UPCONVERSION NANOPARTICLE BASED OPTICAL BIOSENSOR FOR THE DETECTION OF MOLECULAR BIOMARKERS

By

Yinghui Chen

Institute for Biomedical Materials & Devices,

School of Mathematical and Physical Sciences, Faculty of Science

Supervisors:

Prof. Dayong Jin & Prof. Stella M Valenzuela

This thesis is presented for the degree of Doctor of Philosophy

February 2019

Certificate of Original Authorship

I, Yinghui Chen declare that this thesis, submitted in fulfilment of the requirements for the award of Doctor of Philosophy, in the School of Mathematical and Physical Sciences, Faculty of Science, University of Technology Sydney.

This thesis is wholly my own work unless otherwise reference or acknowledged. In addition, I certify that all information sources and literatures used are indicated in the thesis.

This document has not been submitted for qualifications at any other academic institution.

This research is supported by an Australian Government Research Training Program.

Signature: Production Note:
Signature removed prior to publication.

Date: 6/2/2019

Acknowledgements

Completing my PhD study is one of my proudest achievements. Over the course of this four-year period, a lot of people have given me help, care, and encouragement. All of these people will be kept in the bottom of my heart as an invaluable treasure which I will never forget.

To my principle supervisor, distinguished Prof. Dayong Jin, I count myself so lucky to have been your student. I still remember the first time that I heard him describe committing to a PhD. He said, 'As a doctor of philosophy, what you should learn is the philosophy behind the science, instead of only the science.' This motto has stayed with me always and guides me as I explore the scientific world, and the world around me in my ever day life. Professor Jin sets an excellent example for others, never giving up, staying enthusiastic, enjoying science, loving life, learning and giving. I am so grateful to him; he is a respected teacher and a lovely friend.

My co-supervisor, Prof. Stella M Valenzuela, is a wonderfully kind lady. I will never forget her tender supervision and warm encouragement, they are like a colourful rainbow, always making me feel hopeful in my dark days. Her careful and serious attitude to scientific study, makes me feel the responsibility being as a scientific researcher. I really enjoyed the moments where we shared interesting knowledge or techniques with each other. We designed

experiments together, found solutions together and discussed the results together. I really appreciate her help.

Dr. Olga Shimoni, I thank from my bottom heart. She helped me solve lots of experimental problems, working and fighting through challenges with me like a comrade-in-arms. She was so considerate of my thoughts and feelings, and her patience guided me towards a positive attitude. I thank her for always being by my side whenever I needed her.

Dr. Hien T.T. Huong, helped me overcome the surface modification bottle-neck which troubled my project and was a roadblock for quite some time. Dr. Jie Lu, I thank for teaching me the fundamental knowledge and techniques of molecular biology and biochemistry during my initial PhD study, which made me interested in and confident in my PhD research.

Special acknowledgement is also given to Ms Elizabeth Gurung Tamang, the School Manager. She guided me through many complicated procedures, such as my scholarship extension, which allowed me to devote more time and energy towards my work.

I would like to acknowledge all my colleagues who have given me help over the last four years. Hao He, Claudia D'amario, Yingzhu Zhou, Guocheng Fang, for helping me the processing of experiments; Shihui Wen, Jiayan Liao, Xiaoxue Xu, for being reliable collaborators providing me nanomaterials; Dr. Fan Wang, Dr. Jiajia Zhou, Zhiguang Zhou,

Yongtao Liu, Chaohao Chen, Chao Mi, for their excellent contributions in the establishment and maintenance of optical facilities.

Deep appreciation should be also given to my parents, my boyfriend, my relatives and my friends. I thank my parents, my father-Liangyi Chen and my mother-Jie Miao, for understanding me and supporting my decisions. I thank my boyfriend, Xiaolong Meng, for his endless tolerance and sincere company. Every night, you take away any loneliness I may feel, even we are far apart. I also thank my friends, Libing Fu, Huan Wu, Xiaofei Wang, Steven Vasilescu; they have given me a lot of support.

Finally, I acknowledge the financial support from the University of Technology Sydney and Institution of Biomedical and Materials Devices Scholarship, they provided me with precious opportunities to freely discover in scientific world.

Format of Thesis

This is a conventional thesis with five chapters (illustrated by the flow chart below).

Chapter 1 is an introduction chapter, including a comprehensive literature review. The motivation, background, specific aims, and advances made in biomarker detection, optical sensors and upconversion nanoparticles are discussed in details within this chapter.

Chapter 2 is the first result chapter to identify the most suitable ligand molecule for surface modification, and the result Chapters 3 and 4 are parallel investigations of optical biosensors for DNA and protein biomarker assays, and in progressive relation of Chapter 2. Each result chapter follows a paper-publication style, including introduction, experimental section, results and discussion.

Chapter 5 first summarizes the key research outcomes of this thesis, followed by a discussion of the future prospects using upconversion biosensor in molecular biomarker testing.

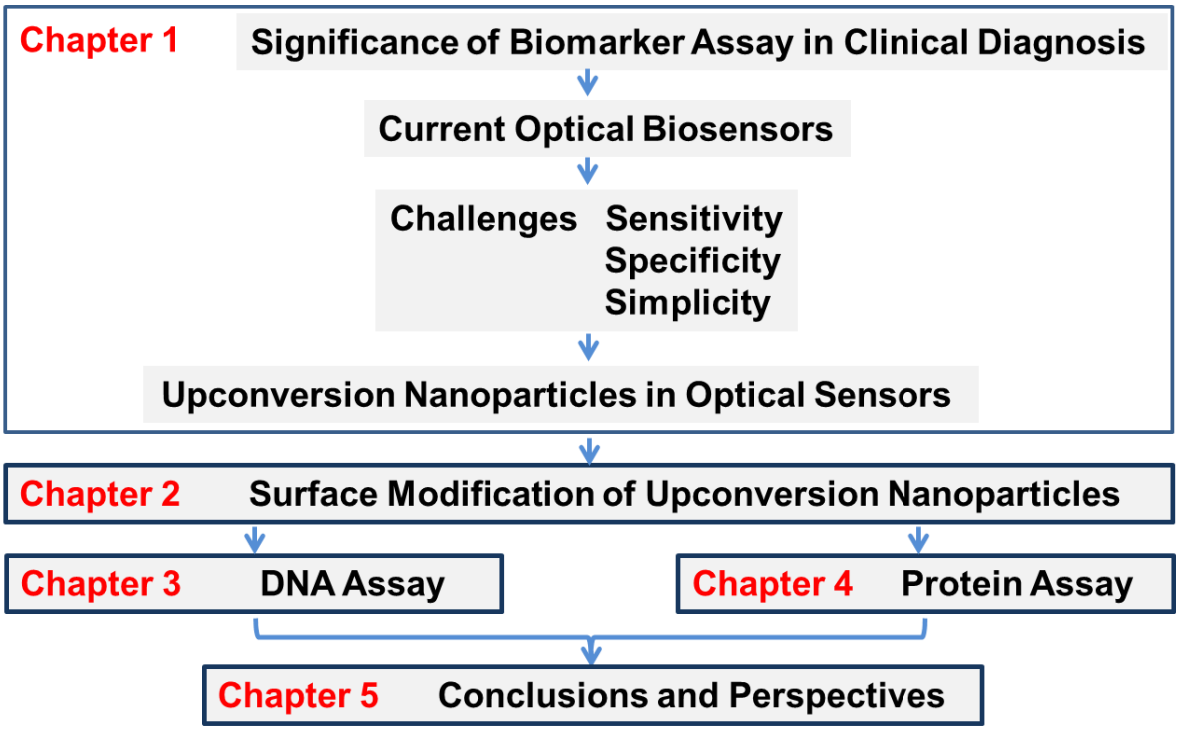

The flow chart outlines the thesis structure.

List of Publications

Research papers:

[1] Yingzhu Zhou, **Yinghui Chen**, Hao He, Jiayan Liao, Hien T. T. Duong, Maryam Parviz, Dayong Jin. A Homogeneous DNA Assay by Recovering Inhibited Emission of Rare Earth Ions-Doped Upconversion Nanoparticles. Journal of Rare Earths. Doi:10.1016/j.jre.2018.05.008.

[2] Hao He, Christopher B. Howard*, **Yinghui Chen**, Shihui Wen, Gungun Lin, Jiajia Zhou, Kristofer J. Thurecht and Dayong Jin*. Bispecific Antibody-Functionalized Upconversion Nanoprobe. Analytical Chemistry. 2018, 90 (5), 3024-3029.

[3] **Yinghui Chen**, Hien T. T. Duong, Shihui Wen, Chao Mi, Yingzhu Zhou, Olga Shimoni, Stella M Valenzuela and Dayong Jin*. Exonuclease III-Assisted Upconversion Resonance Energy Transfer in a Wash-Free Suspension DNA Assay. Analytical Chemistry. 2018, 90 (1), 663-668.

[4] Hien T. T. Duong*, **Yinghui Chen**, Sherif Abdulkader Tawfik, Shihui Wen, Maryam Parviz, Olga Shimoni and Dayong Jin. Systematic Investigation of Functional Ligands for Colloidal Stable Upconversion Nanoparticles. RSC Advances. 2018, 8 (9), 4842-4849.

[5] Jie Lu, **Yinghui Chen**, Deming Liu, Wei Ren, Yiqing Lu, Yu Shi, James Piper, Ian Paulsen and Dayong Jin*. One-Step Protein Conjugation to Upconversion Nanoparticles. Analytical Chemistry. 2015, 87, 10406-10413.

([1] – [5] are closely related to my PhD program)

List of Acronyms (in alphabetic order)

3,4-DHCA	3,4-dihyrocinnamic acid
AD	Alzeimer's disease
AIBN	2,2'-azobisisobutyronitrile
AMPA	(aminomethyl)phosphonic acid
APTES	(3-aminopropy)trienthoxylsilane
AuNPs	gold nanoparticles
BTPA	2-(*n*-butyltrithiocarbonate)-proionic acid
CCD	charge coupled device
cfNA	cell-free nucleic acids
CHO	Chinese hamster ovary
CRC	colorectal cancer
CTAB	cetyl trimethylammonium bromide
CTCs	circulating tumor cells
ctDNA	circulating tumor deoxyribonucleic acid
DC	down-conversion
DLS	dynamic light scattering
DNA	deoxyribonucleic acid
DOX	doxorubicin
DPBS	Dulbecco's phosphate-buffered saline
ECL	electro-chemiluminescence

EDC	1-ethyl-3(3-dimethylaminopropyl)carbodiimide
ELISA	enzyme-linked immunosorbent assay
ESA	excited-state absorption
ETU	energy transfer upconversion
Exo III	Exonuclease III
FBS	fetal bovine serum
FDA	food and drug administration
FTIR	Fourier-transform infrared spectroscopy
GO	graphene oxide
GSA	ground-state absorption
GSH	glutathione
HIV	human immunodeficiency virus
HPLC	high performance liquid chromatograph
HRTEM	high-transmission electron microscopy
LOD	limit of detection
LOQ	limit of quantification
LRET	luminescence resonance energy transfer
MAEP	monoacryloxythyl phosphate
MES	2-(N-Morpholino)ethanesulfonic acid
MIPs	molecularly imprinted polymers
NIR	near infrared
NMR	nuclear magnetic resonance

OA	oleate acid
ODE	1-octadecene
OM	oleylamine
PAA	poly(acrylic acid)
PCR	polymerase chain reaction
PEG	polyethylene glycol
PEI	polyethylenimine
PMAO	amphiphilic poly(maleic anhydride-*alt*-1-octadecence)
QCM	quartz crystal microbalance
RE	rare earth
REEs	rare earth elements
REMs	rare earth metals
RNA	ribonucleic acid
S/N	signal-to-noise
SNPs	single-nucleotide polymorphisms
SPR	surface plasma resonance
TAMRA™	carboxyltetramethyl rhodamine™
TEM	transmission electron microscope
TEOS	tetraethyl orthosilicate
THF	tetrahydrofuran
UC	up-conversion
UCL	upconversion luminescence

UCNPs	upconversion nanoparticles
XO	xylenol orange
XRD	X-ray diffraction

Abstract

Developing sensitive, specific and user-friendly biosensors in order to detect and quantify disease-related molecular biomarkers, is highly significant for early stage diagnosis in the clinic. Current optical biosensors have limitations due to high auto-fluorescent background noise, low detection sensitivity, and are labour intensive.

This thesis explores the surface properties of upconversion nanoparticles (UCNPs), along with identification of a suitable surface modification ligand, which ultimately results in the development of a set of optical biosensors for use in the detection and quantification of both nucleic acid and protein molecular biomarkers for diagnostic purposes. This project has employed UCNPs as a new generation optical nanomaterial for biosensing applications, which have the distinct advantage of eliminating background interference arising from auto-fluorescence. This favourable advantage comes from the physicochemical properties of the UCNPs as they stepwise absorb near-infrared photons and emit anti-Stokes visible luminescence within a narrow spectral bandwidth. This project further explores the use of UCNPs in luminescence resonance energy transfer (LRET) to simplify biomolecular assays, as their distance-dependent energy transfer properties can be exploited to avoid tedious washing steps, resulting in simplicity by saving both labour and analytical time. To realize this, an enzyme-assisted signal amplification technique has been applied to further improve the detection sensitivity of trace amounts of nucleic acids.

The research program reported herein involves three core projects with three key

techniques successfully implemented: the first project contains a systematic and comparative study on the colloidal stability and biocompatibility of hydrophilic UCNPs capped with four ligands. In this project, a newly designed polymer ligand have been identified to form highly water stable and biocompatible UCNPs (Chapter 2); the second project reports an Exonuclease III-assisted upconversion resonance energy transfer in a wash-free suspension DNA assay. Using this approach, an ultra-high sensitivity assay with a detection limit of 15 pM of DNA has been achieved. This assay has achieved one order of magnitude higher sensitivity compared to conventional LRET DNA assay systems using UCNPs (Chapter 3); the third project introduces UCNP based resonance energy transfer for immunoassay of glypican-1 (GPC-1), as a molecular biomarker for prostate cancer diagnosis. In this system, a rational core-shell structure of UCNPs was designed to increase the on/off ratio of detection, and a bispecific antibody was used to improve immune-affinity and simplicity. As a result, a labour-saving, specific and rapid optical biosensor to detect the prostate cancer-relevant GPC-1 biomarker has been demonstrated (Chapter 4).

Several advances in biosensor development have been achieved and reported in this thesis, and further developments are still required towards real world applications. By the end of this thesis, the simplicity of detecting devices and exploitation in point-of-care application are further discussed, which present an array of new opportunities for biomarker assays (conclusions and perspectives Chapter 5).

Key words: biomarker assay, upconversion nanoparticles, surface modification, luminescence resonance energy transfer, signal amplification.

Table of Contents

CHAPTER 1

Introduction

This PhD thesis focuses on developing optical biosensors for application in disease diagnosis, using upconversion nanoparticles (UCNPs) as probes for molecular biomarker detection and quantification. This introductory chapter serves to provide a clear description about the motivation behind the plan. It includes the significance of biomarkers in diagnosis, challenges in current optical biosensor development, the current applications of UCNPs in luminescence resonance energy transfer (LRET) technique for molecular biomarkers detection and quantification, and the advantages of upconversion LRET in combination with advanced enzyme-assisted signal amplification technique and bispecific antibody technique for nucleic acid and protein biomarkers detection and quantification.

1.1 Biomarkers

1.1.1 Definition of Biomarkers

'Biomarker', a term coined as a portmanteau of 'biological marker', has been defined by Hulka and colleagues[1] in 1990 as 'cellular, biochemical or molecular alterations that are measurable in biological media such as human tissues, cells, or fluids.' As biomarker research has expanded over the past decades, so too did the ambiguity of naming and terminology within the biomarker literature. This uncertainty over the specific definition of a biomarker, prompted the National Institutes of Health to form the Biomarker Definitions Working Group to alleviate this growing confusion and provide clarity to

scientists within the field. Thus, in 2001, an authoritative definition for a biomarker was proposed by this special group which states that: 'a biomarker is a characteristic that is objectively measured and evaluated as an indicator for normal biological process, pathogenic process, or pharmacologic response to a therapeutic intervention[2]'. More recently, the definition has been further extended to a broad subcategory of medical signs, which can be accurately and reproducibly measured as objective indications of a medical state observed from outside the patient[3].

1.1.2 Significance of Biomarkers

Biomarkers play a critical role in deepening our understanding of both normal and healthy physiology as well as in improving the drug development process, so they are popular in epidemiological[4] and therapeutic[5] studies. Biomarkers can be considered as helpful tools or technologies aiding in understanding the prediction, cause, diagnosis, progression, regression, or outcome of treatment of diseases[6]. Particularly, the application of biomarkers in the diagnosis and management of major diseases are well known, such as cardiovascular disease[5,7], infections[8], immune disorders[9] and cancers[10]. By monitoring biomarkers' behaviours, it is possible to comprehend the entire progress of disease from very early manifestations to the terminal stages. What's more, when used as outcomes in clinical trials, biomarkers are considered to be surrogate endpoints; that is, they act as surrogates or substitutes for clinically meaningful endpoints. It is advocated by the FDA that it is necessary to use biomarkers in basic and clinical research as surrogate outcomes in large trials of major diseases[11]. Figure 1.1 shows an example of various biomarkers in clinical use for colorectal cancer (CRC)[12].

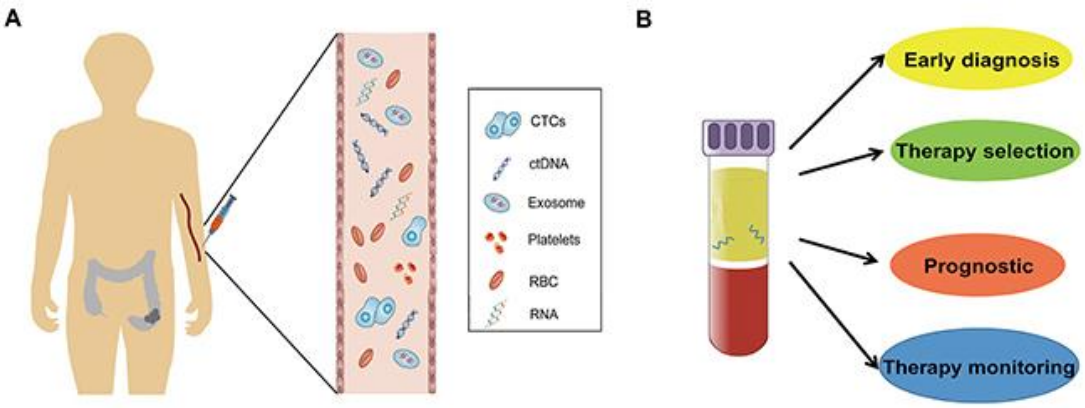

Figure 1.1 Circulating biomarkers in CRC patient (A) and the clinical application of liquid biopsy (B). Reprinted from Ref.[12].

1.1.3 Classification of Biomarkers

According to Perera and Weinstein, biomarkers can simply be classified into two major types based on the sequence of events from exposure to disease: biomarkers of exposure are used in risk prediction; biomarkers of disease are used in screening, diagnosis and monitoring of disease progression[4]. When a disease is suspected of resulting from a toxic exposure in an individual immediate environment, direct measurement of the degree of alleged toxin in air[13], water[14], soil[15], or food[16] can provide indicative value for estimating the individual susceptibility to disease. However, the external dose measured sometimes provides the basis to understand the relationship to the disease process. The measurement of internal dose from the tissues or body fluids of the suspected individuals, such as blood, urine and cerebrospinal fluids may provide more accurate information for screening, diagnosis and prognosis[17-19]. More recently, biomarkers have been defined into six categories in more detail in light of their contribution to clinical research[20], namely: (1) biomarkers for risk-predicting whether an individual is predisposed to developing any physiological disorder; (2) biomarkers for diagnosis/trait-reflecting the possibility and presence of disease state; (3) biomarkers for state/acuity-reflecting the severity of a

particular disease process; (4) biomarkers for stage-reflecting extant staging classification allowing categorization of an individual's present stage of illness; (5) biomarkers for treatment response-as an index and signal of certain treatment; (6) biomarkers for prognosis-predicting the likely course and outcome of an illness.

On the other hand, based on their characteristics, biomarkers can also be classified into physiological biomarkers, like blood pressure or heart rate, and molecular biomarkers, like prostate specific antigen for prostate cancer. More recently, molecular biomarkers are becoming synonymous for the various biomarkers currently being pursued, including four major types - DNA, RNA, protein and small chemicals[21] (Figure 1.2).

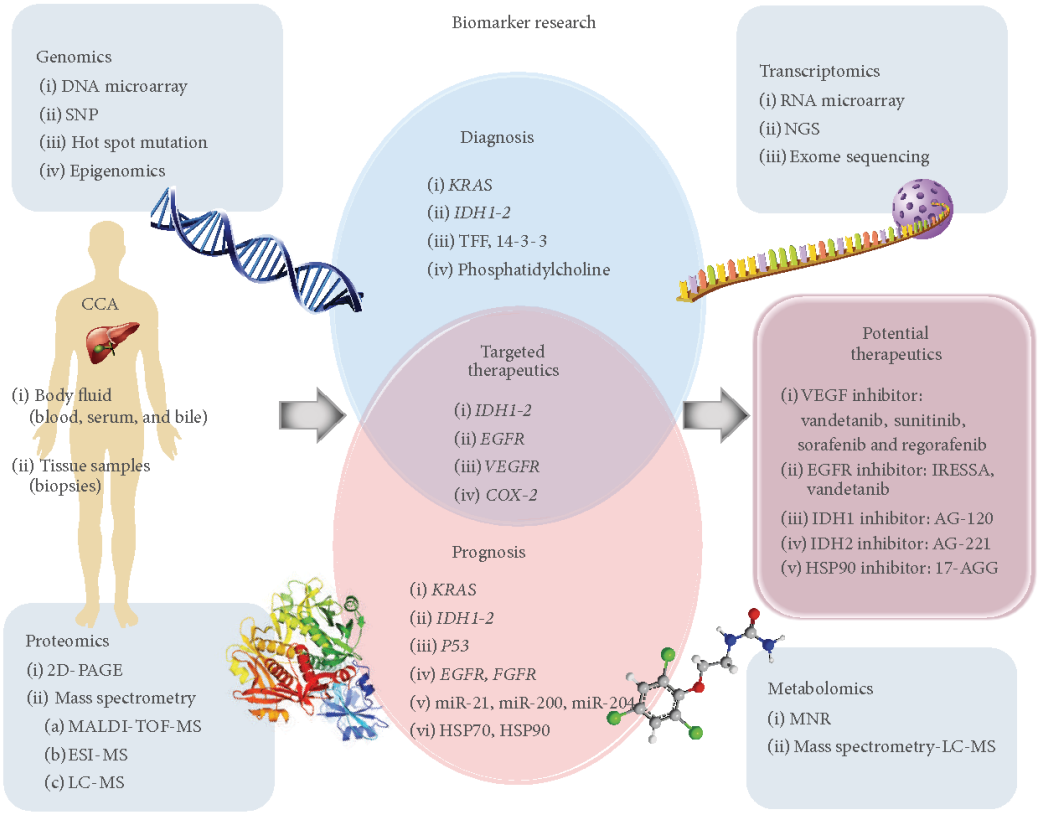

Figure 1.2 Classification and examples of molecular biomarkers. Reprinted from Ref.[21].

1.2 Current Biosensors of Molecular Biomarker Detection

Development of reliable and practical techniques for biomarker monitoring is urgently needed in order to transfer laboratory-technique to clinic application. The rapid growth of molecular biology and laboratory technology has expanded to the point at which the application of technically advanced biomarkers will soon become even more feasible. As for the composition of biomarkers, it includes protein, nucleic acid, enzyme, heavy metal, cell and small chemical[17,22-25]. Among this group, protein and nucleic acid based biomarkers attract most popularity and attention. In this thesis, the focus will be mainly on development of optical biosensors for nucleic acid and protein based biomarkers detection. Thus, here, we emphasize current methods for these two molecular markers.

1.2.1 Nucleic Acids

ctDNA. Dating back to 1948, was the first time that Mandel and Metais reported the presence of cell-free nucleic acids (cfNA) circulating in blood plasma of healthy individuals and patients[26]. However, at that moment, due to the lack of clear understanding about cfNA, their work did not attract much attention. It was not until 1994 that the importance of cfNA was recognized, when it firstly reported the presence of mutated oncogene products (K-ras) in the plasma of pancreatic cancer patients[27]. Nowadays, it is an agreed consensus that increased levels of cfNA circulating in patients' blood can act as a useful indicator in diagnosis of various kinds of diseases, especially cancer. Over the past decade, increasing attention has been paid to cfNAs (such as DNA, mRNA and microRNA (miRNA)) whose presence at high concentration in the blood of cancer patients, and their potential values in clinical research was broadly highlighted[28]. Circulating tumour DNA (ctDNA) released by circulating tumour cells (CTCs) into the circulation and found in the plasma of cancer patients with increased quantities compared

with healthy people, is a potential biomarker to detect and monitor tumours in a non-invasive way[29,30]. It has been fully considered that ctDNA contains oncogenes, and clinical data demonstrate that these oncogenes are identical to those found in the tumour tissue sample from the same patient[31-33]. However, at the early stage of cancer, the number of CTCs is very low, usually around one to ten CTCs together with several millions of blood cells[34,35], that means the amount of ctDNA released from CTCs is extremely low. Thus, developing highly sensitive biosensor strategies are urgently needed for measuring ctDNA markers at ultralow levels during early stages of disease.

Signal amplification. Conventional nucleic acid quantitative detection based on hybridization assays, usually provide insufficient sensitivity to detect target nucleic acid existing in low abundance below the picomolar level. To overcome this challenge, a variety of target-triggered signal amplification techniques have emerged recently, providing ultrahigh sensitive and quantitative performance for nucleic acid detection. They exploit repeated reaction cycles to duplicate the specific targets or target-dependent complexes for continuous signal generation.

Polymerase chain reaction (PCR), developed by Kary Mullis in 1983[36], is a nucleic acid amplification technique, whereby a few copies or a small fraction of DNA are amplified in orders of magnitude, to generate thousands, or even millions of copies of the target DNA sequence to achieve substantially enhanced signal output. PCR methods rely on thermal cycling, with a heat-stable DNA polymerase necessarily employed. In addition, it needs highly experienced operator and very sophisticated temperature-controlled machine. Thus, as for this stringent reaction condition, PCR-driven techniques are not ideal for developing user-friendly point-of-care devices.

Other enzyme-assisted signal amplification techniques through amplifying the target DNA-dependent complexes at room temperature to generate substantial measurable signals can also achieve high detection sensitivity in nucleic acid assays[37-39]. Such isothermal approaches can avoid interferences from primer dims and cross-contamination as well as costly equipment for precise temperature control, in comparison with PCR. These methods rely on special approaches capable of releasing the target DNA sequence after hybridization, often through enzymes that can recognize and manipulate specific sites of DNA, such as exonuclease, endonuclease and polymerase. The released target DNA is then recycled to bind to other complementary DNA probes repeatedly, leading to the accumulation of signal over time. As for different enzymes' functions, the strategies of processing the target DNA recycling are different: the strategy using exonucleases is to digest nucleotides in the binding sites from the end of the complementary DNA probe in a duplex without damaging the target DNA sequence; the strategy using endonucleases is to nick and remove a small part in the middle of the complementary DNA probe, resulting in reduced binding affinity with target DNA sequence; the strategy using polymerases is to produce a new DNA strand possessing stronger binding affinity with complementary DNA probe, to replace the target DNA sequence. Usually, the application of endonuclease is not a good option for developing general methods, for most of the time, it requires very specific sequences that matches the enzyme's recognition quite well. However, most targeted sequences do not have that specific sequences. In comparison, using exonucleases is much more flexible, by adjusting the design of probe-DNA to meet the requirement of either 3' or 5' end of the formed duplex.

Target DNA-triggered signal amplification assisted by Exonuclease III (Exo III) enzyme

for ultrasensitive quantitation of DNA has been extensively developed and applied[37,40]. Exo III has a double-strand specific, non-processive 3'-5' exo-deoxyribonulease activity that produces a step-by-step mononucleotide removal from the 3'-end of DNA. However, if the 3'-end of the DNA overhangs by more than four bases in length, it can be protected from Exo III activity[41]. Typically, the mononucleotides of designed probe DNA can be stepwise removed without damaging the target DNA sequence. Like the assay shown in Figure 1.3, in addition of target DNA, the formed double stranded DNA are recognized by Exo III. Subsequently, only the probe DNA with 3'-end exposed outside can be digested by Exo III, and the modified dye at 3'-end are released from probe DNA during the digestion. The intact target DNA goes to the next probe DNA to form another duplex, triggering the cycle. In this case, many fluorescent dyes are released from probe DNA to be taken as the loss of signal just induced by one target DNA, and the signal amplification can be realized. In this thesis, this selective nucleotide digestion feature has been exploited in Chapter 3 to significantly enhance the limit of detection in upconversion LRET DNA assay. The obtained experimental LOD value is 15 pM, one order of magnitude enhanced sensitivity of DNA detection, compared to the conventional DNA-DNA direct hybridization upconversion LRET assay[42-45].

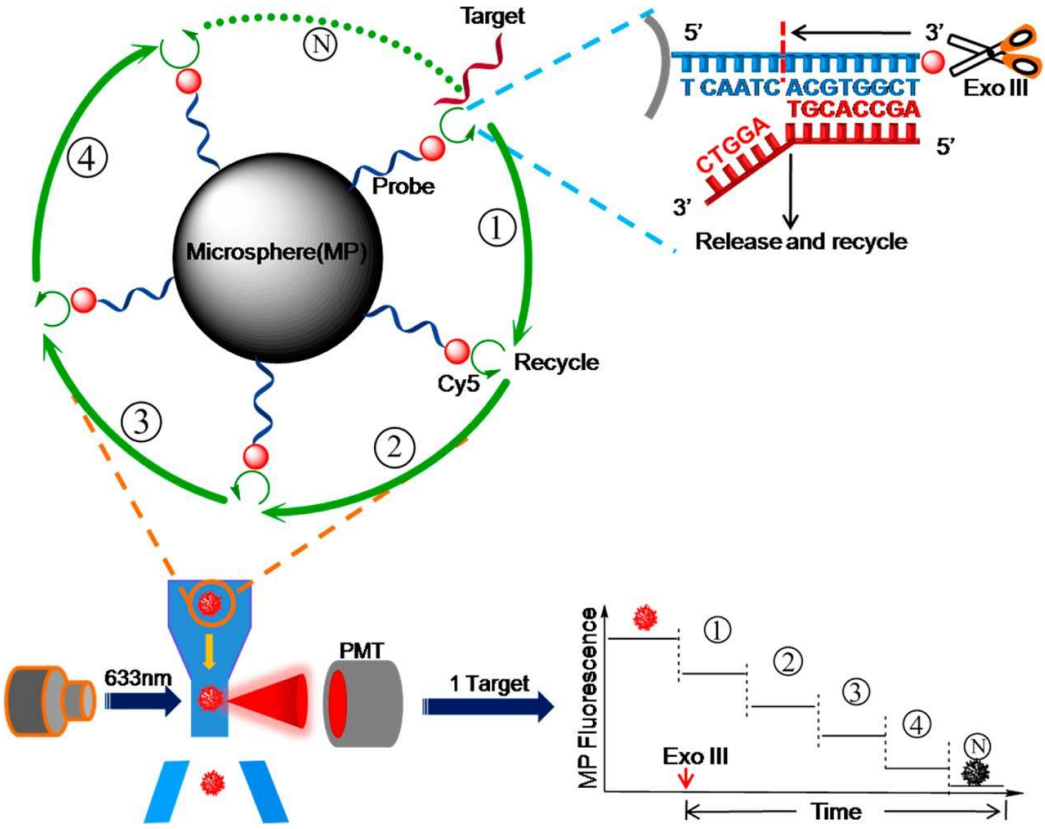

Figure 1.3 Scheme of Exo III based target recycling coupled to amplified flow cytometry DNA bead assay. Reprinted from Ref.[40].

1.2.2 Protein Antigens

In the development of diagnostic tests, an alternate approach is based on a panel of protein biomarkers, those are detectable in body fluids and tissues and can be used to differentiate among diseases with population-wide robustness. Protein biomarkers play a significant role in the diagnosis of several major diseases, such as Alzheimer's disease (AD)[17,46], cancer[47], and cardiovascular disease[48].

Immunoassays. Protein-based detection techniques, commonly referred to as immunoassays, determine the presence of a specific protein, or even the amount of protein in samples. The most crucial element of the detection strategy is a highly specific antibody-antigen interaction. Immunoassays used jointly with other techniques have

demonstrated excellent progress for the development and application of protein biosensors[49]. Protein biosensors are comprised of two closely associated elements: a biological recognition element (enzyme, antibody, receptor, microorganism, nucleic acids) and a transducer (electrochemical, mass, optical and thermal). This fabrication can realize the specific detection *via* specific binding affinity between target protein with recognition element, and also the conjunction of the signal transducer can provide a relatively high sensitive outcome[50]. The most famous immunoassay is enzyme-linked immunosorbent assay (ELISA)[51]. It is a plate-based technique designed for detecting and quantifying protein-structure based substances. In direct ELISA, target antigens should be pre-immobilized onto a solid phase *via* high levels of physical absorption, and then antibodies conjugated with enzyme can be introduced in the liquid phase to produce a measurable product, due to specific affinity between antigen-antibody.

Aptamer. The interactions between an antibody and an antigen, or a receptor and an antibody are well known to be very specific reactions. In the case of aptamers, more attention is placed on the selection of a certain nucleic acid sequence as the capture element, called “aptasensor”, which serves a similar function to that of the antibody[52]. These are RNA or DNA molecules (25-80 nucleotides) selected *in vitro* by an “evolutionary” method called SELEX (systematic evolution of ligands by exponential enrichment) from a vast population of random sequences that recognize specific ligands by forming binding pockets[53,544]. Usually, in the absence of the target protein, aptamers act as normal nucleic acids. The presence of target protein molecules results in a conformational change of the aptamers, this newly formed spatial structure can only allow target protein binding. DNA aptamers are more resistant to denaturation and degradation, and their binding affinities and specificities can easily be manipulated and improved by

rational design or by techniques of molecular evolution, and they can be modified with functional groups or tags that allow covalent, detected immobilization on biochips, resulting in highly ordered receptor layers[55]. In contrast, RNA aptamers are susceptible to degradation by the endogenous ribonucleases typically found in cell lysates and serum.

BsAb. Antibodies containing two different antigen-binding sites in one molecule are called bispecific antibodies (BsAbs). BsAbs can be roughly divided into two categories: immunoglobulin G (IgG)-like molecules and non-IgG-like molecules[56]. Non-IgG-like antibodies lack an Fc region entirely, consisting of only the Fab regions, and various types of bivalent and trivalent single-chain variable fragments (scFvs). One scFvs BsAb, as one active domain can specifically recognize and bind to methoxyl polyethylene glycol (mPEG) molecules, have gained increased attention in the application of both diagnosis and therapy[57-59] (Figure 1.4). Antibody fragments can be tethered to the mPEG-functionalized nanomaterials through simple mixing, show advantages over the traditional chemical conjugation as the chemical conjugation may alter the structure of nanomaterials encapsulated drugs, and deactivate the antibodies. In this thesis, this kind of scFvs- structured BsAb has been applied in joint with upconversion LRET for the protein antigen assay.

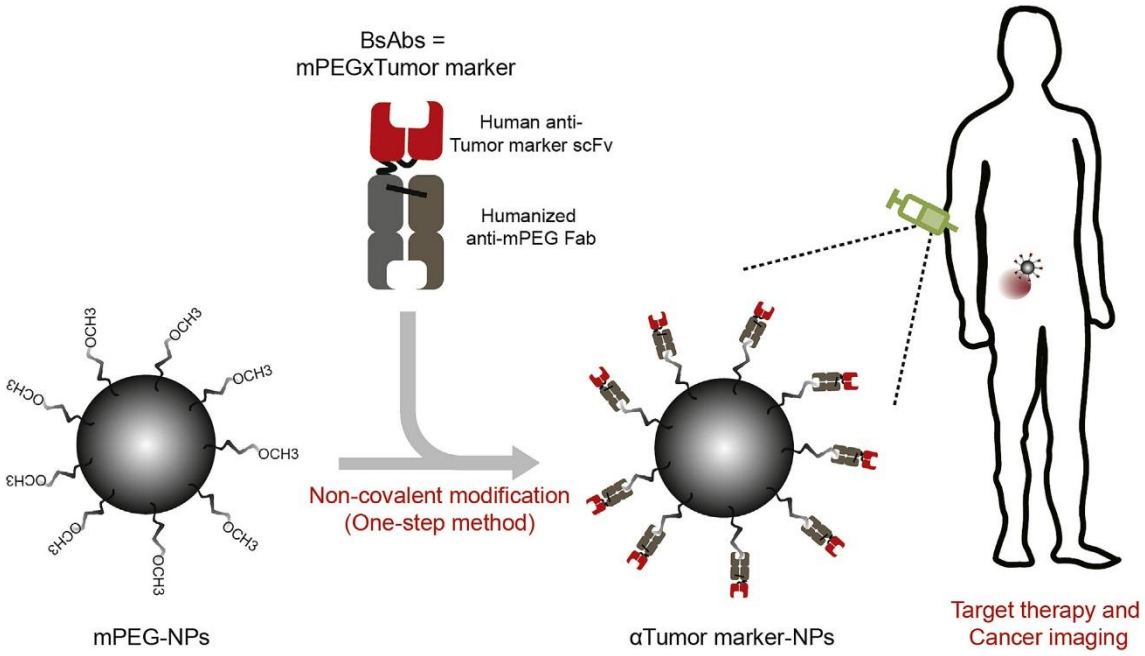

Figure 1.4 Scheme of one-step mixing with humanized anti-mPEG bispecific antibody enhances tumour accumulation and therapeutic efficacy of mPEGylated nanoparticles. Reprinted from Ref.[59].

1.2.3 Current Biosensors of Nucleic Acids and Protein Antigens

Based on the types of signal transduction, biosensors can be classified into five groups: electrical, electrochemical, piezoelectric, magnetic and optical[60]. Figure 1.5 demonstrates the typical biosensors examples.

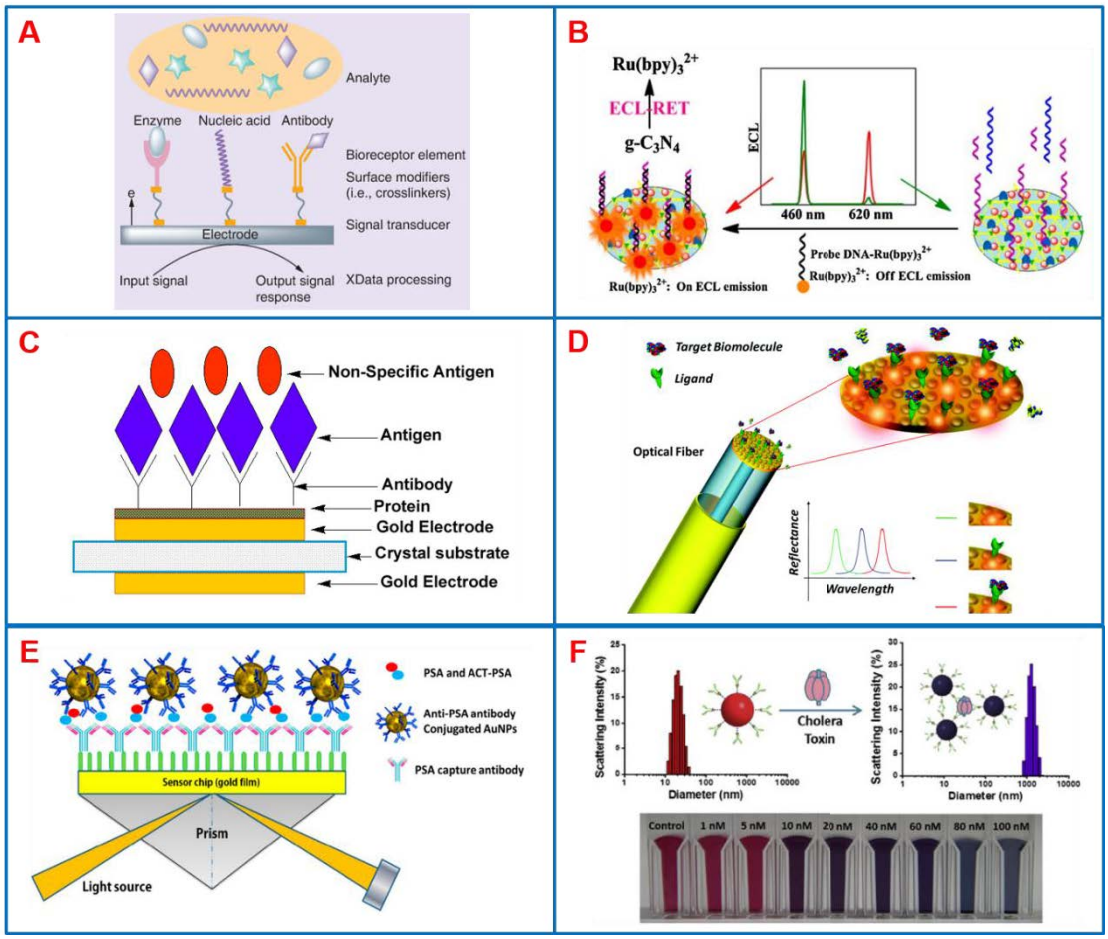

Figure 1.5 Typical examples of biosensors. (A) Electrical biosensor. (B) Electrochemical biosensor. (C) Piezoelectric biosensor. (D-F) Optical biosensor: optical fibre sensor, surface plasmon resonance sensor, gold nanoparticle-based colorimetric sensor. Figures are reprinted from Ref.[61-66].

1.2.3.1 Electro-chemiluminescence

Electro-chemiluminescence (ECL), is a technique in which luminescence is produced during electrochemical reaction in solution. There are two main ECL modes in broad application in the fields of enzyme or immunochemical biosensors[67] based on different luminescent reactions: the luminol and ruthenium complexes. Luminol oxidation leads to the formation of an aminophthalate ion in an excited state, which emits light when returning to the ground state. In Sakura's work, it is proposed that luminol was first

oxidized at the electrode surface and then reacted, mole to mole, with hydrogen peroxide to generate the blue emission spectrum maximum at 425 nm[68,69]. On the other hand, ruthenium complexes, especially $[Ru(Bpy)_3]^{2+}$ (which releases a photon at ~620 nm) regenerates with TPrA (Tripropylamine) in liquid phase or liquid–solid interface (Figure 1.5B)[62]. One of the most attractive characteristics of ruthenium metal chelate complexes, is their ability to be regenerated in their native form after having completed the light emission reaction sequence[70,71]. A single molecule could then theoretically generate more photons than the luminol in destructive electro-chemiluminescence. Since 1972, when the Rubipy-based electrochemiluminescence was first reported, it has been used in development of immunoassays and DNA probe assays for clinical diagnostics[72]. These types of small molecules used to label proteins or oligonucleotides have little or no effect in their immunoreactivity, solubility or ability to hybridize, which can result in extremely low detection limit.

1.2.3.2 Quartz Crystal Microbalance

Quartz is one member of a family of crystals that experience the piezoelectric effect. A quartz crystal microbalance (QCM) measures a mass variation per unit area by measuring the change in frequency of a quartz crystal resonator. As the change in quartz resonance frequency is in direct linear correlation with changes in mass, the measurable increase of its mass due to the binding of an analyte can be calculated from the frequency change based on Sauerbrey's initial formula[73]. The property of measuring the mass change of quartz crystal microbalance for protein detection, avoids the need to fluorescently label either the analyte or receptor and the subsequent complex photophysics and photochemistry accompanying detection by optical biosensors. The utility of quartz crystal microbalance coupled with immunoassays has been wide spread, with both

antibody and aptamers selected as the receptors pre-coated onto the surface of the quartz crystal[74,75].

1.2.3.3 Optical Biosensors

Optical biosensors show numerous advantages over other analytical techniques, because of their capability of direct and real-time detection of a range of biological and chemical substances. Various advanced concepts and approaches are applied in the implementation of new optical biosensors, especially with the rapid advances in nanotechnology and biotechnology, optical biosensors based on nano-biotechnology are becoming the most popular class. Optical biosensors can be simply split into two general modes[76]: label-free and label-based. In brief, label-free mode means the measurable signal is generated directly through the interaction of the analytes with the transducers. On the contrary, label-based sensors involve using a label to generate an optical signal by a colorimetric, fluorescent or luminescent method. In the following section provides a detailed description of the three most popular optical biosensors.

Optical fibre. Optical fibres are currently used as transducers for various physical phenomena. Compared with other biosensors, optical fibres demonstrate several advantages: small size, flexible geometry, remote working capability and noise immunity. Many optical biosensors use an optical fibre to propagate the signal emitted by a fluorescent label[77-79]. The fibre-optic evanescent wave biosensor is based on total internal reflection. The light travelling in a fibre core penetrates into the surrounding medium, during which the intensity of the evanescent field decays exponentially from the fibre core surface into the medium. The pre-immobilized or flowing fluorophores around the core surface can be excited by evanescent wave, and the produced fluorescence is coupled

back into the fibre core as an optical signal for transmission to an optical measuring device (Figure 1.5 D)[64].

Surface plasmon resonance. Optical sensors based on excitation of surface plasmons, referred to as surface plasmon resonance (SPR), mainly rely on measuring changes in the refractive index occurring in the field of an electromagnetic wave supported by the optical structure of the sensor (Figure 1.5 E)[65]. Ever since the first application of SPR for gas detection demonstrated by Nylander and Liedberg in the 1980s[80], during the following decades, the development and application of SPR biosensing have gained remarkable achievements in various kinds of biomarker detection[81,82], including DNA[83,84] and protein[85,86]. SPR immunoassay was first reported in 1983, to detect anti-human IgG in water solution based on a silver film coated with human IgG[87], and from then on, SPR biosensors have been broadly used in biomarker detection in clinic, such as breast cancer, prostate cancer, colorectal cancer and sepsis[88,89]. SPR biosensor, which allows for real-time analysis of bio-specific interactions without the use of labelled molecules, has become a leading technology in the field of direct real-time observation of biomolecular interactions. SPR sensors, in principle, are thin-film refractometers that measure changes in the refractive index occurring at the surface of a metal film (typically gold or silver) supporting a surface plasmon. Briefly, it is the changes of refractive index produced by the capture of biomolecules at the sensor surface that reflect the presence and even concentration of analyte molecules. Since then, On the basis of which characteristic of light wave modulated by a surface plasmon is measured, SPR sensors can be classified into four modes: angular, wavelength, intensity and phase.

Gold nanoparticles. Nanomaterial based optical biosensors for DNA and protein (Figure

1.5 F)[66], such as gold nanoparticles, are becoming a popular technique[90,91]. Colorimetric detection of DNA hybridization in a homogeneous solution based on the formation of oligonucleotide-functionalized gold nanoparticles aggregates in the presence of target DNA, was firstly developed by Mirkin in 1997[92]. It provides an easy way for DNA detection by observing the colour change of the solution from red to purple by naked eyes. However, its biggest challenge is the low detection sensitivity. Later on, a signal amplification method based on nanoparticles-promoted reduction of silver(I) was successfully coupled with a new 'scanometric' chip-based DNA array, and grey-scale achieves two orders of magnitude of sensitivity compared with analogous fluorophore systems[93]. Furthermore, gold nanoparticles that facilitate formation of a silver coating acting as a surface-enhanced Raman scattering promoter for dye-labelled particles has been developed for ultra-high sensitivity of DNA and RNA detection[94]. What's more, as for the utility of large light scattering cross section of AuNPs in DNA detection, Huo and co-workers developed a dynamic light scattering (DLS) method allowing for highly sensitive DNA detection[95]. In the presence of target DNA, the two kinds of capture DNAs - that are complementary to different parts of the target DNA – located on modified-AuNPS will be caused to form dimers, trimers and larger aggregates. This nanoparticle aggregation will increase the average diameter of the whole nanoparticle population, detected by DLS analysis.

1.2.4 Challenges in Optical Biosensor Development

Even though numerous optical biosensors for use in molecular detection have been reported, several major challenges still exist, such as auto-fluorescent background, low sensitivity, and labour-intensive. Amongst the rapid developments in nanotechnology, a new kind of nanomaterial, UCNP, is considered as particularly promising, due to its

unique optical properties that are superior to conventional nanomaterials. Due to its outstanding performance in recent years, it is considered as a potential candidate in use in the development of optical biosensors, leading to a new generation of optical biosensors, able to achieve high-sensitivity and labour-savings.

1.3 Lanthanide-Doped Upconversion Nanoparticles

1.3.1 Definition of Rare Earth Materials

Rare earth (RE) materials include a kind of phosphor which can absorb and convert certain types of energy into radiation of light, are often characterized by various names, such as rare earth elements (REEs), rare earth metals (REMs), rare earth oxides, or yttrium-based rare earth materials. REMs are composed of a set of 17 chemical elements (15 lanthanides plus scandium and yttrium) and are essentially classified into two distinct categories: light rare earth elements, known as the cerium group, from lanthanum to europium; and heavy rare earth elements, known as the yttrium group, from gadolinium to lutetium, plus scandium and yttrium. Scandium and yttrium are considered to be rare earth elements because of their same core deposits as lanthanides and exhibit identical chemical properties[96]. Lanthanides are mostly stable in the trivalent form (Ln^{3+}) and their 4f inner shell is (partially) filled with electrons, and the Ln^{3+} ions have the electronic configuration $4f^n\ 5s^2\ 5p^6$ where n varies from 0 to 14. The 4f electrons are shielded by the completely filled $5s^2$ and $5p^6$ orbitals resulting in weak electron-phonon coupling and the f-f transitions are in principle parity forbidden. Consequently, their absorption and emission feature narrow f-f transition bands with low transition probabilities and substantially long lifetimes[97].

1.3.2 Advantages of Upconversion in Biological Applications

On the basis of the mechanism of luminescence, RE luminescence can be divided into down-conversion (DC) and up-conversion (UC) emission; the DC process obeys the Stoke's shift that is converting higher energy photons with shorter wavelength into lower energy photons with longer wavelength; the UC process is anti-Stoke's shift that absorbs two or more lower energy photons with longer wavelength and converts into higher energy photons with shorter wavelength, on the basis of sequential adsorption and energy transfer steps[98]. Compared with the DC process with UV excitation, currently, much attention has been paid to the UC process, as its anti-Stoke's shift demonstrates significant advantages in biological applications: (1) It can achieve high penetration depth in biological tissues near-infrared resulting in negligible photodamage due to the longer wavelength and lower energy level of near-infrared light[99-102] (Figure 1.6A). (2) It is capable of eliminating strong auto-fluorescence interference[103] and to improve the accuracy and sensitivity of bioimaging and biomolecular detection, as most auto-fluorescent biomolecules are unable to be excited under near-infrared light with lower power. (3) The narrow luminescence bands and multi-colour output, due to being doped with different lanthanides of upconversion nanoparticles, play a significant role in realizing multiplexing in biological application assays[104-106] (Figure 1.6B). (4) The luminescence within the visible range is easy to measure, so both of the NIR exciting sources and measuring devices are cheap and easier to obtain. This cost-effective property makes upconversion techniques applicable in not only academic studies but also technical applications[107,108].

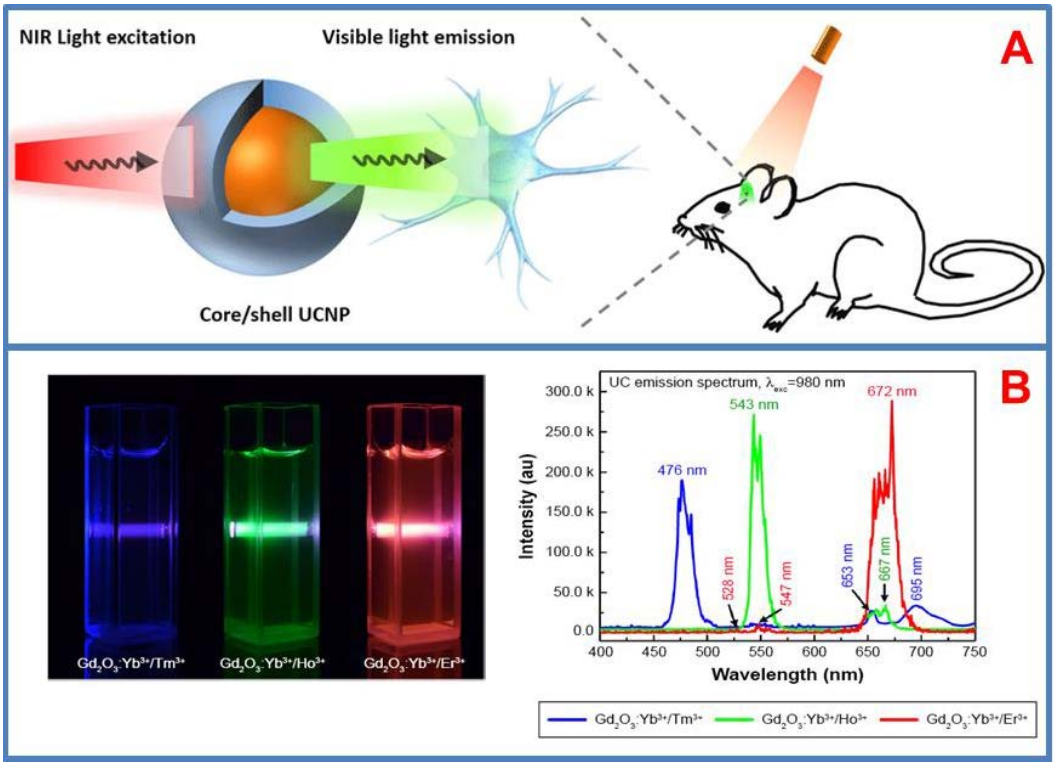

Figure 1.6 Optical properties of UCNPs. (A) is reprinted from Ref[109]*. (B) is reprinted from Ref*[110]*.*

1.3.3 Mechanism of Upconversion Emission Including GSA/ESA and ETU

The most efficient and common mechanisms of lanthanide-doped upconversion process can be roughly summarized into two classes: ground-state absorption followed by excited-state absorption (GSA/ESA) and subsequent energy transfer upconversion (ETU, also known as addition de photon par transfers d'energies, the APTE effect). Both mechanisms are based on the sequential absorption of two or more photons by metastable, long-lived energy states[111]. This kind of sequential absorption induces the population of photons at a highly excited state from where the upconversion emission occurs.

GSA/ESA. GSA/ESA is a single ion based process whose excitation takes the form of successive absorption of at least two photons by a single ion that provides enough energy to reach the emitting level. Firstly, if excitation energy is resonant with the transition

energy from ground state to excited metastable state, the GSA will occur to make the photons populate at E_1 state from ground state. A second pump photon that promotes the ion from E_1 to higher-lying state E_2 results in UCL, corresponding to the E_2-G optical transition (Figure 1.7A). In single-ion doped nanocrystals, the distance between the two neighbouring activator ions and the absorption cross-section of the ions are the two key factors of the upconversion process. There are two major factors influencing upconversion processes. High doping concentration of activator ions can lead to severe cross-relaxation due to the too short distance between two ions, resulting in quenching of excitation energy. Most lanthanide activator ions show low absorption cross-section, leading to low pump efficiency. Therefore, the overall upconversion efficiency for single-ion doped nanocrystals is relatively low.

ETU. ETU is different from GSA/ESA, and one photon is absorbed by the ion, and subsequent energy transfer from neighbouring ion also at excited state results in the population of a highly excited state of the emitting ion (Figure1.7B). Usually, the neighbouring ion transferring energy at its excited state is called sensitizer, who possesses a relatively strong absorption cross-section in the NIR region. Specifically, excitation takes the form of successive absorption of pump photons by two neighbouring ions. Both the sensitizer and activator ions can absorb a pump photon in the same energy, thereby populating the intermediate reservoir level E_1. Then the activator ion is promoted to upper emitting state E_2 according to a non-radiative energy transfer process from the neighbouring sensitizer ion, while the ion relaxes back to ground state G. A short wavelength photon is released from the activator ion when the promoted photon is back to the ground state G. The most commonly used lanthanide as sensitizer is Yb^{3+} which possesses an extremely simple energy level scheme with only one excited 4f level of $^2F_{5/2}$.

The $^2F_{7/2}$-$^2F_{5/2}$ transition of Yb^{3+} can resonant well with many f-f transitions of typical upconverting lanthanide ions (Er^{3+}, Tm^{3+} and Ho^{3+}), and enables multicolour emissions[112].

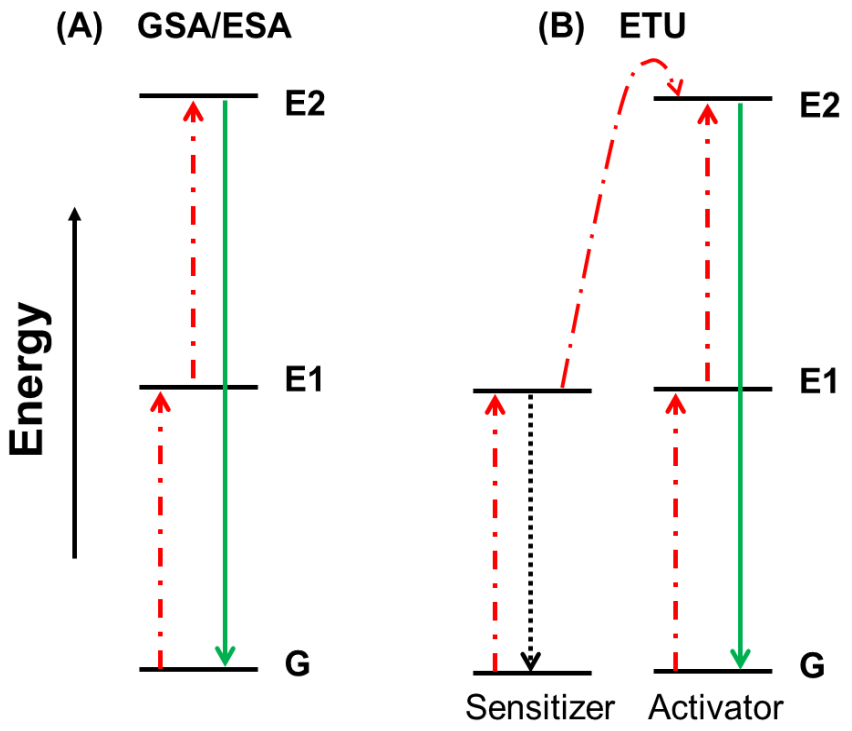

Figure 1.7 Schematic illustration of the mechanism of upconversion luminescence.

1.3.4 Yb^{3+} and Er^{3+} Co-doped $NaYF_4$ UCNPs

The most efficient UCNP to date, Yb^{3+} and Er^{3+} co-doped $NaYF_4$, was introduced by Menyuk et al. in 1972[113] and Kano et al. in 1973[114]. In this thesis, the typical co-doped Yb^{3+}/Er^{3+} nanoparticles yielding strong green at around 545 nm originated from the transitions $^4S_{3/2}$-$^4I_{15/2}$ and red emission at around 660 nm originated from the transition $^4F_{9/2}$-$^4I_{15/2}$ were utilized in Chapter 3 and Chapter 4. In Chapter 3, the absorbance of acceptor dye is around 560 nm, and the absorbance of gold nanoparticle in Chapter 4 is around 520 nm. Thus the co-doped Yb^{3+}/Er^{3+} nanoparticles with 545 nm emission is applied because of the well-matched wavelength overlapping. Additionally, the unchanged red emission around 650 nm has functioned as internal signal reference. The

mechanism of Yb^{3+} and Er^{3+} co-doped $NaYF_4$ upconverting luminescence is illustrated in Figure 1.8. The visible green emission around 540 nm is popular in upconverting luminescence resonance energy transfer bio-assay coupling with wavelength-matched various traditional fluorescent dyes[103,115] and other optical materials such as gold nanoparticles[116,117] and graphene oxide[118,119]. These two luminescence emissions will be mainly applied for optical signal measurement in this thesis.

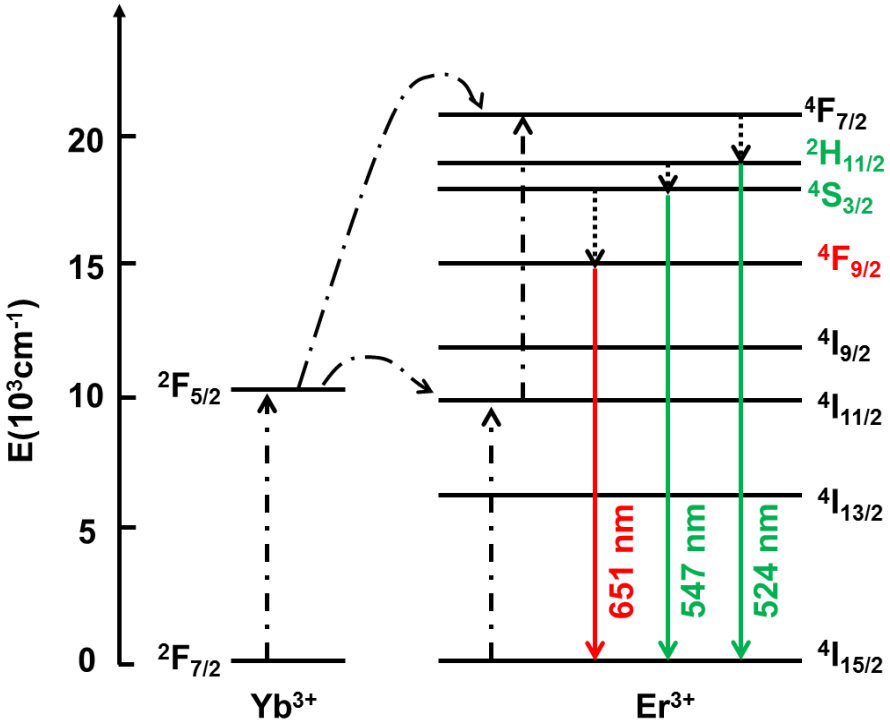

Figure 1.8 The illustration of upconversion mechanism of Yb^{3+}/Er^{3+}-$NaYF_4$ nanoparticles.

1.3.5 Surface Modification of Lanthanide-doped UCNPs

The typical synthesized UCNPs are organic-soluble with hydrophobic surfactant-coating[120], demonstrating more uniform size, morphology and higher crystallinity than directly synthesized water-soluble particles[121,122]. Oleate acid (OA) and oleylamine (OM) are the most used surfactants to assist particles suspended in organic solvents during synthesis and storage. Bare UCNPs stick closely with carboxyl or amine groups of OA or OM, and leaving the long fatty acid chain outside. It is necessary to transfer the

hydrophobic particles into hydrophilic through surface modification, in order to apply the nanoparticles into biological application. Currently, there are four most popular surface modification methods including ligand oxidation[123,124], inorganic shell coating[125,126], ligand exchange[127,128] and amphiphilic ligand encapsulation[129-130].

Ligand oxidation. The chemical structure of both OA and OM consist an unsaturated carbon-carbon double bond in the middle of the fatty acid chain, and it is usually based on the direct oxidation of that carbon-carbon double bond of OA or OM ligands pre-coated on the surface of UCNPs to generate carboxyl groups. The double bonds are broken down and the newly generated carboxyl groups are exposed on the outside of the particles, leading to hydrophilic dispersion in aqueous solution (Figure 1.9). This ligand oxidation needs catalysis by strong oxidants, such as Lemieux-von Rudloff reagent and ozone. Lemieux-von Rudloff reagent consisting of $KMnO_4$ and $NaIO_4$ as oxidant, has been widely applied to selectively oxidize the carbon-carbon double bond followed by immersed in hydrochloric acid to obtain the carboxyl groups[131,132,133]. Less popular but also reliable, ozone has also been employed for the ozonolysis of OA ligands *via* epoxidation to selectively cleave the carbon-carbon double bond, combined with a subsequent oxidation by mixture of H_2O_2 and CH_3COOH to bare carboxyl groups. Besides the subsequent oxidation following ozonolysis, at the same time, researchers in this work also conduct subsequent reduction treatment following ozonolysis with CH_3SGH_3 to generate aldehyde groups for further conjugation with amino-containing molecules *via* easier Schiff-base condensation[123]. In another case, the oxidation was firstly catalysed by 3-chloroperoxybenzoic acid to generate a three-membered-ring epoxide; and the polyethylene glycol monomethyl ether (PEG-OH) was secondly reacted with the highly reactive epoxide product to introduce the PEG polymer onto the surface

of the nanoparticles[124]. PEG has been broadly applied for the surface modification of nanoparticles in bio-application as it can provide higher water solubility. Through ligand oxidation, the morphology, phase, composition and luminescence of the UCNPs can remain unaffected. However, it also shows disadvantages like complicated processing, poor colloidal water stability and low yields of functional groups.

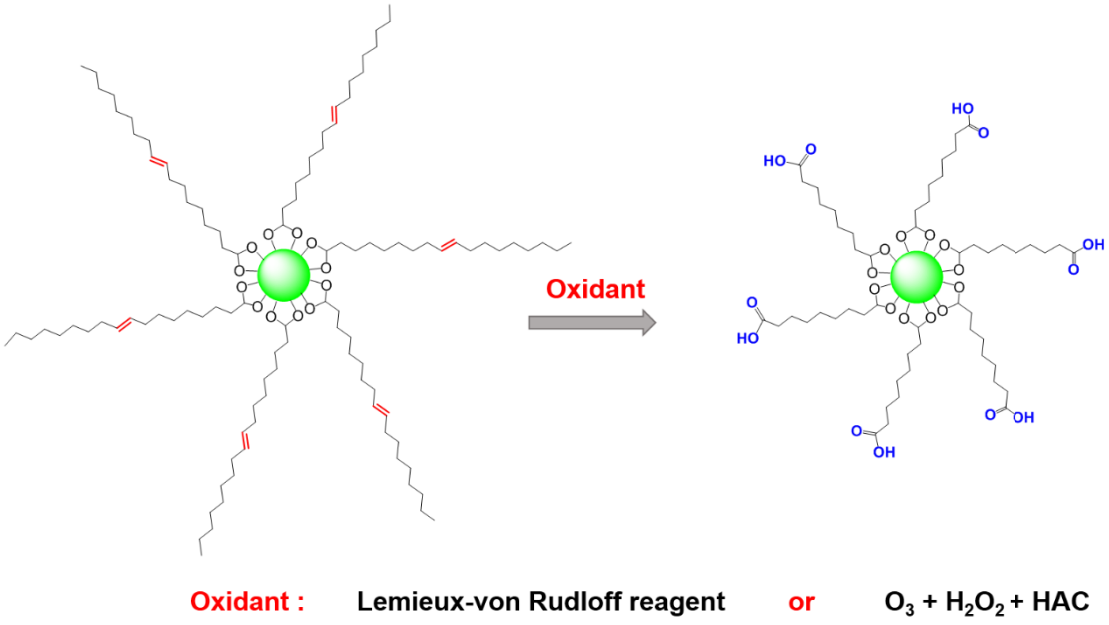

Figure 1.9 The illustration of surface modification of UCNPs via ligand oxidation.

Amphiphilic ligand encapsulation. Amphiphilic molecules are also popular in UCNPs surface modification, due to their special chemical structure. They consist of two basic sections including a hydrophobic long alkyl chain to form a bilayer with the oleate ligands on the surface of UCNPs *via* van-der-Waals, and a hydrophilic head outside of the bilayer enabling good water solubility of UCNPs. Currently applied amphiphilic molecules for surface modification of UCNPs includes, PEG-phospholipids, amphiphilic poly(maleic anhydride-*alt*-1-octadecence) (PMAO), amphiphilic chitosan[134], CTAB[135] and TWEEN[136]. Among them, PEG-phospholipids and PMAO are two used highly for such applications (Figure 1.10). Phospholipids are a major component of cell membranes that

possess special amphiphilic structures to form the hydrophilic bilayers. Similarly, the hydrophobic fatty acid chains from PEG-phospholipids attract and insert into the fatty acid chains from OA ligand that wrap the outside of the UCNPs, forming the bilayer surface coating. At the same time, the hydrophilic head of PEG, kept outside of the formed bilayer, provides strong water solubility and stability[137,138]. Incorporation of modifying functional groups (carboxyl, amine, maleimide, biotin) at the end of the PEG molecules are used to mimic surface bio-engineering of UCNPs for further conjugation[118,129]. PMAO, also known as C_{18}PMH, has a similar chemical structure to phospholipids, with its long fatty acid chain used to attract and form the bilayer coating[103,139-141,142]. Amphiphilic ligand encapsulation can keep the crystal stability of the particle's surface, resulting in relatively bright luminescence during the modification. However, amphiphilic ligands themselves can easily form micelles, and these 'empty' encapsulations will also take part in the following bio-conjugation, therefore influencing detection sensitivity.

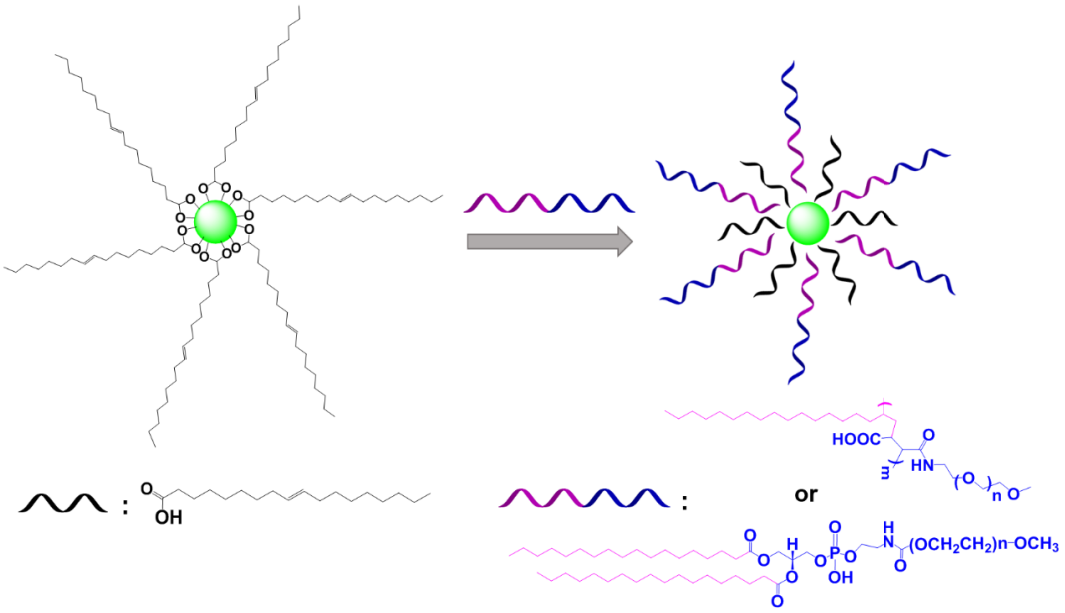

Figure 1.10 The illustration of surface modification of UCNPs via amphiphilic ligand encapsulation.

Silica shell coating. The deposition of a silica shell on a UCNP is a useful technique to

generate water soluble nanoparticles. Both hydrophilic and hydrophobic UCNPs can be coated using either the Stober method[125,126,142-149] or the reverse microemulsion method[117,150-154], and the latter gains much more attentions as it can provide uniform silica layer (Figure 1.11). As for reverse microemulsion, there are commonly two steps: Firstly, Igepal CO-520, a kind of surfactant, is added into cyclohexane to form a microemulsion (water-in-oil), followed by adding OA-capped UCNPs, so that OA ligands are detached from the surface of the particles and the bare particles can be wrapped inside the microemulsion; Secondly, ammonia liquid and TEOS are added into the solution. Catalysed by the ammonia, TEOS hydrolyses to form silanol. The silanol condenses with its neighbouring silanol to form a relatively solid layer coating the surface of UCNP by replacing the pre-microemulsion. It can form multilayers of silica shell and it is easier to adjust the thickness of the silica shell by controlling the input amount of CO-520 and TEOS. CO-520 can also be substituted by other molecules like PVP[104,155,156] and CTAB[116,157]. TEOS-based silica coating lacks functional groups restricting the application of the nanoparticles. (3-aminopropyl)trienthoxysilane (APTES), an amino siloxane, is often preformed to generate functional amino groups on the surface of the silica coated nanoparticles for further bioconjugation. The silanization begins with the hydrolysis of ethoxy groups in APTES[126,151], a process catalysed by water, leading to the formation of silanols; and then, the silanols condensed with surface silanols of the silicon substrate forming a monolayer of APTES *via* a lateral siloxane network. The amino groups are oriented away from the underlying silicon surface leading the convenient and efficient chemical reaction in conjugation. The silica-coated nanoparticles are water soluble, but unstable and always tend to aggregate in water. Furthermore, the additional modification step with APTES is time-consuming.

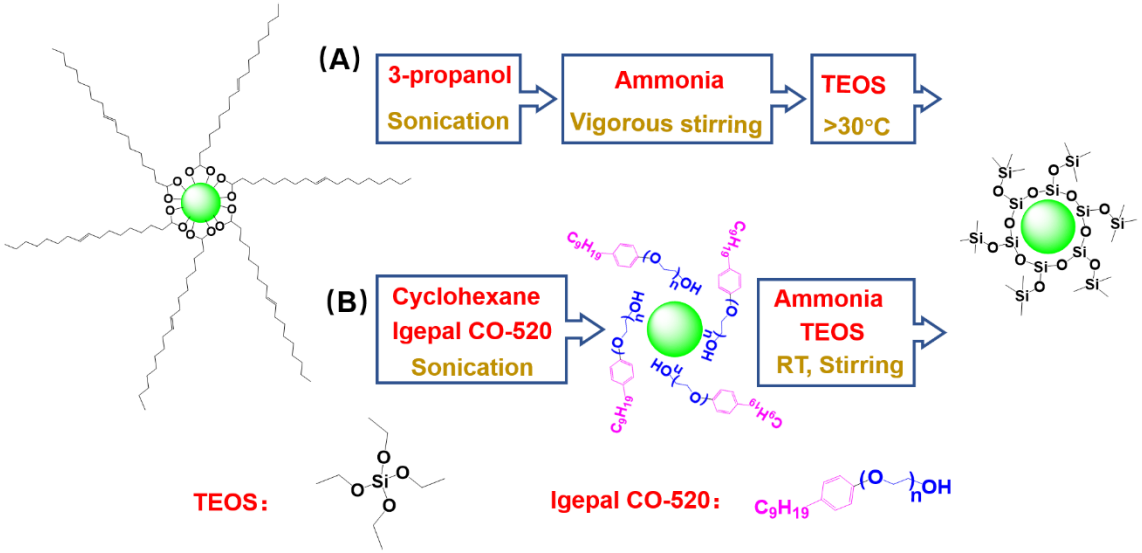

Figure 1.11 An illustration of surface modification of UCNPs via silica coating.

Ligand exchange. Ligand exchange, a one-step in combination of replacement of hydrophobic OA or OM ligands with functionalization by hydrophilic molecules, is becoming a popular surface modification in recent years. The ideal hydrophilic ligands should possess both replacing heads with stronger chemical binding or chelating affinity to lanthanide ions to remove the OA ligands, and also functional ends avoiding further modification. The binding strength of the reacting groups is the key element for the replacement of the OA molecules, and the decisive factor for the stability of the nanoparticles in biological reagents containing various molecules which may have higher binding strength over the reacting groups to the metal ions. The functional groups displaying different charges always act as the important role for the bio-conjugation and excellent dispersion in aqueous buffer with various pH levels. Exchange conducted in one-phase is much more efficient than in two-phases. The so-called two-phases means OA-capped UCNPs and replacing ligands are separately pre-dissolved in non-polar phase and polar phase, as the replacing ligands in this case are hydrophilic biomolecules, such as DNA[128,158,159] and peptide[160]. The ligand exchange mainly happens around the interface

between the organic and aqueous solution with vigorous shaking. Under this situation, hydrophobic particles and hydrophilic ligands do not easily have access to contact with each other, resulting in incomplete exchange and low production yields. In addition, for most of the time, the interface between organic and aqueous solution needs to be discarded because there exists the mixture of hydrophobic and hydrophilic particles, leading to loss of particles[128,161]. In contrast, mixing the replacing ligands with OA-UCNPs within one solvent only under gentle shake, can increase the chance of touching, leading to thorough replacement and high productivity[162]. Tetrahydrofuran (THF) usually acts as the processing reagent[162,163], having the capability to dissolve both hydrophilic ligands and hydrophobic nanoparticles. The popular ligands for one-phase ligand exchange includes bigger polymer, such as poly(acrylic acid) PAA[162-173], PEI[108,117,174], phosphate-PEG polymer[162,175-178]; and smaller molecules, such as DHCA[163,179] and citrate acid[180] (Figure 1.12). Sometimes, in order to achieve high binding yield of hydrophilic ligands on the surface of particles, OA ligands are removed by acidic solvent (commonly hydrochloride acid) firstly, followed by attachment of ligands in water[115,181-184]. Ligand exchange is a rapid, high-efficient, labour-saving surface modification method of nanoparticles.

In general, for ligand oxidation, amphiphilic ligand encapsulation and silica coating, the biggest advantage is that the morphology and luminescence of the UCNPs can remain unaffected. However, each method also has its own drawbacks: ligand oxidation shows the disadvantages like complicated processing, poor colloidal water dispersible and low yields of functional groups; amphiphilic ligands themselves are easy to form micelles, and these ‘empty’ encapsulation will also take part in the following bio-conjugation, influencing detection sensitivity; the silica-coated nanoparticles always tend to aggregate

in water, and the additional modification step with APTES is time-consuming. In comparison, ligand exchange is high-yield and easy to process. Particles through ligand exchange are quite water dispersible and luminescent bright.

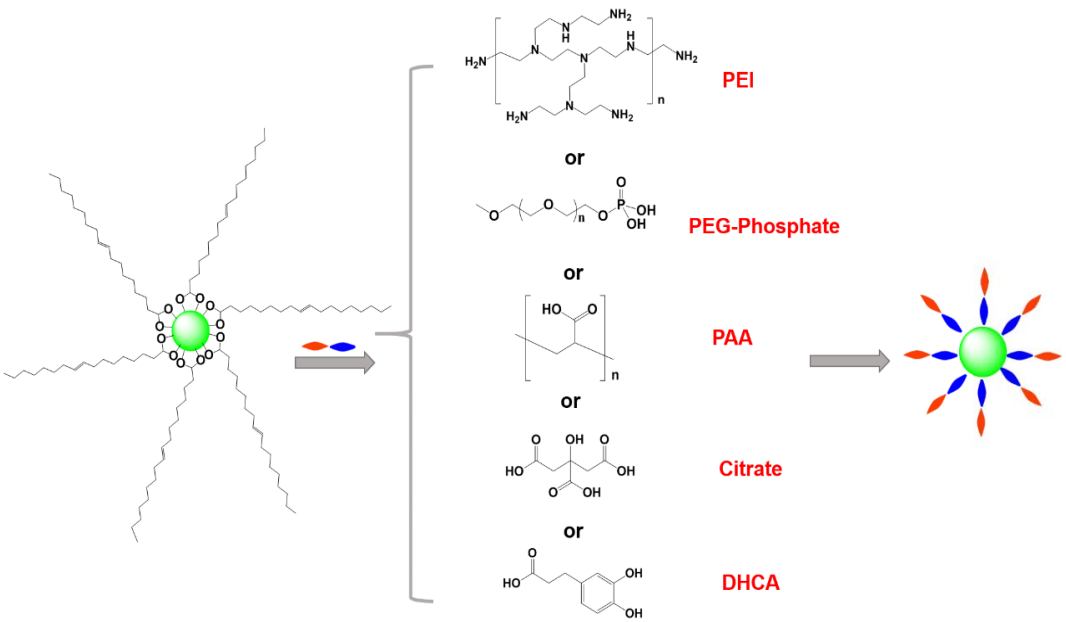

Figure 1.12 An illustration of surface modification of UCNPs via ligand exchange.

1.3.6 *In vitro* Applications of Upconversion LRET in Molecular Biomarker Detection

For the application of UCNPs in biomolecule detection, there are two main pathways: simply being as optical signal in replacement of traditional chromophores; not only being as the measurable signal, also taking the role as donor in resonance energy transfer technique. Every single UCNP usually contains thousands of photon sensitizers and hundreds of trivalent lanthanide ions (Ln^{3+}) as photon activators within an inorganic crystalline host matrix, and therefore deliver bright luminescence within the visible range. By using these brighter nanoparticles under NIR excitation to replace small molecular chromophores under UV excitation, it can achieve higher signal observation, for instance, in the lateral-flow strip test application[144,166,185]. However, it is more attractive for the research to take this special UCNPs being a new generation of energy donor in resonance

energy transfer technique, to develop simple and sensitive bioassays.

Due to the wavelength cross-section between the excitation of the acceptor with upconversion luminescence of the donor, the energy transfer occurs from the doped-activator at the excited state to the molecular acceptor at the ground state. In this case, the energy is transferred in a non-radiation pathway, and no upconversion luminescence is emitted, and subsequent the radiation of the excited acceptor results in its fluorescence.

This thesis emphasizes the application of UCNPs in combination with RET technique for bioassays, and a more detail description of various kinds of upconversion LRET approaches is provided below.

1.3.6.1 Target-triggered absorption wavelength shift of acceptor. Acceptors chosen in this case are target-sensitive fluorescent molecules, in which their excitation wavelength can passively change only in the presence of detectable targets. Mostly, the targets are metal ions. Chelate complexes can be formed between some metal ions with molecular fluorophores, leading to the conjugation system change and absorption range shift of molecules. It is simply classified into two ways: ‘switch-on’ and ‘switch-off’.

‘Switch-on’, can be easily understood that the ‘stolen’ energy is returned back to the donors from acceptors, leading into the emission of upconversion luminescence again. Specifically, the target-sensitive acceptors are pre-immobilized close to UCNPs, and in the absence of target, the luminescence emission was prohibited *via* LRET. Once the target is present, the coordination of the target with the acceptor triggers the blue/red shift of the acceptor’s excitation wavelength beyond the cross-section with upconversion

luminescence. The pre-quenched upconversion luminescence is recovered along with LRET disappearing (Fig.1.13). Either the intensity of recovered upconversion luminescence or reduced acceptor's, or the ratio between them, can be used as optical signal to monitor target concentration[117,186,187].

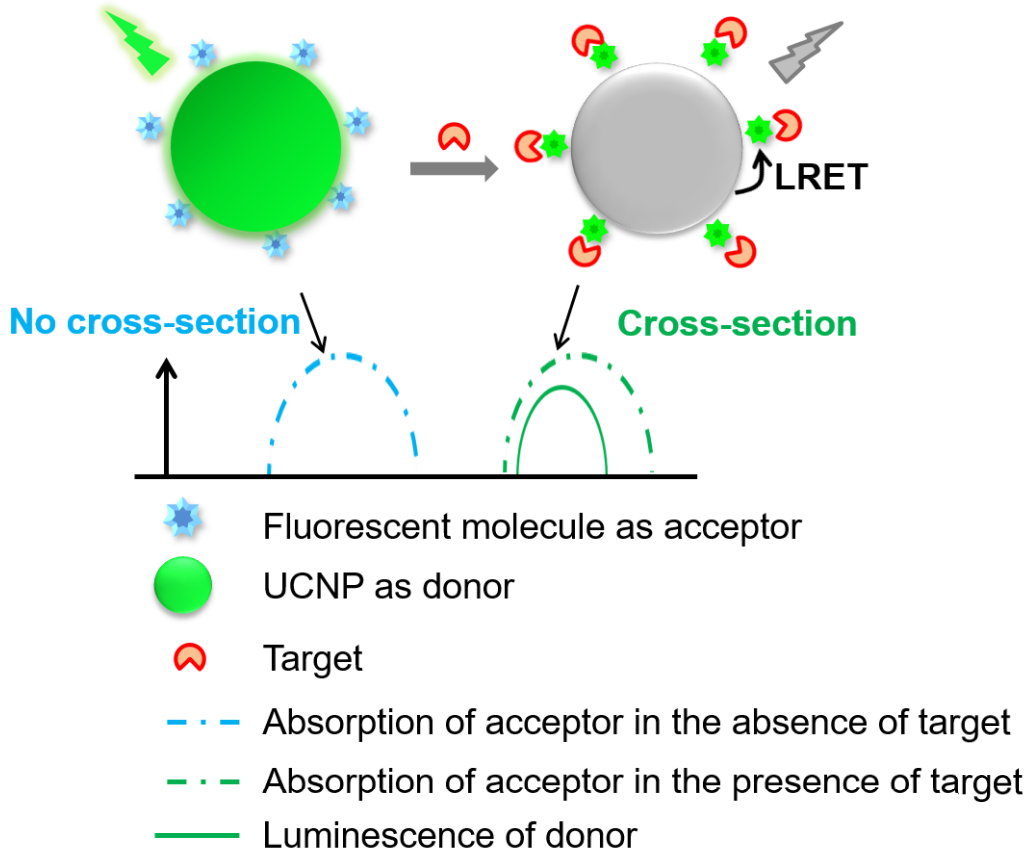

Figure 1.13 The illustration of 'switch-off' upconversion LRET assay based on target-triggered absorption wavelength shift of acceptor.

'Switch-off', conversely, the energy is 'stolen' by acceptor with the assistance of the target to prohibit the upconversion luminescence[143,188]. The excitation wavelength of pre-immobilized acceptors onto particles does not overlap with upconversion luminescence. The addition of target induces the cross-section between donor and acceptor, and then upconversion luminescence is quenched along with the enhanced acceptor's

fluorescence[131].

Table 1.1 lists the fluorescent molecules as the acceptors used in upconversion LRET assays in both 'switch-on' and 'switch-off' models, based on the mechanism that the presence of the target can induce the absorption wavelength shift of the fluorescent molecules.

Table 1.1 Target-triggered absorption wavelength change of acceptor.

Upconversion LRET based on target-triggered absorption wavelength shift of fluorescent acceptors					
	Acceptor absorption (nm)	**Acceptor absorption with target (nm)**	**UCNP doping**	**Detective target**	**Sensitivity**
Switch-on	**540**	450	Er^{3+}	Hg^{2+} [186]	0.21 μM
	790	510	Tm^{3+}	$ONOO^{-}$ [187]	0.08 μM
	470	360	Tm^{3+}	Zn^{2+} [115]	0.78 μM
Switch-off	660	**840**	Er^{3+}, Tm^{3+}	$MgHg^{2+}$ [131]	0.18 ppb
	400	**580**	Er^{3+}, Tm^{3+}	F^{-} [143]	5 μM
	510	**540**	Er^{3+}	Cu^{2+} [188]	2.16 μM

1.3.6.2 Target-triggered absorption intensity change of acceptor. Besides the fluorescent molecules mentioned above, another type of fluorescent molecules are also target-sensitive. Rather than the absorption wavelength shift, it is the absorption capacity at certain wavelength that changes in addition of target. Thereby, capability of LRET is influenced[103,157,167,179,189-191]. Take the detection of chromium (Cr^{3+}) as an example[103]. A Cr^{3+}-responsive rhodamine derivative (CRD) was assembled on the surface of Ho^{3+} doped UCNPs. Upon addition of Cr^{3+} into the probe solution, the absorption peak of CRD at 560 nm was significantly enhanced, which greatly reduced the upconverting green emission, leading to an obvious colour evolution from green to yellow to orange and to red with increasing the concentration of Cr^{3+}. The colour change can be distinguished by the naked eye, as predicted, and the achieved LOD is as low as 4.1 μM.

1.3.6.3 Upconversion LRET based on pH-sensitive fluorophores as acceptors. Intracellular pH is one of a number of factors determining cellular proliferation, apoptosis, enzymatic activity, ion transport and muscle contraction. UCNPs are powerful tools for monitoring intracellular pH changing because of their high signal-to-noise ratio resulting in excellent sensitivity and specificity[164,174,162,184,192,193]. Some molecular fluorophores can show various behaviours of absorbance under different pH conditions. In the application of upconversion LRET for pH monitoring, pH as the stimulator induces the change of acceptors' absorbance in the cross-section with upconversion luminescence. Consequently, the upconversion LRET can be either strengthened or weakened, as an optical signal for monitoring pH change. Take UCNP-xylenol orange (XO) as an example[193] (Figure 1.14). The absorption spectrum of XO is very sensitive to pH in the range of 5-8, covering most of the physiological pH range. XO exhibits the maximum absorbance around 435 nm at low pH (<6.0) and around 576 nm at high pH (>7.0). So

the absorption around 435 nm possesses a good spectral crosstalk with the upconversion blue emission around 450 nm of Tm-doped UCNPs in low pH conditions (<6.0), leading to efficient LRET. As the pH increases, the absorption of XO was observed red-shift gradually, resulting in poor crosstalk with the blue emission of Tm^{3+}-doped UCNPs and the quenched luminescence was released. This probe cannot only detect pH values in buffer solution, but also in living cells. It is very evident that with the increase of the intracellular pH value from 5 to 8, the ratio of the blue UCL channel to the red one was increased correspondingly. Table 1.2 lists the pH-sensitive fluorescent molecules as the acceptors used in upconversion LRET assays.

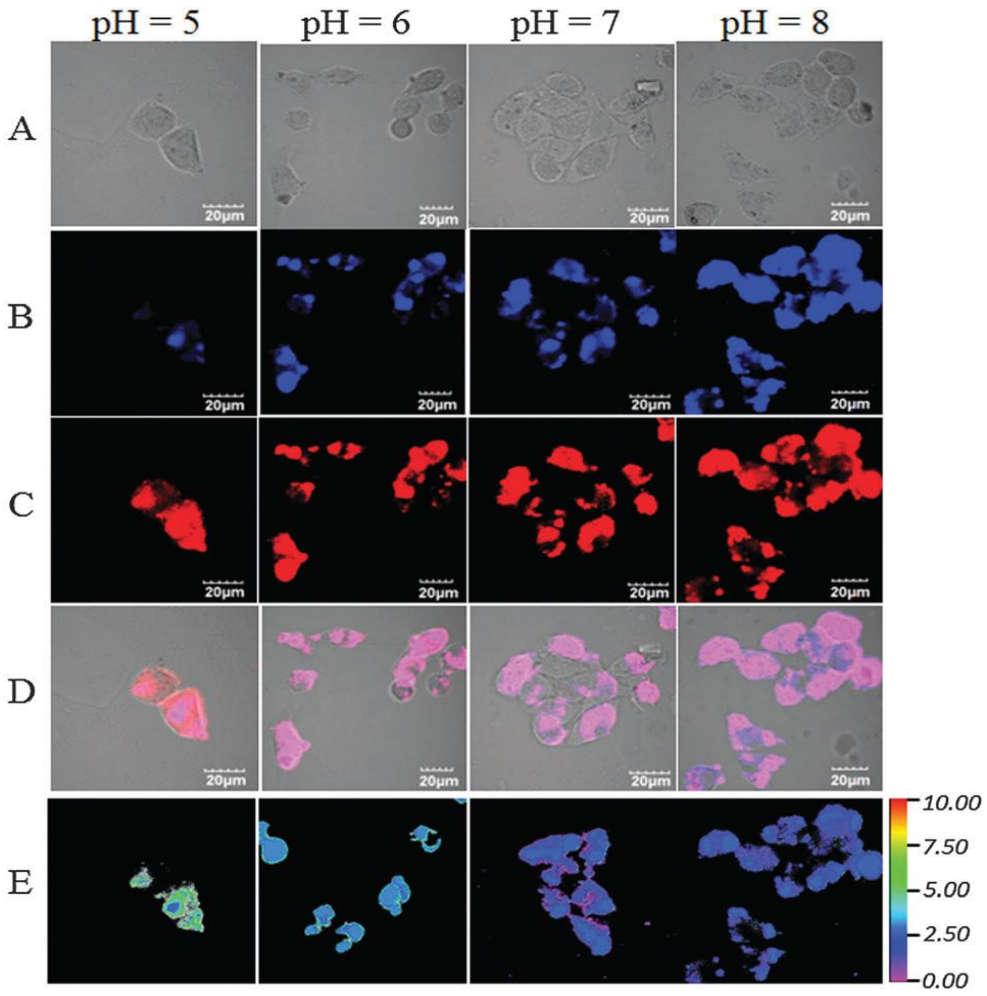

Figure 1.14 UCL images of UCNP@SiO2–XO at different pH values in HeLa cells (lex = 980 nm). (A) Bright field images, (B) collected at emission wavelengths of 430–520 nm; (C) collected at emission wavelengths of 580–680 nm; (D) overlay of (A), (B) and (C); (E) ratio of emission intensity at 430–520 nm to that at 580–680 nm. Figure is reprinted from Ref.[193].

Table 1.2 Upconversion LRET based on pH-sensitive fluorophores as acceptors.

Upconversion LRET based on pH-sensitive fluorophores as acceptors		
Acceptor	**UCNP doping**	**pH range**
Hemicyanine dye [164]	Tm^{3+}	5.0-9.0
Fluorescein [174]	Tm^{3+}	5.0-8.0
pHrodo Red [182]	Er^{3+}	5.0-7.0
Fluorescein isothiocyanate [184]	Tm^{3+}	3.0-7.0
pHrodo™ Red [192]	Er^{3+}	2.5-7.2
Xylenol orange [193]	Tm^{3+}	5.0-8.0

1.3.6.4 Target-triggered detachment of acceptors from UCNPs. LRET is a distance-dependent phenomenon, and by controlling the distance between UCNPs with fluorescent molecules, LRET efficiency is easy to be adjusted (Figure 1.15). Normally, the specific

fluorescent molecules are pre-immobilized onto the surface of UCNPs[160,173,194,195] *via* non-covalent bonds. These acceptors can recognize specific targets and detach from UCNPs to bind with targets, resulting in a long distance of donor-acceptor beyond the energy transfer range. Thus, the introduction of targets leads to recovery of the upconversion luminescence. It is the key point in this case that the binding affinity of acceptor to target is much stronger than that to UCNPs. What's more, no chemical reaction is allowed for the conjugation of acceptors onto UCNPs, and simply physical absorption is preferred. Table 1.3 lists the upconversion LRET based on target-triggered detachment of acceptors from UCNPs.

It is worth mentioning that this upconversion LRET based on target-triggered detachment of acceptors from UCNPs is also popular and applicable to drug-release tracking during intracellular therapeutic study[116,168]. Take the common cancer drug-DOX as an example. The Mn-doped UCNPs coated with silica shell are responsive to mild reductive and acidic tumour conditions, enabling the breakup of Si-O-Si bonds within the silica framework. This tumour-sensitive degradation of the shell can facilitate the pre-loaded DOX in the internal space of nanoparticles releasing in the tumour location. The release of DOX brings recovery to the total emission intensity and a drastic decline to the red/green ratio, which can be used to sense the drug release extent.

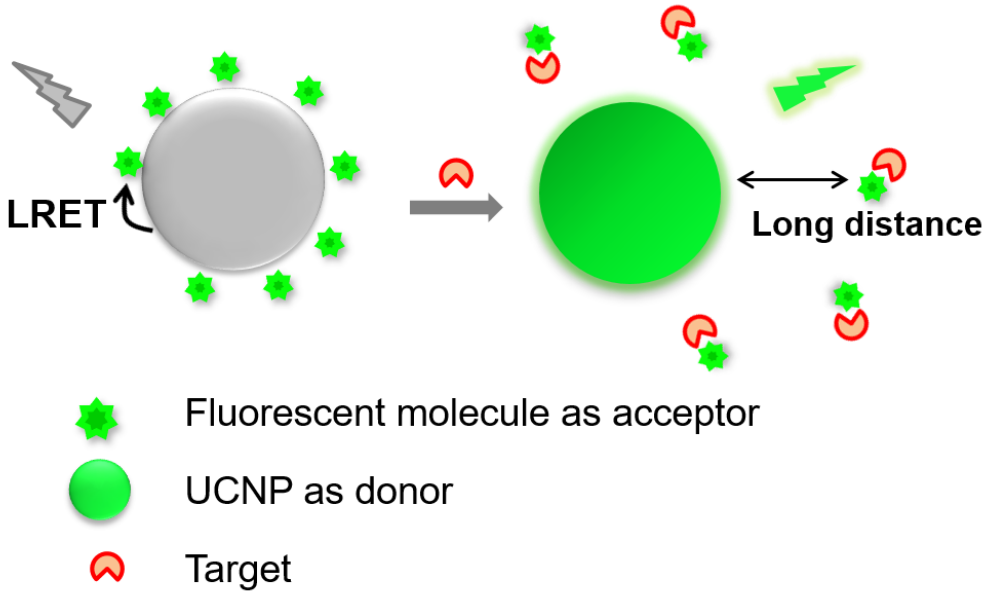

Figure 1.15 The illustration of upconversion LRET assay based on target-triggered detachment of acceptors from UCNPs.

Table 1.3 Upconversion LRET based on target-triggered detachment of acceptors from UCNPs.

Upconversion LRET based on target-triggered detachment of acceptors from UCNPs			
Acceptor	**UCNP doping**	**Target**	**Sensitivity**
TAMRA	Er^{3+}	Trypsin [160]	0.05 nM
TAMRA	Er^{3+}	Lysozyme [173]	2.5 nM
Fluo-4	Er^{3+}, Tm^{3+}	Ca^{2+} [194]	15 pM
CoOOH	Er^{3+}	Ascorbic acid [195]	3.32 μmol/L

1.3.6.5 The application of enzymatic-assisted signal amplification in the upconversion LRET with DNA double helix-sensitive fluorophores. It is a robust ideal to combine enzymatic-assisted signal amplified technique with upconversion LRET for DNA assay. Through the upconversion to eliminate auto-fluorescence background, the amplified optical signal is able to achieve a higher signal-to-noise ratio. The fluorescent acceptors chosen here are capable of intercalating with the double-stranded DNA, like SYTOX Orange and SYBR Green I[38,196,197]. In fact, it is the target DNA template being amplified in the form of double-stranded structure, which attracts labelling dyes to intercalate within the double-stranded DNA. The more double-stranded structures produced on the surface of UCNPs, the more fluorescent dyes get closer to the surface of UCNPs to obtain a higher chance of LRET. DNA polymerase assisted PCR and DNA ligase assisted ligation are two popular amplification techniques applied in upconversion LRET. For instance, as for the application of PCR-upconversion LRET in detecting the *IS6110* sequence of *Mycobacterium tuberculosis* complex (MTBC) in sputum[196] (Figure 1.16), the PCR amplicon with biotinylated primers are mixed with streptavidin-conjugated UCNPs, followed by intercalation with SYTOX Orange dyes. The intercalated dyes are close enough to the UCNPs for LRET occurring, and the reduction part of upconversion luminescence is applied as optical signal for target DNA monitoring. The kappa agreement of the UCNP-LRET assay with conventional PCR was 0.8464 and false-negative results were reduced, demonstrating the successful implementation of the UCNP-LRET system in detecting the *IS6110* sequence of the MTBC.

Another ligase-assisted upconversion LRET DNA assay also displays high sensitivity and specificity for DNA detection[38]. Using target DNA as a bridge to join the two probe

sequences into a single DNA strand by ligase, the newly-produced DNA sequence can form a hairpin loop-stem structure spontaneously. Thus, the number of hairpins can be increased during the thermal cycling between ligation at a lower temperature and dehybridisation at a higher temperature. One of the two probes is pre-immobilized onto the surface of UCNPs. Thus, after the longer-hairpin-formation, the intercalating dye, SYBR Green I can be trapped in the double-stranded stem portion and get approximate close to UCNPs to trigger LRET happening. Similarly, the reduction part of upconversion luminescence is applied as an optical signal for target DNA monitoring. SYBR Green I is a commonly used DNA staining dye showing higher bind affinity towards double-stranded DNAs than single-stranded DNA. Furthermore, because of the overlap of its absorption band with upconversion emission, it is also a good acceptor in upconversion LRET DNA assays[198]. However, the LOD obtained in this assay is not as low as expected, just at nanogram level.

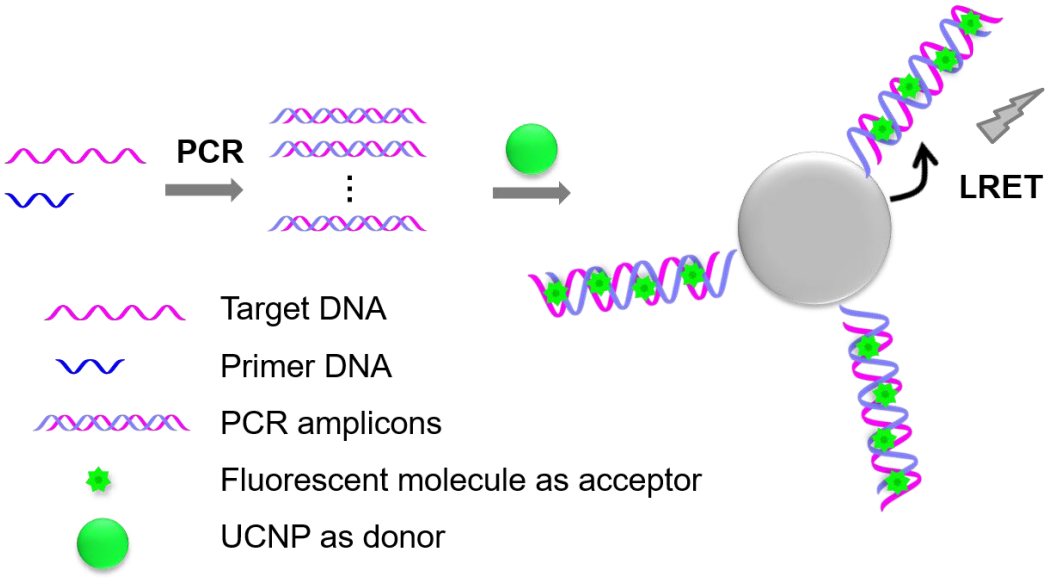

Figure 1.16 The illustration of upconversion LRET assay in joint with PCR technique for DNA detection, with DNA double helix-sensitive fluorophores as acceptors.

1.3.6.6 Upconversion LRET with graphene oxide as acceptors. The absorption band of graphene oxide (GO) is broad enough to overlap with upconversion luminescence. In addition, GO is composed of a lot of unsaturated sp^2 carbons, which can form π–π stacking interaction with the aromatic nucleobases of the single-stranded DNA, and thus UCNP-GO fabrication can be applied for DNA assay. Usually, the capture DNA (single-stranded) designed to be complementary with the target DNA, is pre-immobilized onto UCNPs. In the presence of the target DNA, the double-stranded p-electrons are involved in forming the duplex *via* base-stacking interactions between capture DNA with target DNA, and there is no chance for GO to interact with capture DNA. In this case, GO is randomly distributed in the solution far from UCNPs, meaning, no LRET[119] (Figure 1.17). The efficiency of upconversion LRET is considered as optical signal for target concentration measurement. On the other hand, once the capture DNA functionalizes as certain protein aptamer, the similar idea can also be directly applied for protein molecules detection[118,159,169,199]. Upon introduction of target protein, the random-coiled aptamer transforms into a special three-dimensional structure and prefers to bind with the target, resulting in no LRET. Table 1.4 lists the application of GO as acceptor in upconversion LRET assays.

Besides GO, carbon nanocrystals[200,201] and molybdenum disulphide nanosheets[202] also show the π–π stacking interaction with the aromatic nucleobases of the single-strand DNA. In a similar proof-of-concept to upconversion LRET based on GO, upconversion LRET based on carbon nanocrystals or molybdenum disulphide nanosheets have also been developed for bio-assay applications[200,201,202].

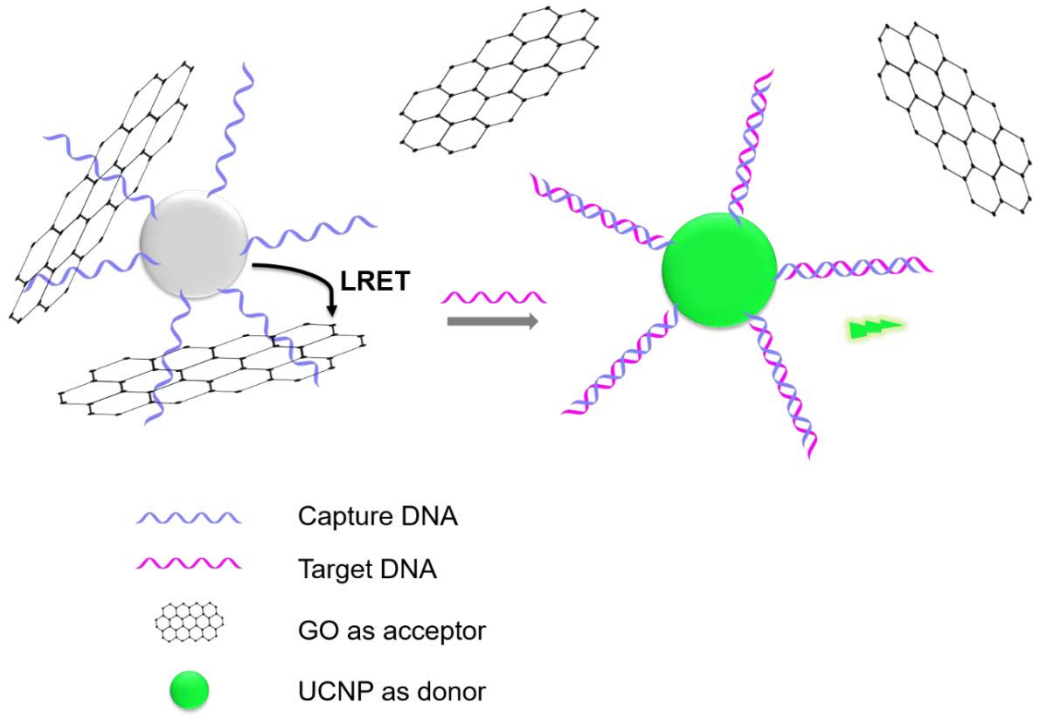

Figure 1.17 The illustration of upconversion LRET assay with GO as acceptor for DNA detection.

Table 1.4 Upconversion LRET based on graphene oxide as acceptors.

Upconversion LRET based on graphene oxide as acceptors		
Target	**UCNP doping**	**Sensitivity**
HIV antibody [118]	Er^{3+}	2 nM
DNA [119]	Er^{3+}	5 pM
Kanamycin [159]	Er^{3+}	18 pM
Ochratoxin A [169]	Er^{3+}	0.001 ng/ml
Exonuclease I [199]	Er^{3+}	0.02 U/ml

1.3.6.7 Upconversion LRET based on MnO_2-nanosheets as acceptors. The first fabrication of UCNPs with MnO_2 nanosheets in LRET system is applied for glutathione (GSH) monitoring in cancer cells in 2011[133]. MnO_2 nanosheets wrapped outside of nanoparticles can quench the upconversion luminescence in the absence of GSH. GSH can reduce MnO_2 to Mn^{2+}, resulting in degradation of MnO_2 nanosheets. Thus, in the presence of GSH, the quenched luminescence can be turned on, which is able to monitor the concentration of GSH intracellularly. Illuminated by that idea, the strategy for H_2O_2 detection based on upconversion LRET with MnO_2 nanosheets has been designed[132]. Similar to GSH, H_2O_2 can reduce MnO_2 to Mn^{2+}, leading to decomposition of the MnO2 nanosheets. Moreover, because glucose can be oxidized to produce H_2O_2 in the presence of glucose oxidase, this LRET assay can also be used for monitoring the blood glucose through the detection of enzymatically generated H_2O_2. Due to the negligible background interference and non-autofluorescence resulting from NIR excitation, the proposed method enables the direct monitoring of glucose levels in whole blood with a relatively low detection limit. The general approach process is illustrated in Figure 1.18.

Furthermore, it is possible to extend the application of upconversion-MnO_2 nanosheet into nanomedicine. The microenvironment in solid tumours is always acidic and H_2O_2-rich[203,204]. During the reduction from MnO_2 nanosheets into Mn^{2+} by acidic H_2O_2, a great deal of oxygen is generated enabling oxygen-dependent photodynamic therapy within tumour cells. Thus, a concurrent pH-/H_2O_2-responsive upconversion tracking and oxygen-elevated synergetic radio/photodynamic therapy *in vivo* based on MnO_2-UCNPs nanosystem has been developed[116,205].

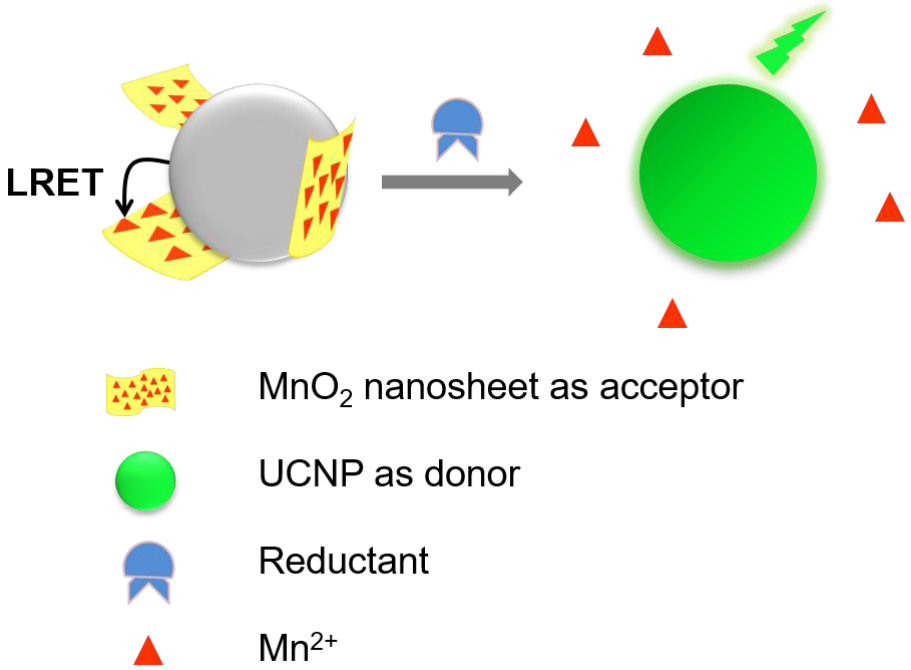

Figure 1.18 The illustration of upconversion LRET assay with MnO2-nanosheets as acceptors.

1.3.6.8 Upconversion LRET with gold nanoparticles as acceptors. As the absorption band of AuNPs or gold nanorods (AuNRs) can overlap with upconversion luminescence, optical nanosensors based on UCNP-AuNP LRET for biomolecules have been broadly developed. The design of upconversion LRET with gold nanocrystals as acceptors can also be classified into two ways: 'switch-on'[206] and 'switch-off'[117,207], with the former attracting more attention in recent years. Trypsin detection based on switch-on is a good example[207] (Figure 1.19). Trypsin can cleave certain peptide sequence. This special peptide can be used to link UCNPs with AuNPs for LRET. In the presence of trypsin, the peptide linker is cleaved to set free the two kinds of nanoparticles. The restored upconversion luminescence is therefore proportional to the concentration of trypsin in the solution. Compared with the upconversion LRET with fluorescent molecules as acceptors, the working distance of UCNP-AuNP pair is much longer than that of UCNP-fluorophore

pair, so upconversion LRET coupled with AuNPs as acceptors has broader applicability in biomolecular assays, especially in protein based immunoassays.

The upconversion LRET assay with AuNPs as acceptors, usually is applied in joint with other mature and advanced analytical techniques, to achieve broader applications in various fields.

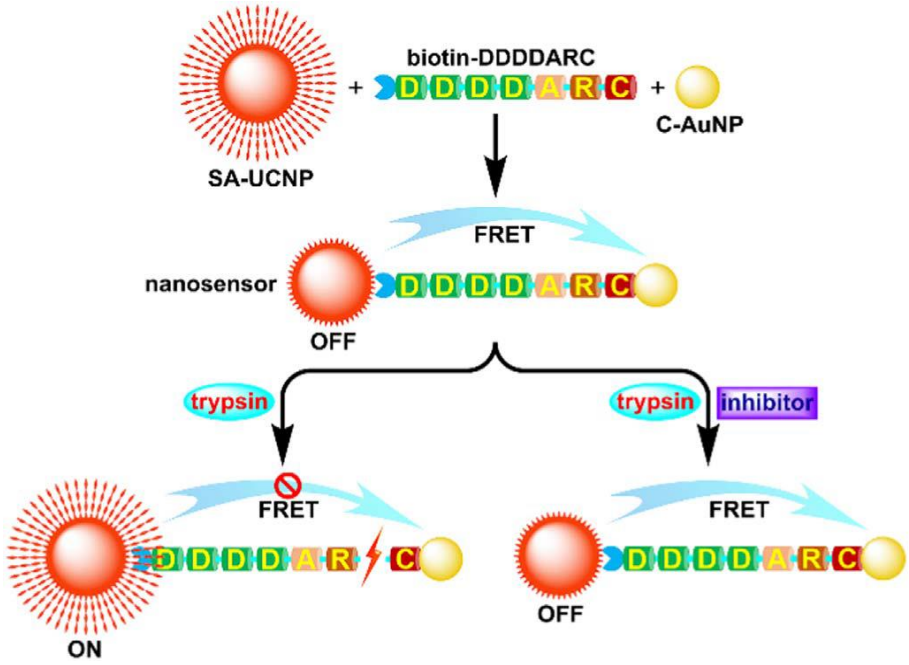

Figure 1.19 The illustration of 'switch-on' upconversion LRET assay with AuNPs as acceptors for trypsin detection. Figure is reprinted from Ref.[207].

a) Application of competitive immunoassay. In one case, UCNP-AuNP LRET has been applied to a competitive immunoassay[149,208]. Through the immune-affinity, the antibody-conjugated UCNPs get very close to the antigen-conjugated AuNPs and the luminescence of UCNPs are quenched. Once the free antigens to be measured from patients, antigen-coupled AuNPs and antibody-coupled UCNPs coexist in the solution, the competition between free antigens and antigen-AuNPs binding to antibody-UCNPs will result in some

of the antigen-AuNPs being unable to bind with antibody-UCNPs. In that case, part of the luminescence of UCNPs can be restored and the recovery of the quenched luminescence is used for quantification of target antigens (Figure 1.20). However, the disadvantage of this approach is that the binding affinity of free antigens is same as that of antigen-AuNPs, and there is no chance for all free antigens can bind with antibody-UCNPs. To some extent, the precise quantification cannot be ensured.

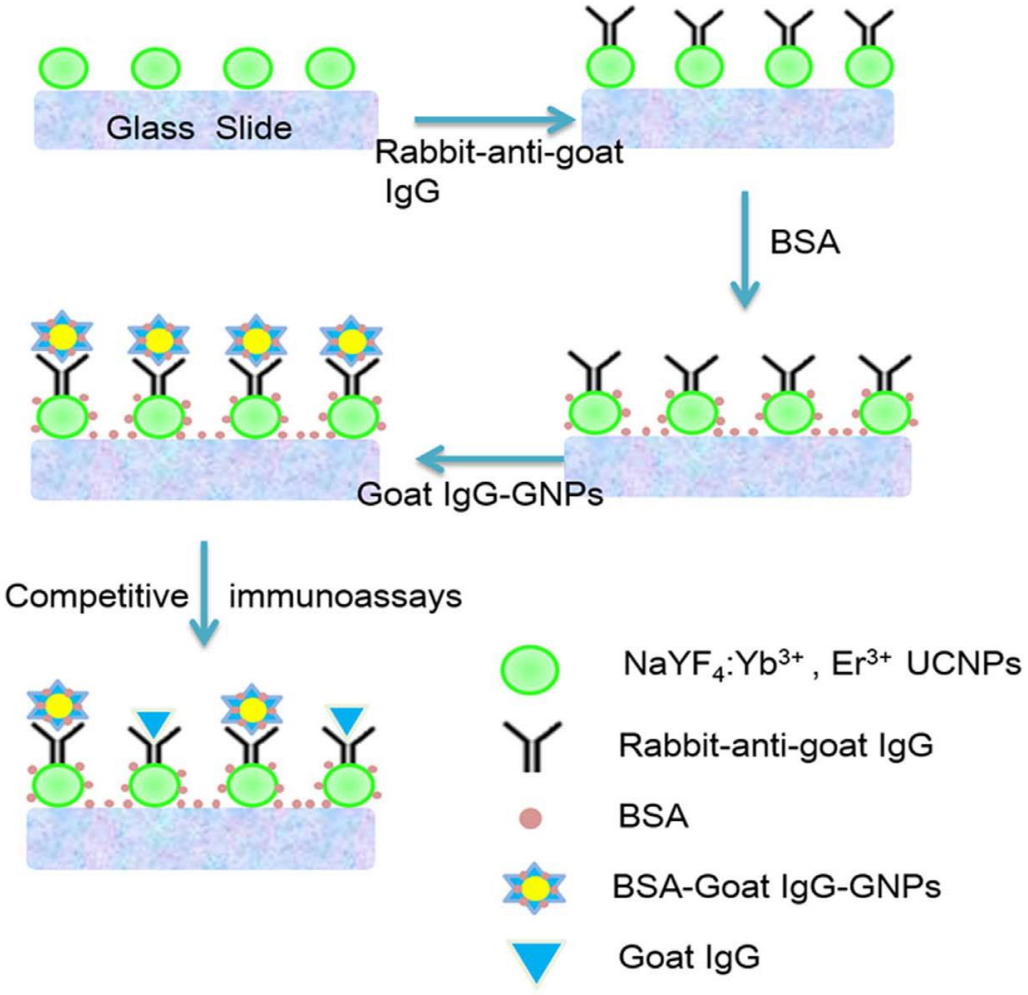

Figure 1.20 One-step in situ solid-substrate-based whole blood immunoassay based on LRET between UCNPs and AuNPs. Figure is reprinted from Ref.[208].

b) Application of DNA aptamer. Another kind of UCNP-AuNP fabrication assay shares the similar idea of competitive immunoassay. Due to the application of DNA aptamer,

the UCNP-AuNP fabrication is attributed to electric-interaction or DNA hybridization[209,210]. In Cheng's work for *Salmonella typhimurium* detection[209], the negatively charged DNA aptamer functionalized-UCNPs are fabricated with attachment of positively charged surfactant-free AuNRs, resulting in luminescence quenching. The addition of target will release the AuNPs from UCNPs to restore the luminescence, as the target can bind with the DNA aptamer-UCNPs. In Dai's work[210], OTA aptamer-DNA-UCNPs firstly hybridize with complementary-DNA-AuNRs for luminescence quenching. The addition of OTA triggers the re-configuration of aptamer and the coordination of OTA with aptamer. Complementary DNA is no longer able to hybridize with re-configurated aptamer DNA, resulting in restoration of upconversion luminescence with the long distance between donor-acceptor. Whereas, the configuration of aptamer is an equilibrium state, and the very precise quantification cannot be ensured. Besides the two examples described above, targeted induced 'switch-on' fabricated UCNP-AuNP pyramids have also been used for quantification of miRNA in living cells[211]. It achieved a luminescence intensity ranging from 0.16 to 43.65 fmol/10μg$_{RNA}$ with a LOD of 0.12 fmol/10μg$_{RNA}$, opening up a new avenue for the ultrasensitive detection and quantification of miRNA in living cells.

c) Application of electrostatics. As for the electrostatic interaction of UCNP-AuNP, Yao's group apply this in a very special way[212-214] (Figure 1.21). CTAB-capped UCNPs display positively charged and citrate-capped AuNPs that are negatively charged. The chemical substrates pre-existing in the reaction can be catalysed rapidly to forming N-Au or S-Au bond with AuNPs. The replacement of the citrate from the AuNPs makes the AuNPs non-charged and thus prone to aggregation. Thus, the AuNPs escape from UCNPs

due to non-charged surface and their absorption red-shifts, because of their aggregation. The pre-quenched UCNPs is restored.

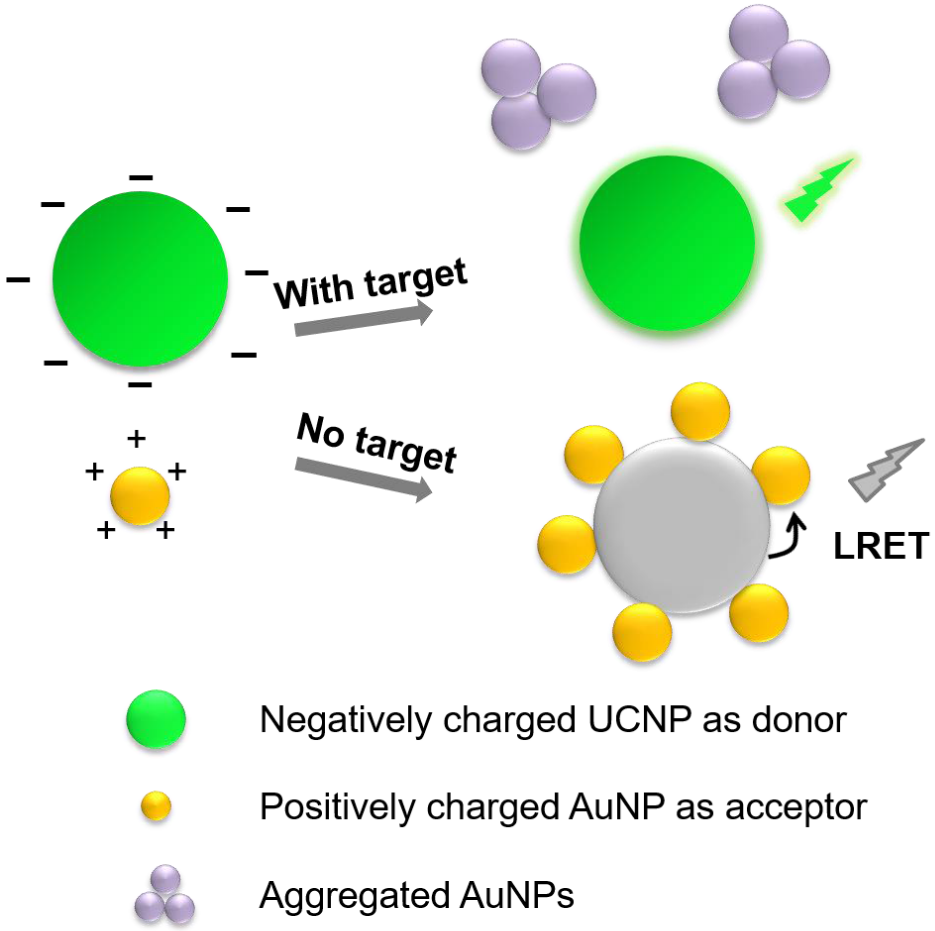

Figure 1.21 The illustration of upconversion LRET assay with AuNPs as acceptors based on electrostatic interaction.

1.3.6.9 Modulation of upconversion luminescence by heavy metal ions. Heavy metal ions are known as efficient quenchers of phosphors, with the quenching of upconversion luminescence by free heavy metal ions in solution, firstly reported by Wolfbeis and co-workers in 2011[215]. The follow-up application into proof-of-concept UC probe for monitoring biothiols[216] (Figure 1.22), was constructed with Cu^{2+} as the quencher. The quencher can anchor onto the surface of UCNPs through coordination with a molecular ligand. In the presence of biothiols, competition exists between the molecular ligands and

the biothiols to coordinate with Cu^{2+}. Part of the quenched upconversion luminescence is recovered upon removal of Cu^{2+} by the biothiols from the UCNPs, enabling monitoring of biothiol level in living cells and deep tissues. What's more, application of Fe^{3+} into upconversion quenching systems has also been conducted to monitor GSH/Cys/AA simultaneously[217].

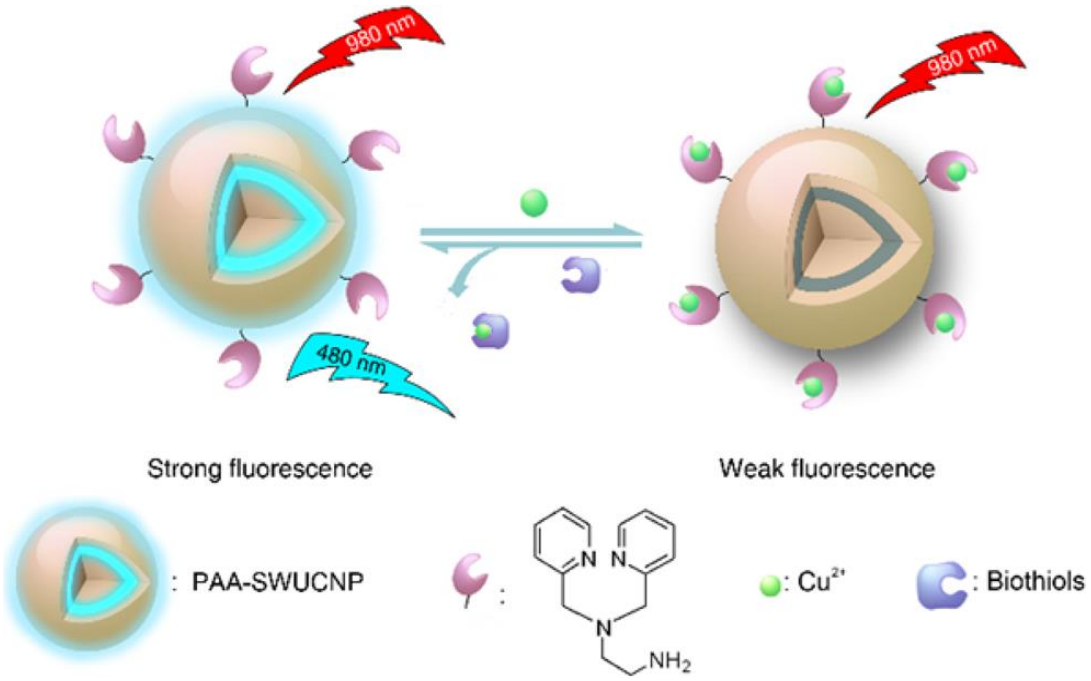

Figure 1.22 Biothiols monitoring through the modulation of upconversion luminescence by heavy metal ions. The figure is reprinted from Ref.[181].

1.3.6.10 Application of molecular imprinting techniques in upconversion LRET. Molecular imprinting is a technique creating complementary cavities for the specific targeting by polymerizing functional monomers in the presence of template molecules. After removal of templates, molecular imprinted polymers (MIPs) can exhibit affinity and selectivity for the template molecules. Compared with antibodies, MIPs possess excellent mechanical and chemical stability, ease of preparation, low cost and are reusable. Building a hybrid synergistic identification system by integrating two or more of the recognition elements is a potential promising idea to elevate the detection sensitivity. The

concept of upconversion MIPs is by polymerizing the functional monomers around the surface of the UCNPs in the presence of template molecules. Following removal of the templates, the complementary cavities are created for target recognition and affinity. Usually, these interactions occurring *via* hydrogen bonding between the targets with the MIPs. Once the cavities are blocked, the integrated polymers surrounding the UCNPs quench the upconversion luminescence. MIPs-UCNP fabrication for specific recognition of biomolecules has been broadly demonstrated[145,153,170,218-221]. Figure 1.23 is an example of clenbuterol detection reported by Li's group[219]. A three-dimensional network complemented with clenbuterol is formed as a polymer, followed by removal of clenbuterol templates by hydrolysis and the binding sites in the cavities are left. The fluorescence quenching of the MIPs-UCNPs occurs when the clenbuterol is bound to the fluorescent probe. In addition, in this paper, researchers also try to investigate the mechanism of the upconversion luminescence quenched by the MIPs. LRET is not suggested as a possible mechanism of quenching because of lack of observation of an overlap between the absorption band of target and the emission. Alternatively, the mechanism for the luminescence quenching of the MIPs-UCNPs was probably the photo-induced electron transfer due to the formation of hydrogen bonds and the lone pair of electrons in the oxygen-containing groups which are available for photo-induced electron transfer, leading to a decrease in the emission. Table 1.5 lists the Application of molecular imprinting techniques in upconversion LRET.

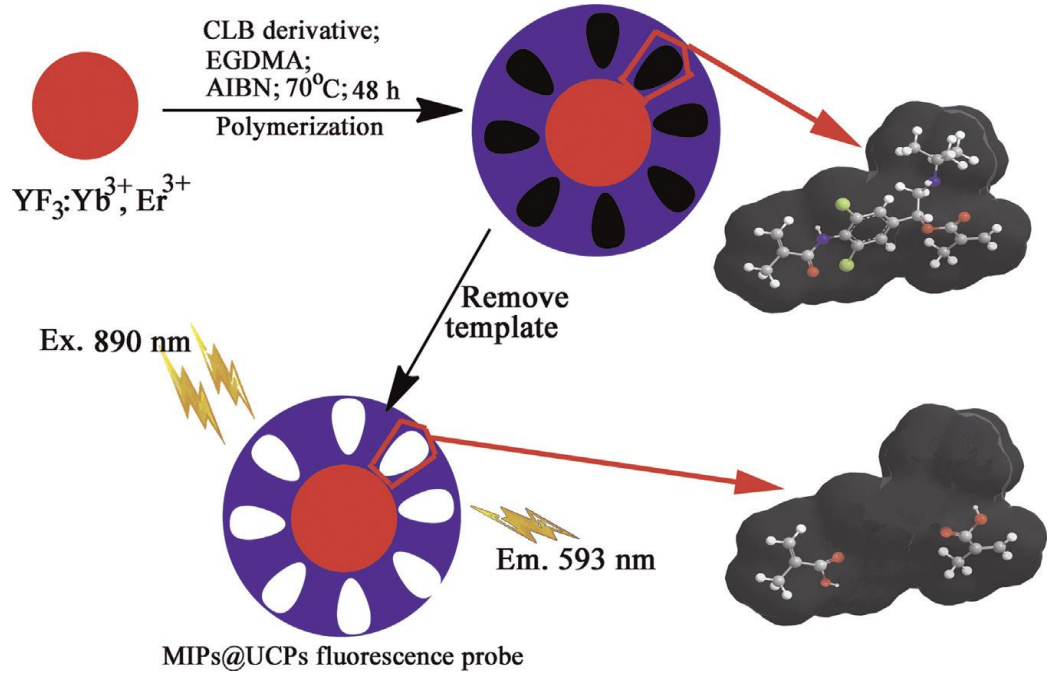

Figure 1.23 The illustration of upconversion LRET assay in joint with MIPs. The figure is reprinted from Ref.[219].

Table 1.5 Upconversion LRET based on the MIPs.

Upconversion LRET based on the MIPs		
Target	**UCNP doping**	**Sensitivity**
Enrofloxacin [145]	Tm^{3+}	0.04 ng/ml
Sulfamethazine [153]	Er^{3+}	34 ng/ml
Cytochrome c [170]	Er^{3+}	0.73 μM
Ractopamine [218]	Er^{3+}	8.6×10^{-10} mol/L
Clenbuterol [219]	Er^{3+}	0.12 μg/L
Diethylstilbestrol [220]	Er^{3+}	12.8 ng/ml
Enrofloxacin [221]	Er^{3+}	8 ng/L

1.4 Detection Limit and Quantitation Limit

The criteria for evaluating an analytical method include recovery and stability of analyte, sensitivity and specificity, procedural ease, reproducibility, time and cost. Limit of detection (LOD) and limit of quantification (LOQ) are two main parameters in method validation. LOD and LOQ are related but have distinct definitions. The LOD is defined as the lowest concentration of analyte in a sample that can be detected but not necessarily correctly quantified; the LOQ is defined as the lowest concentration of an analyte in a sample that can be determined with acceptable precision and accuracy. Some common methods for estimating the detection and quantitation limit include: visual definition, signal-to-noise ratio (S/N), standard deviation of the blank, linear regression, limit of blank and precision-based approaches[222]. Among these, two methods commonly used are described briefly below:

1.4.1 Signal-to-noise

Signal (S), stands for the corresponding value of the analyte; noise (N) stands for the peak-to-peak value of the baseline around the analyte retention time. Sometimes, certain concentration of the analyte would yield a signal equal to that value of noise, in that case it is hard to tell if the signal is induced only by the analyte or not. In order to obtain the accurate and precise detection and quantification, an S/N ratio of 3 is accepted for estimating LOD and S/N of 10 is accepted for estimating LOQ. This method is specified in the European Pharmacopoeia[223] and popularly applied to analytical chemistry that exhibit baseline noise.

1.4.2 Blank Determination

The blank determination is applied when the blank analysis can also obtain low amount

of signal with a non-zero standard deviation[224]. LOD is expressed as the analyte concentration corresponding to the sample blank value plus three standard deviations (SD), and LOQ is the analyte concentration corresponding to the sample blank value plus ten SDs as shown in the following equations: LOD = (Xb) + 3*Sb; LOQ = (Xb) + 10*Sb. Xb is the mean concentration of the blank and Sb is the standard deviation of the blank. Before the measurement, a calibration curve should be established with equation Y = f (X), where Y is the signal and X is the corresponding concentration of analyte. When the false positive signal values Yb given by blanks, the corresponding concentration of the blanks are measured as Xb according to the calibration curve. Then the (Xb) and Sb can be measured. And in Chapter 3, the LOD was calculated *via* this method.

1.5 Aims of This Project

First, owing to the advanced polymerization techniques, the newly designed and laboratory-synthesized di-block copolymer composed of poly(ethylene glycol) methyl ether acrylate and poly(monoacryloxyethyl phosphate) coated UCNPs can solve the bottleneck of nanoparticles' surface modification, resulting in highly water-stable UCNPs, co-functionalized with carboxylation and mPEG. Second, on top of the water stable carboxyl-UCNPs and conventional upconversion LRET approaches, applying the enzyme-assisted target-triggered signal amplification technique to detect and quantify low abundance disease-related DNA biomarkers, in order to enhance the detection sensitivity for disease diagnosis at early stage. Third, apply the new concept of core-shell UCNPs, traditional sandwich immunoassay and advanced BsAb techniques, on top of the mPEG-UCNPs and conventional upconversion LRET approaches, to realize the detection and quantification of protein antigen biomarkers for prostate cancer diagnosis. This upconversion LRET immunoassay is designed to achieve even lower detection limits than

the conventional beads assay, and greatly shorten detection time and simplify the detection process. Together, these activities are all aimed at ultimately developing user-friendly point-of-care devices.

1.6 References

[1] Griffith, J. D., Hulka, B. S. & Wilcosky, T. C. Biological Markers in Epidemiology. (*Oxford University Press*, **1990**).

[2] Biomarkers Definition Working Group. Biomarkers and Surrogate Endpoints: Preferred Definitions and Conceptural framwork. *Clin Pharmacol Theraperutics* 69:89-95 (**2001**).

[3] Strimbu, K. & Tavel, J. A. What Are Biomarkers? *Current Opinion in HIV and AIDS* 5, 463 **(2010)**.

[4] Perera, F. P. & Weinstein, I. B. Molecular Epidemiology: Recent Advances and Future Directions. *Carcinogenesis* 21, 517-524 **(2000)**.

[5] Felker, G. M., Hasselblad, V., Hernandez, A. F. & O'connor, C. M. Biomarker-Guided Therapy in Chronic Heart Failure: A Meta-Analysis of Randomized Controlled Trials. *American Heart Journal* 158, 422-430 **(2009)**.

[6] Mayeux, R. Biomarkers: Potential Uses and Limitations. *NeuroRx* 1, 182-188 **(2004)**.

[7] Sen, S., McDonald, S. P., Coates, P. T. H. & Bonder, C. S. Endothelial Progenitor Cells: Novel Biomarker and Promising Cell Therapy for Cardiovascular Disease. *Clinical Science* 120, 263-283 **(2011)**.

[8] Bihrer, V., Friedrich-Rust, M., Kronenberger, B., Forestier, N., Haupenthal, J., Shi, Y., Peveling-Oberhag, J., Radeke, H. H., Sarrazin, C. & Herrmann, E. Serum MIR-122 as a Biomarker of Necroinflammation in Patients with Chronic Hepatitis C Virus Infection. *The American Journal of Gastroenterology* 106, 1663 **(2011)**.

[9] Kalichman, S. C. & Simbayi, L. C. HIV Testing Attitudes, Aids Stigma, and Voluntary HIV Counselling and Testing in a Black Township in Cape Town, South Africa. *Sexually Transmitted Infections* 79, 442-447 **(2003)**.

[10] Kosaka, N., Iguchi, H. & Ochiya, T. Circulating Microrna in Body Fluid: A New Potential Biomarker for Cancer Diagnosis and Prognosis. *Cancer Science* 101, 2087-2092 **(2010)**.

[11] Food and Drug Administration. Innovation and Stagnation: Challenges and

Opportunity on the Critical Path to New Medical Products *(White Paper).* **2004**. updated **2010**.

[12] Jia, S., Zhang, R., Li, Z. & Li, J. Clinical and Biological Significance of Circulating Tumor Cells, Circulating Tumor DNA, and Exosomes as Biomarkers in Colorectal Cancer. *Oncotarget* 8, 55632 **(2017)**.

[13] Benowitz, N. L. Cotinine as a Biomarker of Environmental Tobacco Smoke Exposure. *Epidemiologic Reviews* 18, 188-204 **(1996)**.

[14] Sumpter, J. P. & Jobling, S. Vitellogenesis as a Biomarker for Estrogenic Contamination of the Aquatic Environment. *Environmental Health Perspectives* 103, 173 **(1995)**.

[15] Sanchez-Hernandez, J. C. Earthworm Biomarkers in Ecological Risk Assessment. *Reviews of Environmental Contamination and Toxicology* 85-126 (**2006**).

[16] Goodsaid, F. & Frueh, F. Biomarker Qualification Pilot Process at the US Food and Drug Administration. *The AAPS Journal* 9, E105-E108 **(2007)**.

[17] Doecke, J. D., Laws, S. M., Faux, N. G., Wilson, W., Burnham, S. C., Lam, C. P., Mondal, A., Bedo, J., Bush, A. I. & Brown, B. Blood-Based Protein Biomarkers for Diagnosis of Alzheimer Disease. *Archives of Neurology* 69, 1318-1325 **(2012)**.

[18] Laxman, B., Morris, D. S., Yu, J., Siddiqui, J., Cao, J., Mehra, R., Lonigro, R. J., Tsodikov, A., Wei, J. T. & Tomlins, S. A. A First-Generation Multiplex Biomarker Analysis of Urine for the Early Detection of Prostate Cancer. *Cancer Research* 68, 645-649 **(2008)**.

[19] Shaw, L. M., Vanderstichele, H., Knapik-Czajka, M., Clark, C. M., Aisen, P. S., Petersen, R. C., Blennow, K., Soares, H., Simon, A. & Lewczuk, P. Cerebrospinal Fluid Biomarker Signature in Alzheimer's Disease Neuroimaging Initiative Subjects. *Annals of Neurology* 65, 403-413 **(2009)**.

[20] Davis, J., Maes, M., Andreazza, A., McGrath, J., Tye, S. J. & Berk, M. Towards a Classification of Biomarkers of Neuropsychiatric Disease: From Encompass to Compass. *Molecular Psychiatry* 20, 152 **(2015)**.

[21] Seeree, P., Pearngam, P., Kumkate, S. & Janvilisri, T. An Omics Perspective on Molecular Biomarkers for Diagnosis, Prognosis, and Therapeutics of Cholangiocarcinoma. *International Journal of Genomics* **(2015)**.

[22] Wu, L. & Qu, X. Cancer Biomarker Detection: Recent Achievements and Challenges. *Chemical Society Reviews* 44, 2963-2997 **(2015)**.

[23] Ryo, M., Nakamura, T., Kihara, S., Kumada, M., Shibazaki, S., Takahashi, M., Nagai,

M., Matsuzawa, Y. & Funahashi, T. Adiponectin as a Biomarker of the Metabolic Syndrome. *Circulation Journal* 68, 975-981 **(2004)**.

[24] Nielsen, F., Mikkelsen, B. B., Nielsen, J. B., Andersen, H. R. & Grandjean, P. Plasma Malondialdehyde as Biomarker for Oxidative Stress: Reference Interval and Effects of Life-Style Factors. *Clinical Chemistry* 43, 1209-1214 **(1997)**.

[25] Mendiola, J., Moreno, J. M., Roca, M., Vergara-Juárez, N., Martínez-García, M. J., García-Sánchez, A., Elvira-Rendueles, B., Moreno-Grau, S., López-Espín, J. J. & Ten, J. Relationships between Heavy Metal Concentrations in Three Different Body Fluids and Male Reproductive Parameters: A Pilot Study. *Environmental Health* 10, 6 **(2011)**.

[26] Mandel, P. Les Acides Nucleiques Du Plasma Sanguin Chez L'homme. *CR Acad Sci Paris* 142, 241-243 **(1948)**.

[27] Sorenson, G. D., Pribish, D. M., Valone, F. H., Memoli, V. A., Bzik, D. J. & Yao, S.-L. Soluble Normal and Mutated DNA Sequences from Single-Copy Genes in Human Blood. *Cancer Epidemiology and Prevention Biomarkers* 3, 67-71 **(1994)**.

[28] Swarup, V. & Rajeswari, M. Circulating (Cell-Free) Nucleic Acids−a Promising, Non-Invasive Tool for Early Detection of Several Human Diseases. *FEBS letters* 581, 795-799 **(2007)**.

[29] Anker, P., Mulcahy, H., Chen, X. Q. & Stroun, M. Detection of Circulating Tumour DNA in the Blood (Plasma/Serum) of Cancer Patients. *Cancer and Metastasis Reviews* 18, 65-73 **(1999)**.

[30] Sozzi, G., Conte, D., Leon, M., Cirincione, R., Roz, L., Ratcliffe, C., Roz, E., Cirenei, N., Bellomi, M. & Pelosi, G. Quantification of Free Circulating DNA as a Diagnostic Marker in Lung Cancer. *Journal of Clinical Oncology* 21, 3902-3908 **(2003)**.

[31] Johnson, P. J. & Lo, Y. D. Plasma Nucleic Acids in the Diagnosis and Management of Malignant Disease. *Clinical Chemistry* 48, 1186-1193 **(2002)**.

[32] Taback, B., O'DAY, S. J. & HOON, D. S. Quantification of Circulating DNA in the Plasma and Serum of Cancer Patients. *Annals of the New York Academy of Sciences* 1022, 17-24 **(2004)**.

[33] Chen, Z., Fadiel, A., Naftolin, F., Eichenbaum, K. & Xia, Y. Circulation DNA: Biological Implications for Cancer Metastasis and Immunology. *Medical Hypotheses* 65, 956-961 **(2005)**.

[34] Ghossein, R. A., Bhattacharya, S. & Rosai, J. Molecular Detection of Micrometastases and Circulating Tumor Cells in Solid Tumors. *Clinical Cancer*

Research 5, 1950-1960 **(1999)**.

[35] Pelkey, T., Frierson, H. & Bruns, D. Molecular and Immunological Detection of Circulating Tumor Cells and Micrometastases from Solid Tumors. *Clinical Chemistry* 42, 1369-1381 **(1996)**.

[36] Mullis, K. B., Erlich, H. A., Arnheim, N., Horn, G. T., Saiki, R. K. & Scharf, S. J. Process for Amplifying, Detecting, and/or-Cloning Nucleic Acid Sequences. U.S. Patent 4,683,195 **(1987)**.

[37] Zuo, X., Xia, F., Xiao, Y. & Plaxco, K. W. Sensitive and Selective Amplified Fluorescence DNA Detection Based on Exonuclease III-Aided Target Recycling. *Journal of the American Chemical Society* 132, 1816-1818 **(2010)**.

[38] Wang, P., Ahmadov, T. O., Lee, C. & Zhang, P. Ligase-Assisted Signal-Amplifiable DNA Detection Using Upconversion Nanoparticles. *RSC Advances* 3, 16326-16329 **(2013)**.

[39] Ren, W., Liu, H., Yang, W., Fan, Y., Yang, L., Wang, Y., Liu, C. & Li, Z. A Cytometric Bead Assay for Sensitive DNA Detection Based on Enzyme-Free Signal Amplification of Hybridization Chain Reaction. *Biosensors and Bioelectronics* 49, 380-386 **(2013)**.

[40] Lu, J., Paulsen, I. T. & Jin, D. Application of Exonuclease III-Aided Target Recycling in Flow Cytometry: DNA Detection Sensitivity Enhanced by Orders of Magnitude. *Analytical Chemistry* 85, 8240-8245 **(2013)**.

[41] Weiss, B. Endonuclease II of Escherichia Coli is Exonuclease III. *Journal of Biological Chemistry* 251, 1896-1901 **(1976)**.

[42] Zhang, P., Rogelj, S., Nguyen, K. & Wheeler, D. Design of a Highly Sensitive and Specific Nucleotide Sensor Based on Photon Upconverting Particles. *Journal of the American Chemical Society* 128, 12410-12411 **(2006)**.

[43] Liu, J., Cheng, J. & Zhang, Y. Upconversion Nanoparticle Based LRET System for Sensitive Detection of Mrsa DNA Sequence. *Biosensors and Bioelectronics* 43, 252-256 **(2013)**.

[44] Zhu, H., Lu, F., Wu, X. C. & Zhu, J. J. An Upconversion Fluorescent Resonant Energy Transfer Biosensor for Hepatitis B Virus (HBV) DNA Hybridization Detection. *Analyst* 140, 7622-7628 **(2015)**.

[45] Wang, P., Ahmadov, T. O., Lee, C. & Zhang, P. Ligase-Assisted Signal-Amplifiable DNA Detection Using Upconversion Nanoparticles. *RSC Advances* 3, 16326-16329 **(2013)**.

[46] Blennow, K. Cerebrospinal Fluid Protein Biomarkers for Alzheimer's Disease. *NeuroRx* 1, 213-225 **(2004)**.

[47] Welsh, J. B., Sapinoso, L. M., Kern, S. G., Brown, D. A., Liu, T., Bauskin, A. R., Ward, R. L., Hawkins, N. J., Quinn, D. I. & Russell, P. J. Large-Scale Delineation of Secreted Protein Biomarkers Overexpressed in Cancer Tissue and Serum. *Proceedings of the National Academy of Sciences* 100, 3410-3415 **(2003)**.

[48] Addona, T. A., Shi, X., Keshishian, H., Mani, D., Burgess, M., Gillette, M. A., Clauser, K. R., Shen, D., Lewis, G. D. & Farrell, L. A. A Pipeline That Integrates the Discovery and Verification of Plasma Protein Biomarkers Reveals Candidate Markers for Cardiovascular Disease. *Nature Biotechnology* 29, 635 **(2011)**.

[49] Chikkaveeraiah, B. V., Bhirde, A. A., Morgan, N. Y., Eden, H. S. & Chen, X. Electrochemical Immunosensors for Detection of Cancer Protein Biomarkers. *ACS Nano* 6, 6546-6561 **(2012)**.

[50] Leca-Bouvier, B. & Blum, L. J. Biosensors for Protein Detection: A Review. *Analytical Letters* 38, 1491-1517 **(2005)**.

[51] Butler, J. E. Enzyme-Linked Immunosorbent Assay. *Journal of Immunoassay* 21, 165-209 **(2000)**.

[52] Strehlitz, B., Nikolaus, N. & Stoltenburg, R. Protein Detection with Aptamer Biosensors. *Sensors* 8, 4296-4307 **(2008)**.

[53] Ellington, A. D. & Szostak, J. W. In Vitro Selection of Rna Molecules That Bind Specific Ligands. *Nature* 346, 818 **(1990)**.

[54] Centi, S., Tombelli, S., Minunni, M. & Mascini, M. Aptamer-Based Detection of Plasma Proteins by an Electrochemical Assay Coupled to Magnetic Beads. *Analytical Chemistry* 79, 1466-1473 **(2007)**.

[55] Stadtherr, K., Wolf, H. & Lindner, P. An Aptamer-Based Protein Biochip. *Analytical Chemistry* 77, 3437-3443 **(2005)**.

[56] Fan, G., Wang, Z., Hao, M. & Li, J. Bispecific Antibodies and Their Applications. *Journal of Hematology & Oncology* 8, 130 **(2015)**.

[57] Howard, C. B., Fletcher, N., Houston, Z. H., Fuchs, A. V., Boase, N. R., Simpson, J. D., Raftery, L. J., Ruder, T., Jones, M. L. & de Bakker, C. J. Overcoming Instability of Antibody-Nanomaterial Conjugates: Next Generation Targeted Nanomedicines Using Bispecific Antibodies. *Advanced Healthcare Materials* 5, 2055-2068 **(2016)**.

[58] He, H., Howard, C. B., Chen, Y., Wen, S., Lin, G., Zhou, J., Thurecht, K. J. & Jin, D. Bispecific Antibody-Functionalized Upconversion Nanoprobe. *Analytical*

Chemistry 90, 3024-3029 **(2018)**.

[59] Kao, C. H., Wang, J. Y., Chuang, K. H., Chuang, C. H., Cheng, T. C., Hsieh, Y. C., Tseng, Y. l., Chen, B. M., Roffler, S. R. & Cheng, T. L. One-Step Mixing with Humanized Anti-mPEG Bispecific Antibody Enhances Tumor Accumulation and Therapeutic Efficacy of Mpegylated Nanoparticles. *Biomaterials* 35, 9930-9940 **(2014)**.

[60] Teles, F. & Fonseca, L. Trends in DNA Biosensors. *Talanta* 77, 606-623 **(2008)**.

[61] Shanmugam, N. R., Muthukumar, S. & Prasad, S. A Review on ZnO-Based Electrical Biosensors for Cardiac Biomarker Detection. *Future Science OA* 3(4), FSO196 **(2017)**.

[62] Chen, Y., Zhou, S., Li, L. & Zhu, J. J. Nanomaterials-Based Sensitive Electrochemiluminescence Biosensing. *Nano Today* 12, 98-115 **(2017)**.

[63] Kumar, A. Biosensors Based on Piezoelectric Crystal Detectors: Theory and Application. *JOM-e* 52, 1-6 **(2000)**.

[64] Ricciardi, A., Crescitelli, A., Vaiano, P., Quero, G., Consales, M., Pisco, M., Esposito, E. & Cusano, A. Lab-on-Fiber Technology: A New Vision for Chemical and Biological Sensing. *Analyst* 140, 8068-8079 **(2015)**.

[65] Nguyen, H. H., Park, J., Kang, S. & Kim, M. Surface Plasmon Resonance: A Versatile Technique for Biosensor Applications. *Sensors* 15, 10481-10510 **(2015)**.

[66] Khan, S. A., DeGrasse, J. A., Yakes, B. J. & Croley, T. R. Rapid and Sensitive Detection of Cholera Toxin Using Gold Nanoparticle-Based Simple Colorimetric and Dynamic Light Scattering Assay. *Analytica Chimica Acta* 892, 167-174 **(2015)**.

[67] Marquette, C. A. & Blum, L. J. Electro-Chemiluminescent Biosensing. *Analytical and Bioanalytical Chemistry* 390, 155-168 **(2008)**.

[68] Sakura, S. Electrochemiluminescence of Hydrogen Peroxide-Luminol at a Carbon Electrode. *Analytica Chimica Acta* 262, 49-57 **(1992)**.

[69] Roswell, D. F. & White, E. H. The Chemiluminescence of Luminol and Related Hydrazides. *Methods in Enzymology* 57, 409-423 **(1978)**.

[70] Lee, W. Y. Tris (2,2'-Bipyridyl) Ruthenium (II) Electrogenerated Chemiluminescence in Analytical Science. *Microchimica Acta* 127, 19-39 **(1997)**.

[71] Knight, A. W. & Greenway, G. M. Occurrence, Mechanisms and Analytical Applications of Electrogenerated Chemiluminescence. *Analyst* 119, 879-890 **(1994)**.

[72] Blackburn, G. F., Shah, H. P., Kenten, J. H., Leland, J., Kamin, R. A., Link, J., Peterman, J., Powell, M. J., Shah, A. & Talley, D. B. Electrochemiluminescence

Detection for Development of Immunoassays and DNA Probe Assays for Clinical Diagnostics. *Clinical Chemistry* 37, 1534-1539 **(1991)**.

[73] Sauerbrey, G. Use of Quartz Crystal Units for Weighing Thin Films and Microweighing. *Magzine for Physics* 155, 206-222 **(1959)**.

[74] Muratsugu, M., Ohta, F., Miya, Y., Hosokawa, T., Kurosawa, S., Kamo, N. & Ikeda, H. Quartz Crystal Microbalance for the Detection of Microgram Quantities of Human Serum Albumin: Relationship between the Frequency Change and the Mass of Protein Adsorbed. *Analytical chemistry* 65, 2933-2937 **(1993)**.

[75] Liss, M., Petersen, B., Wolf, H. & Prohaska, E. An Aptamer-Based Quartz Crystal Protein Biosensor. *Analytical Chemistry* 74, 4488-4495 **(2002)**.

[76] Damborský, P., Švitel, J. & Katrlík, J. Optical Biosensors. *Essays in Biochemistry* 60, 91-100 **(2016)**.

[77] Liu, X. & Tan, W. A Fiber-Optic Evanescent Wave DNA Biosensor Based on Novel Molecular Beacons. *Analytical Chemistry* 71, 5054-5059 **(1999)**.

[78] Piunno, P. A., Krull, U. J., Hudson, R. H., Damha, M. J. & Cohen, H. Fiber-Optic DNA Sensor for Fluorometric Nucleic Acid Determination. *Analytical Chemistry* 67, 2635-2643 **(1995)**.

[79] Ko, S. & Grant, S. A. A Novel FRET-Based Optical Fiber Biosensor for Rapid Detection of Salmonella Typhimurium. *Biosensors and Bioelectronics* 21, 1283-1290 **(2006)**.

[80] Nylander, C., Liedberg, B. & Lind, T. Gas Detection by Means of Surface Plasmon Resonance. *Sensors and Actuators* 3, 79-88 **(1982)**.

[81] Homola, J., Yee, S. S. & Gauglitz, G. Surface Plasmon Resonance Sensors. *Sensors and Actuators B: Chemical* 54, 3-15 **(1999)**.

[82] Homola, J. Surface Plasmon Resonance Sensors for Detection of Chemical and Biological Species. *Chemical Reviews* 108, 462-493 **(2008)**.

[83] Endo, T., Kerman, K., Nagatani, N., Takamura, Y. & Tamiya, E. Label-Free Detection of Peptide Nucleic Acid−DNA Hybridization Using Localized Surface Plasmon Resonance Based Optical Biosensor. *Analytical Chemistry* 77, 6976-6984 **(2005)**.

[84] Nelson, B. P., Grimsrud, T. E., Liles, M. R., Goodman, R. M. & Corn, R. M. Surface Plasmon Resonance Imaging Measurements of DNA and RNA Hybridization Adsorption onto DNA Microarrays. *Analytical Chemistry* 73, 1-7 **(2001)**.

[85] Lee, H. J., Nedelkov, D. & Corn, R. M. Surface Plasmon Resonance Imaging

Measurements of Antibody Arrays for the Multiplexed Detection of Low Molecular Weight Protein Biomarkers. *Analytical Chemistry* 78, 6504-6510 **(2006)**.

[86] Li, Y., Lee, H. J. & Corn, R. M. Detection of Protein Biomarkers Using RNA Aptamer Microarrays and Enzymatically Amplified Surface Plasmon Resonance Imaging. *Analytical Chemistry* 79, 1082-1088 **(2007)**.

[87] Liedberg, B., Nylander, C. and Lunström, I. Surface Plasmon Resonance for Gas Detection and Biosensing. *Sensors and Actuators 4*, pp.299-304 **(1983)**.

[88] Reddy, P.J., Sadhu, S., Ray, S. and Srivastava, S. Cancer Biomarker Detection by Surface Plasmon Resonance Biosensors. *Clinics in Laboratory Medicine*, *32*(1), pp.47-72 **(2012)**.

[89] Canovi, M., Lucchetti, J., Stravalaci, M., Valentino, S., Bottazzi, B., Salmona, M., Bastone, A. and Gobbi, M. A New Surface Plasmon Resonance-based Immunoassay for Rapid, Reproducible and Sensitive Quantification of Pentraxin-3 in Human Plasma. *Sensors 14*(6), pp.10864-10875 **(2014)**.

[90] Parolo, C., de la Escosura-Muñiz, A. & Merkoçi, A. Enhanced Lateral Flow Immunoassay Using Gold Nanoparticles Loaded with Enzymes. *Biosensors and Bioelectronics* 40, 412-416 **(2013)**.

[91] Liu, X., Dai, Q., Austin, L., Coutts, J., Knowles, G., Zou, J., Chen, H. & Huo, Q. A One-Step Homogeneous Immunoassay for Cancer Biomarker Detection Using Gold Nanoparticle Probes Coupled with Dynamic Light Scattering. *Journal of the American Chemical Society* 130, 2780-2782 **(2008)**.

[92] Elghanian, R., Storhoff, J. J., Mucic, R. C., Letsinger, R. L. & Mirkin, C. A. Selective Colorimetric Detection of Polynucleotides Based on the Distance-Dependent Optical Properties of Gold Nanoparticles. *Science* 277, 1078-1081 **(1997)**.

[93] Taton, T. A., Mirkin, C. A. & Letsinger, R. L. Scanometric DNA Array Detection with Nanoparticle Probes. *Science* 289, 1757-1760 **(2000)**.

[94] Cao, Y. C., Jin, R. & Mirkin, C. A. Nanoparticles with Raman Spectroscopic Fingerprints for DNA and Rna Detection. *Science* 297, 1536-1540 **(2002)**.

[95] Dai, Q., Liu, X., Coutts, J., Austin, L. & Huo, Q. A One-Step Highly Sensitive Method for DNA Detection Using Dynamic Light Scattering. *Journal of the American Chemical Society* 130, 8138-8139 **(2008)**.

[96] Jha, A. R. Rare Earth Materials: Properties and Applications. (CRC Press, **2014**).

[97] Tu, L., Liu, X., Wu, F. & Zhang, H. Excitation Energy Migration Dynamics in

Upconversion Nanomaterials. *Chemical Society Reviews* 44, 1331-1345 **(2015)**.

[98] Tropper, A. C., Carter, J. N., Lauder, R., Hanna, D. C., Davey, S. T. & Szebesta, D. Analysis of Blue and Red Laser Performance of the Infrared-Pumped Praseodymium-Doped Fluoride Fiber Laser. *Journal of the Optical Society of America B* 11, 886-893 **(1994)**.

[99] Chatterjee, D. K., Rufaihah, A. J. & Zhang, Y. Upconversion Fluorescence Imaging of Cells and Small Animals Using Lanthanide Doped Nanocrystals. *Biomaterials* 29, 937-943 **(2008)**.

[100] Chen, G., Shen, J., Ohulchanskyy, T. Y., Patel, N. J., Kutikov, A., Li, Z., Song, J., Pandey, R. K., Ågren, H. & Prasad, P. N. (α-$NaYbF_4$:Tm^{3+})/CaF_2 Core/Shell Nanoparticles with Efficient Near-Infrared to Near-Infrared Upconversion for High-Contrast Deep Tissue Bioimaging. *ACS nano* 6, 8280-8287 **(2012)**.

[101] Sun, M., Xu, L., Ma, W., Wu, X., Kuang, H., Wang, L. & Xu, C. Hierarchical Plasmonic Nanorods and Upconversion Core−Satellite Nanoassemblies for Multimodal Imaging-Guided Combination Phototherapy. *Advanced Materials* 28, 898-904 **(2016)**.

[102] Chen, Q., Wang, C., Cheng, L., He, W., Cheng, Z. & Liu, Z. Protein Modified Upconversion Nanoparticles for Imaging-Guided Combined Photothermal and Photodynamic Therapy. *Biomaterials* 35, 2915-2923 **(2014)**.

[103] Liu, S., Li, Y., Zhang, C., Yang, L., Zhao, T., Zhang, R. & Jiang, C. Upconversion Color Tuning in Ce^{3+}-Doped $LiYF_4$: Yb^{3+}/Ho^{3+}@ $LiYF_4$ Nanoparticles Towards Ratiometric Fluorescence Detection of Chromium (III). *Journal of Colloid and Interface Science* 493, 10-16 **(2017)**.

[104] Wu, S., Duan, N., Ma, X., Xia, Y., Wang, H., Wang, Z. & Zhang, Q. Multiplexed Fluorescence Resonance Energy Transfer Aptasensor between Upconversion Nanoparticles and Graphene Oxide for the Simultaneous Determination of Mycotoxins. *Analytical Chemistry* 84, 6263-6270 **(2012)**.

[105] Cheng, L., Yang, K., Zhang, S., Shao, M., Lee, S. & Liu, Z. Highly-Sensitive Multiplexed in Vivo Imaging Using Pegylated Upconversion Nanoparticles. *Nano Research* 3, 722-732 **(2010)**.

[106] Gorris, H. H. & Wolfbeis, O. S. Photon-Upconverting Nanoparticles for Optical Encoding and Multiplexing of Cells, Biomolecules, and Microspheres. *Angewandte Chemie International Edition* 52, 3584-3600 **(2013)**.

[107] Zhang, M., Shi, S., Meng, J., Wang, X., Fan, H., Zhu, Y., Wang, X. & Qian, Y.

Preparation and Characterization of Near-Infrared Luminescent Bifunctional Core/Shell Nanocomposites. *The Journal of Physical Chemistry C* 112, 2825-2830 **(2008)**.

[108] He, M., Li, Z., Ge, Y. & Liu, Z. Portable Upconversion Nanoparticles-Based Paper Device for Field Testing of Drug Abuse. *Analytical Chemistry* 88, 1530-1534 **(2016)**.

[109] Lin, X., Wang, Y., Chen, X., Yang, R., Wang, Z., Feng, J., Wang, H., Lai, K. W., He, J. & Wang, F. Multiplexed Optogenetic Stimulation of Neurons with Spectrum-Selective Upconversion Nanoparticles. *Advanced Healthcare Materials* 6 **(2017)**.

[110] Liu, J., Huang, L., Tian, X., Chen, X., Shao, Y., Xie, F., Chen, D. & Li, L. Magnetic and Fluorescent Gd_2O_3: Yb^{3+}/Ln^{3+} Nanoparticles for Simultaneous Upconversion Luminescence/MR Dual Modal Imaging and NIR-Induced Photodynamic Therapy. *International Journal of Nanomedicine* 12, 1 **(2017)**.

[111] Haase, M. & Schäfer, H. Upconverting Nanoparticles. *Angewandte Chemie International Edition* 50, 5808-5829 **(2011)**.

[112] Li, X., Zhang, F. & Zhao, D. Lab on Upconversion Nanoparticles: Optical Properties and Applications Engineering Via Designed Nanostructure. *Chemical Society Reviews* 44, 1346-1378 **(2015)**.

[113] Menyuk, N., Dwight, K. & Pierce, J. $NaYF_4$:Yb, Er−an Efficient Upconversion Phosphor. *Applied Physics Letters* 21, 159-161 **(1972)**.

[114] Kano, T., Suzuki, T., Suzuki, A. & Minagawa, S. Fabrication of Efficient up-Conversion Type Green Led Using $NaYF_4$-Yb, Er Phosphor. *Journal of the Electrochemical Society* 120, C87 **(1973)**.

[115] Peng, J., Xu, W., Teoh, C. L., Han, S., Kim, B., Samanta, A., Er, J. C., Wang, L., Yuan, L. & Liu, X. High-Efficiency in Vitro and in Vivo Detection of Zn^{2+} by Dye-Assembled Upconversion Nanoparticles. *Journal of the American Chemical Society* 137, 2336-2342 **(2015)**.

[116] Xu, J., He, F., Cheng, Z., Lv, R., Dai, Y., Gulzar, A., Liu, B., Bi, H., Yang, D. & Gai, S. Yolk-Structured Upconversion Nanoparticles with Biodegradable Silica Shell for FRET Sensing of Drug Release and Imaging-Guided Chemotherapy. *Chemistry of Materials* 29, 7615-7628 **(2017)**.

[117] Wu, M., Wang, X., Wang, K. & Guo, Z. Sequence-Specific Detection of Cytosine Methylation in DNA via the FRET Mechanism between Upconversion Nanoparticles and Gold Nanorods. *Chemical Communications* 52, 8377-8380 **(2016)**.

[118] Wu, Y. M., Cen, Y., Huang, L. J., Yu, R. Q. & Chu, X. Upconversion Fluorescence Resonance Energy Transfer Biosensor for Sensitive Detection of Human Immunodeficiency Virus Antibodies in Human Serum. *Chemical Communications* 50, 4759-4762 **(2014)**.

[119] Alonso-Cristobal, P., Vilela, P., El-Sagheer, A., Lopez-Cabarcos, E., Brown, T., Muskens, O., Rubio-Retama, J. & Kanaras, A. Highly Sensitive DNA Sensor Based on Upconversion Nanoparticles and Graphene Oxide. *ACS Applied Materials & Interfaces* 7, 12422-12429 **(2015)**.

[120] Ma, C., Xu, X., Wang, F., Zhou, Z., Liu, D., Zhao, J., Guan, M., Lang, C. I. & Jin, D. Optimal Sensitizer Concentration in Single Upconversion Nanocrystals. *Nano Letters* 17, 2858-2864 **(2017)**.

[121] Cao, T., Yang, Y., Gao, Y., Zhou, J., Li, Z. & Li, F. High-Quality Water-Soluble and Surface-Functionalized Upconversion Nanocrystals as Luminescent Probes for Bioimaging. *Biomaterials* 32, 2959-2968 **(2011)**.

[122] Wang, Z. L., Hao, J., Chan, H. L., Law, G. L., Wong, W. T., Wong, K. L., Murphy, M. B., Su, T., Zhang, Z. & Zeng, S. Simultaneous Synthesis and Functionalization of Water-Soluble up-Conversion Nanoparticles for in Vitro Cell and Nude Mouse Imaging. *Nanoscale* 3, 2175-2181 **(2011)**.

[123] Zhou, H. P., Xu, C. H., Sun, W. & Yan, C. H. Clean and Flexible Modification Strategy for Carboxyl/Aldehyde-Functionalized Upconversion Nanoparticles and Their Optical Applications. *Advanced Functional Materials* 19, 3892-3900 **(2009)**.

[124] Hu, H., Yu, M., Li, F., Chen, Z., Gao, X., Xiong, L. & Huang, C. Facile Epoxidation Strategy for Producing Amphiphilic up-Converting Rare-Earth Nanophosphors as Biological Labels. *Chemistry of Materials* 20, 7003-7009 **(2008)**.

[125] Lü, Q., Guo, F., Sun, L., Li, A. & Zhao, L. Silica-/Titania-Coated Y_2O_3:Tm^{3+}, Yb^{3+} Nanoparticles with Improvement in Upconversion Luminescence Induced by Different Thickness Shells. *Journal of Applied Physics* 103, 123533 **(2008)**.

[126] Wang, M., Mi, C., Zhang, Y., Liu, J., Li, F., Mao, C. & Xu, S. NIR-Responsive Silica-Coated $NaYbF_4$:Er/Tm/Ho Upconversion Fluorescent Nanoparticles with Tunable Emission Colors and Their Applications in Immunolabeling and Fluorescent Imaging of Cancer Cells. *The Journal of Physical Chemistry C* 113, 19021-19027 **(2009)**.

[127] Duong, H., Chen, Y., Tawfik, S. A., Wen, S., Parviz, M., Ford, M. J., Shimoni, O. & Jin, D. Systematic Investigation of Functional Ligands for Colloidal Stable

Upconversion Nanoparticles. *RSC Advances* 8(9), 4842-4849 **(2018)**.

[128] Lu, J., Chen, Y., Liu, D., Ren, W., Lu, Y., Shi, Y., Piper, J., Paulsen, I. & Jin, D. One-Step Protein Conjugation to Upconversion Nanoparticles. *Analytical Chemistry* 87, 10406-10413 **(2015)**.

[129] Li, L. L., Zhang, R., Yin, L., Zheng, K., Qin, W., Selvin, P. R. & Lu, Y. Biomimetic Surface Engineering of Lanthanide-Doped Upconversion Nanoparticles as Versatile Bioprobes. *Angewandte Chemie International Edition* 51, 6121-6125 **(2012)**.

[130] Chen, Z., Chen, H., Hu, H., Yu, M., Li, F., Zhang, Q., Zhou, Z., Yi, T. & Huang, C. Versatile Synthesis Strategy for Carboxylic Acid−Functionalized Upconverting Nanophosphors as Biological Labels. *Journal of the American Chemical Society* 130, 3023-3029 **(2008)**.

[131] Liu, Y., Chen, M., Cao, T., Sun, Y., Li, C., Liu, Q., Yang, T., Yao, L., Feng, W. & Li, F. A Cyanine-Modified Nanosystem for in Vivo Upconversion Luminescence Bioimaging of Methylmercury. *Journal of the American Chemical Society* 135, 9869-9876 **(2013)**.

[132] Yuan, J., Cen, Y., Kong, X.-J., Wu, S., Liu, C. L., Yu, R. Q. & Chu, X. MnO_2-Nanosheet-Modified Upconversion Nanosystem for Sensitive Turn-on Fluorescence Detection of H_2O_2 and Glucose in Blood. *ACS Applied Materials & Interfaces* 7, 10548-10555 **(2015)**.

[133] Deng, R., Xie, X., Vendrell, M., Chang, Y. T. & Liu, X. Intracellular Glutathione Detection Using MnO_2-Nanosheet-Modified Upconversion Nanoparticles. *Journal of the American Chemical Society* 133, 20168-20171 **(2011)**.

[134] Cui, S., Chen, H., Zhu, H., Tian, J., Chi, X., Qian, Z., Achilefu, S. & Gu, Y. Amphiphilic Chitosan Modified Upconversion Nanoparticles for in Vivo Photodynamic Therapy Induced by near-Infrared Light. *Journal of Materials Chemistry* 22, 4861-4873 **(2012)**.

[135] Liang, S., Zhang, X., Wu, Z., Liu, Y., Zhang, H., Sun, H., Sun, H. & Yang, B. Decoration of up-Converting $NaYF_4$:Yb, Er (Tm) Nanoparticles with Surfactant Bilayer. A Versatile Strategy to Perform Oil-to-Water Phase Transfer and Subsequently Surface Silication. *CrystEngComm* 14, 3484-3489 **(2012)**.

[136] Ren, W., Tian, G., Jian, S., Gu, Z., Zhou, L., Yan, L., Jin, S., Yin, W. & Zhao, Y. Tween Coated $NaYF_4$:Yb, Er/ $NaYF_4$ Core/Shell Upconversion Nanoparticles for Bioimaging and Drug Delivery. *RSC Advances* 2, 7037-7041 **(2012)**.

[137] Park, Y. I., Kim, J. H., Lee, K. T., Jeon, K. S., Na, H. B., Yu, J. H., Kim, H. M.,

Lee, N., Choi, S. H. & Baik, S. I. Nonblinking and Nonbleaching Upconverting Nanoparticles as an Optical Imaging Nanoprobe and T1 Magnetic Resonance Imaging Contrast Agent. *Advanced Materials* 21, 4467-4471 **(2009)**.

[138] Nam, S. H., Bae, Y. M., Park, Y. I., Kim, J. H., Kim, H. M., Choi, J. S., Lee, K. T., Hyeon, T. & Suh, Y. D. Long-Term Real-Time Tracking of Lanthanide Ion Doped Upconverting Nanoparticles in Living Cells. *Angewandte Chemie* 123, 6217-6221 **(2011)**.

[139] Wang, C., Tao, H., Cheng, L. & Liu, Z. Near-Infrared Light Induced in Vivo Photodynamic Therapy of Cancer Based on Upconversion Nanoparticles. *Biomaterials* 32, 6145-6154 **(2011)**.

[140] Li, X., Wu, Y., Liu, Y., Zou, X., Yao, L., Li, F. & Feng, W. Cyclometallated Ruthenium Complex-Modified Upconversion Nanophosphors for Selective Detection of Hg^{2+} Ions in Water. *Nanoscale* 6, 1020-1028 **(2014)**.

[141] Fang, S., Wang, C., Xiang, J., Cheng, L., Song, X., Xu, L., Peng, R. & Liu, Z. Aptamer-Conjugated Upconversion Nanoprobes Assisted by Magnetic Separation for Effective Isolation and Sensitive Detection of Circulating Tumor Cells. *Nano Research* 7, 1327-1336 **(2014)**.

[142] Jiang, G., Pichaandi, J., Johnson, N. J., Burke, R. D. & Van Veggel, F. C. An Effective Polymer Cross-Linking Strategy to Obtain Stable Dispersions of Upconverting Nayf4 Nanoparticles in Buffers and Biological Growth Media for Biolabeling Applications. *Langmuir* 28, 3239-3247 **(2012)**.

[143] Liu, Y., Ouyang, Q., Li, H., Zhang, Z. & Chen, Q. Development of an Inner Filter Effects-Based Upconversion Nanoparticles-Curcumin Nanosystem for the Sensitive Sensing of Fluoride Ion. *ACS Applied Materials & Interfaces* **(2017)**.

[144] Liang, Z., Wang, X., Zhu, W., Zhang, P., Yang, Y., Sun, C., Zhang, J., Wang, X., Xu, Z. & Zhao, Y. Upconversion Nanocrystals Mediated Lateral-Flow Nanoplatform for in Vitro Detection. *ACS Applied Materials & Interfaces* 9, 3497-3504 **(2017)**.

[145] Liu, X., Ren, J., Su, L., Gao, X., Tang, Y., Ma, T., Zhu, L. & Li, J. Novel Hybrid Probe Based on Double Recognition of Aptamer-Molecularly Imprinted Polymer Grafted on Upconversion Nanoparticles for Enrofloxacin Sensing. *Biosensors and Bioelectronics* 87, 203-208 **(2017)**.

[146] Wu, Z., Xu, E., Chughtai, M. F., Jin, Z. & Irudayaraj, J. Highly Sensitive Fluorescence Sensing of Zearalenone Using a Novel Aptasensor Based on

Upconverting Nanoparticles. *Food Chemistry* 230, 673-680 **(2017)**.

[147] Ouyang, Q., Liu, Y., Chen, Q., Guo, Z., Zhao, J., Li, H. & Hu, W. Rapid and Specific Sensing of Tetracycline in Food Using a Novel Upconversion Aptasensor. *Food Control* 81, 156-163 **(2017)**.

[148] Zhang, P., Rogelj, S., Nguyen, K. & Wheeler, D. Design of a Highly Sensitive and Specific Nucleotide Sensor Based on Photon Upconverting Particles. *Journal of the American Chemical Society* 128, 12410-12411 **(2006)**.

[149] You, H., Hua, X., Feng, L., Sun, N., Rui, Q., Wang, L. & Wang, M. Competitive Immunoassay for Imidaclothiz Using Upconversion Nanoparticles and Gold Nanoparticles as Labels. *Microchimica Acta* 184, 1085-1092 **(2017)**.

[150] Wilhelm, S., Hirsch, T., Patterson, W. M., Scheucher, E., Mayr, T. & Wolfbeis, O. S. Multicolor Upconversion Nanoparticles for Protein Conjugation. *Theranostics* 3, 239 **(2013)**.

[151] Xing, H., Bu, W., Zhang, S., Zheng, X., Li, M., Chen, F., He, Q., Zhou, L., Peng, W. & Hua, Y. Multifunctional Nanoprobes for Upconversion Fluorescence, MR and CT Trimodal Imaging. *Biomaterials* 33, 1079-1089 **(2012)**.

[152] Fu, L., Morsch, M., Shi, B., Wang, G., Lee, A., Radford, R., Lu, Y., Jin, D. & Chung, R. A Versatile Upconversion Surface Evaluation Platform for Bio-Nano Surface Selection for the Nervous System. *Nanoscale* 9, 13683-13692 **(2017)**.

[153] Tian, J., Bai, J., Peng, Y., Qie, Z., Zhao, Y., Ning, B., Xiao, D. & Gao, Z. A Core-Shell-Structured Molecularly Imprinted Polymer on Upconverting Nanoparticles for Selective and Sensitive Fluorescence Sensing of Sulfamethazine. *Analyst* 140, 5301-5307 **(2015)**.

[154] Fang, C., Wu, S., Duan, N., Dai, S. & Wang, Z. Highly Sensitive Aptasensor for Oxytetracycline Based on Upconversion and Magnetic Nanoparticles. *Analytical Methods* 7, 2585-2593 **(2015)**.

[155] Jiang, L. F., Chen, B. C., Chen, B., Li, X. J., Liao, H. L., Huang, H. M., Guo, Z. J., Zhang, W. Y. & Wu, L. Detection of Aβ Oligomers Based on Magnetic-Field-Assisted Separation of Aptamer-Functionalized Fe_3O_4 Magnetic Nanoparticles and $BaYF_5$:Yb, Er Nanoparticles as Upconversion Fluorescence Labels. *Talanta* 170, 350-357 **(2017)**.

[156] Johnson, N. J., Sangeetha, N. M., Boyer, J. C. & van Veggel, F. C. Facile Ligand-Exchange with Polyvinylpyrrolidone and Subsequent Silica Coating of Hydrophobic Upconverting β-$NaYF_4$:Yb^{3+}/Er^{3+} Nanoparticles. *Nanoscale* 2, 771-

777 **(2010)**.

[157] Mou, X., Wang, J., Meng, X., Liu, J., Shi, L. & Sun, L. Multifunctional Nanoprobe Based on Upconversion Nanoparticles for Luminescent Sensing and Magnetic Resonance Imaging. *Journal of Luminescence* 190, 16-22 **(2017)**.

[158] Huang, L. J., Yu, R. Q. & Chu, X. DNA-Functionalized Upconversion Nanoparticles as Biosensors for Rapid, Sensitive, and Selective Detection of Hg^{2+} in Complex Matrices. *Analyst* 140, 4987-4990 **(2015)**.

[159] Li, H., Sun, D. E., Liu, Y. & Liu, Z. An Ultrasensitive Homogeneous Aptasensor for Kanamycin Based on Upconversion Fluorescence Resonance Energy Transfer. *Biosensors and Bioelectronics* 55, 149-156 **(2014)**.

[160] Zeng, T., Zhang, T., Wei, W., Li, Z., Wu, D., Wang, L., Guo, J., He, X. & Ma, N. Compact, Programmable, and Stable Biofunctionalized Upconversion Nanoparticles Prepared through Peptide-Mediated Phase Transfer for High-Sensitive Protease Sensing and in Vivo Apoptosis Imaging. *ACS Applied Materials & Interfaces* 7, 11849-11856 **(2015)**.

[161] Li, L. L., Wu, P., Hwang, K. & Lu, Y. An Exceptionally Simple Strategy for DNA-Functionalized Up-Conversion Nanoparticles as Biocompatible Agents for Nanoassembly, DNA Delivery, and Imaging. *Journal of the American Chemical Society* 135, 2411-2414 **(2013)**.

[162] Duong, H. T., Chen, Y., Tawfik, S. A., Wen, S., Parviz, M., Shimoni, O. & Jin, D. Systematic Investigation of Functional Ligands for Colloidal Stable Upconversion Nanoparticles. *RSC Advances* 8, 4842-4849 **(2018)**.

[163] Liu, Y., Purich, D. L., Wu, C., Wu, Y., Chen, T., Cui, C., Zhang, L., Cansiz, S., Hou, W. & Wang, Y. Ionic Functionalization of Hydrophobic Colloidal Nanoparticles to Form Ionic Nanoparticles with Enzymelike Properties. *Journal of the American Chemical Society* 137, 14952-14958 **(2015)**.

[164] Li, H., Dong, H., Yu, M., Liu, C., Li, Z., Wei, L., Sun, L. D. & Zhang, H. NIR Ratiometric Luminescence Detection of pH Fluctuation in Living Cells with Hemicyanine Derivative-Assembled Upconversion Nanophosphors. *Analytical Chemistry* 89, 8863-8869 **(2017)**.

[165] Wu, S., Duan, N., Shi, Z., Fang, C. & Wang, Z. Simultaneous Aptasensor for Multiplex Pathogenic Bacteria Detection Based on Multicolor Upconversion Nanoparticles Labels. *Analytical Chemistry* 86, 3100-3107 **(2014)**.

[166] You, M., Lin, M., Gong, Y., Wang, S., Li, A., Ji, L., Zhao, H., Ling, K., Wen, T. &

Huang, Y. Household Fluorescent Lateral Flow Strip Platform for Sensitive and Quantitative Prognosis of Heart Failure Using Dual-Color Upconversion Nanoparticles. *ACS Nano* 11, 6261-6270 **(2017)**.

[167] Han, J., Zhang, C., Liu, F., Liu, B., Han, M., Zou, W., Yang, L. & Zhang, Z. Upconversion Nanoparticles for Ratiometric Fluorescence Detection of Nitrite. *Analyst* 139, 3032-3038 **(2014)**.

[168] Lin, M., Gao, Y., Diefenbach, T. J., Shen, J. K., Hornicek, F. J., Park, Y. I., Xu, F., Lu, T. J., Amiji, M. & Duan, Z. Facial Layer-by-Layer Engineering of Upconversion Nanoparticles for Gene Delivery: Near-Infrared-Initiated Fluorescence Resonance Energy Transfer Tracking and Overcoming Drug Resistance in Ovarian Cancer. *ACS Applied Materials & Interfaces* 9, 7941-7949 **(2017)**.

[169] Dai, S., Wu, S., Duan, N., Chen, J., Zheng, Z. & Wang, Z. An Ultrasensitive Aptasensor for Ochratoxin a Using Hexagonal Core/Shell Upconversion Nanoparticles as Luminophores. *Biosensors and Bioelectronics* 91, 538-544 **(2017)**.

[170] Guo, T., Deng, Q., Fang, G., Liu, C., Huang, X. & Wang, S. Molecularly Imprinted Upconversion Nanoparticles for Highly Selective and Sensitive Sensing of Cytochrome C. *Biosensors and Bioelectronics* 74, 498-503 **(2015)**.

[171] Li, Z., Lv, S., Wang, Y., Chen, S. & Liu, Z. Construction of LRET-Based Nanoprobe Using Upconversion Nanoparticles with Confined Emitters and Bared Surface as Luminophore. *Journal of the American Chemical Society* 137, 3421-3427 **(2015)**.

[172] Hu, G., Sheng, W., Zhang, Y., Wang, J., Wu, X. & Wang, S. Upconversion Nanoparticles and Monodispersed Magnetic Polystyrene Microsphere Based Fluorescence Immunoassay for the Detection of Sulfaquinoxaline in Animal-Derived Foods. *Journal of Agricultural and Food Chemistry* 64, 3908-3915 **(2016)**.

[173] Zhu, H., Ding, Y., Wang, A., Sun, X., Wu, X. C. & Zhu, J. J. A Simple Strategy Based on Upconversion Nanoparticles for a Fluorescent Resonant Energy Transfer Biosensor. *Journal of Materials Chemistry B* 3, 458-464 **(2015)**.

[174] Du, S., Hernandez-Gil, J., Dong, H., Zheng, X., Lyu, G.-M., Bañobre-López, M., Gallo, J., Sun, L., Yan, C. H. & Long, N. J. Design and Validation of a New Ratiometric Intracellular pH Imaging Probe Using Lanthanide-Containing Upconverting Nanoparticles. *Dalton Transactions* **(2017)**.

[175] Chen, Y., Duong, H., Wen, S., Mi, C., Zhou, Y., Shimoni, O., Valenzuela, S. M. & Jin, D. Exonuclease III-Assisted Upconversion Resonance Energy Transfer in a

Wash-Free Suspension DNA Assay. *Analytical Chemistry* **(2017)**.

[176] Cao, P., Tong, L., Hou, Y., Zhao, G., Guerin, G., Winnik, M. A. & Nitz, M. Improving Lanthanide Nanocrystal Colloidal Stability in Competitive Aqueous Buffer Solutions Using Multivalent PEG-Phosphonate Ligands. *Langmuir* 28, 12861-12870 **(2012)**.

[177] Zhao, G., Tong, L., Cao, P., Nitz, M. & Winnik, M. A. Functional PEG-Pamam-Tetraphosphonate Capped $NaLnF_4$ Nanoparticles and Their Colloidal Stability in Phosphate Buffer. *Langmuir* 30, 6980-6989 **(2014)**.

[178] Boyer, J. C., Manseau, M. P., Murray, J. I. & van Veggel, F. C. Surface Modification of Upconverting $NaYF_4$ Nanoparticles with PEG-Phosphate Ligands for NIR (800 nm) Biolabeling within the Biological Window. *Langmuir* 26, 1157-1164 **(2009)**.

[179] Wang, D., Chen, C., Ke, X., Kang, N., Shen, Y., Liu, Y., Zhou, X., Wang, H., Chen, C. & Ren, L. Bioinspired near-Infrared-Excited Sensing Platform for in Vitro Antioxidant Capacity Assay Based on Upconversion Nanoparticles and a Dopamine-Melanin Hybrid System. *ACS Applied Materials & Interfaces* 7, 3030-3040 **(2015)**.

[180] Wilhelm, S., Kaiser, M., Würth, C., Heiland, J., Carrillo-Carrion, C., Muhr, V., Wolfbeis, O. S., Parak, W. J., Resch-Genger, U. & Hirsch, T. Water Dispersible Upconverting Nanoparticles: Effects of Surface Modification on Their Luminescence and Colloidal Stability. *Nanoscale* 7, 1403-1410 **(2015)**.

[181] Liang, T., Li, Z., Song, D., Shen, L., Zhuang, Q. & Liu, Z. Modulating the Luminescence of Upconversion Nanoparticles with Heavy Metal Ions: A New Strategy for Probe Design. *Analytical Chemistry* 88, 9989-9995 **(2016)**.

[182] Näreoja, T., Deguchi, T., Christ, S., Peltomaa, R., Prabhakar, N., Fazeli, E., Perälä, N., Rosenholm, J. M., Arppe, R. & Soukka, T. Ratiometric Sensing and Imaging of Intracellular Ph Using Polyethylenimine-Coated Photon Upconversion Nanoprobes. *Analytical Chemistry* 89, 1501-1508 **(2017)**.

[183] Kale, V., Päkkilä, H., Vainio, J., Ahomaa, A., Sirkka, N., Lyytikäinen, A., Talha, S. M., Kutsaya, A., Waris, M. & Julkunen, I. Spectrally and Spatially Multiplexed Serological Array-in-Well Assay Utilizing Two-Color Upconversion Luminescence Imaging. *Analytical Chemistry* 88, 4470-4477 **(2016)**.

[184] Li, C., Zuo, J., Zhang, L., Chang, Y., Zhang, Y., Tu, L., Liu, X., Xue, B., Li, Q. & Zhao, H. Accurate Quantitative Sensing of Intracellular Ph Based on Self-Ratiometric Upconversion Luminescent Nanoprobe. *Scientific Reports* 6, 38617

(2016).

[185] Tang, J., Lei, L., Feng, H., Zhang, H. & Han, Y. Preparation of K^+-Doped Core-Shell $NaYF_4$:Yb, Er Upconversion Nanoparticles and Its Application for Fluorescence Immunochromatographic Assay of Human Procalcitonin. *Journal of Fluorescence* 26, 2237-2246 **(2016)**.

[186] Gu, B., Zhou, Y., Zhang, X., Liu, X., Zhang, Y., Marks, R., Zhang, H., Liu, X. & Zhang, Q. Thiazole Derivative-Modified Upconversion Nanoparticles for Hg^{2+} Detection in Living Cells. *Nanoscale* 8, 276-282 **(2016)**.

[187] Peng, J., Samanta, A., Zeng, X., Han, S., Wang, L., Su, D., Loong, D. T. B., Kang, N. Y., Park, S. J. & Jiang, W. Real-Time in Vivo Hepatotoxicity Monitoring through Chromophore-Conjugated Photon-Upconverting Nanoprobes. *Angewandte Chemie International Edition* 56, 4165-4169 **(2017)**.

[188] Huang, X., Wang, L., Zhang, X., Yin, X., Bin, N., Zhong, F., Liu, Y. & Cai, Q. Dye-Assembled Nanocomposites for Rapid Upconversion Luminescence Sensing of Cu^{2+}. *Sensors and Actuators B: Chemical* 248, 1-8 **(2017)**.

[189] Wang, X., Wang, S., Huang, K., Liu, Z., Gao, Y. & Zeng, W. A Ratiometric Upconversion Nanosensor for Visualized Point-of-Care Assay of Organophosphonate Nerve Agent. *Sensors and Actuators B: Chemical* 241, 1188-1193 **(2017)**.

[190] Zhai, Y., Zhang, H., Zhang, L. & Dong, S. A High Performance Fluorescence Switching System Triggered Electrochemically by Prussian Blue with Upconversion Nanoparticles. *Nanoscale* 8, 9493-9497 **(2016)**.

[191] Liu, J., Liu, Y., Bu, W., Bu, J., Sun, Y., Du, J. & Shi, J. Ultrasensitive Nanosensors Based on Upconversion Nanoparticles for Selective Hypoxia Imaging in Vivo Upon Near-Infrared Excitation. *Journal of the American Chemical Society* 136, 9701-9709 **(2014)**.

[192] Arppe, R., Näreoja, T., Nylund, S., Mattsson, L., Koho, S., Rosenholm, J. M., Soukka, T. & Schäferling, M. Photon Upconversion Sensitized Nanoprobes for Sensing and Imaging of Ph. *Nanoscale* 6, 6837-6843 **(2014)**.

[193] Ma, T., Ma, Y., Liu, S., Zhang, L., Yang, T., Yang, H.-R., Lv, W., Yu, Q., Xu, W. & Zhao, Q. Dye-Conjugated Upconversion Nanoparticles for Ratiometric Imaging of Intracellular Ph Values. *Journal of Materials Chemistry C* 3, 6616-6620 **(2015)**.

[194] Li, Z., Lv, S., Wang, Y., Chen, S. & Liu, Z. Construction of LRET-Based Nanoprobe Using Upconversion Nanoparticles with Confined Emitters and Bared

Surface as Luminophore. *Journal of the American Chemical Society* 137, 3421-3427 **(2015)**.

[195] Chen, Y., Zhang, T., Gao, X., Pan, W., Li, N. & Tang, B. A Highly Selective and Instantaneous Upconversion Fluorescent Nanoprobe for Ascorbic Acid Detection in Biological Samples. *Chinese Chemical Letters* **(2017)**.

[196] Hwang, S. H., Im, S. G., Sung, H., Hah, S. S., Cong, V. T., Lee, D. H., Son, S. J. & Oh, H. B. Upconversion Nanoparticle-Based Förster Resonance Energy Transfer for Detecting the Is6110 Sequence of Mycobacterium Tuberculosis Complex in Sputum. *Biosensors and Bioelectronics* 53, 112-116 **(2014)**.

[197] Kim, S., Hwang, S. H., Im, S. G., Lee, M. K., Lee, C. H., Son, S. J. & Oh, H. B. Upconversion Nanoparticle-Based Förster Resonance Energy Transfer for Detecting DNA Methylation. *Sensors* 16, 1259 **(2016)**.

[198] Wu, B., Cao, Z., Zhang, Q. & Wang, G. NIR-Responsive DNA Hybridization Detection by High Efficient FRET from 10-nm Upconversion Nanoparticles to Sybr Green I. *Sensors and Actuators B: Chemical* **(2017)**.

[199] Han, G.-M., Li, H., Huang, X. X. & Kong, D.-M. Simple Synthesis of Carboxyl-Functionalized Upconversion Nanoparticles for Biosensing and Bioimaging Applications. *Talanta* 147, 207-212 **(2016)**.

[200] Xu, Y., Meng, X., Liu, J., Dang, S., Shi, L. & Sun, L. Luminescent Nanoprobes Based on Upconversion Nanoparticles and Single-Walled Carbon Nanohorns or Graphene Oxide for Detection of Pb^{2+} Ion. *CrystEngComm* 18, 4032-4037 **(2016)**.

[201] Jiang, P., He, M., Shen, L., Shi, A. & Liu, Z. A Paper-Supported Aptasensor for Total Ige Based on Luminescence Resonance Energy Transfer from Upconversion Nanoparticles to Carbon Nanoparticles. *Sensors and Actuators B: Chemical* 239, 319-324 **(2017)**.

[202] Lv, J., Zhao, S., Wu, S. & Wang, Z. Upconversion Nanoparticles Grafted Molybdenum Disulfide Nanosheets Platform for Microcystin-LR Sensing. *Biosensors and Bioelectronics* 90, 203-209 **(2017)**.

[203] Chiche, J., Brahimi-Horn, M. C. & Pouysségur, J. Tumour Hypoxia Induces a Metabolic Shift Causing Acidosis: A Common Feature in Cancer. *Journal of Cellular and Molecular Medicine* 14, 771-794 **(2010)**.

[204] Kuang, Y., Balakrishnan, K., Gandhi, V. & Peng, X. Hydrogen Peroxide Inducible DNA Cross-Linking Agents: Targeted Anticancer Prodrugs. *Journal of the American Chemical Society* 133, 19278-19281 **(2011)**.

[205] Fan, W., Bu, W., Shen, B., He, Q., Cui, Z., Liu, Y., Zheng, X., Zhao, K. & Shi, J. Intelligent MnO_2 Nanosheets Anchored with Upconversion Nanoprobes for Concurrent pH-/H_2O_2-Responsive UCL Imaging and Oxygen-Elevated Synergetic Therapy. *Advanced Materials* 27, 4155-4161 **(2015)**.

[206] Wu, S., Duan, N., Shi, Z., Fang, C. & Wang, Z. Dual Fluorescence Resonance Energy Transfer Assay between Tunable Upconversion Nanoparticles and Controlled Gold Nanoparticles for the Simultaneous Detection of Pb^{2+} and Hg^{2+}. *Talanta* 128, 327-336 **(2014)**.

[207] Wu, M., Wang, X., Wang, K. & Guo, Z. An Ultrasensitive Fluorescent Nanosensor for Trypsin Based on Upconversion Nanoparticles. *Talanta* 174, 797-802 **(2017)**.

[208] Li, C., Zuo, J., Li, Q., Chang, Y., Zhang, Y., Tu, L., Liu, X., Xue, B., Zhao, H. & Zhang, H. One-Step in Situ Solid-Substrate-Based Whole Blood Immunoassay Based on FRET between Upconversion and Gold Nanoparticles. *Biosensors and Bioelectronics* 92, 335-341 **(2017)**.

[209] Cheng, K., Zhang, J., Zhang, L., Wang, L. & Chen, H. Aptamer Biosensor for Salmonella Typhimurium Detection Based on Luminescence Energy Transfer from Mn^{2+}-Doped $NaYF_4$:Yb, Tm Upconverting Nanoparticles to Gold Nanorods. *Spectrochimica Acta Part A: Molecular and Biomolecular Spectroscopy* 171, 168-173 **(2017)**.

[210] Dai, S., Wu, S., Duan, N. & Wang, Z. A Luminescence Resonance Energy Transfer Based Aptasensor for the Mycotoxin Ochratoxin a Using Upconversion Nanoparticles and Gold Nanorods. *Microchimica Acta* 183, 1909-1916 **(2016)**.

[211] Li, S., Xu, L., Ma, W., Wu, X., Sun, M., Kuang, H., Wang, L., Kotov, N. A. & Xu, C. Dual-Mode Ultrasensitive Quantification of Microrna in Living Cells by Chiroplasmonic Nanopyramids Self-Assembled from Gold and Upconversion Nanoparticles. *Journal of the American Chemical Society* 138, 306-312 **(2015)**.

[212] Wu, Q., Long, Q., Li, H., Zhang, Y. & Yao, S. An Upconversion Fluorescence Resonance Energy Transfer Nanosensor for One Step Detection of Melamine in Raw Milk. *Talanta* 136, 47-53 **(2015)**.

[213] Long, Q., Li, H., Zhang, Y. & Yao, S. Upconversion Nanoparticle-Based Fluorescence Resonance Energy Transfer Assay for Organophosphorus Pesticides. *Biosensors and Bioelectronics* 68, 168-174 **(2015)**.

[214] Fang, A., Chen, H., Li, H., Liu, M., Zhang, Y. & Yao, S. Glutathione Regulation-Based Dual-Functional Upconversion Sensing-Platform for Acetylcholinesterase

Activity and Cadmium Ions. *Biosensors and Bioelectronics* 87, 545-551 **(2017)**.

[215] Saleh, S. M., Ali, R. & Wolfbeis, O. S. Quenching of the Luminescence of Upconverting Luminescent Nanoparticles by Heavy Metal Ions. *Chemistry-A European Journal* 17, 14611-14617 **(2011)**.

[216] Liang, T., Li, Z., Song, D., Shen, L., Zhuang, Q. & Liu, Z. Modulating the Luminescence of Upconversion Nanoparticles with Heavy Metal Ions: A New Strategy for Probe Design. *Analytical Chemistry* 88, 9989-9995 **(2016)**.

[217] Zhang, L., Ling, B., Wang, L. & Chen, H. A near-Infrared Luminescent Mn^{2+}-Doped $NaYF_4$:Yb, Tm/Fe^{3+} Upconversion Nanoparticles Redox Reaction System for the Detection of GSH/Cys/AA. *Talanta* 172, 95-101 **(2017)**.

[218] Tang, Y., Li, M., Gao, Z., Liu, X., Gao, X., Ma, T., Lu, X. & Li, J. Upconversion Nanoparticles Capped with Molecularly Imprinted Polymer as Fluorescence Probe for the Determination of Ractopamine in Water and Pork. *Food Analytical Methods*, 1-10 **(2017)**.

[219] Tang, Y., Gao, Z., Wang, S., Gao, X., Gao, J., Ma, Y., Liu, X. & Li, J. Upconversion Particles Coated with Molecularly Imprinted Polymers as Fluorescence Probe for Detection of Clenbuterol. *Biosensors and Bioelectronics* 71, 44-50 **(2015)**.

[220] Wang, Y., Ren, S., Jiang, H., Peng, Y., Bai, J., Li, Q., Li, C., Gao, Z. & Ning, B. A Label-Free Detection of Diethylstilbestrol Based on Molecularly Imprinted Polymer-Coated Upconversion Nanoparticles Obtained by Surface Grafting. *RSC Advances* 7, 22215-22221 **(2017)**.

[221] Tang, Y., Li, M., Gao, X., Liu, X., Gao, J., Ma, T. & Li, J. A NIR-Responsive up-Conversion Nanoparticle Probe of the $NaYF_4$:Er, Yb Type and Coated with a Molecularly Imprinted Polymer for Fluorometric Determination of Enrofloxacin. *Microchimica Acta* 184, 3469-3475 **(2017)**.

[222] Armbruster, D. A. & Pry, T. Limit of Blank, Limit of Detection and Limit of Quantitation. *The Clinical Biochemist Reviews* 29, S49 **(2008)**.

[223] European Pharmacopoeia. European Directorate for the Quality of Medicines. **(2007)**.

[224] Shrivastava, A. and Gupta, V.B. Methods for the Determination of Limit of Detection and Limit of Quantitation of the Analytical Methods. Chronicles of Young Scientists 2(1), p.21 **(2011)**.

CHAPTER 2

Systematic and Comparative Investigation of the Colloidal Stability and Biocompatibility of Hydrophilic Upconversion Nanoparticles Capped with Four Ligands

Abstract: Surface modification resulting in good stability and biocompatibility is key for the bio-application of upconversion nanoparticles (UCNPs). We present a systematic and comparative study of the physical and cellular interaction properties of four hydrophilic ligand-capped UCNPs. Four molecules, including (aminomethyl)phosphonic acid (AMPA), (3-Aminopropyl)triethoxysilane (APTES), 3,4-dihyrocinnamic acid (3,4-DHCA) and one kind of di-block copolymer composed of poly(ethylene glycol) methyl ether acrylate and poly(monoacryloxyethyl phosphate) (simply named as MAEP in this chapter), were respectively applied to replace the hydrophobic oleic acids *via* a one-step ligand exchange method resulting in carboxyl and amino functionalized aqueous-dispersible UCNPs. Modification with these ligands has no obvious effect on the ratio between the green and red emission from the spectrum measurement; while the single nanoparticle luminescence measurement indicates that all four attached ligands have the quenching effect on the upconversion emission. Carboxyl-functionalised UCNPs demonstrate better aqueous stability compared with amino-functonalised UCNPs,

particularly in a slightly basic biological environment due to the negative charge of the carboxyl-containing UCNPs. In contrast, the amino-functionalized UCNPs can only remain monodispersed in acidic environments due to their positive charge. Furthermore, polymer modified MAEP-UCNPs, that incorporate carboxyl group in the polymer chain, demonstrates the best stability in all three biological buffers (HEPES buffer, SSC buffer and Tris-HCl buffer) with unchanged and uniform size distribution compared with DHCA-UCNPs. Study of cellular *in vitro* compatibility using CHO-K1 cells, MAEP-UCNPs show non-cytotoxic behavior with low uptake level of non-aggregated particles into cells. The other three compounds on the surface of nanoparticles were all cytotoxic and demonstrate high cellular uptake levels, and most particles show a highly aggreged state within the cell cytoplasm resulting in increased toxicity to cells. This study result has the potential as a guideline for the surface modification of UCNPs in bio-applications.

Key words: surface modification, upconversion nanoparticles, water stability, cellular uptake, cytotoxicity.

2.1 Introduction

Upconversion nanoparticles (UCNPs) have attracted a great deal of attention in biomolecular detection[1,2] and biological imaging[3,4]. These nanoparticles are capable of emitting visible and near-infrared (NIR) light when excited with NIR radiation[5]. Every single UCNP contains thousands of photon sensitizers and hundreds of trivalent lanthanide ions as photo activators within an inorganic crystalline host matrix, and therefore delivers bright luminescence in the darkness *via* either anti-Stokes spectrum filtering or time-gated detection. What is more, through the intermediate energy levels to

increase the absorption efficiency by orders of magnitude compared with conventional fluorescent dyes and quantum dots, it allows for the use of low excitation densities. Thus, the major appeal of UCNPs for bioimaging is that it can achieve deeper tissue penetration as well as higher-contrast optical imaging due to their ability to suppress autofluorescence and minimize photodamage to living cells[6,7]. Furthermore, they are capable of tunable multicolor emission[8] and lifetime[9] with exceptional photostability, and also have nonoverlapping emission bands, which are all of great potential use in high-throughput multiplex molecular detection and imaging.

Despite these promises, the poor dispersity and stability of UCNPs in aqueous phase still remains a major challenge, as a layer of hydrophobic surfactant is often needed for the colloidal UCNPs to remain stable under synthesis in organic media at high temperature. To improve the application of UCNPs for biological studies, transferring them from a hydrophobic into a hydrophilic state *via* surface modification is therefore necessary. Most current methods include ligand oxidation[10,11], inorganic shell coating[12,13], ligand exchange[14,15] and amphiphilic ligand encapsulation[16,17]. Usually, the synthesized upconversion nanoparticles dispersed in organic solvent are oleate or oleylamine capped. As for the original ligand oxidation, it is usually based on the oxidation of the carbon-carbon double bond of the oleate or oleyamine to generate carboxyl groups or epoxy groups catalyzed by strong oxidants. Even though it has been found that the morphology, composition and upconversion luminescence of the UCNPs are not influenced by the oxidation process, this method is not commonly used due to the complicated processing, poor colloidal water stability and low yields of functional groups. In some cases, surface modification with an inorganic shell layer is achieved *via* surface silanization of amorphous silica, the mostly used is tetraethoxysilance (TEOS), according to the well-

known Stober procedure[12,18]. It is easier to adjust the thickness of the silica shell for the various requests[13]. However, the silica-coated nanoparticles tend to be aggregate in aqueous buffer and lack the required functional groups for bioconjugation. So usually, one more step is needed to obtain the functionalized UCNPs following the silica coating, making the modification process more comprehensive. Amphiphilic molecules are popular for use in UCNPs surface modification, as they contain special components of two basic sections including a hydrophobic long alkyl chain to form a bilayer with the oleic acid *via* van-der Waals and a hydrophilic head outside the bilayer enabling good stability of UCNPs dispersed in water. The disadvantage of the amphiphilic bilayer modification is that the ligands are easily detached from the particles as the binding between carboxyl with UCNPs surface is not strong enough[19], and amphiphilic ligand encapsulation is usually performed at high temperature and requires extra washing steps and harsh sonication[16], leading to low transfer efficiency, poor stability and damaged photostability. Previously, the ligand exchange methods were usually conducted in a two-phase system with hydrophobic UCNPs in the nonpolar phase and the reacting ligands in the polar phase[15,20], and this two-phase transfer leads to insufficient reacting ligands on the surface of the nanoparticles and low transfer efficiency, and further resulting in serious aggregation and poor stability. However, recently, ligand exchange has been updated to one-phase transfer to overcome the disadvantages. Tetrahydrofuran (THF) usually acts as the processing reagent, both of the hydrophobic nanoparticles and the reacting ligands are mixed in a single phase at RT or slightly increased temperature[14,21].

In ligand exchange, the ligand consists of two necessary parts, reacting groups and the functional groups. The binding strength of the reacting groups is the key element for the replacement of the OA molecules, and the decisive factor for the stability of the

nanoparticles in biological reagents containing various molecules, which may have higher binding strength over the reacting groups to the metal ions. Here, four molecules are applied in surface modification of upconversion nanoparticles *via* ligand exchange, containing (aminomethyl)phosphonic (AMPA), (3-Aminopropyl)triethoxysilane (APTES), 3,4-dihydrocinnamic acid (3,4-DHCA) and one kind of di-block copolymer composed of poly(ethylene glycol) methyl ether acrylate and poly(monoacryloxyethyl phosphate) (simply named as MAEP in this chapter), (Figure 2.1). Both of AMPA and MAEP consist of the phosphonate group which has been widely used in the surface modification of the nanoparticles due to its strong binding capacity to the rare earth ions[14,22]. 3,4-DHCA, owing to the phenolic group, can replace the OA to form a robust anchor on the surface of nanoparticles *via* a metallocyclic chelate[23,24]. APTES[12], an amino siloxane, is often preformed to generate functional amino groups on the surface of the silica coated nanoparticles for further bioconjugation. Usually, the silanization begins with the hydrolysis of ethoxy groups in APTES, a process catalyzed by water, leading to the formation of silanols; and then, the silanols condense with surface silanols of the silicon substrate forming a monolayer of APTES *via* a lateral siloxane network in which amino groups are oriented away from the underlying silicon surface[25,26]. In this work, parts of the hydrolyzed silanols can remove the OA to form stable chemical bonds with rare earth ions and other silanols condense amongst each other, resulting in a relatively dense film on the surface of UCNPs.

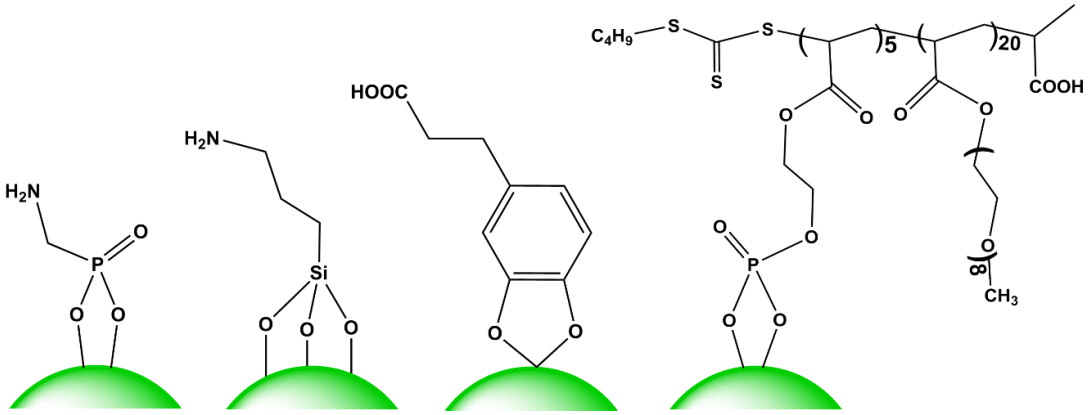

Figure 2.1 Schematic image of chemical structure of ligand-capped water-dispersible UCNPs. From left to right, AMPA-UCNP, APTES-UCNP, 3,4-DHCA-UCNP, MAEP-UCNP.

The functional groups displaying different charges always play an important role in the bio-conjugation and assist in good stability in aqueous buffer at various pH levels. The ideal surface modification should also demonstrate good cellular response, such as no cytotoxicity and minimal non-specific cellular uptake. Herein, we report a systematic and comparative investigation of hydrophilic nanoparticles capped with four ligands consisting of distinct reacting groups and functional groups, including the dispersity, stability and luminescence in aqueous buffer, and the relationship between cytotoxicity and cellular uptake. This study result has the potential to serve as a guideline for the surface modification of UCNPs in bio-applications.

2.2 Experiments

2.2.1 Materials

Rare-earth chloride hexahydrates used in this work for UCNPs synthesis, including yttrium (III) chloride hexahydrate ($YCl_3 \cdot 6H_2O$, 99.99%), ytterbium chloride hexahydrate

($YbCl_3 \cdot 6H_2O$, 99.99%), and erbium chloride hexahydrate ($ErCl_3 \cdot 6H_2O$, 99.9%), were purchased from Sigma-Aldrich. For the synthesis of di-block copolymer composed of poly(ethylene glycol) methyl ether acrylate and poly(monoacryloxyethyl phosphate), the chemicals including 2-bromopropionic acid (99%), zinc acetylacetonate hydrate, 4-cyano-4-(phenylcarbonothioylthio)pentanoic acid (97%), Monomer oligo(ethylene glycol) methyl ether acrylate (OEGA), ethylene glycol (99%), 1-butanethiol (99%) and poly(ethylene glycol) methyl ether acrylate were purchased from Sigma-Aldrich, and monoacryloxyethyl phosphate (MAEP) from Polysciences, Inc. OEGA and MAEP were used as received. 2,2'-Azobisisobutyronitrile (AIBN) was purified by recrystallization twice from methanol. All other materials and reagents, ammonium fluoride (NH_4F), sodium fluoride (NaF), cyclohexane, methanol, sodium hydroxide (NaOH), acetonitrile, tetrahydrofuran (THF), 3,4-DHCA, AMPA, APTES, Tris-buffer, SSC-buffer, Hepes-buffer were purchased from Sigma-Aldrich with reagent grade or higher. For cell culture, trypan-blue, trypsin, cell culture media DMEM-Dulbecco's Modified Eagle Medium and PBS-buffer, were purchased from ThermoFisher Scientific. Fetal bovine serum (FBS) was purchased from Scienitifix.

2.2.2 Instrumentation

UCNPs were characterized using the FEI Tecnai transmission electron microscope (FEI, U.S.A.) and D8 Discover X-ray diffraction (Bruker, Germany). The synthesized polymers were characterized with Agilent 500 MHz nuclear magnetic resonance (Agilent Technologies, U.S.A.). The hydrodynamic size of UCNPs was determined by a zetasizer nano (Malvern, U.K.). The surface ligand measurement was conducted by the Thermo Scientific Nicolet 6700 FTIR spectrometer (Thermo Fisher Scientific, Australia). Upconversion luminescent spectra were measured by an iHR550 imaging spectrometer

(Horiba Scientific, U.K.) modified with an external 980 nm laser (Figure 2.2). A single mode continuous-wave 980 nm diode laser beam launched through the UV quartz cuvette produced excitation irradiance values of up to 1.36×10^6 W/cm^2.

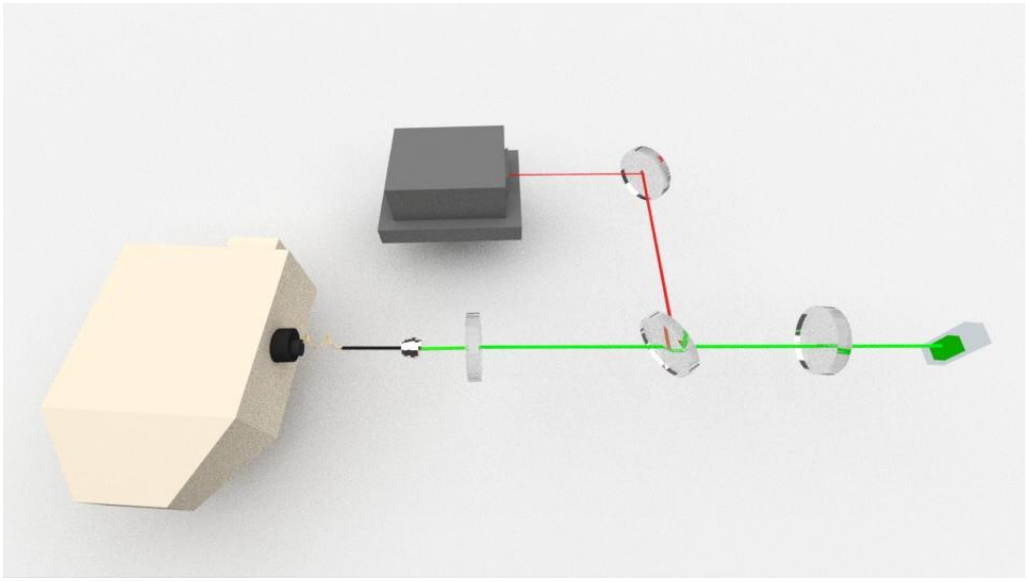

Figure 2.2 Schematic image of the experimental configuration for measuring upconversion luminescent spectrum of nanoparticles under continuous-wave 980-nm diode laser.

The photoluminescent intensity of single UCNP was measured by the home-built stage-scan confocal microscopy with 980 nm excitation source[27] (Figure 2.3).

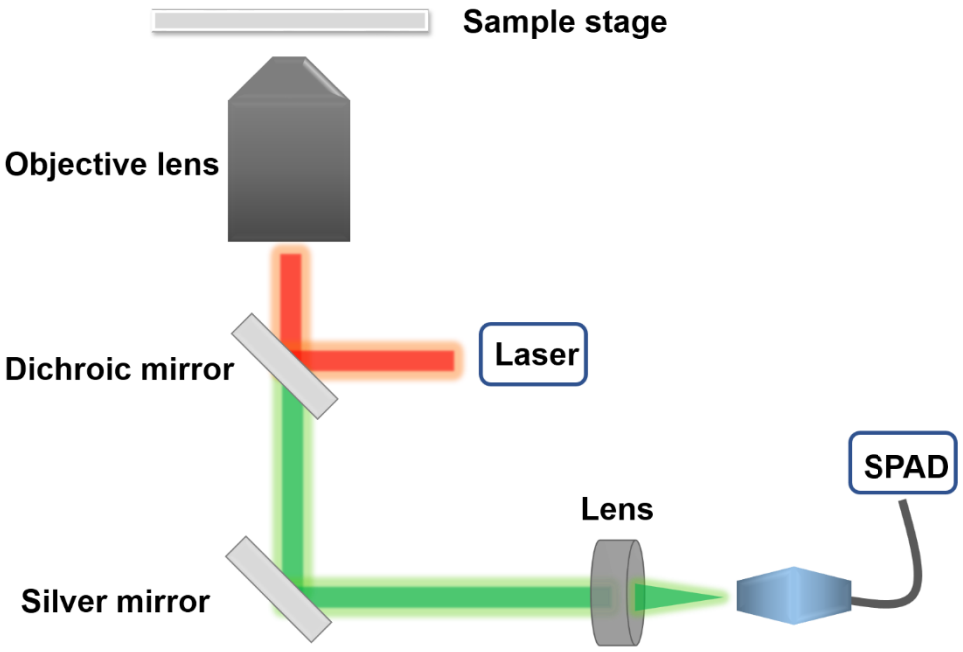

Figure 2.3 Schematic illustration of customized scanning confocal microscope for the measurement of upconversion luminescence intensity of ligand-coated signal nanoparticle.

All the measurements of upconversion luminescence in cellular uptake assay were performed on a home-built microscopy system. A schematic drawing of the experimental setup was presented in Figure 2.4. UCNPs were excited by a polarization-maintaining single-mode fiber-coupled 980 nm diode laser (BL976-PAG900, controller CLD1015, Thorlabs). The half wave plate (HWP, WPH05M-980, Thorlabs) and polarized beam splitter (PBS, CCM1-PBS252/M, Thorlabs) were employed to precisely adjust the excitation power by rotating HWP electronically. After collimation, the excitation beam was reflected by the first short-pass dichroic mirror (DM, T875spxrxt-UF1, Chroma), and focused through a high numerical aperture objective (UPlanSApo, 100×/1.40 oil, Olympus) to the sample slide. Photoluminescence was collected by the same objective and split from the excitation beams by DM. The emission signals were filtered by short

pass filter (SPF, FF01-842/SP-25, Semrock), then detected by a charge coupled device (CCD). Typical excitation powers for the recording images were set at 200 mW. All powers were measured at the back aperture of the objective lens.

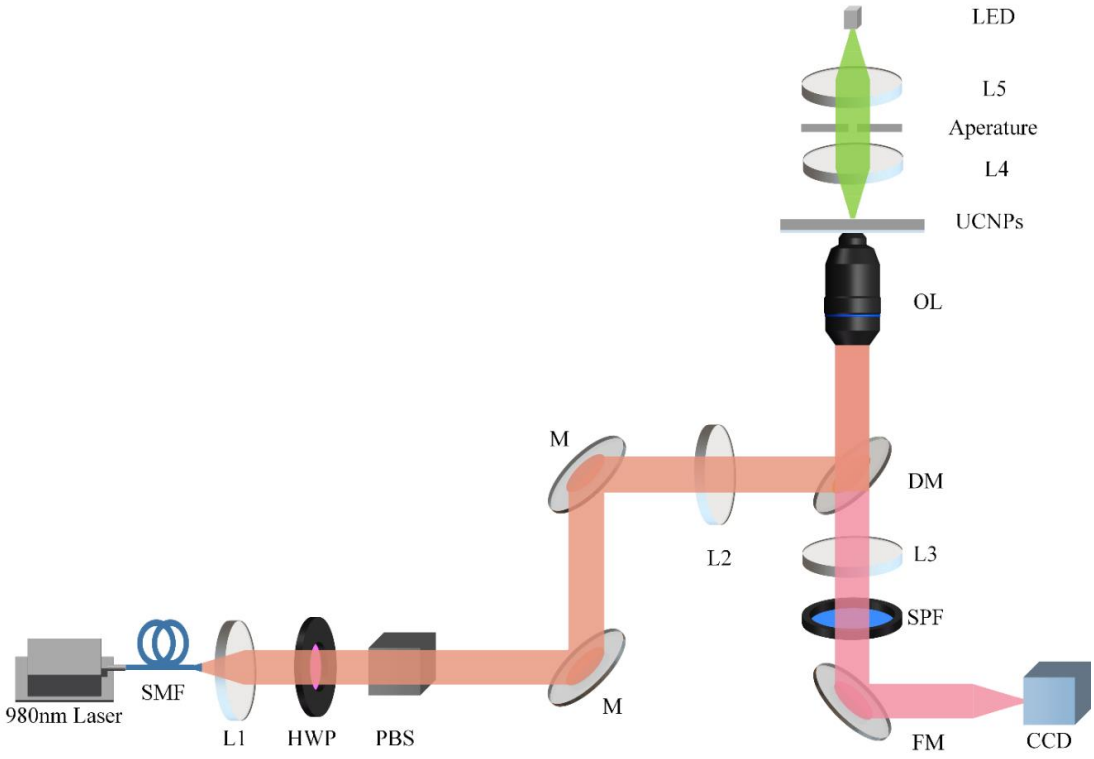

Figure 2.4 Experimental setup of wide field microscope for cell imaging to investigate the non-specific cellular uptake of ligand-capped UCNPs. (SMF, single-mode fiber; L1 to L5, lens; HWP, half-wave plate; PBS, polarized beam splitter; M, mirror; DM, dichroic mirror; OL, objective lens; SPF, short pass filter; CCD, charge coupled device)

2.2.3 Synthesis of Er Doped UCNPs

UCNPs had been synthesized according to our previously reported method[28]. In a typical experiment, 1 mmol $LnCl_3$ (Ln=Y, Yb, Er) with the molar ratio of 78:20:2 were added to a 50 mL flask containing oleic acid (OA, 6 mL) and 1-octadecene (ODE, 15 mL). The mixture was heated to 160°C under argon for 30 min to obtain a clear solution and then

cooled down to room temperature, followed by the addition of 5 mL methanol solution of NH_4F (4 mmol) and NaOH (2.5 mmol). After stirring for 30 min, the solution was heated to 100°C for 20 min to remove methanol and 120°C for 20 min to remove water under argon, followed by heating solution to 300°C for another 90 min. Finally, the reaction solution was cooled down to room temperature, and nanocrystals were precipitated with ethanol and washed with cyclohexane, ethanol and methanol thrice to get the $NaYF_4$:Yb, Er nanoparticles. UCNPs were dispersed in cyclohexane with the concentration of 20 mg/ml, kept in freezer until usage.

2.2.4 Synthesis of di-blcok Copolymer POEGA-*b*-PMAEP

Synthesis of POEGA macro-RAFT agent. The RAFT agent, 2-(*n*-butyltrithiocarbonate)-propionic acid (BTPA) was prepared according to a published procedure[29]. OEGA (5.0 g, 1.04×10^{-2} mol), RAFT agent (1.13×10^{-1} g, 4.73×10^{-4} mol) and AIBN (7.77×10^{-3} g, 4.73×10^{-4} mol) were dissolved in 20 ml of toluene in a round-bottom flask with a magnetic stirring bar. The flask was then sealed with a rubber septum and purged with nitrogen gas for 30 mins. The reaction mixtures were then placed in a preheated oil bath at 70°C. After 17 h, the polymerization was terminated by quenching the samples in an ice bath for 5 min. The POEGA polymer was then purified three times by precipitation with excess petroleum spirits (boiling range of 40-60°C) followed by centrifugation (7000 rpm for 5 min) and was dried under vacuum at room temperature. The samples were stored at 4°C until required for further chain extension to form di-block copolymer.

Synthesis of POEGA-*b*-PMAEP. POEGA macro-RAFT agent (1.0 g, 1.02×10^{-4} mol) and AIBN (3.35×10^{-3} g, 2.04×10^{-5} mol) were dissolved in 5 ml of acetonitrile and MAEP (1.4×10^{-1} g, 7.14×10^{-4} mol) was added. The reaction mixture was purged with nitrogen gas for 30 min in an ice bath. The polymerization was carried out in an oil bath at 70°C and was terminated by placing the samples on ice for 5 min. The POEGA-*b*-PMAEP was purified three times by precipitation in excess of diethyl ether followed by centrifugation (7000 rpm for 5 min) and was then dried under reduced pressure at room temperature.

2.2.5 Analysis of POEGA-*b*-PMEAP

NMR spectroscopy. Monomer conversion and polymer compositions were characterized by ^{1}H NMR using Bruker Avance 300 (300 MHz) spectrometers in d_6-DMSO = 2.46 ppm. ^{31}P NMR spectra of the polymer was carried out in d_6-DMSO for POEGA-*b*-PMAEP.

Monomer OEGA conversion (α^{OEGA}) for POEGA was calculated using the following equation: $\alpha^{\mathrm{OEGA}} = \left[\frac{\int 4.1\ ppm}{\int 4.1\ ppm + \int 4.3\ ppm}\right]$, with $\int 4.1\ ppm$ and $\int 4.3\ ppm$ corresponding to integral of the signal at 4.1 (polymer) and at 4.3 (monomer) ppm, respectively. The experimental molecular weight of POEGA was calculated using the following equation: $M_{\mathrm{n,NMR}}^{\mathrm{POEGA}} = \alpha^{OEGA} \times \left(\frac{[\mathrm{OEGA}]}{[\mathrm{RAFT}]}\right) \times M_{\mathrm{w}}^{\mathrm{OEGA}} + M_{\mathrm{w}}^{\mathrm{RAFT}}$, where $M_{\mathrm{w}}^{\mathrm{OEGA}}$ and $M_{\mathrm{w}}^{\mathrm{RAFT}}$ are the molecular weight of monomer and RAFT agent, respectively.

Monomer conversion for MAEP was also calculated from ^{1}H NMR spectra of the reaction mixture before and after polymerization by comparing the integral ratio of the vinyl protons of monomer and the unchanged methylene protons of the POEGA adjacent to

ester bond at 4.1 ppm, using the equation: $\alpha^{\mathrm{MAEP}} = (\int 6.2\,ppm, 0\,(h) - \int 6.2\,ppm, t(h))/\int 6.2\,ppm, 0(h))$. The experimental molecular weight of the resultant POEGA-*b*-PMAEP was calculated using the following equation: $M_{\mathrm{n,NMR}}^{\mathrm{POEGA}-b-\mathrm{MAEP}} = \alpha^{\mathrm{MAEP}} \times \left(\frac{[\mathrm{MAEP}]}{[\mathrm{POEGA\ maro}-\mathrm{RAFT}]}\right) \times M_{\mathrm{w}}^{\mathrm{MAEP}} + M_{\mathrm{n,NMR}}^{\mathrm{POEGA}}$, where $M_{\mathrm{w}}^{\mathrm{OEGA}}$ and $M_{\mathrm{w}}^{\mathrm{RAFT}}$ are the molecular weight of monomer and macro-RAFT agent, respectively.

2.2.6 Surface Modification of UCNPs with Four Hydrophilic Ligands *via* Ligand Exchange

To produce the 3,4-DHCA -UCNPs, 10 mg of 3,4-DHCA and 10 mg of OA-UCNPs were mixed in 2 ml of THF solution followed by sonication for 10 min. The mixture was left with a gentle shaking at RT overnight. The sample was then washed with THF thrice *via* centrifugation at 14,680 rpm for 25 min (500 ul/vial), followed by two cycles of washing/dispersion with water. The 3,4-DHCA-UCNPs were stored in 1 ml of water for further use.

To produce the APTES-UCNPs, 10 mg of OA-UCNPs dissolved in THF, 30 ul of APTES solution was added and sonicated for 10 min. The mixture was left with a gentle shaking at RT overnight. The sample was then washed with THF thrice *via* centrifugation at 14,680 rpm for 25 min (300 ul/vial), followed by two cycles of washing/dispersion with water. The APTES-UCNPs were stored in 1 ml of water for further use.

To produce the AMPA-UCNPs, 10 mg of AMPA in water and 10 mg of OA-UCNPs in THF were mixed and sonicated for 10 min. The mixture was left with a gentle shaking at

RT overnight. The sample was then washed with THF thrice *via* centrifugation at 14,680 rpm for 25 min (500 ul/vial), followed by two cycles of washing/dispersion with water. AMPA-UCNPs were stored in 1 ml of water for further use.

To produce the MAEP-UCNPs, 5 mg of MAEP and 10 mg of OA-UCNPs in THF were mixed well followed by sonication for 10 min. The mixture was left with a gentle shaking at RT overnight. The sample was then washed with THF thrice *via* centrifugation at 14,680 rpm for 25 min (500 ul/vial), followed by two cycles of washing/dispersion with water. MAEP-UCNPs were stored in 1 ml of water for further use.

To produce the bare-UCNP, 10 mg of OA-UCNPs were dissolved in 2 ml of 0.1 M HCL solution followed by sonication for 30 min. The sample was then washed with THF thrice *via* centrifugation at 14,680 rpm for 25 min (500 ul/vial), followed by two cycles of washing/dispersion with water. Bare-UCNPs were stored in 1 ml of water for further use.

2.2.7 Cytotoxicity Assay of Hydrophilic Ligand-capped UCNPs

Approximately 1×10^5 CHO-K1 cells were seeded per well into 12-well plates (Corning Incorporated) and incubated for 24 h in cell culture media (DMEM/F12 + 5%FBS). The media was removed, and another 1 ml of fresh media (DMEM/F12 + 1% FBS) containing NaF (2 mM) and one of the four ligand-capped UCNPs at concentrations of 10 ug/ml and 100 ug/ml were added into each well, respectively. Cells incubated in equal volume of the media with NaF (2 mM) were used as a control. After incubation for 24 h, 48 h or 72 h, Trypan blue viability test was performed to measure cell viability. The media with

particles was collected into tubes (15 ml), and 1 ml DPBS solution for washing the well was also collected into corresponding tubes. 500 ul of 0.25% trypsin was added into each well for cell detachment under 37°C for 3-5 min, followed by adding 500 ul of media (DMEM/F12 + 5%FBS) into each well to inactive trypsin. The 1 ml of detached cell media was collected and mixed with pre-collected 2 ml supernatant, followed by centrifuge at 1400 rpm for 3.5 min. The supernatant was discarded, and the pelleted cells were re-suspended in 1 ml of DMEM/F12. 20 ul of the media was mixed with equal volume of 0.4% trypan blue solution for cell staining. 10 ul of mixture was pipetted into the hemocytometer chamber, and cells were counted under a light microscope. Cell viability was determined using the formula: live cell count/(live cell count + dead cell count) × 100 = viability%. At the same time, the cell number of each assay group was also determined and compared with that of the control group. For the cytotoxicity assay, after the ligand-capped UCNPs were prepared, they were dried out as powder, and keep under UV irradiation for 1 h for sterilization.

2.2.8 Non-specific Cellular Uptake of Hydrophilic Ligand-capped UCNPs

Sterile round, glass coverslips (12 mm, diameter) were placed into individual wells of a 12-well plate and approximately 1×10^5 CHO-K1 cells were added into each well and incubated for 24 h in cell culture media (DMEM/F12 + 5%FBS) in order to seed the cells onto the glass coverslips. The media was removed, and another 1 ml of fresh media (DMEM/F12 + 1% FBS) containing NaF (2 mM) and one of each of the four different ligand-capped UCNPs were individually added at concentrations of 10 ug/ml or 100 ug/ml into each well, respectively. Cells incubated in equal volume of the media with NaF (2 mM) were used as a control. After incubation for another 24 h, the supernatant was discarded and the wells were washed with PBS three times. 1 ml of 4% paraformaldehyde

in PBS was applied to fix the cells onto the coverslips at RT for 15 min, followed by washing the coverslips with PBS for another three times. The coverslips were then mounted onto glass slides and observed under a microscope with 980 nm wavelength laser excitation.

2.3 Results and Discussion

2.3.1 Synthesis of UCNPs

The synthesized OA-UCNPs displayed uniform hexagonal morphology with the mean size of 20 nm from the TEM result (Figure 2.5B). The XRD result (Figure 2.5A) corresponded with the standard pattern of the hexagonal phase $NaYF_4$, indicating the high crystallinity of the nanoparticles.

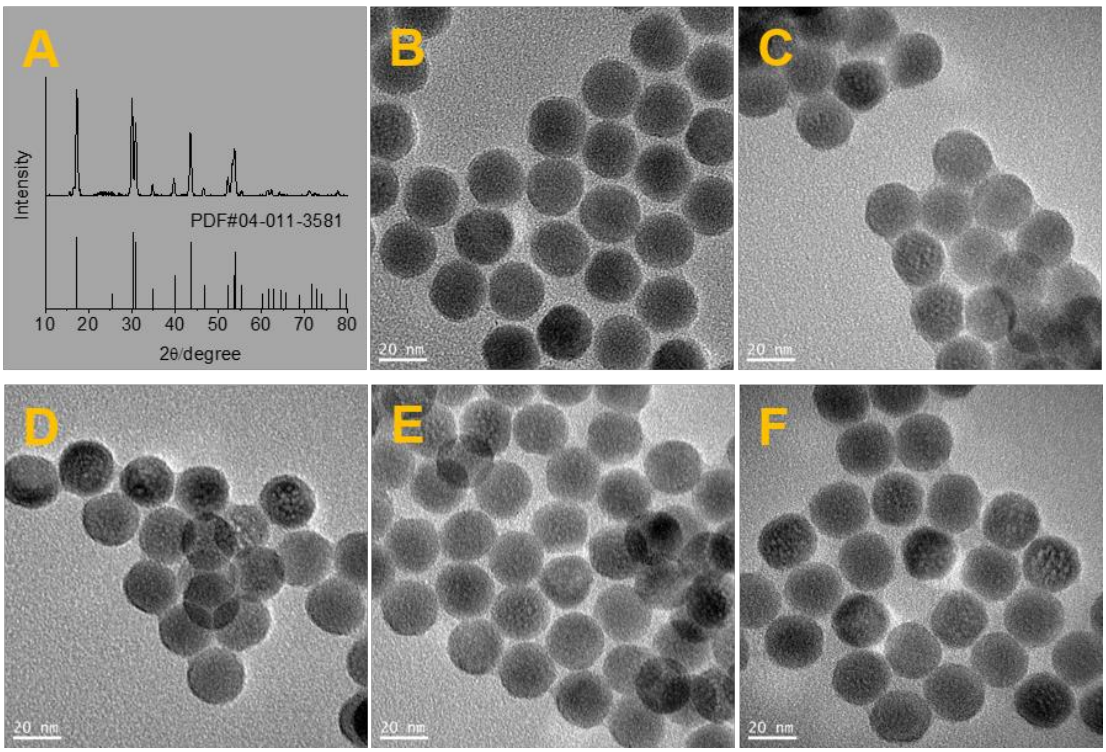

Figure 2.5 (A) The XRD of synthesized OA-UCNPs. (B-F) The TEM of OA-UCNPs, AMPA-UCNPs, APTES-UCNPs, 3,4-DHCA-UCNPs and MAEP-UCNPs, respectively.

2.3.2 Synthesis of POEGA-*b*-PMAEP

The ^{1}H NMR result of POEGA macro-RAFT agent and POEGA-*b*-PMAEP are shown in Figure 2.6 and Figure 2.7, respectively. The conversion of OEGA during the course of polymerization was 90%, and the molecular weight of the POEGA macro-RAFT agent was measured to be $M_{n,NMR}$ = 9500 g/mol. The conversion of MAEP was around 70%, and the molecular weight was measured to be $M_{n,NMR}$ = 10800 g/mol for POEGA-*b*-PMEAP. The obtained di-block co-polymer contained 20 repeating units of OEGA and 5 repeating units of MAEP from the analysis of ^{1}H NMR.

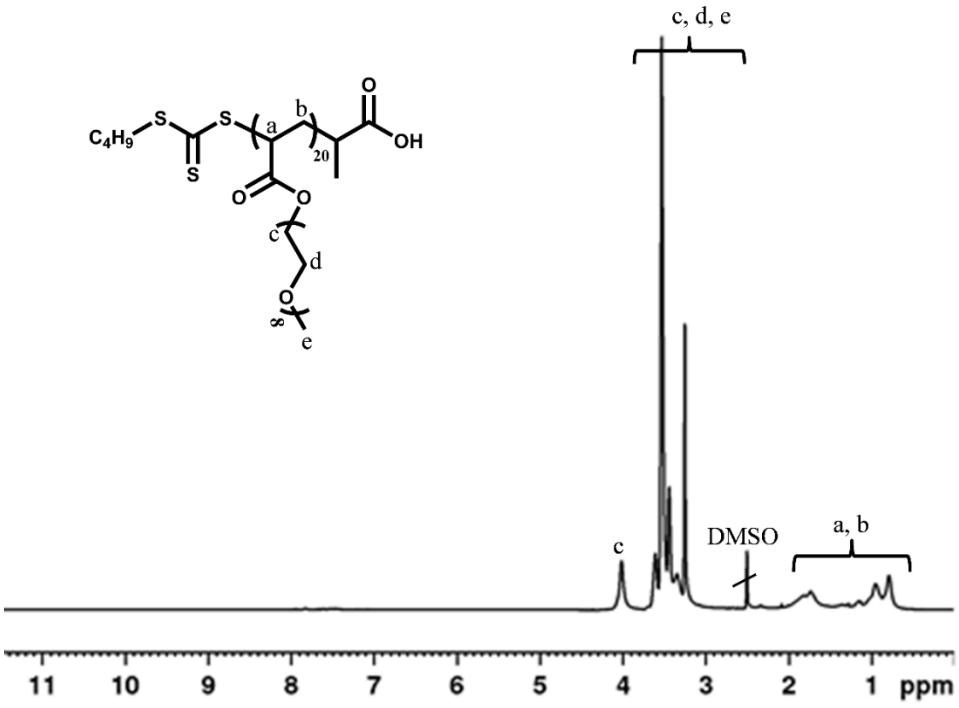

Figure 2.6 ^{1}H NMR spectrum of POEGA.

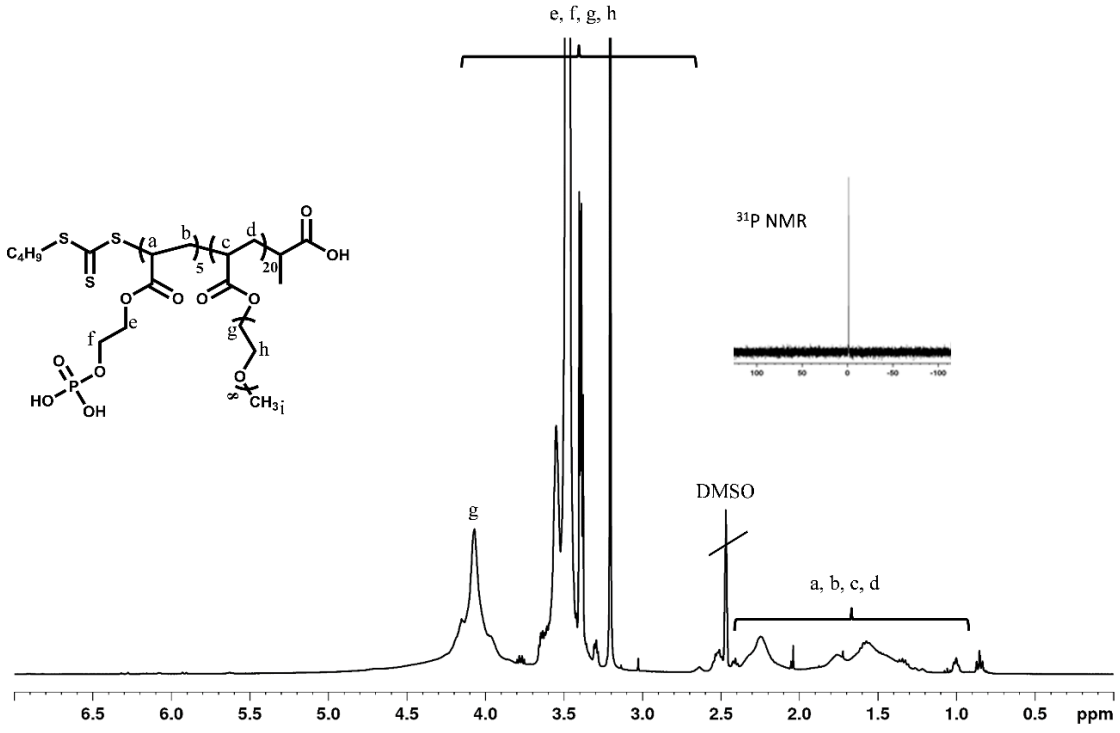

Figure 2.7 ^{1}H NMR spectrum of POEGA-b-PMAEP.

2.3.3 Characterization of Hydrophilic Ligand-capped UCNPs *via* Ligand Exchange

FTIR. The ligand exchange of the capping molecules on the surface of UCNPs was investigated using FTIR spectroscopy. As shown in Figure 2.8, four FTIR spectra of UCNPs with different hydrophilic surfaces were compared with that of as-prepared OA-UCNPs. The peaks at approximately 2921 and 2851 cm^{-1} were respectively assigned to the asymmetric and symmetric stretching vibration of the C-H bond[30]. A peak at 3005 cm^{-1} attributed to the =CH– stretching vibration was observed in the spectrum of the OA-UCNPs as the existence of the –HC=CH– group[31]. While in all four ligand-modified UCNPs, this peak disappeared, indicating the remove of the OA molecules. The peaks at 1089 cm^{-1} and 1096 cm^{-1} of respectively AMPA-UCNPs and MAEP-UCNPs were the typical P=O stretching vibration[14], confirming the attachment of AMPA and MAEP on the surface of nanoparticles. The peak at 1008 cm^{-1} was Si-O-Si stretching vibration[32],

which demonstrated the attachment of APTES onto the surface of nanoparticles. The bands around 1490 and 1300 cm^{-1} presented when catechol bond covalently to metal oxides as catechol anions, which were attributed to the benzene ring vibration and a C–O stretch, respectively[24,33,34]. While in this FTIR result of the 3,4-DHCA-UCNP, only a sharp peak at 1288 cm^{-1} was obviously observed as the C–O stretch within an acceptable shift.

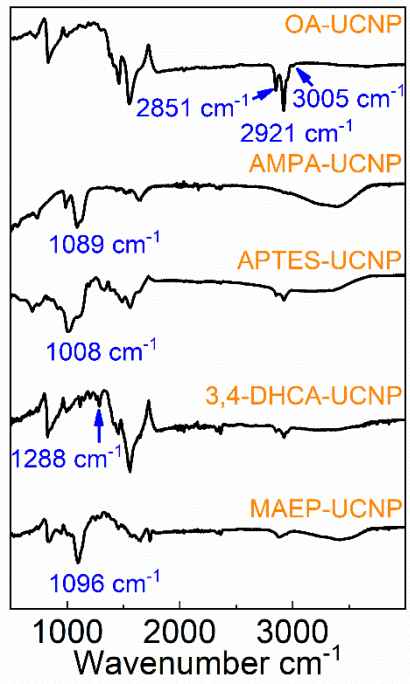

Figure 2.8 FTIR spectrum of OA-UCNPs, AMPA-UCNPs, APTES-UCNPs, 3,4-DHCA-UCNPs and MAEP-UCNPs.

TEM. TEM observations reveal that OA-UCNPs, 3,4-DHA-UCNPs, APTES-UCNPs, AMPA-UCNPs and MAEP-UCNPs were uniform in shape without obvious change in morphology after surface modification *via* ligand exchange (Figure 2.5 B-F).

Zeta potential. Table 2.1 displayed the average value of the zeta potential of the four hydrophilic ligand-capped UCNPs suspended in water. The Milli-Q water showed weak acidic (pH 6). The amino-functionalized UCNPs capped by AMPA and APTES showed positive zeta potentials, and the value of AMPA was much stronger than APTES. The carboxyl-functionalized UCNPs capped by 3,4-DHCA and MEAP were negative zeta potential, and the values were not as strong as the positive ones.

Table 2.1 Zeta potential of four ligand-capped UCNPs.

Ligand	Surface functional group	Zeta potential (mV)
AMPA	$-NH_2$	+26.9
APTES	$-NH_2$	+7.13
3,4-DHCA	-COOH	–3.41
MAEP	-COOH	–4.94

DLS. The dynamic light scattering (DLS) was applied for measuring the hydrodynamic diameter of UCNPs dispersed in aqueous buffer (Figure 2.9). The mean hydrodynamic diameter of OA-UCNPs dispersed in cyclohexane was 22 ± 1 nm, which was closely correspondent to the value measured under TEM. For the hydrophilic ligand capped-UCNPs dispersed in water, the hydrodynamic diameter was to some extent pH-dependent, as the pH value influenced the surface charge, especially for the small molecular ligands. The average diameter of the AMPA-UCNPs in water was 93 ± 5 nm (pH 6, PDI=0.481).

The diameter of AMPA-UCNPs slightly changed to smaller in acidic solution, while the diameter value got extremely bigger once in basic condition (Figure 2.9A). The average hydrodynamic diameter of the APTES-UCNPs in water was 492 ± 5 nm (pH 6, PDI=0.479), and it became much smaller in acidic condition, which was related to the surface charge getting more positive. Similar with the AMPA-UCNPs, once in basic condition, the particles aggregated severely and showed very large hydrodynamic diameter (Figure 2.9B). For 3,4-DHCA-UCNPs, the average diameter in water was 59 ± 1 nm (pH 6, PDI=0.474). In the contrast to the distribution behaviour of amino-functionalized UCNPs, DHCA-UCNPs showed the aggregates in acidic condition and stable in basic condition (Figure 2.9C). The hydrodynamic diameter of MAEP-UCNPs was 34 ± 1 nm in water (pH 6, PDI=0.514). Different from the small molecular ligands, the PEG-derived hydrophilic MAEP-UCNPs displayed very colloidal stable and uniform hydrodynamic diameter of 34 ± 1 nm in both of the acidic and basic conditions (Figure 2.9D).

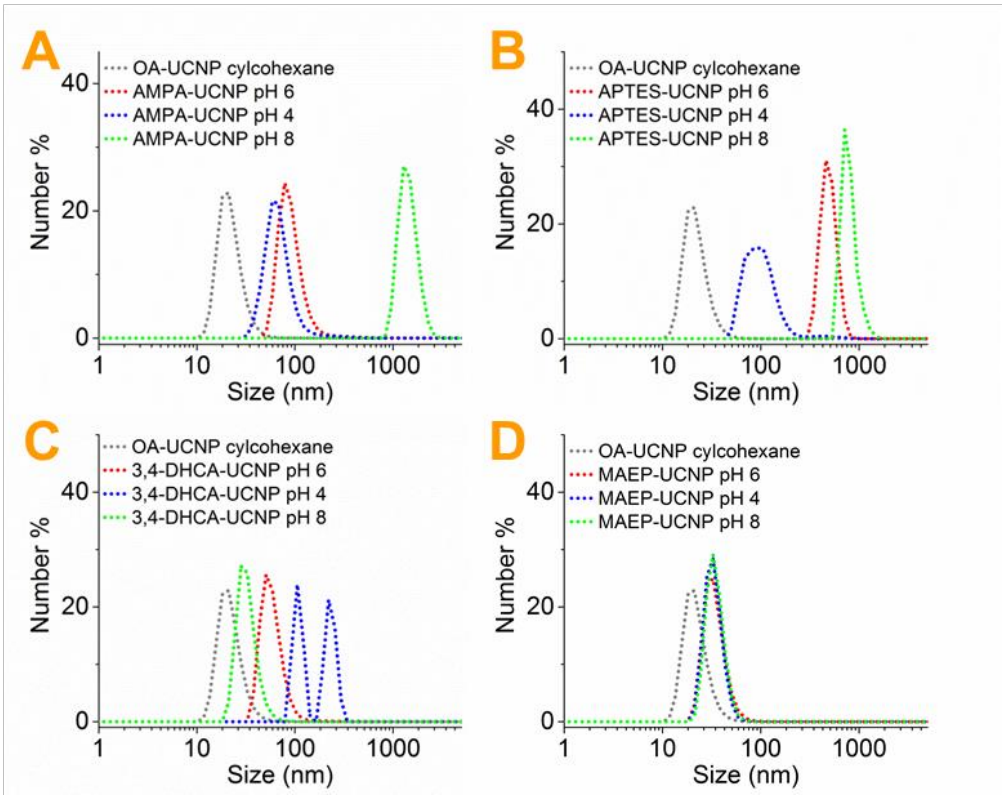

Figure 2.9 Comparative size distribution of AMPA-UCNPs (A), APTES-UCNPs (B), 3,4-DHCA-UCNPs (C), MAEP-UCNPs (D) with OA-UCNPs in water at three pH levels via dynamic light scattering (DLS).

The aforementioned DLS results showed the particles dispersed in water, and there were no other molecules in the solution that could induce competition with the surface ligands. In fact, most bioassays are conducted in weak basic conditions to ensure the bioactivity of the biomolecules. So, here, carboxyl-functionalized nanoparticles, 3,4-DHCA-UCNPs and MEAP-UCNPs, were further studied for the stability in different biological buffers which correspond with the environment of the human body, such as Tris-HCL buffer, SSC buffer and HEPES buffer. Tris-buffer contained 15 mM of tris(hydroxymethyl)aminomethanetris and 150 mM NaCl (pH 7.6); SSC-buffer contained 15 mM of citrate and 150 mM NaCl (pH 7.0); HEPES buffer contained 15 mM 4-(2-Hydroxyethyl)piperazine-1-ethanesulfonic acid and 150 mM NaCl (pH 7.0). Figure 2.10 displayed the DLS result of the 3,4-DHCA-UCNPs and MEAP-UCNPs in three buffers. Particles were dissolved in different buffers and were measured at three time points (0, 12 and 24h), respectively. From the result, 3,4-DHCA-UCNPs dispersed in HEPES and Tris-HCL buffer, the size of the particles increased and did not overlay closely among the three measurements. But for the 3,4-DHCA-UCNPs dispersed in SSC buffer, the dynamic size of the particles at three time points did not change and the distribution was very uniform. The comparative study of 3,4-DHCA-UCNPs in three buffers, indicating that the optimal condition of 3,4-DHCA-UCNPs in bio-application was in SSC buffer. On the other hand, for MEAP-UCNPs, the dynamic size of the nanoparticles dispersed in all three buffers did not change and size distribution was very uniform as for the high overlap of the three measurements. This systematic investigation of MAEP-UCNPs in three

buffers indicated that this kind ligand-capped nanoparticle was very stable in various ionic liquids under basic condition, and was a potential candidate as nanoprobe in bioassay.

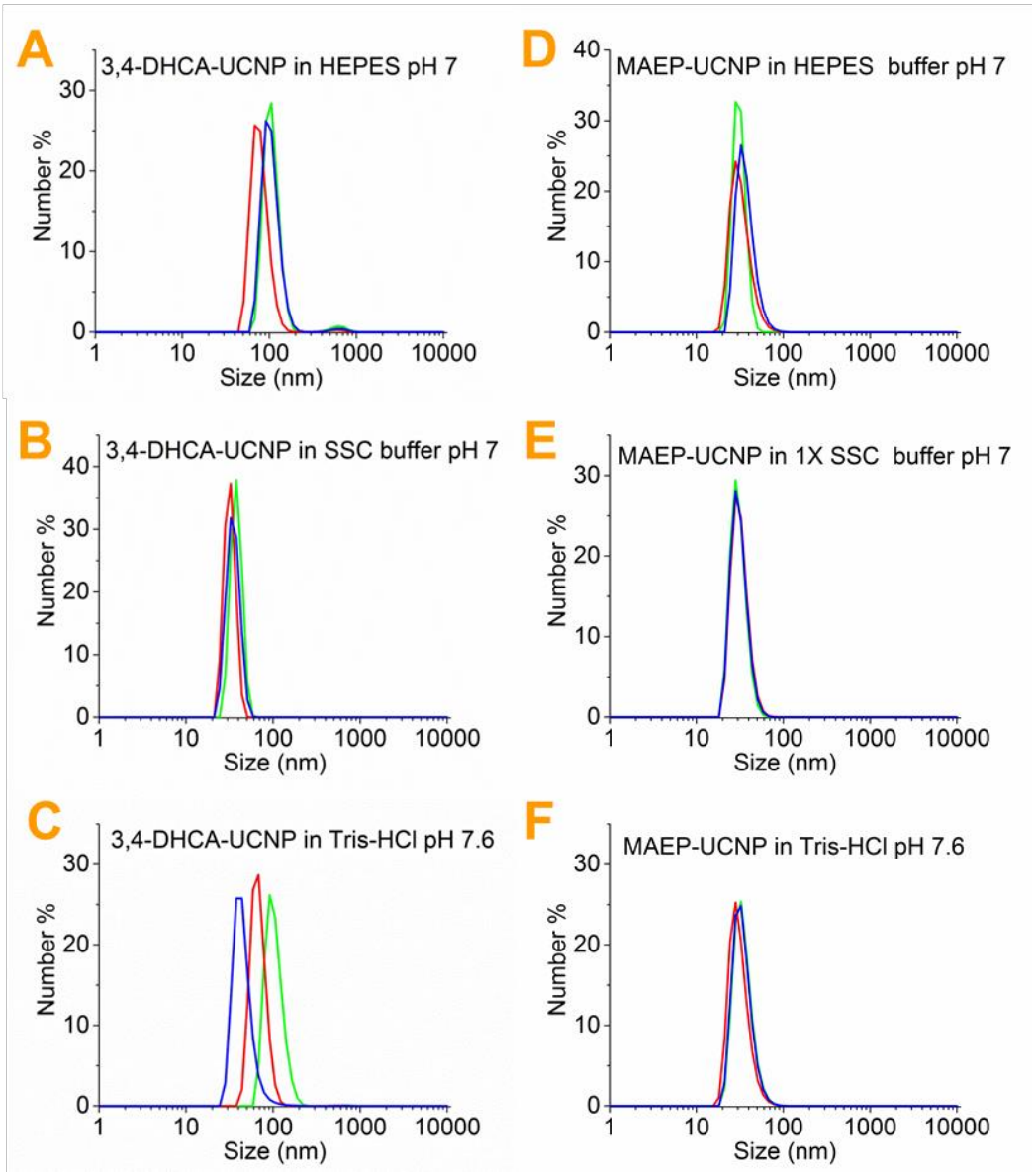

Figure 2.10 Size distribution of 3,4-DHCA-UCNPs (A, B, C) and MAEP-UCNPs (D, E, F) in HEPES buffer, SSC buffer and Tris-HCl buffer, respectively. Red, green and blue lines stand for measurement of particles in buffers at three time points, 0, 12 and 24 h, respectively.

Spectra of upconversion luminescence. The spectra of nanoparticles dissolved in water excited under NIR light at 980 nm were measured and normalized to investigate the effect of the ligands on the ratio of the green (539 nm) to red (653 nm) emission (Figure 2.11A-F). The bare-UCNPs dispersed in water were compared with the OA-UCNPs dispersed in THF, and the spectrum showed the reduction of green emission that can be attributed to the strong vibration between water molecules with surface metal ions[35]. The similar quenching efficiency of the green emission under normalization of red emission occured in all four ligand-capped UCNPs. This spectrum measurement of upconversion luminescence in suspension demonstrated that modification with these four ligands onto the surface of UCNPs had no obvious effect on the ratio between the green and red emission (Figure 2.11G).

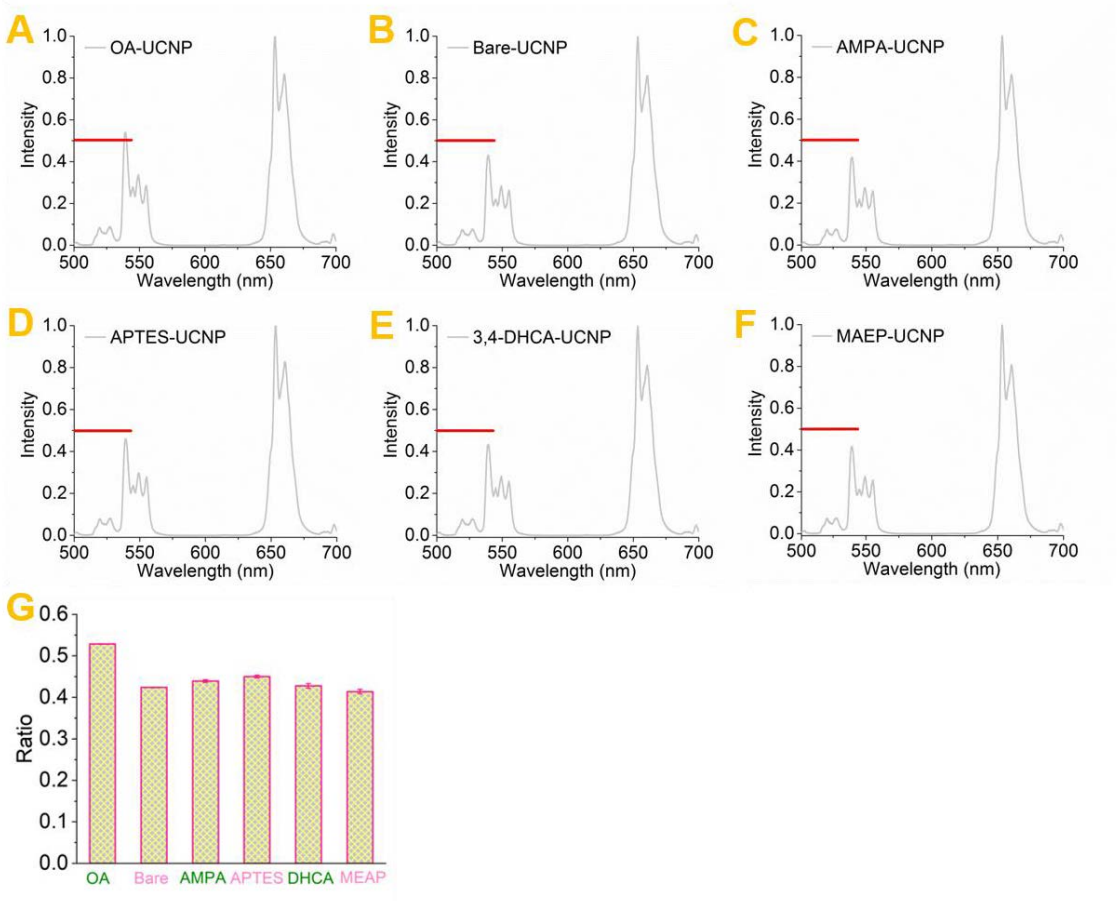

Figure 2.11 Spectra of OA-UCNPs in cyclohexane (A), bare-UCNPs (B), AMPA-UCNPs (C), APTES-UCNPs (D), 3,4-DHCA-UCNPs (E), MAEP-UCNPs (F) in water under homemade spectrometer with 980 nm excitation. The ratio of green (539 nm) to red (653 nm) of upcoversion emission (G). For the statistic analysis of the ratio between green and red emission, there are three replicates for each kind of ligand modified UCNPs.

Luminescence of single UCNP. To investigate the exact influence of the ligand on the luminescence intensity of UCNPs, luminescence of single nanoparticle completely dried was tested. This is a more accurate measurement in comparison with nanoparticles suspension, as it is difficult to make the concentration exactly equal for each ligand-decorated UCNPs, and also, water molecules have been confirmed to have an influence on the upconversion luminescence. These two factors may result in inaccurate testing outcomes. Thus, particles were dissolved in water under extreme dilution and dropped on the cover slide, and then measured under homebuilt microscopy with 980 nm until the sample was completely dried out. Compared with the luminescence of OA-UCNPs, all four hydrophilic ligand-capped UCNPs demonstrated severely reduced luminescence, and in particular MAEP-UCNPs sample. The upconversion luminescence of MAEP-UCNP was quenched about fifty percent compared with that of OA-UCNP (Figure 2.12). It was unclear about the cause of the upconversion quenching, as for all four hydrophilic ligand-capped UCNPs plus hydrophobic OA-UCNPs, the reagents were completely evaporated, so the quenching should be attributed to the ligands. However, the mechanism of different quenching efficiency of each ligand is unrevealed, and still under investigation.

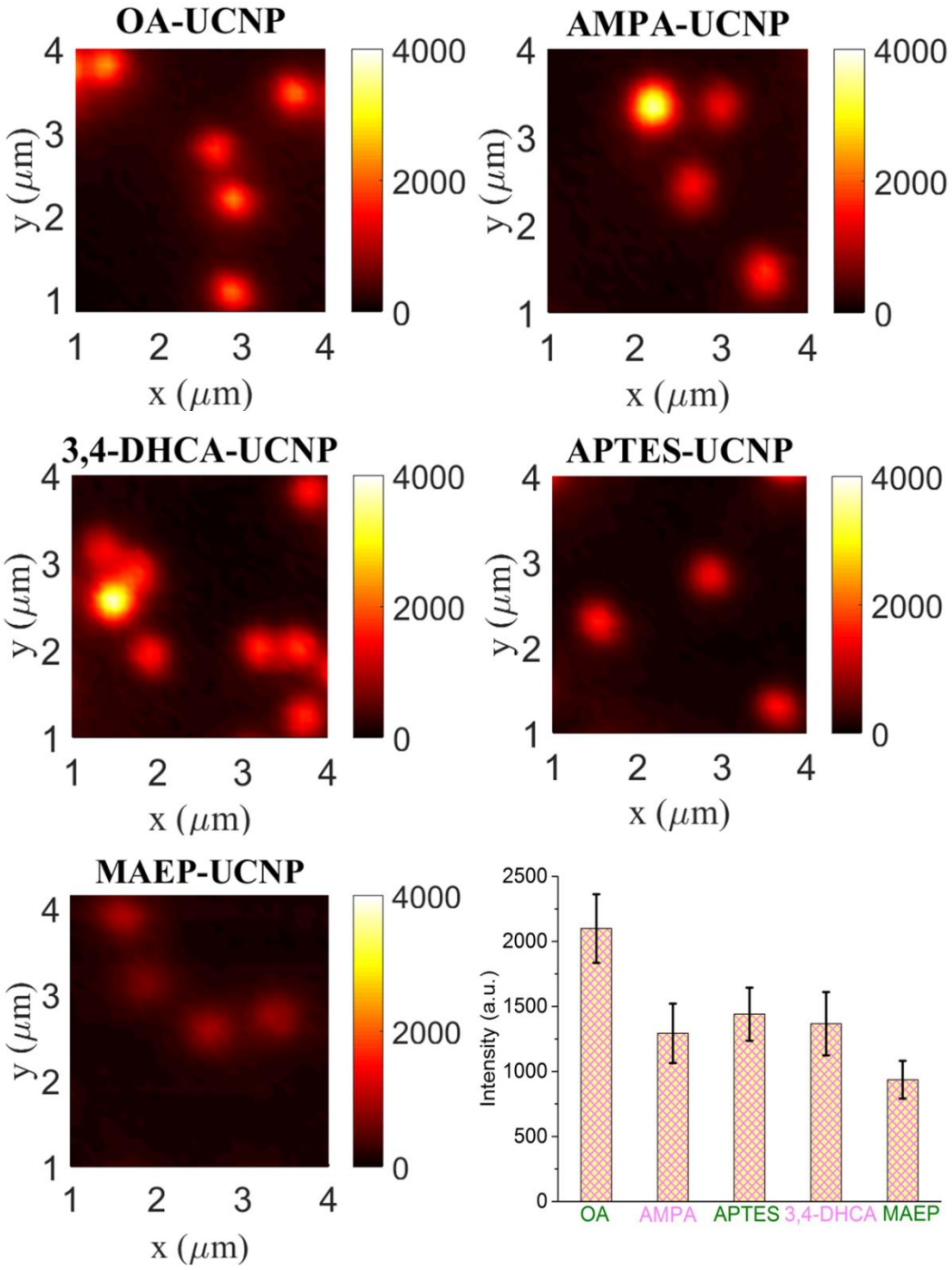

Figure 2.12 Luminescence intensity measurement of single nanoparticle for OA-UCNP, AMPA-UCNP, APTES-UCNP, 3,4-DHCA-UCNP and MEAP-UCNP, and the average intensity value of twenty particles for each kind of ligand-UCNP.

2.3.4 Cytotoxicity Assay of Hydrophilic Ligand-capped UCNPs

Trypan-blue viability test was applied to evaluate the viability of CHO-K1 cells incubated with each of the four ligand-capped hydrophilic UCNPs at 37°C with 5% CO_2 at concentrations of 10 ug/ml or 100 ug/ml for 24 h, 48 h and 72 h. Trypan-blue is a small fluorescent dye, it can pass through the cell membrane of damaged or dead cells only. As particles dissociated at low concentration, 2 mM of NaF was kept in the media to provide enough F^- when incubating the particles with cells in order to prevent the dissociation[36]. The obtained results demonstrated that the viability of the CHO-K1 cells remained unaffected by exposure to the four ligand-capped UCNPs at a concentration of 10 ug/ml for as long as 72 h (Figure 2.13A), and the proliferation of the cells almost followed an exponential growth pattern (Figure 2.13C). For MAEP-UCNPs, even the concentration of the particles was increased 10 times to 100 ug/ml for incubated with CHO-K1, cell viability and proliferation were not noticeably changed compared with the control. However, once the cells were incubated with AMPA-UCNPs, APTES-UCNPs and DHCA-UCNPs at 100 ug/ml, the cell viability gradually decreased (Figure 2.13B) over time and the cell proliferation was also inhibited (Figure 2.13D). For DHCA-UCNPs incubated with cells, after 72 h, the cell viability was reduced to only 54%, and the total cell number was approximately nine (9) times lower than the control group. Particles incubated with DHCA were regarded as the most cytotoxic amongst all four ligand molecules. For AMPA-UCNP and APTES-UCNP, the cell viability of CHO-K1 following incubation with the particles for 72 h, was 75% and 82%, respectively. The total CHO-K1 cell number following incubation with AMPA- and APTES-UCNPs for 72 h was approximately four and five times lower than that of untreated cells. T-test analysis was applied to statistically compare the control group with each assay group at 72 h. Both the cell viability and cell proliferation in the three assay groups (AMPA-, APTES, DHCA-

UCNP) showed a statistically significant difference from the control group after incubation for 72 h. The result was clear to demonstrate that MAEP-UCNPs were cell friendly at both high and low concentrations. However, AMPA-UCNPs, APTES-UCNPs and DHCA-UCNPs were cell friendly only at low concentrations, and they showed cytotoxicity at high concentrations.

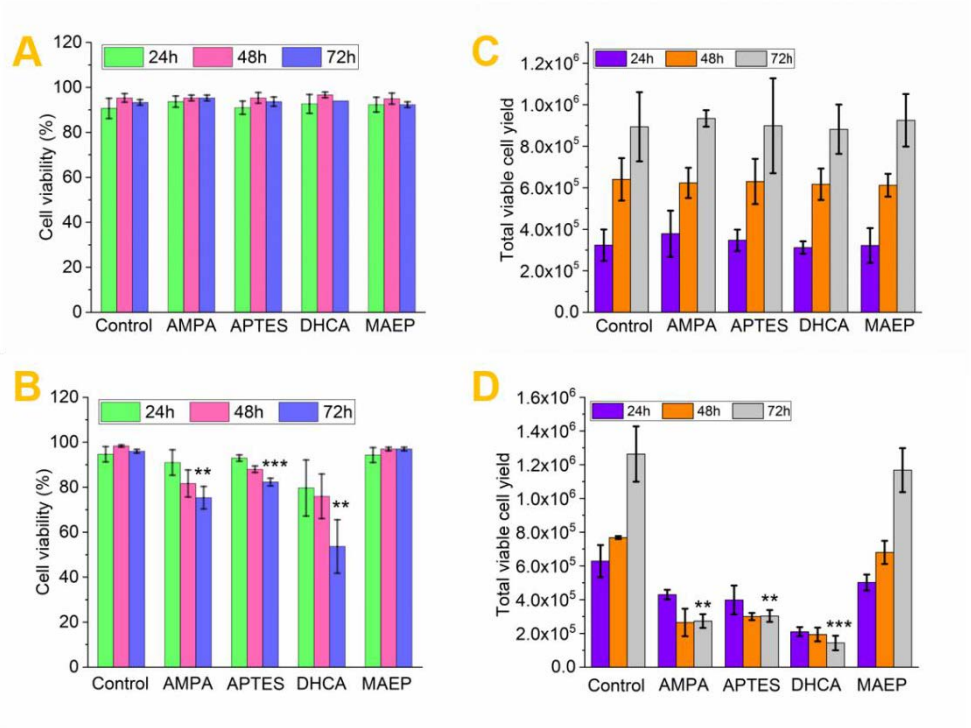

Figure 2.13 Cytotoxicity investigation of ligand-UCNPs at 10 ug/ml and 100 ug/ml incubated with CHO-K1 cells at 37℃ under 5% CO_2, for 24 h, 48 h and 72 h. Cell viability testing by trypan-blue method at 10 ug/ml (A) and 100 ug/ml (B); Cell proliferation testing at 10 ug/ml (C) and 100 ug/ml (D). Each data point was represented as mean ± SD from triplicate trials.

2.3.5 Non-specific Cellular Uptake of Hydrophilic Ligand-capped UCNPs

AMPA-UCNPs, APTES-UCNPs and DHCA-UCNPs demonstrated higher cellular uptake than MAEP-UCNPs, and more nanoparticles were trapped within the cell cytoplasm when incubated with 100 ug/ml compared with the 10 ug/ml samples (Figure 2.14). The result of the cellular uptake correlated with the result of the cytotoxicity assay, indicating that cellular uptake was increased at high doses of nanoparticles for AMPA-UCNPs, APTES-UCNP and DHCA-UCNPs, leading to reduced cell viability and prohibited proliferation. At first, there were no visible MAEP-UCNPs associated with CHO-K1 cells at same measurement condition with other three groups, but upon increasing the acquisition gain value on the microscope system during measurement, some single MAEP-UCNP in the cells were observed and some single particles were also seen to localize within or close to cell nucleus (Figure 2.15). This result of non-specific cellular uptake of four ligand-capped UCNPs investigation, was to some extent related with the particles stability and dispersity modified with different surface ligands. Besides MAEP-UCNPs, the other three particles were easier to aggregate in such complex condition of cell culture media, which increased the chance of contact with cells. On the other hand, the low level of cellular uptake of MAEP-UCNP showed its potential in bioimaging application to achieve a relatively accurate and specific detection.

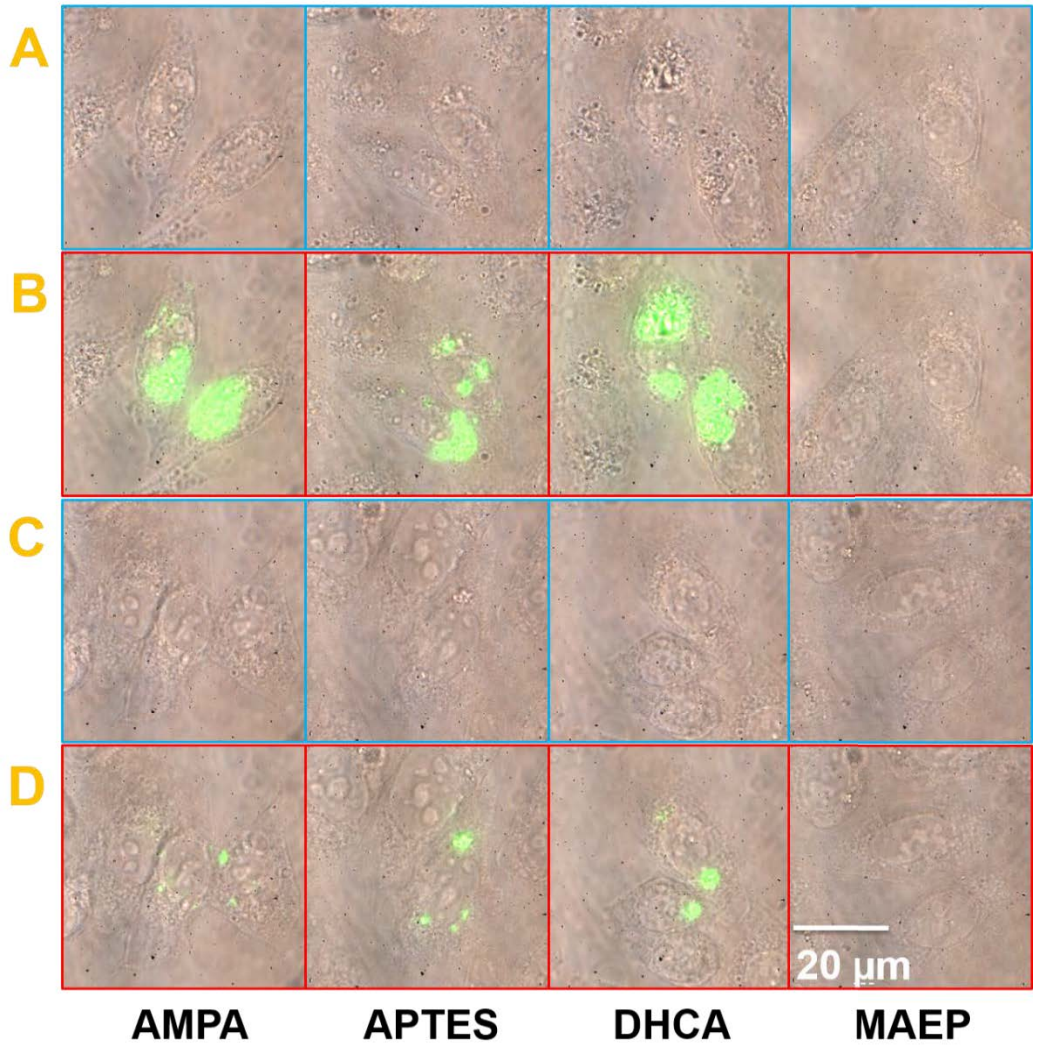

Figure 2.14 Fluorescence imaging of CHO-K1 cells after incubated with ligand-UCNPs in cell culture medium at 100 ug/ml (A, B) and 10 ug/ml (C, D) at 37℃ under 5% CO_2 for 24 h excited by 980 nm. Bright field (A, C) and overlay (B, D). The gain value is 7.

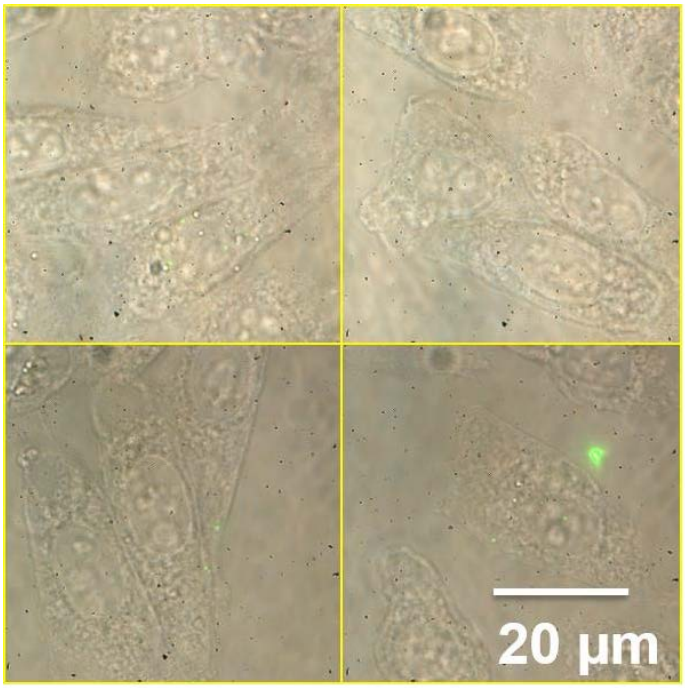

Figure 2.15 Fluorescence imaging of CHO-K1 cells after incubation with MAEP-UCNPs at 37℃ under 5% CO_2 for 24 h at 100 ug/ml excited by 980 nm. The gain value is 26.

In general, taking the main characteristics into consideration, including colloidal stability in water and buffer, as well as biocompatibility (cytotoxicity and non-specific cellular uptake), the best molecule for ligand exchange of UCNPs is MAEP. This outcome coincides with our prediction. MAEP consists of phosphate group, PEG linker and carboxyl group: phosphate group takes an important role to bind with lanthanide ions, to compete with other molecules; PEG linker is an inevitable section to keep the particles monodisperse in various conditions, even in comprehensive cell culture medium; carboxyl group, as functional group with negative charge for further conjugation is prior to amino group with positive charge, especially in basic condition. However, similar structure of MAEP with amino as functional group, was not investigated in this chapter. It is hypothesised that MAEP constructed as phosphate-PEG-NH_2 will also perform as

well as phosphate-PEG-COOH, if the PEG linker takes the most responsibility of the excellent colloidal stability of the particles. In that case, two kinds of di-block co-polymer sharing same construction with either carboxyl or amino functional group will provide broader bioconjugation methods, and the very stable modified-UCNPs can be not only used for bimolecular testing in vitro, but also tracking and therapy in vivo.

2.4 Conclusion

In summary, in this chapter, hydrophilic UCNPs capped with four molecules separately *via* a one-step ligand exchange surface modification process was systematically investigated. MAEP-UCNPs were found to perform the best in terms of their water/aqueous stability and bio-compatibility owing to the strong binding affinity of the phosphonate group and negatively charged carboxyl group, and the most importantly inclusion of stealth property of PEG-derived groups. The amino-functional UCNPs, namely AMPA-UCNPs and APTES-UCNPs, were found to remain monodispersed only in acidic condition due to their positive charge. 3,4-DHCA-UCNPs, was a good choice for bio-applications in basic water with sodium salt, but for aqueous buffers containing other small molecules, it showed instability. For the investigation of nanoparticles interacted with cells, MAEP-UCNPs were found to be most cell friendly, while the other three nanoparticles were cytotoxic at 100 ug/ml. This cytotoxicity result was further demonstrated relative to the cellular uptake level. It is also worth to mention that, even though MAEP-UCNPs demonstrated proper water colloidal property, the upconversion luminescence in fact was severely quenched. However, a number of reports in the literature indicated that the quenching could be eliminated by core-shell structure of the UCNP during synthesis[27]. Only four ligands were used in this work, but the protocol

established here can serve as a good guide for the assessment of the surface modification of UCNPs for subsequent bio-applications.

As surface modification of UCNPs *via* one-step ligand exchange with homemade *POEGA-b-PMAEP* polymers (MAEP-UCNPs) is a robust method to produce hydrophilic, stable and biocompatible UCNPs for bio-application. This method were used in the next two chapters for bioassays.

2.5 References

[1] Chen, Y., Duong, H., Wen, S., Mi, C., Zhou, Y., Shimoni, O., Valenzuela, S. M. & Jin, D. Exonuclease III-Assisted Upconversion Resonance Energy Transfer in a Wash-Free Suspension DNA Assay. *Analytical Chemistry* 90(1). 663-668 **(2018)**.

[2] Gu, B., Zhou, Y., Zhang, X., Liu, X., Zhang, Y., Marks, R., Zhang, H., Liu, X. & Zhang, Q. Thiazole Derivative-Modified Upconversion Nanoparticles for Hg^{2+} Detection in Living Cells. *Nanoscale* 8, 276-282 **(2016)**.

[3] Liu, Q., Sun, Y., Yang, T., Feng, W., Li, C. & Li, F. Sub-10 nm Hexagonal Lanthanide-Doped $NaLuF_4$ Upconversion Nanocrystals for Sensitive Bioimaging in Vivo. *Journal of the American Chemical Society* 133, 17122-17125 **(2011)**.

[4] Mader, H. S., Kele, P., Saleh, S. M. & Wolfbeis, O. S. Upconverting Luminescent Nanoparticles for Use in Bioconjugation and Bioimaging. *Current Opinion in Chemical Biology* 14, 582-596 **(2010)**.

[5] Zhao, J., Jin, D., Schartner, E. P., Lu, Y., Liu, Y., Zvyagin, A. V., Zhang, L., Dawes, J. M., Xi, P. & Piper, J. A. Single-Nanocrystal Sensitivity Achieved by Enhanced Upconversion Luminescence. *Nature Nanotechnology* 8, 729 **(2013)**.

[6] Chen, G., Shen, J., Ohulchanskyy, T. Y., Patel, N. J., Kutikov, A., Li, Z., Song, J., Pandey, R. K., Ågren, H. & Prasad, P. N. (α-$NaYbF_4$:Tm^{3+})/CaF_2 Core/Shell Nanoparticles with Efficient near-Infrared to near-Infrared Upconversion for High-Contrast Deep Tissue Bioimaging. *ACS Nano* 6, 8280-8287 **(2012)**.

[7] Jayakumar, M. K. G., Idris, N. M. & Zhang, Y. Remote Activation of Biomolecules in Deep Tissues Using Near-Infrared-to-UV Upconversion Nanotransducers. Proceedings of the National Academy of Sciences 109, 8483-8488 (**2012**).

[8] Wang, F. & Liu, X. Upconversion Multicolor Fine-Tuning: Visible to near-Infrared Emission from Lanthanide-Doped $NaYF_4$ Nanoparticles. *Journal of the American Chemical Society* 130, 5642-5643 **(2008)**.

[9] Lu, Y., Zhao, J., Zhang, R., Liu, Y., Liu, D., Goldys, E. M., Yang, X., Xi, P., Sunna, A. & Lu, J. Tunable Lifetime Multiplexing Using Luminescent Nanocrystals. *Nature Photonics* 8, 32-36 **(2014)**.

[10] Muhr, V., Wilhelm, S., Hirsch, T. & Wolfbeis, O. S. Upconversion Nanoparticles: From Hydrophobic to Hydrophilic Surfaces. *Accounts of Chemical Research* 47, 3481-3493 **(2014)**.

[11] Zhou, H. P., Xu, C. H., Sun, W. & Yan, C. H. Clean and Flexible Modification Strategy for Carboxyl/Aldehyde-Functionalized Upconversion Nanoparticles and Their Optical Applications. *Advanced Functional Materials* 19, 3892-3900 **(2009)**.

[12] Wang, M., Mi, C., Zhang, Y., Liu, J., Li, F., Mao, C. & Xu, S. NIR-Responsive Silica-Coated $NaYbF_4$:Er/Tm/Ho Upconversion Fluorescent Nanoparticles with Tunable Emission Colors and Their Applications in Immunolabeling and Fluorescent Imaging of Cancer Cells. *The Journal of Physical Chemistry C* 113, 19021-19027 **(2009)**.

[13] Lü, Q., Guo, F., Sun, L., Li, A. & Zhao, L. Silica-/Titania-Coated Y_2O_3:Tm^{3+}, Yb^{3+} Nanoparticles with Improvement in Upconversion Luminescence Induced by Different Thickness Shells. *Journal of Applied Physics* 103, 123533 **(2008)**.

[14] Duong, H., Chen, Y., Tawfik, S. A., Wen, S., Parviz, M., Ford, M. J., Shimoni, O. & Jin, D. Systematic Investigation of Functional Ligands for Colloidal Stable Upconversion Nanoparticles. *RSC Advances* 8 (9), 4842-4849 **(2018)**.

[15] Lu, J., Chen, Y., Liu, D., Ren, W., Lu, Y., Shi, Y., Piper, J., Paulsen, I. & Jin, D. One-Step Protein Conjugation to Upconversion Nanoparticles. *Analytical Chemistry* 87, 10406-10413 **(2015)**.

[16] Li, L. L., Zhang, R., Yin, L., Zheng, K., Qin, W., Selvin, P. R. & Lu, Y. Biomimetic Surface Engineering of Lanthanide-Doped Upconversion Nanoparticles as Versatile Bioprobes. *Angewandte Chemie International Edition* 51, 6121-6125 **(2012)**.

[17] Liang, S., Zhang, X., Wu, Z., Liu, Y., Zhang, H., Sun, H., Sun, H. & Yang, B. Decoration of up-Converting $NaYF_4$:Yb, Er (Tm) Nanoparticles with Surfactant

Bilayer. A Versatile Strategy to Perform Oil-to-Water Phase Transfer and Subsequently Surface Silication. *CrystEngComm* 14, 3484-3489 **(2012)**.

[18] Stöber, W., Fink, A. & Bohn, E. Controlled Growth of Monodisperse Silica Spheres in the Micron Size Range. *Journal of Colloid and Interface Science* 26, 62-69 **(1968)**.

[19] Jiang, G., Pichaandi, J., Johnson, N. J., Burke, R. D. & Van Veggel, F. C. An Effective Polymer Cross-Linking Strategy to Obtain Stable Dispersions of Upconverting $NaYF_4$ Nanoparticles in Buffers and Biological Growth Media for Biolabeling Applications. *Langmuir* 28, 3239-3247 **(2012)**.

[20] Li, L. L., Wu, P., Hwang, K. & Lu, Y. An Exceptionally Simple Strategy for DNA-Functionalized up-Conversion Nanoparticles as Biocompatible Agents for Nanoassembly, DNA Delivery, and Imaging. *Journal of the American Chemical Society* 135, 2411-2414 **(2013)**.

[21] Liu, Y., Purich, D. L., Wu, C., Wu, Y., Chen, T., Cui, C., Zhang, L., Cansiz, S., Hou, W. & Wang, Y. Ionic Functionalization of Hydrophobic Colloidal Nanoparticles to Form Ionic Nanoparticles with Enzymelike Properties. *Journal of the American Chemical Society* 137, 14952-14958 **(2015)**.

[22] Li, R., Ji, Z., Dong, J., Chang, C. H., Wang, X., Sun, B., Wang, M., Liao, Y.-P., Zink, J. I. & Nel, A. E. Enhancing the Imaging and Biosafety of Upconversion Nanoparticles through Phosphonate Coating. *ACS Nano* 9, 3293-3306 **(2015)**.

[23] Liu, Y., Chen, T., Wu, C., Qiu, L., Hu, R., Li, J., Cansiz, S., Zhang, L., Cui, C. & Zhu, G. Facile Surface Functionalization of Hydrophobic Magnetic Nanoparticles. *Journal of the American Chemical Society* 136, 12552-12555 **(2014)**.

[24] Hojo, D., Togashi, T., Iwasa, D., Arita, T., Minami, K., Takami, S. & Adschiri, T. Fabrication of Two-Dimensional Structures of Metal Oxide Nanocrystals Using Si Substrate Modified with 3,4-Dihydroxyhydrocinnamic Acid. *Chemistry of Materials* 22, 1862-1869 **(2010)**.

[25] Liu, Y., Li, Y., Li, X. M. & He, T. Kinetics of (3-Aminopropyl) Triethoxylsilane (APTES) Silanization of Superparamagnetic Iron Oxide Nanoparticles. *Langmuir* 29, 15275-15282 **(2013)**.

[26] Kim, J. Investigation of the Formation and Structure of Aptes Films on Silicon Substrates. *Pike Technologies.* 4, 47-49 **(2010)**.

[27] Ma, C., Xu, X., Wang, F., Zhou, Z., Liu, D., Zhao, J., Guan, M., Lang, C. I. & Jin, D. Optimal Sensitizer Concentration in Single Upconversion Nanocrystals. *Nano Letters* 17, 2858-2864 **(2017)**.

[28] Zhao, J., Lu, Z., Yin, Y., McRae, C., Piper, J. A., Dawes, J. M., Jin, D. & Goldys, E. M. Upconversion Luminescence with Tunable Lifetime in $NaYF_4$:Yb, Er Nanocrystals: Role of Nanocrystal Size. *Nanoscale* 5, 944-952 **(2013)**.

[29] Ferguson, C. J., Hughes, R. J., Nguyen, D., Pham, B. T., Gilbert, R. G., Serelis, A. K., Such, C. H. & Hawkett, B. S. Ab Initio Emulsion Polymerization by RAFT-Controlled Self-Assembly. *Macromolecules* 38, 2191-2204 **(2005)**.

[30] Wu, L., Zhang, Y., Yang, G., Zhang, S., Yu, L. & Zhang, P. Tribological Properties of Oleic Acid-Modified Zinc Oxide Nanoparticles as the Lubricant Additive in Poly-Alpha Olefin and Diisooctyl Sebacate Base Oils. *RSC Advances* 6, 69836-69844 **(2016)**.

[31] Chen, Z., Chen, H., Hu, H., Yu, M., Li, F., Zhang, Q., Zhou, Z., Yi, T. & Huang, C. Versatile Synthesis Strategy for Carboxylic Acid-Functionalized Upconverting Nanophosphors as Biological Labels. *Journal of the American Chemical Society* 130, 3023-3029 **(2008)**.

[32] Tansub, W., Tuitemwong, K., Limsuwan, P., Theparoonrat, S. & Tuitemwong, P. Synthesis of Antibodies-Conjugated Fluorescent Dye-Doped Silica Nanoparticles for a Rapid Single Step Detection of Campylobacter Jejuni in Live Poultry. *Journal of Nanomaterials* 2012, 60 **(2012)**.

[33] Hachani, R., Lowdell, M., Birchall, M., Hervault, A., Mertz, D., Begin-Colin, S. & Thanh, N. T. K. Polyol Synthesis, Functionalisation, and Biocompatibility Studies of Superparamagnetic Iron Oxide Nanoparticles as Potential Mri Contrast Agents. *Nanoscale* 8, 3278-3287 **(2016)**.

[34] Togashi, T., Takami, S., Kawakami, K., Yamamoto, H., Naka, T., Sato, K., Abe, K. & Adschiri, T. Continuous Hydrothermal Synthesis of 3,4-Dihydroxyhydrocinnamic Acid-Modified Magnetite Nanoparticles with Stealth-Functionality against Immunological Response. *Journal of Materials Chemistry* 22, 9041-9045 **(2012)**.

[35] Arppe, R., Hyppänen, I., Perälä, N., Peltomaa, R., Kaiser, M., Würth, C., Christ, S., Resch-Genger, U., Schäferling, M. & Soukka, T. Quenching of the Upconversion Luminescence of $NaYF_4:Yb^{3+}$, Er^{3+} and $NaYF_4:Yb^{3+}$, Tm^{3+} Nanophosphors by Water: The Role of the Sensitizer Yb^{3+} in Non-Radiative Relaxation. *Nanoscale* 7, 11746-11757 **(2015)**.

[36] Plohl, O., Kraft, M., Kovač, J., Belec, B., Ponikvar-Svet, M., Würth, C., Lisjak, D. & Resch-Genger, U. Optically Detected Degradation of $NaYF_4$:Yb, Tm-Based

Upconversion Nanoparticles in Phosphate Buffered Saline Solution. *Langmuir* 33, 553-560 **(2017)**.

CHAPTER 3

Exonuclease III-assisted Upconversion Resonance Energy Transfer in a Wash-Free Suspension DNA Assay

Abstract: Sensitivity is the key in optical detection of low-abundant analytes, such as circulating RNA or DNA. The enzyme Exonuclease III (Exo III) is a useful tool in this regard; its ability to recycle target DNA molecules results in markedly improved detection sensitivity. Lower limits of detection may be further achieved if the detection background of auto-fluorescence can be removed. In this chapter,we report an ultrasensitive and specific method to quantify trace amounts of DNA analytes in a wash-free suspension assay. In the presence of target DNA, the Exo III recycles the target DNA by selectively digesting the dye-tagged sequence-matched probe DNA strand only, so that the amount of free dye removed from the probe DNA is proportional to the number of target DNAs. Remaining intact probe DNAs are then bound onto upconversion nanoparticles (energy donor), which allows for upconversion luminescence resonance energy transfer (LRET) that can be used to quantify the difference between the free dye and tagged dye (energy acceptor). This scheme simply avoids both auto-fluorescence under infrared excitation and many tedious washing steps, as the free dye molecules are physically located away from the nanoparticle surface, and as such they remain “dark” in suspension. Compared to alternative approaches requiring enzyme-assisted amplification on the nanoparticle surface, introduction of probe DNAs onto nanoparticles only after DNA hybridization

and signal amplification steps, effectively avoids steric hindrance. *Via* this approach, we have achieved a detection limit of 15 pM in LRET assays of human immunodeficiency viral DNA.

Key words: Exonuclease III, wash-free, suspension assay, upconversion nanoparticles, luminescence resonance energy transfer.

3.1 Introduction

Rapid detection of low-abundance, specific DNA molecules becomes increasingly important to enable in-depth studies and medical diagnosis of genetic diseases. Optical biosensors for DNA detection, including colorimetric[1] and fluorescent[2,3] methods, have been widely used because of their high detection selectivity and cost-efficiency. However, detection sensitivity is still limited due to the high background interference from auto-fluorescence from bio-samples. In addition, many fluorophores suffer serious photobleaching which leads to the poor reproducibility of the signal measurement.

Upconversion nanoparticles (UCNPs)[4,5] have emerged as a new generation of optical probes for diminishing the interference of auto-fluorescence background, as they stepwise absorb two or more near-infrared photons, and emit long-lifetime anti-Stokes luminescence in the visible spectrum with narrow emission bands. Each single UCNP usually contains thousands of photon sensitizers and hundreds of trivalent lanthanide ions (Ln^{3+}) as photon activators within an inorganic crystalline host matrix, and therefore deliver bright luminescence in the darkness *via* either anti-Stokes spectrum filtering or time-gated detection. Morever, distinct from conventional organic dyes, UCNPs provide high optical stablity for better experimetal reproducibility, and also demonstrate good

biocompatibility and low cytotoxicity[6], as robust molecular probes for biological imaging[7,8] and molecular detection[9-11].

Using UCNPs as the donor in luminescence resonance energy transfer (LRET) systems has been broadly reported in the area of DNA detection[12-15]. Replacing the organic fluorophores as classic energy donors[16] by UCNPs, upconversion LRET assays are now more reliable due to low levels of auto-fluorescence background[17]. Moreover, due to the narrow emission bands, both the donor's and acceptor's emissions have well-defined spectrum windows with minimal levels of cross-talk for quantitative distance-dependent analysis through monitoring the decrease of the donor's intensity and increase of the acceptor's intensity[18,19]. Most of the existing DNA detection assays are based on a sandwich-type hybridization that only allows one DNA probe to detect one target DNA analyte, which holds back this technology from achieving higher detection sensitivity.

Highly sensitive detection of low quantities of target DNA analytes, typically requires direct amplification of the target nucleic acids by use of polymerase chain reaction (PCR)[20,21] to substantially enhance signal output. However, this kind of amplification requires costly equipment, highly trained personnel, along with the requirement of precise temperature control and prevention of primer dimer formation. This makes it difficult to achieve widespread application of this technology. To overcome these challenges, various of enzyme-free[22,23] or enzyme-assisted[1,15,24,25] target-triggered signal amplification techniques, where the replication of target-dependent complexes for continuous signal generation only under isothermal conditions have been developed over the years. Target-triggered signal amplification assisted by Exonuclease III (Exo III) enzyme for ultra-sensitive quantitation of DNA has been extensively developed and applied[25-28]. Exo III

has a double-strand specific, non-processive 3'-5' exo-deoxyribonulease activity that produces a step-by-step mononucleotide removal from the 3'-end of the DNA. However, if the 3'-end of the DNA overhangs by more than four bases in length, it can be protected from Exo III activity[29]. Typically, the mononucleotides of designed probe DNA can be stepwise removed without damaging the target DNA. This selective nucleotide digestion feature can be exploited to significantly enhance the limits of detection in DNA assays.

In this study, we introduce the Exo III-assisted target DNA-triggered signal amplification technique to further improve the detection sensitivity and simplicity of upconversion LRET for the detection and quantification of trace amounts of DNA. As illustrated in Figure 3.1, two in-principle schemes were designed and experimentally verified in this study. In both schemes, carboxytetramethyl rhodamine™ (TAMRA™) is used as the acceptor and is conjugated to the 3'-terminus of the single strand probe DNA. It is selected as a suitable dye due to its maximum absorption at 559 nm, which is well matched to the green emission band of erbium doped UCNPs, resulting in its sensitized luminescence emission at 583 nm, where conveniently UCNPs do not luminesce (Figure 3.2). The sequence of probe DNA is designed to completely hybridize with HIV target DNA. Furthermore, its 5'-end is modified with an amine group in order for it to covalently bind onto the surface of UCNPs that have been modified with polymer linkers ending in carboxyl groups. In addition, the length of the probe DNA is designed to allow the target DNA to overhang by six bases from its 3'-end. This is done to ensure the target DNA escapes digestion by Exo III, therefore allowing it to be recycled in the assay and capable of binding to remaining intact, probe DNAs. These modified probe DNAs are referred to as TAMRA-tagged probe DNAs.

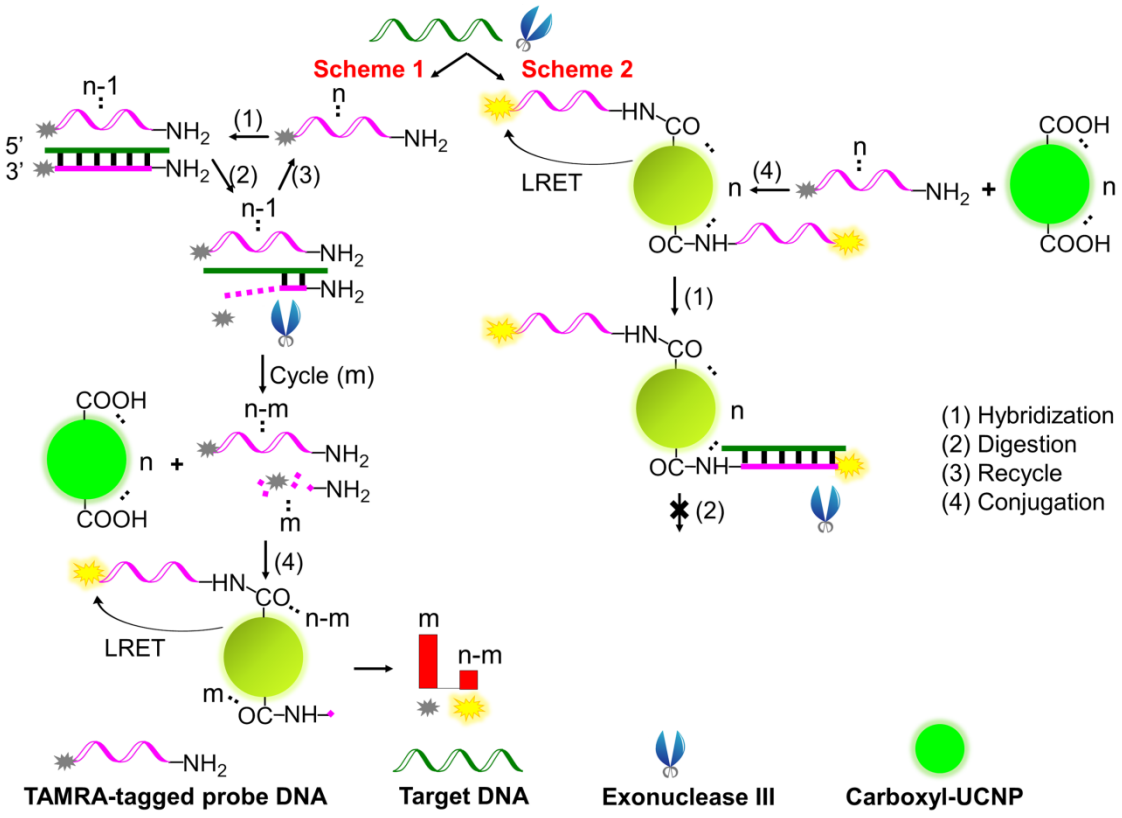

Figure 3.1 Schemas 1 & 2, illustrating the use of Exonuclease III-assisted upconversion resonance energy transfer in a wash-free suspension DNA assay.

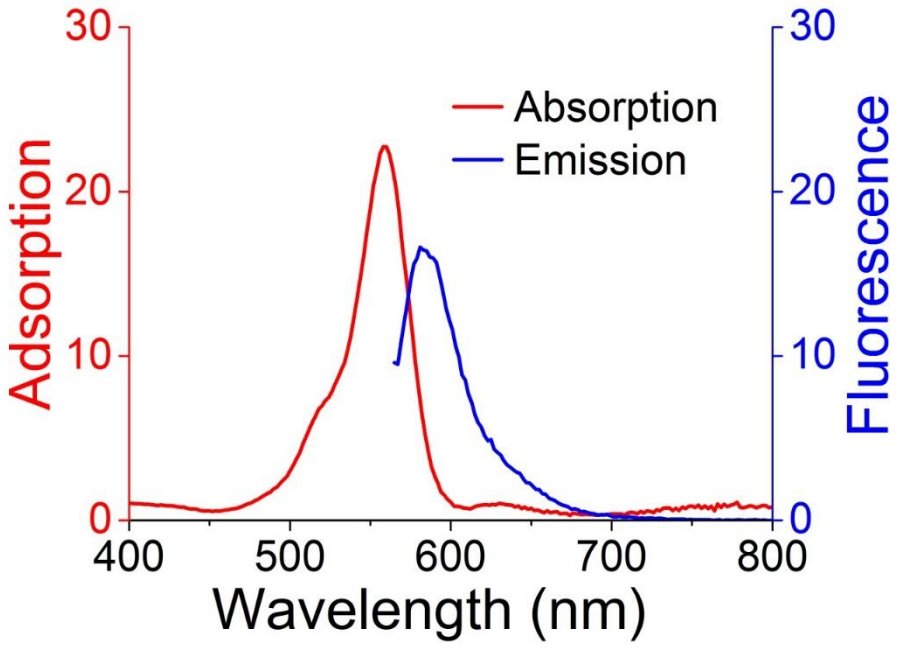

Figure 3.2 The absorption and emission spectra of TAMRA.

Upon hybridization of target DNA to TAMRA-tagged probe DNAs (Figure 3.1, Scheme 1), Exo III recognizes the double-stranded probe-target pairs and selectively digests the TAMRA-tagged probe DNA strand, releasing free-TAMRA. Target DNA remains intact, and is capable of undertaking further rounds of hybridization to TAMRA-tagged probe DNAs. Subsequent addition of EDC-activated carboxyl-UCNPs, results in covalent attachment of the residual full length TAMRA-tagged probe DNAs - *via* their 5' amine group. This in turn results in LRET from the UCNPs to the bound TAMRAs by providing a proportional decrease in luminescence of the UCNPs and an increased fluorescence of the UNCP bound TAMRAs. In contrast, the remaining free TAMRA dye molecules in suspension do not come into close contact with the surface of the UCNPs, contributing no effect to the LRET process. Therefore, the existence of the free TAMRAs in the solution does not influence the result of spectral measurement, eliminating time-consuming and tedious washing steps.

In the case of Scheme 2, the TAMRA-tagged probe DNAs were first conjugated onto UCNPs for efficient LRET, followed by addition of both target DNA and Exo III, designed for signal amplification. However, no obvious change was detected even in the presence of high concentrations of target DNA molecules (Figure 3.3). This comparison experiment confirms Scheme 1 as a simple, reproducible and practical distance-dependent upconversion LRET assay for suspension DNA detection and quantification. In order to meet the distance requirement between UCNP and TAMRA for efficient LRET, we designed relatively short-length probe DNA sequence. As a result, in Scheme 2, short sequence DNA attached to the surface of UCNPs have caused steric hindrance effects, resulting in inhibition and/or failure of enzymatic reactions to proceed on the surface of the UCNPs.

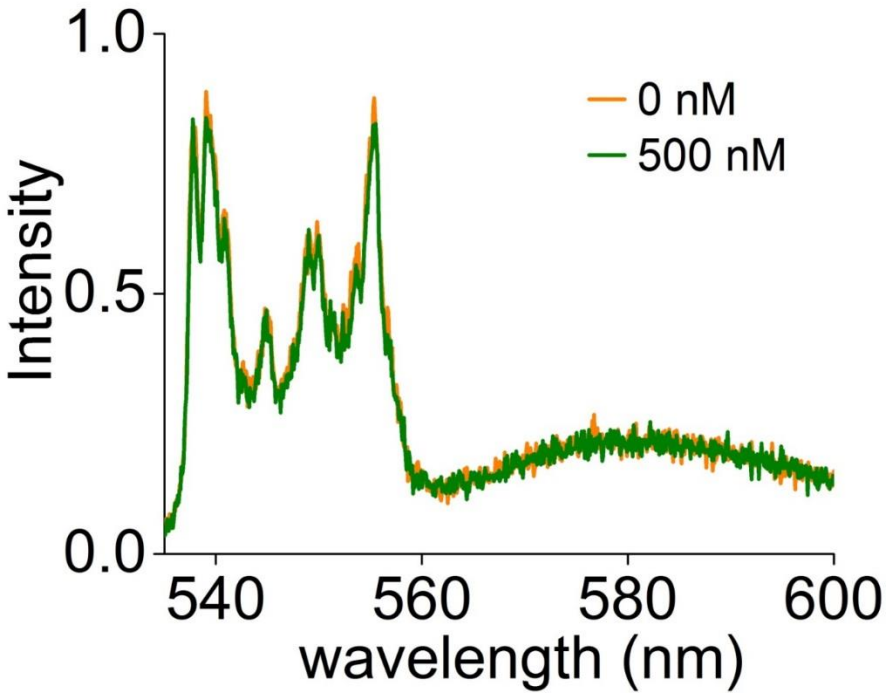

Figure 3.3 Luminescence spectra of TAMRA-UCNPs in Design 2 after Exo III digestion of probe DNA on the surface of UCNPs in the presence of target (0 nM and 500 nM) at 37 ℃ for 4 h.

3.2 Experiments

3.2.1 Materials

Rare-earth chloride hexahydrates used in this work for upconversion nanoparticles (UCNPs) synthesis, including yttrium (III) chloride hexahydrate ($YCl_3 \cdot 6H_2O$, 99.99%), ytterbium chloride hexahydrate ($YbCl_3 \cdot 6H_2O$, 99.99%), and erbium chloride hexahydrate ($ErCl_3 \cdot 6H_2O$, 99.9%), were purchased from Sigma-Aldrich. For polymer synthesis, the chemicals including 2-bromopropionic acid (99%), zinc acetylacetonate hydrate, 4-cyano-4-(phenylcarbonothioylthio)pentanoic acid (97%), ethylene glycol (99%), 1-butanethiol (99%) and poly(ethylene glycol) methyl ether acrylate were purchased from Sigma-Aldrich, and monoacryloxyethyl phosphate from Polysciences, Inc. All other

materials, ammonium fluoride (NH_4F), cyclohexane, methanol, sodium hydroxide (NaOH), acetonitrile, tetrahydrofuran (THF), N-(3-Dimethylaminopropyl)-N′-ethylcarbodiimide hydrochloride (EDC), diethyl ether, 2-(N-Morpholino)ethanesulfonic acid (MES), were purchased from Sigma-Aldrich with analytical grade. Monomer oligo(ethylene glycol) methyl ether acrylate with average Mn of 480 g/ml (OEGA) and monoacryloxyethyl phosphate (MAEP) were used as received. 2,2'-Azobisisobutyronitrile (AIBN) was purified by recrystallization twice from methanol. Exonuclease III (*E.coli*) and NEBuffer 1 were purchased from New England Biolabs Inc. Oligonucleotides were purchased from Integrated DNA Technologies. The sequences of the oligonucleotides use in this work are listed as follows:

Probe DNA: 5'-NH_2-C_6-TTA TTC CAA ATA TCT/TAMK/-3'

HIV target DNA: 5'-AGA AGA TAT TTG GAA TAA CAT GAC-3'

1-base mismatch DNA: 5'-AGA AGA TAT TAG GAA TAA CAT GAC-3'

3-base mismatch DNA: 5'-AGA AGA TAT AAC GAA TAA CAT GAC-3'

Non-match DNA1 (random sequence): 5'-TGT GTG TGT GTG TGT GTG TGT-3'

Non-match DNA2 (HBV sequence): 5'-TTG GCT TTC AGT TAT ATG GAT GTG GTA-3'

3.2.2 Instrumentation

UCNPs were characterized using the FEI Tecnai transmission electron microscope (FEI, U.S.A.) and D8 Discover X-ray diffraction (Bruker, Germany). The synthesized polymers were characterized with Agilent 500 MHz nuclear magnetic resonance (Agilent Technologies, U.S.A.). The hydrodynamic size of upconversion nanoparticles was determined by a zetasizer nano (Malvern, U.K.). The surface ligand measurement was conducted by the Thermo Scientific Nicolet 6700 FTIR spectrometer (Thermo Fisher

Scientific, Australia). The fluorescent spectra of TAMRA were measured using a Cary Eclipse fluorescence spectrophotometer (Agilent, U.S.A.). Upconversion luminescent spectra were measured by an iHR550 imaging spectrometer (Horiba Scientific, U.K.) modified with an external 980 laser (see Figure 2.2). A single mode continuous-wave 980 nm diode laser beam launched through the UV quartz cuvette produced excitation irradiance values of up to 1.36×10^6 W/cm^2 [30].

3.2.3 Synthesis and Surface Modification of $NaYF_4$:Yb, Er UCNPs

UCNPs had been synthesized according to our previously reported method[31]. In a typical experiment, 1 mmol $LnCl_3$ (Ln=Y, Yb, Er) with the molar ratio of 78:20:2 were added to a 50 mL flask containing oleic acid (OA, 6 mL) and 1-octadecene (ODE, 15 mL). The mixture was heated to 160ºC under argon for 30 min to obtain a clear solution and then cooled down to room temperature, followed by the addition of 5 mL methanol solution of NH_4F (4 mmol) and NaOH (2.5 mmol). After stirring for 30 min, the solution was heated to 100ºC for 20 min to remove methanol and 120ºC for 20 min to remove water under argon, followed by heating solution to 300ºC for another 90 min. Finally, the reaction solution was cooled down to room temperature, and nanocrystals were precipitated with ethanol and washed with cyclohexane, ethanol and methanol thrice to get the $NaYF_4$:Yb, Er nanoparticles. UCNPs were dispersed in cyclohexane with the concentration of 20 mg/ml, kept in freezer until usage.

Surface modification of $NaYF_4$:Yb, Er UCNPs was performed via ligand exchange with block copolymer composed of hydrophilic block poly(ethylene glycol) methyl ether acrylate phosphate methacrylate (POEGA-*b*-PMAEP). The synthesis of the POEGA-*b*-PMAEP was following the protocol described in Chapter 2. In typical procedure, 500 ul

of OA-UCNPs (20 mg/mL) kept in cyclohexane, solvent was evaporated to be re-dispersed in THF. Furthermore, OA-UCNPs in THF were mixed with 5 mg of POEGMA-*b*-PMAEP in 2 mL of THF. The reaction was kept mixing overnight, at room temperature. Polymer coated nanoparticles were purified by washing/centrifugation at 14,680 rpm cycles thrice with water to obtain carboxyl-UCNPs. Carboxyl-UCNPs were re-suspended in water at 5 mg/ml.

3.2.4 Optimization of Upconversion LRET DNA Assay

To investigate the optimal ratio of the TAMRA-tagged probe DNAs to UCNPs, by fixing the EDC-activated carboxyl-UCNPs at 1 pmol, different amounts of TAMRA-tagged probe DNAs (1, 2, 5, 10, 20 and 50 pmol) were added into 100 ul of MES buffer.

To investigate the chemical reaction time of carboxyl-UCNPs conjugated with TAMRA-tagged probe DNAs catalyzed *via* EDC, the change of I_{583}/I_{539} was measured under the molar ratio of TAMRA-tagged probe-DNA to UCNPs as 10:1 (10 pmol:1p mol) at different time points (20, 40, 60, 80 and 100 min).

To determine the optimal reaction time for Exo III assisted signal amplification in suspension, TAMRA-tagged probe DNAs (10 pmol), Exo III (10 U) and target DNAs (10 nM = 200 fmol) were incubated in 20 ul of NEBuffer 1 at 37ºC for different reaction time (0, 5, 10, 20, 30, 40, 60, 80, 100 and 120 min), followed by incubation at 70ºC for 20 min to terminate the reaction and then conjugation with activated carboxyl-UCNPs for 1 h at RT.

3.2.5 Detection of HIV DNA Target Based on Upconversion LRET Assay

Mixture of 10 pmol of TAMRA-tagged probe DNAs, 10 U of Exo III, and various concentration of HIV target DNAs (0.025, 0.1, 0.5, 1, 2.5, 5, 10, 25, 50, 100, 250 and 500 nM) in 20 ul of NEBuffer 1 was kept at 37ºC for 1 h in dark, followed by 70ºC for 20 min to terminate the reaction. The final concentration of TAMRA-tagged probe DNAs was 500 nM and that of target DNAs ranged from 0.025 nM to 500 nM.

Conjugation of TAMRA-tagged probe DNAs onto carboxyl-UCNPs was performed according to the protocol of carbodiimide chemistry. The carboxyl-UCNPs were pre-activated by EDC (1000-fold molar ratio to carboxyl-UCNPs) in MES buffer (0.1 M, pH 4.5) with slightly shaking at room temperature for 30 min. The activated carboxyl-UCNPs were centrifuged at 14,680 rpm to remove EDC and re-suspended in MES buffer. The whole reaction of Exo-III assisted signal amplification after termination by heating at 70ºC for 20 min was added into the activated carboxyl-UCNPs (1 pmol) in a final 100 ul of MES buffer. The reaction was slightly shaken at room temperature for 1 h, in dark place to protect TAMRA fluorescence.

3.3 Results and Discussion

Synthesized in organic solvent, UCNPs are hydrophobic due to their capping by surfactant ligands such as oleic acids (OA-UCNPs). Therefore, subsequent surface modification to generate a hydrophilic layer is a prerequisite to yield well-dispersed nanoparticles in aqueous media for bioanalytical applications. In this work, OA-UCNPs were transferred into an aqueous environment *via* a ligand-exchange and carboxyl-functionalization (carboxyl-UCNPs) by POEGA-*b*-PMAEP[32]. For upconversion LRET, carbodiimide crosslinker chemistry was further applied for the conjugation of carboxyl-

UCNPs with TAMRA-tagged probe DNAs (TAMRA-UCNPs) under EDC catalysis after the enzymatic digestion step.

3.3.1 Characterization

X-ray powder diffraction (XRD), high-transmission electron microscopy (HRTEM), Fourier transform infrared (FTIR) spectroscopy, dynamic light scattering (DLS), transmission electron microscopy (TEM), were used to characterize each step of the surface modification and functionalization of the UCNPs. XRD results of the OA-UCNPs synthesized in this experiment corresponded with the standard pattern of the hexagonal phase $NaYF_4$ (Figure 3.4A). The high-transmission electron microscopy (HRTEM) image of OA-UCNPs (Figure 3.4B) shows the high crystallinity of particles with an interplanar spacing of 0.58 nm, which is close to the d_{100} value of hexagonal phase $NaYF_4$[33]. FTIR spectra were applied to identify the successful ligand exchange from OA molecules to POEGA-b-PMAEP on the surface of nanoparticles, where the peaks at 1732 cm^{-1} and 1103 cm^{-1} were respectively assigned to the stretching vibration of the carboxylic group (C=O) and phosphine oxides (P=O) in carboxyl-UCNPs (Figure 3.4C). DLS results (Figure 3.4D) showed that the average hydrodynamic size of UCNPs stepwise increased following the ligand-exchange surface modification and EDC coupling conjugation (PDI<0.1). TEM observations revealed that OA-UCNPs, carboxyl-UCNPs and TAMRA-UCNPs were uniform in size without obvious change in morphology (Figure 3.4E-G).

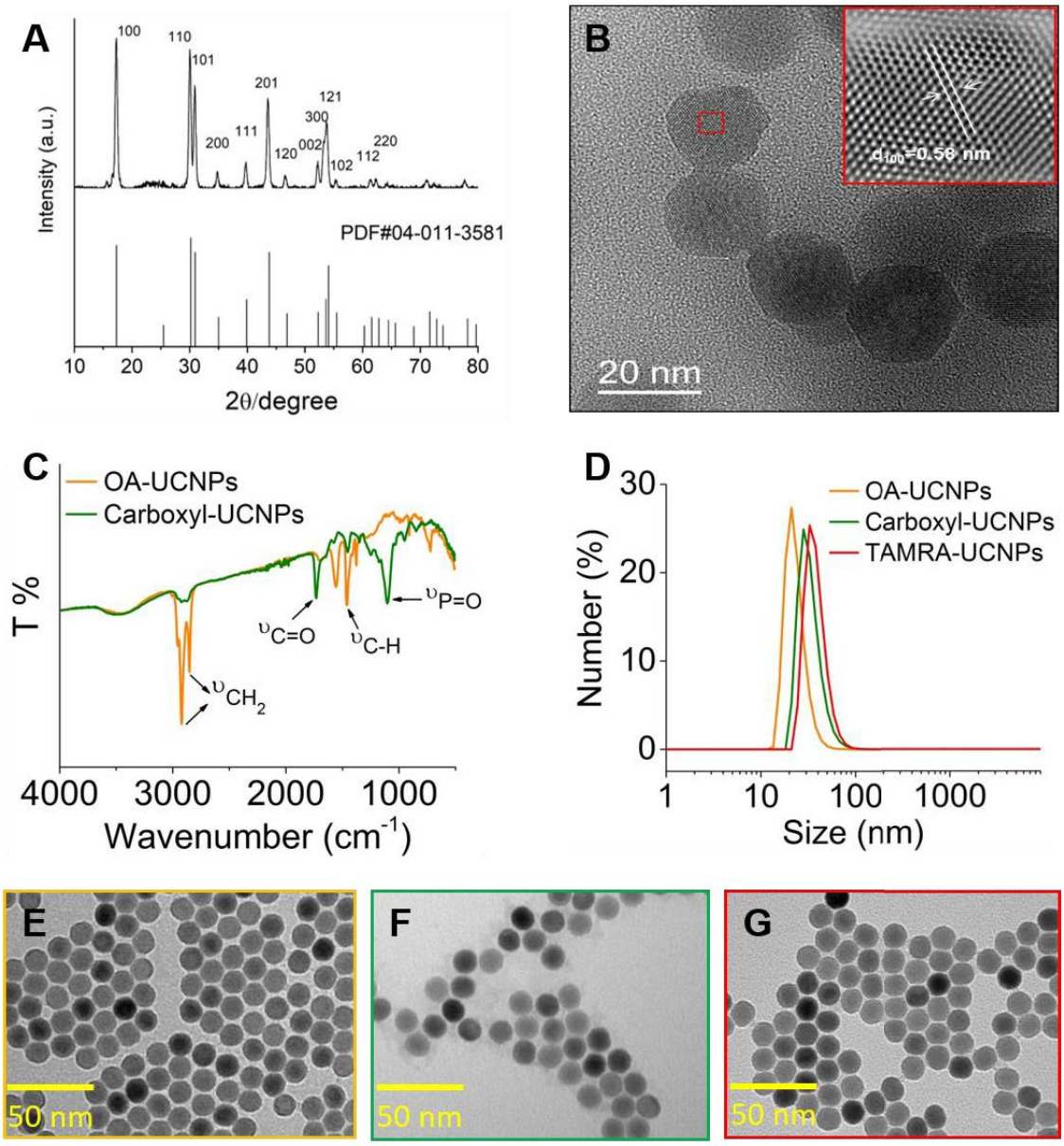

Figure 3.4 Characterization of UCNPs. (A) Diffraction XRD pattern and assigned Miller indices of synthesized OA-UCNP, . (B)HRTEM of OA-UCNPs. (C) FTIR spectra of OA-UCNPs and carboxyl-UCNPs. (D) Size distribution histogram of OA-UCNPs, carboxyl-UCNPs and TAMRA-UCNPs. TEM images of (E) OA-UCNPs, (F) carboxyl-UCNPs and (G) TAMRA-UCNPs.

Figure 3.5 shows the luminescent spectra of OA-UCNPs in cyclohexane, carboxyl-UCNPs and ligand free-UCNPs in MES buffer, under 980 nm laser excitation (1.36×10^6

W/cm^2). The energy transfers from excited state to ground state have been displayed[34]. Though there was no spectrum shift in the peak emission of carboxyl-UCNPs (green line), the green luminescence has been severely quenched compared with OA-UCNPs (orange line). To check if the quenching was caused by the attached polymers, we removed the surface OA molecules by HCL (0.1 M) with 20 min sonication and found that the ligand free-UCNPs (pink line) showed the same level of reduced luminescence, indicating that the quenching was possibly induced by some other factors, especially water molecules[35]. The spectrum intensity changes (shown in Figure 3.5B) confirmed successful energy transfer from UCNPs to TAMRAs, as the fluorescence of TAMRA at 583 nm increased and the luminescence of UCNPs at 539 nm decreased. Moreover, in fact LRET can be clearly observed by the naked eye (shown as the insert photographs) with the luminescent color changing from a green (carboxyl-UCNPs, left) to yellow color (TAMRA-UCNPs, right).

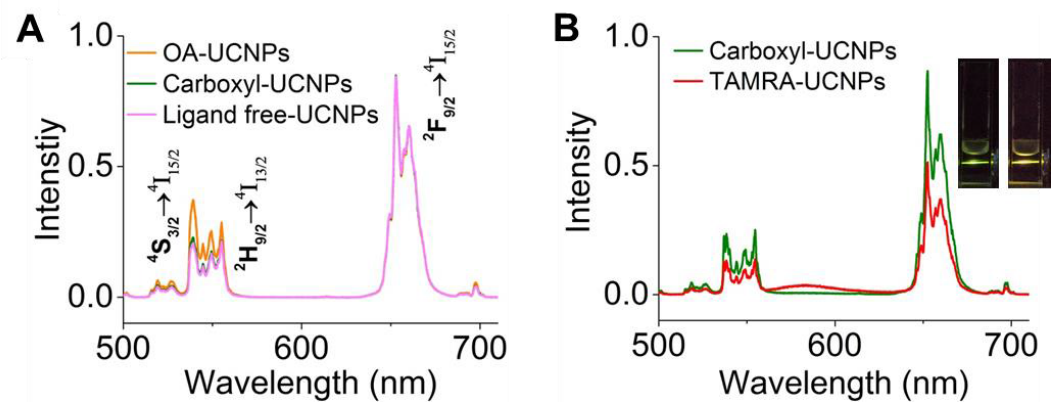

Figure 3.5 (A) Luminescence spectra of OA-UCNPs, carboxyl-UCNPs and ligand free-UCNPs. (B) Luminescence spectra of carboxyl-UCNPs and TAMRA-UCNPs. The inset shows photographs of (left) carboxyl-UCNPs and (right) TAMRA-UCNPs under excitation at 980 nm.

3.3.2 Optimisation of Upconversion LRET DNA Assay

In order to enhance analytical performance, the various experimental conditions were optimised. The molar ratio of TAMRA-tagged probe-DNAs to EDC-activated carboxyl-UCNPs is an important parameter for the detection sensitivity of the HIV DNA target. Increasing the amount of TAMRA-tagged probe DNAs, the fluorescence of TAMRAs at 583 nm was gradually enhanced with the luminescence of UCNPs at 539 nm reduced (Figure 3.6A), and the ratiometric I_{583}/I_{539} (Figure 3.6B) was correspondingly increased until saturated, confirming the optimum molar ratio of TAMRA-tagged probe DNAs to UCNPs as 10:1 were used for LRET assay in this work. Meanwhile, to confirm the observation as the distance-dependent LRET rather than simple reabsorption, by mixing TAMRA-tagged probe DNAs with non-EDC-activated carboxyl-UCNPs, though increasing the amount of TAMRA-tagged probe DNAs, no obvious spectrum and change of I_{583}/I_{539} was observed because of the long distance between TAMRA-UCNP pair (Figure 3.6C&D).

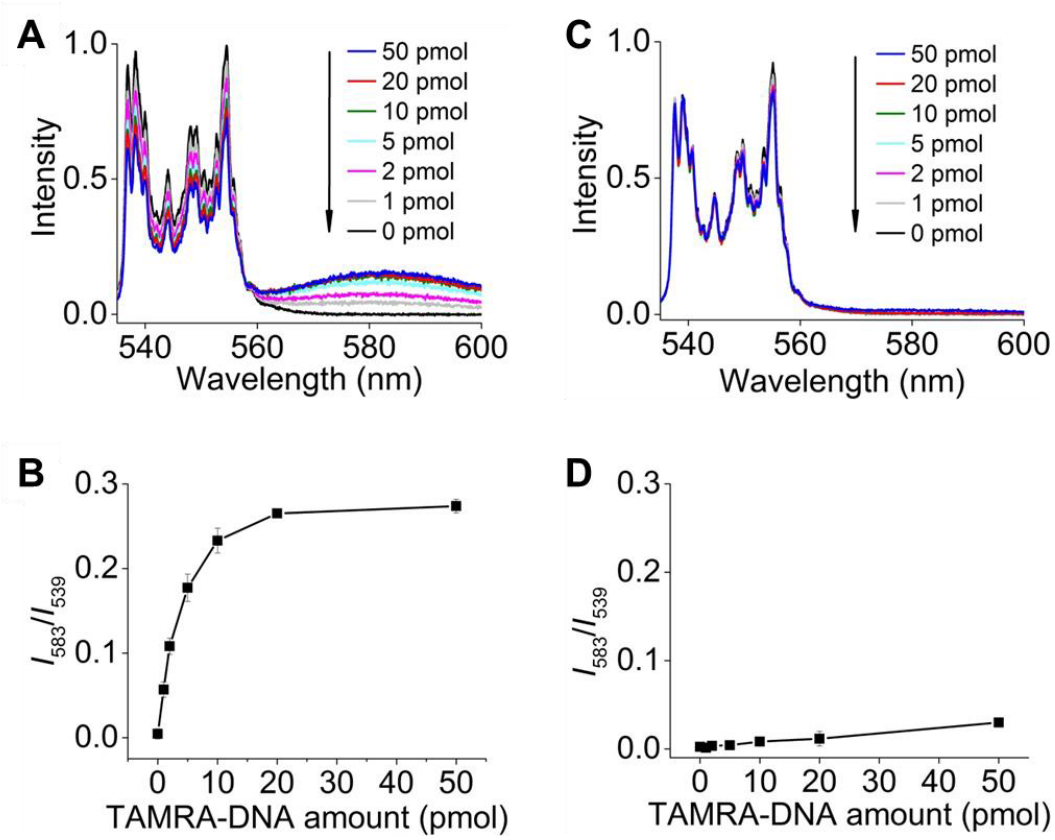

Figure 3.6 Optimization of Exonuclease III-assisted upconversion resonance energy transfer in wash-free suspension DNA assay. (A) Spectrum along incremental amounts of TAMRA-tagged probe DNAs (1, 2, 5, 10, 20 and 50 pmol) with EDC catalysis. (B)Ratio of I_{583}/I_{539} along with incremental amounts of TAMRA-tagged probe DNAs (1, 2, 5, 10, 20 and 50 pmol) with EDC catalysis. (C) Spectrum along incremental amounts of TAMRA-tagged probe DNAs (1, 2, 5, 10, 20 and 50 pmol) without EDC catalysis. (D) I_{583}/I_{539} along with incremental amounts of TAMRA-tagged probe DNAs (1, 2, 5, 10, 20 and 50 pmol) without EDC catalysis. For each figure, the error bars represent the standard deviation calculated from three parallel groups.

The optimal reaction time of this conjugation step was also investigated and the result demonstrated that the carbodiimide chemistry between UCNPs and TAMRA-tagged probe DNAs was completely finished within one hour (Figure 3.7A). To ensure the

complete reaction of Exo III-assisted signal amplification step is another important factor for the sensitive detection. The curve of I_{583}/I_{539} was plotted along reaction time and shown in Figure 3.7B. The reaction efficiency increased during the first forty minutes and reached steady state after one hour. The reaction time of Exo III assisted signal amplification for one hour was subsequently used in this work.

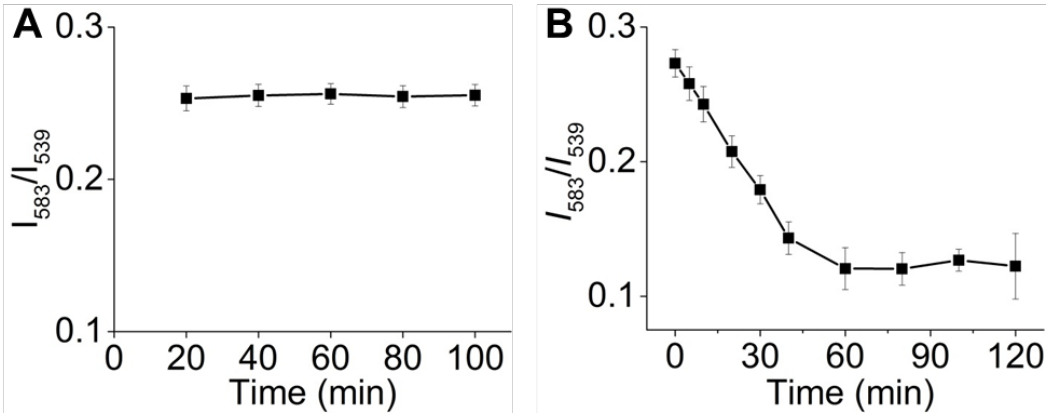

Figure 3.7 Optimisation of Exonuclease III-assisted upconversion resonance energy transfer in wash-free suspension DNA assay. (A) Ratio of I_{583}/I_{539} along with the reaction time for carboxyl-UCNPs conjugation with TAMRA-tagged probe DNAs catalyzed by EDC at different time points (20, 40, 60, 80 and 100 min). (B) Ratio of I_{583}/I_{539} along with the reaction time (0, 5, 10, 20, 30, 40, 60, 80, 100 and 120 min) at Exo III digestion step in the presence of 10 nM target DNAs. For each figure, the error bars represent the standard deviation calculated from three parallel groups.

3.3.3 Detection Sensitivity of HIV DNA Target Based on Upconversion LRET Assay For HIV detection by the Exo III-assisted upconversion LRET assay, varying concentrations of target DNAs were added with fixed values of TAMRA-tagged probe DNAs (10 pmol) and Exo III (10 U) for signal amplification at 37ºC for one hour, and the solution subsequently incubated at 70ºC for 20 min to stop the digestion via deactivating

the Exo III, followed by conjugation onto EDC-activated carboxyl-UCNPs for LRET at RT for one hour. Increasing the concentration of the target DNAs from 0.025 nM to 500 nM, the fluorescent intensity of TAMRAs (583 nm) decreased dramatically with the luminescent intensity of UCNPs (539 nm) increased (Figure 3.8A). The formula of $\frac{R_0\left(\frac{I_{583}}{I_{539}}\right)-R\left(\frac{I_{583}}{I_{539}}\right)}{R_0\left(\frac{I_{583}}{I_{539}}\right)}$ was applied to calculate the percentage of free dye dropped from probe DNAs and as the Y-value of the calibration curve. R refers to experimental group in the presence of target and R_0 refers to control group in the absence of target with Exo III-assisted signal amplification. The changing curve of $(R_0\text{-}R)/R_0$ versus the incremental concentrations of target DNAs was plotted as Figure 3.8B. The trend of the reaction followed a sigmoid increase and the curve was perfectly fitted with Growth/Sigmoidal-Hill 1 equation (r^2 = 0.99). Limit of detection (LOD) via stepwise dilution of the concentration of target DNAs at signal amplification step, was determined by the value of $\bar{x}$+3SD[36], where $\bar{x}$ is the mean value and SD is the standard deviation among three trials of experiment. The reaction in the absence of target DNAs was considered as blank (n = 5). The experimental LOD value in this work is 15 pM, equal to 0.3 fmol, with relative standard deviation (RSD) within 15%.

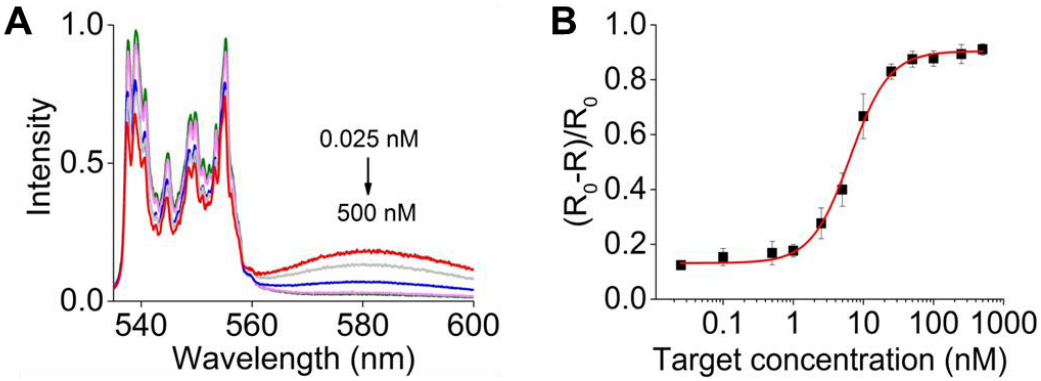

Figure 3.8 Detection sensitivity in Exonuclease III-assisted upconversion resonance energy transfer in a wash-free suspension DNA assay. (A) Luminescence spectra of Exo

III-assisted upconversion LRET DNA assay upon incremental concentrations of target DNAs. (B) The calibration curve along with various concentrations of target DNAs (0.025, 0.1, 0.5, 1, 2.5, 5, 10, 25, 50, 100, 250 and 500 nM). Hill 1 model with 4-parameter equation was applied for curve fitting. The error bars represent the standard deviation calculated from five parallel groups.

3.3.4 Detection Specificity of HIV DNA Target Based on Upconversion LRET Assay To further evaluate the specificity of the as-developed upcoversion LRET assay, TAMRA-tagged probe DNAs and Exo III were incubated with 1-base/3-base mis-match, non-match DNA1 (random sequence) and non-match DNA2 (HBV sequence), respectively, and with three replicate tests for each group. The concentration of target or non-target DNA (four control groups) was 10 nM, three orders of magnitude higher thant the obtained experimental LOD (15 pM) The results displayed in Figure 3.9, showed that this assay method can differentiate between all four mis-/non-match groups with HIV target group ($p < 0.05$), suggesting its potential for single-nucleotide polymorphisms (SNPs) assays.

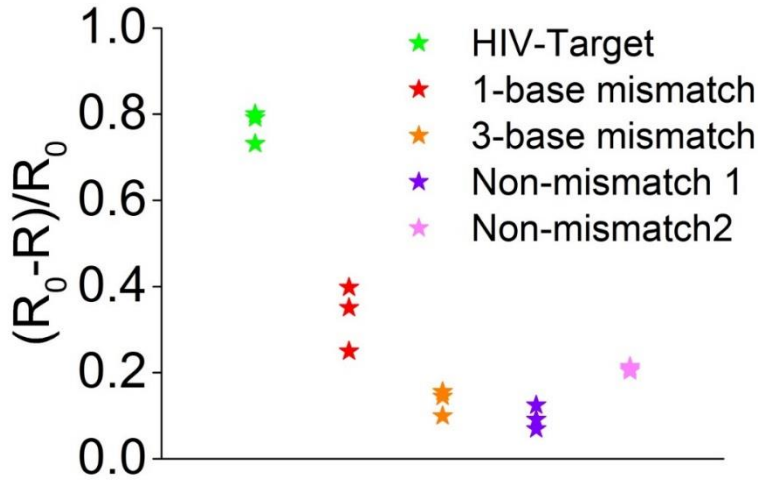

Figure 3.9 Specificity of the Exonuclease III-assisted upconversion resonance energy

transfer in a wash-free suspension DNA assay. Scatter plot shows the $(R_0-R)/R_0$ value for each group respectively.

The developed assay is currently semi-isothermal. In fact, the whole reaction can be conducted at room temperature, realizing fully-isothermal. The activity of Exo III is temperature-dependent, and the enzyme can also work well at room temperature. The following stopping-step with 70℃, can be substituted by addition of EDTA. In this case, the whole assay is isothermal at RT, in terms of development of point-of-care device, much easier than PCR. In this assay, the obtained LOD is 0.3 fmol, equal to 10^8 copies from PCR. Given single copy detection from PCR, in order to achieve similar detection sensitivity, the developed Exo-III assisted upconverting LRET assay should be further conducted in the measurement of single particle. By reducing the amount of upconversion nanoparticles and the reaction volume, the quenching efficiency of one particle by the same amount of acceptors will be significantly enhanced in theory, resulting in high sensitivity.

HIV diagnosis is based on either antigen/antibody testing or nucleic acids testing. Currently, the primary tests include ELISA and western blot for measurement of antigen/antibody, and the viral load test for nucleic acids. Viral load test measures the amount of HIV in human blood. Three are three technologies: reverse transcription polymerase chain reaction (RT-PCR), branched DNA (bDNA) and nucleic acid sequence-based amplification assay (NASBA)[37]. In 2007, Abbott real time HIV-1 amplification kit was approved and licensed by the FDA for sale in the United States. The sensitivity for RT-PCR is between 40 to 1010 copies/ml in clinical settings[38]. Thus, the developed Exo III-assisted upconversion LRET assay cannot achieve the same sensitivity as RT-PCR.

That is why measuring single particle and reducing the reaction volume is under consideration for further work to improve the sensitivity. RNA tests based on PCR looks for the virus itself and can diagnose HIV about 10 days after expose, shortening the diagnosis window of antigen/antibody test. These tests are expensive, and requires highly experienced operators and very sophisticated machine, therefore it is usually not the first test and is hindered for point-of-care development. Thus, it is necessary to exploit isothermal enzyme-assisted signal amplification techniques into point-of-care development for HIV diagnosis. It is worthy to mention that there may be issues for the developed assay if the HIV is in its dsDNA state during the infection, as the assay is currently designed for ssDNA detecting. However, fortunately, for detecting longer virus with longer strands, the assay could still perform well, as long as the 3' end of probe-DNA is blunt or recessed after the formation of duplex.

Application of the developed enzyme-assisted upconverting LRET assay for clinically relevant matrix such as serum in vitro is currently under investigation. Currently, this assay is used for detection of miRNA for tuberculosis diagnosis in clinical samples. The serum contains a lot of proteins and other small molecules with amino groups, which will compete with amine-probe-DNA to conjugate with EDC-activated carboxyl-UCNPs. This disadvantage may be the big challenge to apply the developed assay into clinical serum/plasma samples. As this assay is developed for nucleic acids detection, especially for ctDNA in vitro, the cellular environment was not considered and tested in this case.

3.4 Conclusion

In summary, we have developed an ultra-sensitive and specific detection and quantification method for trace amounts of DNA *via* an Exo III-assisted target DNA-

triggered signal amplification technique and upconversion LRET assay. The Exo III can work under isothermal conditions without costly and sophisticated equipment. The distance-dependent energy transfer avoids the influence of the unbound TAMRA molecules eliminating additional time-consuming washing step and providing a quicker test result turnout. The experimental LOD value in this work is 15 pM, one order of magnitude enhanced sensitivity of DNA detection, compared to the conventional DNA-DNA direct hybridization upconversion LRET assay[12-15]. This wash-free suspension DNA assay has numerous potential clinical applications, along with its main features of high sensitivity, rapid speed, simplicity and low cost.

3.5 References

[1] Xu, W., Xue, X., Li, T., Zeng, H. & Liu, X. Ultrasensitive and Selective Colorimetric DNA Detection by Nicking Endonuclease Assisted Nanoparticle Amplification. *Angewandte Chemie International Edition* 48, 6849-6852 **(2009)**.

[2] Smith, L. M., Sanders, J. Z., Kaiser, R. J., Hughes, P., Dodd, C., Connell, C. R., Heiner, C., Kent, S. & Hood, L. E. Fluorescence Detection in Automated DNA Sequence Analysis. *Nature* 321, 674-679 **(1985)**.

[3] Ren, W., Liu, H., Yang, W., Fan, Y., Yang, L., Wang, Y., Liu, C. & Li, Z. A Cytometric Bead Assay for Sensitive DNA Detection Based on Enzyme-Free Signal Amplification of Hybridization Chain Reaction. *Biosensors and Bioelectronics* 49, 380-386 **(2013)**.

[4] Wu, S., Han, G., Milliron, D. J., Aloni, S., Altoe, V., Talapin, D. V., Cohen, B. E. & Schuck, P. J. Non-Blinking and Photostable Upconverted Luminescence from Single Lanthanide-Doped Nanocrystals. *Proceedings of the National Academy of Sciences* 106, 10917-10921 **(2009)**.

[5] Wang, F., Han, Y., Lim, C. S., Lu, Y., Wang, J., Xu, J., Chen, H., Zhang, C., Hong, M. & Liu, X. Simultaneous Phase and Size Control of Upconversion Nanocrystals through Lanthanide Doping. *Nature* 463, 1061-1065 **(2010)**.

[6] Chatterjee, D. K., Rufaihah, A. J. & Zhang, Y. Upconversion Fluorescence Imaging of Cells and Small Animals Using Lanthanide Doped Nanocrystals. *Biomaterials* 29, 937-943 **(2008)**.

[7] Nyk, M., Kumar, R., Ohulchanskyy, T. Y., Bergey, E. J. & Prasad, P. N. High Contrast in Vitro and in Vivo Photoluminescence Bioimaging Using near Infrared to near Infrared up-Conversion in Tm^{3+} and Yb^{3+} Doped Fluoride Nanophosphors. *Nano Letters* 8, 3834-3838 **(2008)**.

[8] Wang, J., Wei, T., Li, X., Zhang, B., Wang, J., Huang, C. & Yuan, Q. Near-Infrared-Light-Mediated Imaging of Latent Fingerprints Based on Molecular Recognition. *Angewandte Chemie* 126, 1642-1646 **(2014)**.

[9] Deng, R., Xie, X., Vendrell, M., Chang, Y. T. & Liu, X. Intracellular Glutathione Detection Using MnO_2-Nanosheet-Modified Upconversion Nanoparticles. *Journal of the American Chemical Society* 133, 20168-20171 **(2011)**.

[10] Van de Rijke, F., Zijlmans, H., Li, S., Vail, T., Raap, A. K., Niedbala, R. S. & Tanke, H. J. Up-Converting Phosphor Reporters for Nucleic Acid Microarrays. *Nature Biotechnology* 19, 273-276 **(2001)**.

[11] Wang, L., Yan, R., Huo, Z., Wang, L., Zeng, J., Bao, J., Wang, X., Peng, Q. & Li, Y. Fluorescence Resonant Energy Transfer Biosensor Based on Upconversion-Luminescent Nanoparticles. *Angewandte Chemie International Edition* 44, 6054-6057 **(2005)**.

[12] Zhang, P., Rogelj, S., Nguyen, K. & Wheeler, D. Design of a Highly Sensitive and Specific Nucleotide Sensor Based on Photon Upconverting Particles. *Journal of the American Chemical Society* 128, 12410-12411 **(2006)**.

[13] Liu, J., Cheng, J. & Zhang, Y. Upconversion Nanoparticle Based LRET System for Sensitive Detection of Mrsa DNA Sequence. *Biosensors and Bioelectronics* 43, 252-256 **(2013)**.

[14] Zhu, H., Lu, F., Wu, X. C. & Zhu, J. J. An Upconversion Fluorescent Resonant Energy Transfer Biosensor for Hepatitis B Virus (HBV) DNA Hybridization Detection. *Analyst* 140, 7622-7628 **(2015)**.

[15] Wang, P., Ahmadov, T. O., Lee, C. & Zhang, P. Ligase-Assisted Signal-Amplifiable DNA Detection Using Upconversion Nanoparticles. *RSC Advances* 3, 16326-16329 **(2013)**.

[16] Sapsford, K. E., Berti, L. & Medintz, I. L. Materials for Fluorescence Resonance Energy Transfer Analysis: Beyond Traditional Donor-Acceptor Combinations. *Angewandte Chemie International Edition* 45, 4562-4589 **(2006)**.

[17] Su, Q., Feng, W., Yang, D. & Li, F. Resonance Energy Transfer in Upconversion Nanoplatforms for Selective Biodetection. *Accounts of Chemical Research* **(2016)**.

[18] Deng, R., Wang, J., Chen, R., Huang, W. & Liu, X. Enabling FöRster Resonance Energy Transfer from Large Nanocrystals through Energy Migration. *Journal of the American Chemical Society* 138, 15972-15979 **(2016)**.

[19] Soukka, T., Rantanen, T. & Kuningas, K. Photon Upconversion in Homogeneous Fluorescence-Based Bioanalytical Assays. *Annals of the New York Academy of Sciences* 1130, 188-200 **(2008)**.

[20] Heim, A., Ebnet, C., Harste, G. & Pring-Åkerblom, P. Rapid and Quantitative Detection of Human Adenovirus DNA by Real-Time PCR. *Journal of Medical Virology* 70, 228-239 **(2003)**.

[21] Heid, C. A., Stevens, J., Livak, K. J. & Williams, P. M. Real Time Quantitative PCR. *Genome Research* 6, 986-994 **(1996)**.

[22] Gao, F., Lei, J. & Ju, H. Label-Free Surface-Enhanced Raman Spectroscopy for Sensitive DNA Detection by DNA-Mediated Silver Nanoparticle Growth. *Analytical Chemistry* 85, 11788-11793 **(2013)**.

[23] Gao, F., Fan, T., Wu, J., Liu, S., Du, Y., Yao, Y., Zhou, F., Zhang, Y., Liao, X. & Geng, D. Proximity Hybridization Triggered Hemin/G-Quadruplex Formation for Construction a Label-Free and Signal-on Electrochemical DNA Sensor. *Biosensors and Bioelectronics* 96, 62-67 **(2017)**.

[24] Bi, S., Zhang, J. & Zhang, S. Ultrasensitive and Selective DNA Detection Based on Nicking Endonuclease Assisted Signal Amplification and Its Application in Cancer Cell Detection. *Chemical Communications* 46, 5509-5511 **(2010)**.

[25] Gao, F., Lei, J. & Ju, H. Ultrasensitive Fluorescence Detection of Bleomycin Via Exonuclease III-Aided DNA Recycling Amplification. *Chemical Communications* 49, 7561-7563 **(2013)**.

[26] Zuo, X., Xia, F., Xiao, Y. & Plaxco, K. W. Sensitive and Selective Amplified Fluorescence DNA Detection Based on Exonuclease III-Aided Target Recycling. *Journal of the American Chemical Society* 132, 1816-1818 **(2010)**.

[27] Xuan, F., Luo, X. & Hsing, I. M. Ultrasensitive Solution-Phase Electrochemical Molecular Beacon-Based DNA Detection with Signal Amplification by Exonuclease III-Assisted Target Recycling. *Analytical Chemistry* 84, 5216-5220 **(2012)**.

[28] Lu, J., Paulsen, I. T. & Jin, D. Application of Exonuclease III-Aided Target Recycling in Flow Cytometry: DNA Detection Sensitivity Enhanced by Orders of Magnitude. *Analytical Chemistry* 85, 8240-8245 **(2013)**.

[29] Weiss, B. Endonuclease II of Escherichia Coli is Exonuclease III. *Journal of Biological Chemistry* 251, 1896-1901 **(1976)**.

[30] Zhao, J., Jin, D., Schartner, E. P., Lu, Y., Liu, Y., Zvyagin, A. V., Zhang, L., Dawes, J. M., Xi, P. & Piper, J. A. Single-Nanocrystal Sensitivity Achieved by Enhanced Upconversion Luminescence. *Nature Nanotechnology* 8, 729-734 **(2013)**.

[31] Zhao, J., Lu, Z., Yin, Y., McRae, C., Piper, J. A., Dawes, J. M., Jin, D. & Goldys, E. M. Upconversion Luminescence with Tunable Lifetime in $NaYF_4$:Yb, Er Nanocrystals: Role of Nanocrystal Size. *Nanoscale* 5, 944-952 **(2013)**.

[32] Duong, H. T., Chen, Y., Tawfik, S. A., Wen, S., Parviz, M., Shimoni, O. & Jin, D. Systematic Investigation of Functional Ligands for Colloidal Stable Upconversion Nanoparticles. *RSC Advances* 8, 4842-4849 **(2018)**.

[33] Liu, D., Xu, X., Du, Y., Qin, X., Zhang, Y., Ma, C., Wen, S., Ren, W., Goldys, E. M. & Piper, J. A. Three-Dimensional Controlled Growth of Monodisperse Sub-50 nm Heterogeneous Nanocrystals. Nature Communications 7, 10254 (**2016**).

[34] Zhou, J., Gu, F., Liu, X. & Qiu, J. Enhanced Multiphoton Upconversion in Single Nanowires by Waveguiding Excitation. *Advanced Optical Materials* 4, 1174-1178 **(2016)**.

[35] Arppe, R., Hyppänen, I., Perälä, N., Peltomaa, R., Kaiser, M., Würth, C., Christ, S., Resch-Genger, U., Schäferling, M. & Soukka, T. Quenching of the Upconversion Luminescence of $NayYF_4:Yb^{3+}$, Er^{3+} and $NaYF_4:Yb^{3+}$, Tm^{3+} Nanophosphors by Water: The Role of the Sensitizer Yb^{3+} in Non-Radiative Relaxation. *Nanoscale* 7, 11746-11757 **(2015)**.

[36] Armbruster, D. A., Tillman, M. D. & Hubbs, L. M. Limit of Detection (LOD)/Limit of Quantitation (LOQ): Comparison of the Empirical and the Statistical Methods Exemplified with GC-MS Assays of Abused Drugs. *Clinical Chemistry* 40, 1233-1238 **(1994)**.

[37] Calmy, A., Ford, N., Hirschel, B., Reynolds, S.J., Lynen, L., Goemaere, E., de la Vega, F.G., Perrin, L. and Rodriguez, W. HIV Viral Load Monitoring in Resource-limited Regions: Optional or Necessary? *Clinical Infectious Diseases* 44(1), pp.128-134 (**2007**).

[38] Consumer Affairs Branch (CBER)). "Abbott RealTime HIV-1 Amplification Reagent Kit, Abbott RealTime HIV-1 Calibrator Kit, Abbott RealTime HIV-1 Control Kit" (**2007**).

CHAPTER 4

Homogeneous Immunoassay for the Detection of Prostate Cancer Biomarkers Based Upon Upconversion Luminescence Resonance Energy Transfer in Conjunction with Gold Nanoparticles

Abstract: Development of analytical methods for protein-based antigen testing with the property of user-friendly, procedure-simple and high sensitivity is highly sought after, as traditional analytical methods are typically labour-intensive, time-consuming and low-sensitivity. In this chapter, we report a homogenous assay for protein-based antigen detection where we have applied upconversion luminescence resonance energy transfer (LRET) technique in conjunction with gold nanoparticles (AuNPs) as the quencher, within a typical sandwich immunoassay. Using the concept of core(dark)-shell(bright) structure for the upconversion nanoparticle (UCNPs) synthesis and a bispecific antibody technique for the UCNPs conjugation, we aimed to achieve a high quenching efficiency *via* a simple process. It was confirmed that this quenching efficiency is distance-dependent. Through this distance-dependent upconversion LRET sandwich immunoassay working with AuNPs, we have achieved a one-step, wash-free, homogenous detection assay for protein-based biomarkers, which can be used in disease diagnosis.

Key words: upconversion nanoparticles, luminescence resonance energy transfer, gold nanoparticles, core-shell structure, bispecific antibody, prostate cancer.

4.1 Introduction

It is estimated that prostate cancer (PCa) will be the 3rd most common cause of cancer deaths and the 2nd most common cause of male cancer deaths in Australia,according to statistics from the Australian Government Cancer Data, released in 2018[1]. There are estimated to be 17,729 new cases of PCa diagnosed and 3,500 new deaths from PCa in 2018[1]. The main tools to diagnose PCa include digital rectal examination (DRE), serum concentration of prostate specific antigen (PSA), transrectal ultrasound (TRUS)-guided biopsy, and multiparametric magnetic resonance imaging (MRI)[2]. The measurement of total serum PSA is the most widely used method, as it is a continuous parameter: the higher the value, the more likely the existence of PCa. However, testing for total levels of PSA lacks cancer specificity, even if it performs well for organ specificity, as elevated serum PSA levels can also be found in patients with benign prostatic disease and can often be found in older patients, resulting in unnecessary biopsies. A free PSA test only measures the amount of PSA that is floating freely in the bloodstream, without being bound to a different protein. A person may have an increased risk of prostate cancer when they have higher levels of total PSA and lower levels of free PSA. Thus, most recently, the free-to-total PSA ratio is highly recommended for routine measurement. This was shown to result in a significant decrease in the number of unnecessary biopsies, and the accuracy of diagnosis rate of PCa increased significantly with %fPSA[3,4]. However, there remains an urgent need to define better prostate-specific biomarkers that can distinguish

indolent from clinically significant prostate cancer and thus reduce the number of unnecessary invasive biopsies.

The heparan sulfate proteoglycan glypican-1 (GPC-1) has recently been highlighted as a potential protein biomarker for PCa. GPC-1 has been identified to exist in two forms in the body: a membrane bound core protein of 55-60 KDa and as secreted soluble forms of either 40 KDa or 52 KDa[5]. In addition, a sandwich ELISA (enzyme-linked immunosorbent assay) designed for detecting soluble forms of GPC-1 in plasma, serum and urine, has been successfully applied to investigate the range of GPC-1 in normal, benign prostatic hypertrophy (BPH) and prostate cancer patients. The results determined that secreted GPC-1 represents a clinically relevant biomarker for prostate cancer diagnosis[6]. A relatively high specificity of 79% was achieved, which worked to both differentiate between samples from normal / benign versus prostate cancer patients, and worked for patients with PSA ranging between 4-10 ng/ml. However, it shows a low sensitivity of only around 30%. Sensitivity is thus the key factor needed for molecular detection in cancer diagnosis at early stages. Traditional ELISA approaches use multiple washing steps, and each washing step may cause loss of target and resulting in low sensitivity. What is more, so many washing steps are unsuitable for translation of the test into point-of-care diagnostics. Thus, a robust detection method with high sensitivity and simple procedures for detection of the GPC-1 biomarker, is highly desirable.

Upconversion nanoparticles (UCNPs), capable of emitting visible to near-infrared (NIR) light under NIR radiation with anti-Stokes[7], have been widely developed for biomolecular detection both *in vivo*[8,9] and *in vitro*[10,11]. Use of UCNPs as the donor in luminescence

resonance energy transfer (LRET) assays for biomolecular detection, has been broadly reported with various materials as the acceptors, such as small fluorescent dyes[10,12], heavy metal ions[13,14], MnO_2 nanosheets[9,15], graphene oxide[16,17] and gold nanoparticles[18,19]. Upconversion LRET, distance-dependent assay, is where the energy transfer can only occur if the donor and acceptor are within a set distance from each other. Both the 'switch-off'[17,20] and 'switch-on'[21] model by quenching or recovering the upconversion luminescence can be used for molecular biomarker detection. This one-step, wash-free technique, therefore has the potential to be developed as a simple, user-friendly point-of-care detection system.

Using gold nanoparticles (AuNPs) as the acceptor, is superior to traditional fluorescent dyes, allowing the upconverting energy transferto be applied in competitive immunoassays for both large protein detection[18] and small molecule detection[22], since the plasmonic effect from AuNPs can work at quite a long distance. Thus, in this chapter, AuNPs are used as either energy acceptor or quencher, rather than small fluorescent dyes, such as TAMRA (used in Chapter 2). The main consideration here was the application of energy transfer in a sandwich immunoassay requires stronger quenchers for longer working distance, and AuNPs were most appropriate for this purpose.

In addition, in order to achieve higher quenching efficiency of upconversion luminescence, the concept of a rational core-shell structure has been applied to the design and synthesis of UCNPs, with the dark core wrapped within a bright-upconversion shell. For traditionally synthesized UCNPs, the luminescence from the inner part of the particles is not easily quenched, as the distance between the donor-acceptor is beyond the energy

transfer range, which results in a lower quenching percentage. In contrast, the newly designed core-shell structure, where the inner part does not reveal any upconversion luminescence, results in the total luminescent intensity much lower compared with traditional particles. In this case, the quenching percentage is high and it is therefore easy to achieve higher detection sensitivity. Figure 4.1 is the schematic image of the comparison between core-shell and traditional UCNPs.

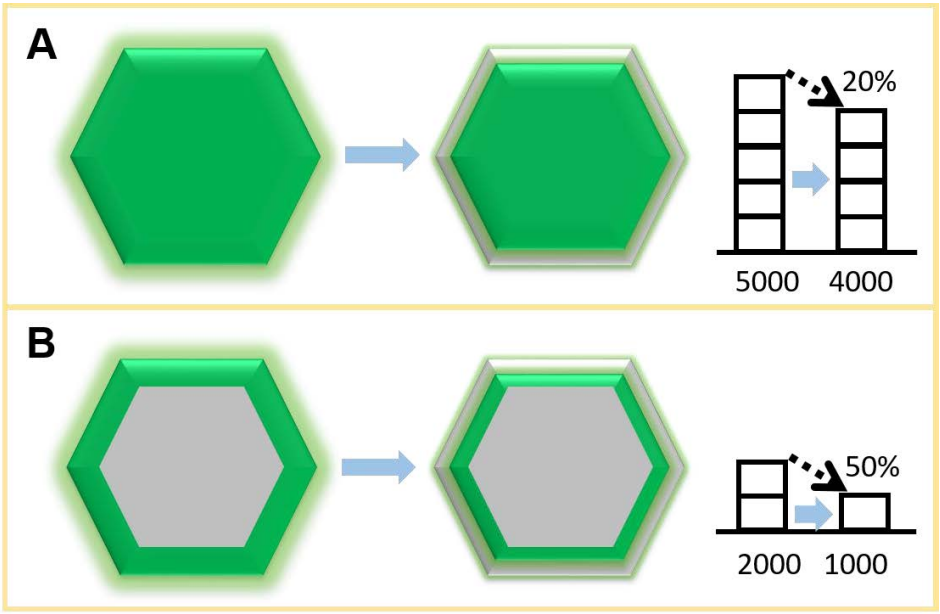

Figure 4.1 Schematic image of the comparison between traditional (A) and advanced core-shell (B) UCNPs for the quenching efficiency.

Antibodies (Abs) with specificity against two distinct antigens, contained within the one antibody molecule are called bispecific antibodies (BsAbs). Thus, these antibodies contain dual antigen-binding sites. BsAbs can be roughly divided into two categories: immunoglobulin G (IgG)-like molecules and non-IgG-like molecules[23]. Non-IgG-like antibodies lack an Fc region entirely, consisting of only the Fab regions, and various types

of bivalent and trivalent single-chain variable fragments (scFvs). One scFvs BsAb, as one active domain can specifically recognize and bind to methoxyl polyethylene glycol (mPEG) molecules. These antibodies have gained increased attention and application in nano-biotechnology[24,25] in recent times. These anti-mPEG fragments can be tethered to mPEG-functionalized nanomaterials through simple mixing, overcoming the extensive procedures of chemical conjugation. Based on Chapter 2, the homemade di-block copolymer POEGA-*b*-PMAEP for nanoparticle surface modification is also a kind of mPEG-polymer. Thus, in this project, the application of scFvs BsAb with one domain specifically targeting the mPEG-coated UCNPs was used to replace the chemical-catalyzed nanomaterial conjugations, resulting in simplicity.

In this study, an upconversion LRET assay using the donor-acceptor pair of UCNP-AuNP was applied in conjunction with a sandwich immunoassay, to realize the detection of GPC-1 biomarker for PCa diagnosis. For the sandwich immunoassay, the selection of two primary antibodies were (MIL38)-(anti-mPEG) bispecific scFvs antibodies and 3G5-antibodies. These two types of antibodies can recognize a specific target GPC-1 antigen at two distinct binding domains, according to recent reports[26]. The BsAb consists two scFvs, named MIL38 scFv and anti-mPEG scFv. MIL38 scFv shares the same sequence with the variable region of MIL38 antibody. MIL38 antibody has been confirmed to have a strong binding affinity to GPC-1.

Newly designed core-shell UCNPs and BsAbs techniques were applied to achieve high detection sensitivity and specificity, and procedural simplicity. This newly developed technique is user-friendly and cost-effective.

4.2 Experiments

4.2.1 Materials

Rare-earth chloride hexahydrates used in this work for UCNPs synthesis, including yttrium chloride hexahydrate ($YCl_3 \cdot 6H_2O$, 99.99%), ytterbium chloride hexahydrate ($YbCl_3 \cdot 6H_2O$, 99.99%), and erbium chloride hexahydrate ($ErCl_3 \cdot 6H_2O$, 99.9%), were purchased from Sigma-Aldrich. For polymer synthesis, the chemicals including 2-bromopropionic acid (99%), zinc acetylacetonate hydrate, 4-cyano-4-(phenylcarbonothioylthio)pentanoic acid (97%), ethylene glycol (99%), 1-butanethiol (99%) and poly(ethylene glycol) methyl ether acrylate were purchased from Sigma-Aldrich, and monoacryloxyethyl phosphate from Polysciences, Inc. All other materials, ammonium fluoride (NH_4F), cyclohexane, methanol, sodium hydroxide (NaOH), acetonitrile, tetrahydrofuran (THF), N-(3-Dimethylaminopropyl)-N′-ethylcarbodiimide hydrochloride (EDC) and Tris-buffer were purchased from Sigma-aldrich. 3G5 antibodies were purchased from GenScript. GPC-1 antigens were purchased from R&D Systems. (MIL38)-(anti-mPEG) BsAbs were provided by Dr. Thurecht's group, the Queensland University.

4.2.2 Instrumentation

Upconversion luminescence measurement for the microparticle-based sandwich assay with BsAb-UCNPs was implemented under the homemade microscopy with 980 nm excitation (Figure 4.2). The optical path of the imaging system consists of the bright-field imaging and fluorescence imaging. LED 980 nm laser was used as a light source for bright-field imaging and fluorescence imaging. Dichroic mirror was used to reflect the

light with >808 nm wavelength and transmit the light with <808 nm wavelength. Objective lens was used for the fluorescence collection. Olympus DP70 camera was used for imaging.

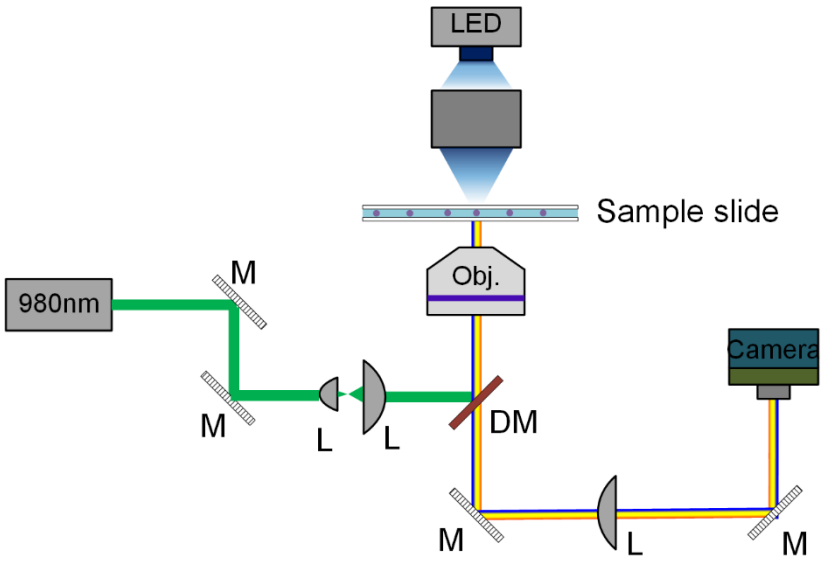

Figure 4.2 Illustration of the path way for the microparticles-based sandwich Immunoassay for GPC-1 with BsAb-UCNPs.

The upconversion luminescence measurement for the upconversion LRET immunoassay with AuNPs was implemented under the homemade spectrometer with 980 nm excitation, which has been describe in Chapter 2.

4.2.2 Synthesis of Core-Shell UCNPs

Synthesis of $NaYF_4$: 20%Yb core. $NaYF_4$:Yb nanoparticles were synthesized using a coprecipitation method. 5 ml of methanol solution containing $LnCl_3$ (1.0 mmol, Ln = Y (0.6 mmol), Yb (0.4 mmol)) together with 6 ml of oleic acid (OA) and 15 ml of 1-octadecene (ODE) were added into a three-neck round-bottom flask. The mixture was

heated at 160°C under argon flow for 30 min to form a transparent yellowish solution. The solution was cooled down to room temperature, and 10 ml of a methanol solution containing 0.16 g NH_4F and 0.10 g NaOH was added with vigorous stirring for 30 min. Then, the slurry was slowly heated to 150°C for 30 min under vacuum to remove methanol and small amount of water. Next, the reaction mixture was protected by an argon atmosphere, quickly heated to 300°C, and maintained at that temperature for 1.5 hour. The solution was cooled down and the products were isolated by addition of ethanol and centrifugation (9000 rpm).

Synthesis of $NaYF_4$: 20%Yb, 2%Er pure precursors. The $NaYF_4$: 20%Yb, 2%Er precursors were prepared as above procedure until the step where the reaction solution was slowly heated to 150°C after adding NaOH/NH_4F solution and kept for 30 min. Instead of further heating to 300°C to trigger nanoparticles' growth, the solution was cooled down to room temperature. The solution was considered as the shell precursors.

Synthesis of $NaYF_4$: 20%Yb@$NaYF_4$: 20%Yb, 2%Er core-shell nanoparticles. The core-shell nanoparticles were prepared with layer-by-layer epitaxial growth method. The pre-synthesized core nanoparticles were used as seeds for shell modification. 0.2 mmol prepared core nanoparticles were added to a 50 ml flask containing 3 ml of OA and 8 ml of ODE. The mixture was heated to 150°C under argon for 30 min, and then was further heated to 300°C. After that, 0.2 ml prepared shell precursors were injected into the reaction mixture and ripened at 300°C for 4 min, followed by the same injection and ripening cycles for approximately several times to get around 5 nm thickness shell. Finally, the slurry was cooled down to room temperature and the formed nanoparticles

were isolated by addition of ethanol and centrifugation (9000 rpm). The final nanoparticles were re-dispersed in cyclohexane at a concentration of 10 mg/ml.

4.2.3 Surface Modification of UCNPs with POEGA-*b*-PMAEP *via* Ligand Exchange

Surface modification of $NaYF_4$:Yb, Er UCNPs was performed *via* ligand exchange with di-block copolymer composed of hydrophilic block poly(ethylene glycol) methyl ether acrylate phosphate methacrylate (POEGA-*b*-PMAEP). The synthesis of the POEGA-*b*-PMAEP was described in Chapter 2. In typical procedure, 500 ul of OA-UCNPs (20 mg/mL) kept in cyclohexane was evaporated, and the particles were re-dispersed and mixed with 5 mg of POEGMA-*b*-PMAEP in 2 mL of THF. The reaction was kept mixing overnight, at room temperature. Nanoparticles were purified by washing/centrifugation at 8,000 rpm in three cycles with THF and another three cycles with water to obtain mPEG-UCNPs. mPEG-UCNPs were re-suspended in water at 10 mg/ml.

4.2.4 Preparation of BsAbs

The BsAbs fragment consists of a single chain variable region (scFv) specific for mPEG linked to a variable region specific for GPC-1. The two scFvs are linked by a glycine serine (G4s) linker. Genes encoding BsAbs fragment which bind to mPEG and GPC-1 were synthesized by Geneart. Genes were transfected into CHO cells for expression. The BsAb production and purification were performed as outlined in published work[23].

4.2.5 Conjugation of UCNPs and AuNPs

Conjugation of UCNPs with BsAbs. Affinity binding of BsAbs onto mPEG-UCNPs. The concentration of BsAbs in stock solution is 0.5 mg/ml. Three amounts (2.5, 5, 10 ug) of BsAbs were dissolved in 300 ul of Tris-buffer (50 mM Tris, 150 mM NaCl, pH 7.6), followed by centrifuge at 14,680 rpm for 5 min with 30K filter, respectively. The supernatant containing BsAbs was then mixed with 2 ul of mPEG-UCNPs (10 mg/ml, 5 $\times 10^{-2}$ nmol/ml) in 100 ul of Tris-buffer. The mixture was kept at RT for 1 h with slightly shaking. The unbound BsAbs were removed by centrifuge at 8,000 rpm for 4 min. The obtained BsAb-UCNPs (0.2 mg/ml, 1×10^{-3} nmol/ml) were kept in 100 ul of Tris-buffer containing NaF (2 mM) at 4ºC until use.

Conjugation of AuNPs with 3G5-antibodies. 3G5-antibodies were conjugated onto the surface of surfactant-free AuNPs *via* physical absorption. Three sizes of AuNPs (30 nm, 40 nm, 50 nm) have been tested: all three have the same level of absorbance around 540 nm at the equal volume, but the molar concentration of each size is different at the equal volume. 200 ul of AuNPs (50 nm-5×10^{-5} nmol/ml, 40 nm-1×10^{-4} nmol/ml, 30 nm-3×10^{-4} nmol/ml) were mixed with 5 ul of 3G5-antibodies (1 mg/ml), kept at RT for 2 h with slightly shaking. Another 200 ul of 0.5% BSA solution was added into the mixture for 1 h incubation at RT. The mixture was divided into two vials (200 ul/vial) for centrifugation at 8,000 rpm for 5 min to obtain the 3G5-AuNPs. The particles were stored in 100 ul of 0.5% BSA solution at 4ºC until further use. The molar concentration for each size of 3G5-AuNPs was 1×10^{-4} nmol/ml for 50 nm, 2×10^{-4} nmol/ml for 40 nm and 3×10^{-4} nmol/ml for 30 nm.

4.2.6 Microparticle-based Sandwich Immunoassay for GPC-1 Detection with BsAb-UCNPs

Conjugation of 3G5-antibodies onto microparticles. Carboxyl-microparticles (Bangs Laboratories, Inc.) were pre-activated with EDC in Hepes-buffer (20 mM, pH 7.0) for 15 min, then 5 ul of 3G5-antibodies (1 mg/ml) was added into the reaction for 2 h at RT. The solution was washed once by centrifugation at 2000 rpm for 2 min. The pellet was resuspended in Tris-buffer containing 0.5% BSA (pH 7.6), kept at RT for 1 h. The particles were washed twice, then the obtained 3G5-microparticles were stored in Tris-buffer containing 0.5% BSA. For control group, BSA was applied to replace 3G5-antibodies for covalent attachment onto the surface of microparticles, all other steps were as same as the above.

Microparticle-based sandwich immunoassay. BsAb-UCNPs and GPC-1 were mixed with 3G5-microparticles or BSA-microparticles in 100 ul of Tris-buffer containing 0.5% BSA, for 1 h at RT. Following this, the mixture was washed with centrifugation/re-dispersion four cycles (2000 rpm for 2 min). The microparticles were redissolved in 10 ul of Tris-buffer and observed under home-built microscope with external 980 nm excitation, to detect upconversion luminescence.

4.2.7 Plate-based Direct ELISA Assay with 3G5-AuNPs

100 ul of GPC-1 at 0.5 ug/ml in Na_2CO_3-buffer (10 mM, pH 9.0) was incubated in 96-well plate at 4°C overnight. The well was then blocked with Na_2CO_3-buffer containing 1% BSA at RT for 2 h, and then washed with 300 ul of PBST (phosphate buffer with 0.1%Tween-20) for three times. 100 ul of 3G5-AuNPs in Tris-buffer (pH 7.6) was added

into the well and incubated at 37°C for 1 h. The well was washed with 300 ul of PBST for three times. 100 ul of anti-mouse-IgG-HRP secondary antibody in Tris-buffer (pH 7.6) was added into the well and incubated at 37°C for 30 min. The well was washed with 300 ul of PBST for three times. 100 ul of TMB substrate was added into the well to observe the colour change. For the control group, the difference was the first step that 100 ul of BSA at 0.5% ug/ml in Na_2CO_3-buffer (10 mM, pH 9.0) was incubated in 96-well plate at 4°C overnight, and all other steps followed the experimental group mentioned above.

4.2.8 Optimisation

Molar ratio between BsAb-UCNPs and 3G5-AuNPs. 2 ul of BsAb-UCNPs was mixed with different volumes of 3G5-AuNPs (0 ul, 10 ul, 20 ul, 40 ul and 80 ul), in 100 ul Tris-buffer. In this case, the molar ratio of BsAb-UCNPs to 3G5-AuNPs at 30 nm is 1:0, 1:3, 1:6, 1:12,1:24; that ratio for AuNPs at 40 nm is 1:0, 1:1, 1:2, 1:4, 1:8; ratio for AuNPs at 50 nm is 1:0, 1:0.5, 1:1, 1:2, 1:4. The upconversion luminescence was measured with the spectrometer with external 980 nm excitation.

Distance-dependent energy transfer between BsAb-UCNPs and 3G5-AuNPs. 2 ul of BsAb-UCNPs was mixed with 80 ul of 3G5-AuNPs at three sizes (30 nm, 40 nm, 50 nm) in various volumes of Tris-buffer (100, 200, 300, 400, 500, 600 and 700 ul). The spectrum was measured under 980 nm excitation.

4.2.9 GPC-1 Detection Based on Upconversion LRET Assay

For AuNPs at 40 nm and 50 nm, once the antibody-coated AuNPs were dissolved in Tris-buffer in 1.5 ml of eppendorf tube with slightly shaking for only half an hour, the particles

were found sticking onto the inner wall of the tube. Whereas, this did not happen to 3G5-AuNPs at 30 nm. Thus, for the application of upconversion LRET assay with AuNPs for GPC-1 detection, 30 nm of AuNPs were selected. BsAb-UCNPs were mixed with 3G5-AuNPs in the molar ratio of 1:24 in Tris-buffer containing 0.5% BSA. Different amounts of GPC-1 were added into the mixture at the final volume of 100 ul (0, 25, 50, 100 and 200 ng/ml), kept at RT for 1 h with slightly shaking. Spectral properties of the mixture were measured with external 980 nm excitation laser. For each concentration, three independent measurements have been performed.

4.2.10 Specificity of Upconversion LRET Assay

BsAb-UCNPs were mixed with 3G5-AuNPs (30 nm) in the molar ratio of 1:24 in Tris-buffer containing 0.5% BSA. Equal amount of GPC-1 and PSA antigens were added into the mixture to make the final concentration of 100 ng/ml, respectively. The 100 ul of mixture was kept at RT for 1 h with slightly shaking, and then spectral properties have been measured with external 980 nm excitation laser. For each concentration, three independent measurements have been performed.

4.3 Results and Discussion

4.3.1 Assay Principle of Upconversion LRET for GPC-1 Detection

In the absence of GPC-1 antigen, the BsAb-UCNPs are spatially distant from the 3G5-AuNPs and therefore, there is no energy transfer. However, in the presence of GPC-1 antigen, because the BsAbs and 3G5-antibodies can bind to two different sites of the GPC-1 molecule simultaneously, BsAb-UCNPs can be brought into close contact with 3G5-AuNPs, resulting in quenching of the upconversion luminescence. The quenching

level of luminescence is proportional to the concentration of GPC-1 in the solution (Figure 4.3).

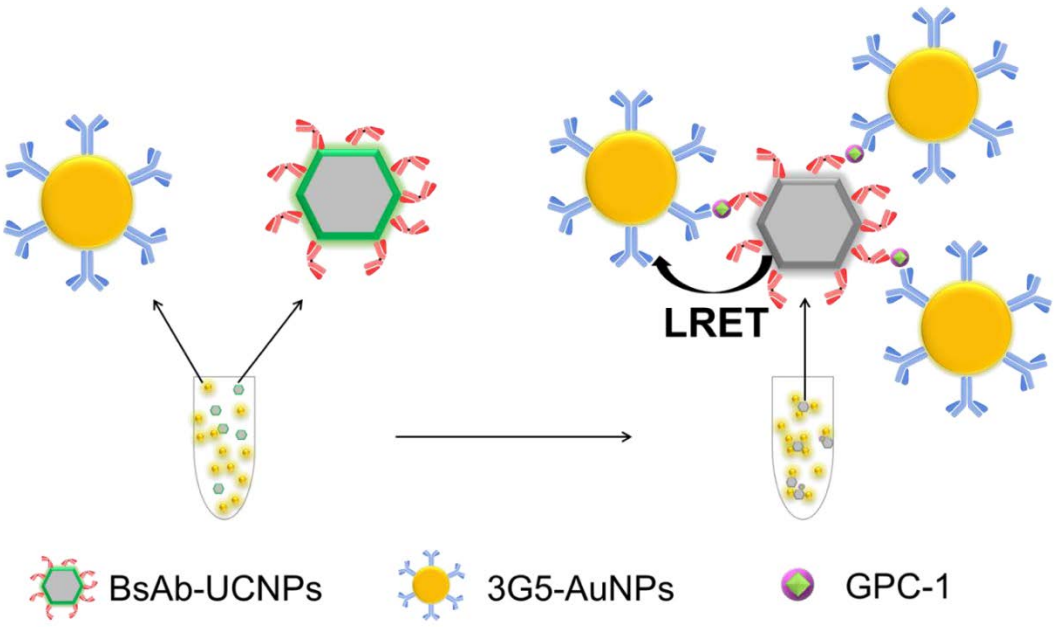

Figure 4.3 Schematic illustration of upconversion LRET sandwich immunoassay with 3G5-AuNPs for GPC-1 detection.

4.3.2 Characterisation of $NaYF_4$:20%Yb@$NaYF_4$:20%Yb, 2%Er Core-Shell Nanoparticles

TEM results of $NaYF_4$:20%Yb core and $NaYF_4$:20%Yb@$NaYF_4$:20%Yb, 2%Er core-shell nanoparticles are displayed in Figure 4.4. The diameter of the core is about 40 nm and the core-shell structure is about 50 nm, indicating the shell thickness is around 5 nm.

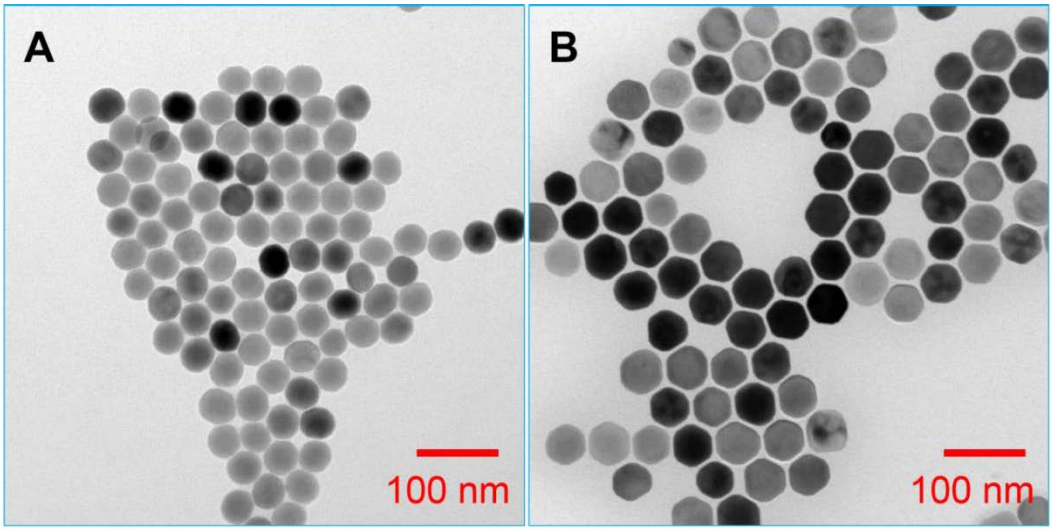

Figure 4.4 (A) The inner core of $NaYF_4$:20%Yb and (B) Core-shell structure of $NaYF_4$:20%Yb@$NaYF_4$:20%Yb, 2%Er under TEM.

4.3.3 Characterisation of BsAb-UCNPs

The BsAbs are artificial antibodies containing two different binding sites with specificity to two different targets[23]. The BsAbs in this study consist of a single chain variable region (scFv) specific for mPEG linked to another variable region specific for GPC-1. From the DLS result in Figure 4.5, the hydrodynamic diameter of mPEG-UCNPs is approximately 44 nm, and the particle size distribution has shifted to a larger particle size indicating the attachment of BsAbs onto mPEG-UCNPs due to one of the scFv regions of the BsAbs can target the PEG-polymer, and phenomenon has been reported by our lab[25]. Once the amount of BsAbs is increased from 2.5 ug to 5 ug, the particles' hydrodynamic size has become larger further (from ~59 nm to ~79 nm). However, the size remains unchanged once the input is increased to 10 ug (~79 nm). This result indicates that the input amount of BsAbs should be at least 5 ug for the conjugation of mPEG-UCNPs.

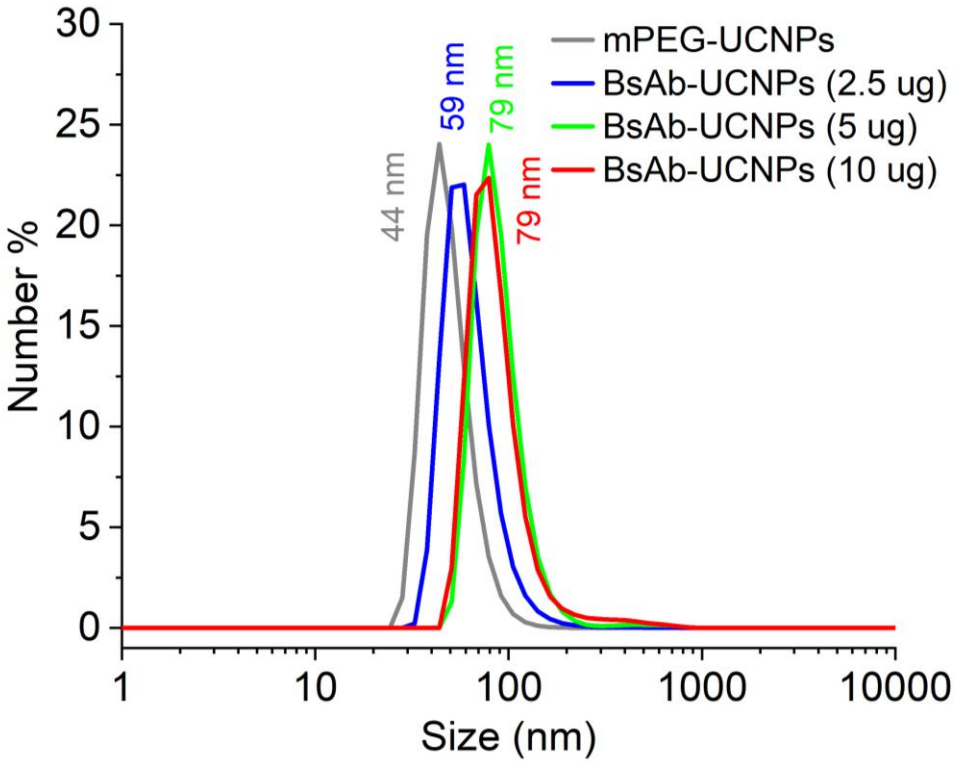

Figure 4.5 DLS result of conjugation of mPEG-UCNPs with various amount of BsAbs (2.5, 5, 10 ug) in Tris-buffer.

4.3.4 Characterisation of 3G5-AuNPs

After the incubation of AuNPs with 3G5-antibodies, according to the DLS result (Figure 4.6A, B, C) the hydrodynamic diameter of the particles has increased because of the physical attachment of the antibodies onto the nanoparticles compared with the bare-AuNPs. The size distribution shift among AuNPs at three sizes after conjugation is very close around 12 nm. The absorbance of the 3G5-AuNPs also shows a red shift in comparison of surfactant-free bare-AuNPs, also confirming the attachment of antibodies onto the surface of AuNPs (Figure 4.6D, E, F). There is approximately 5 nm shift of maximum absorption peak average, amongst the AuNPs at three sizes.

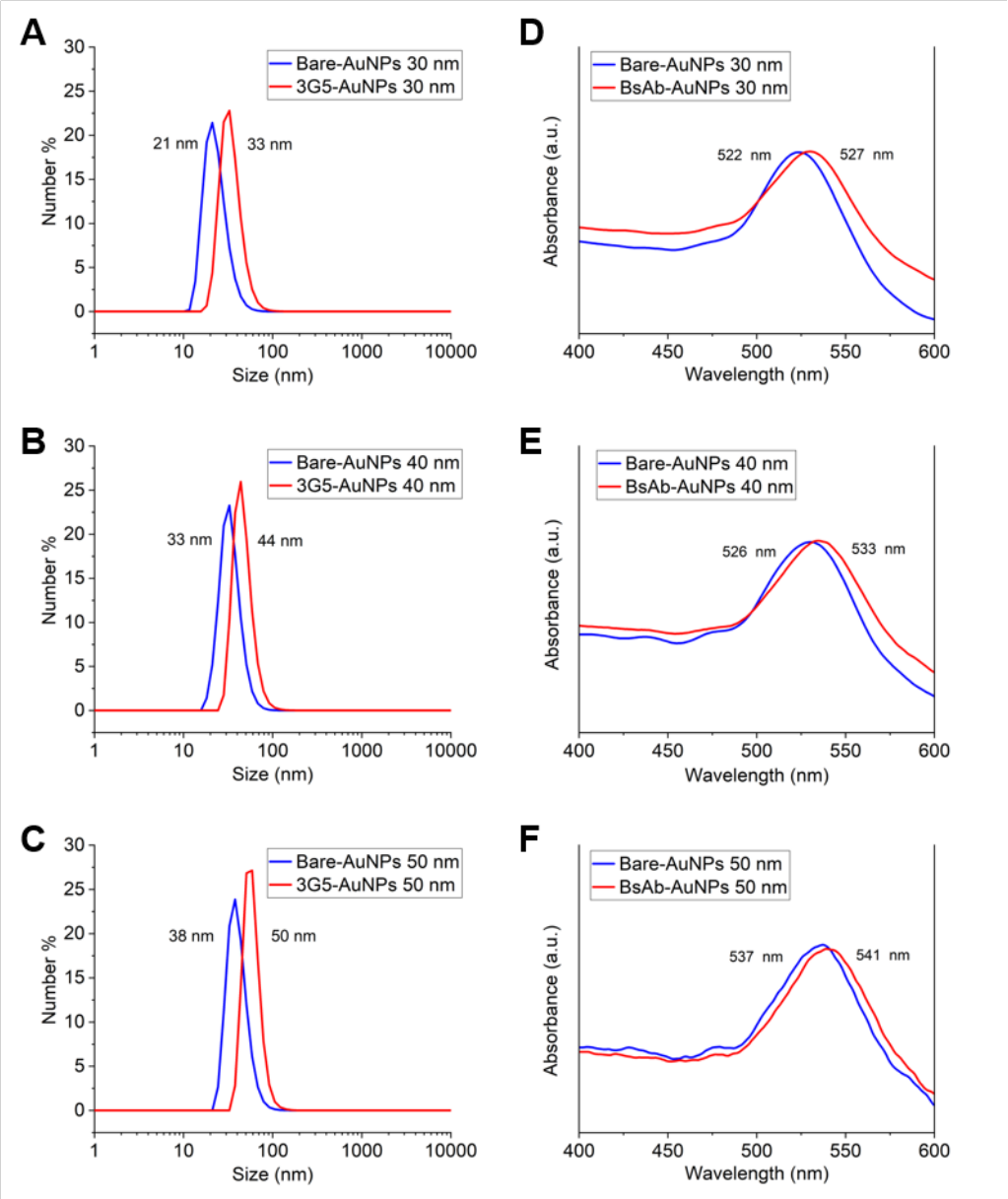

Figure 4.6 The DLS distribution (A, B, C) and the absorbance spectrum (D, E, F) of the conjugation of AuNPs with 3G5-antibodies in comparison with bare-AuNPs.

Figure 4.7 is the overlap spectrum between upconversion luminescence of BsAb-UCNPs with absorbance of 3G5-AuNPs. The absorbance of AuNPs at three sizes ranges from 525 nm to 540 nm as the size increases, and they all match well with upconversion

luminescence. This spectrum cross-talk between two kinds of nanoparticles is the basic factor for occurring resonance energy transfer.

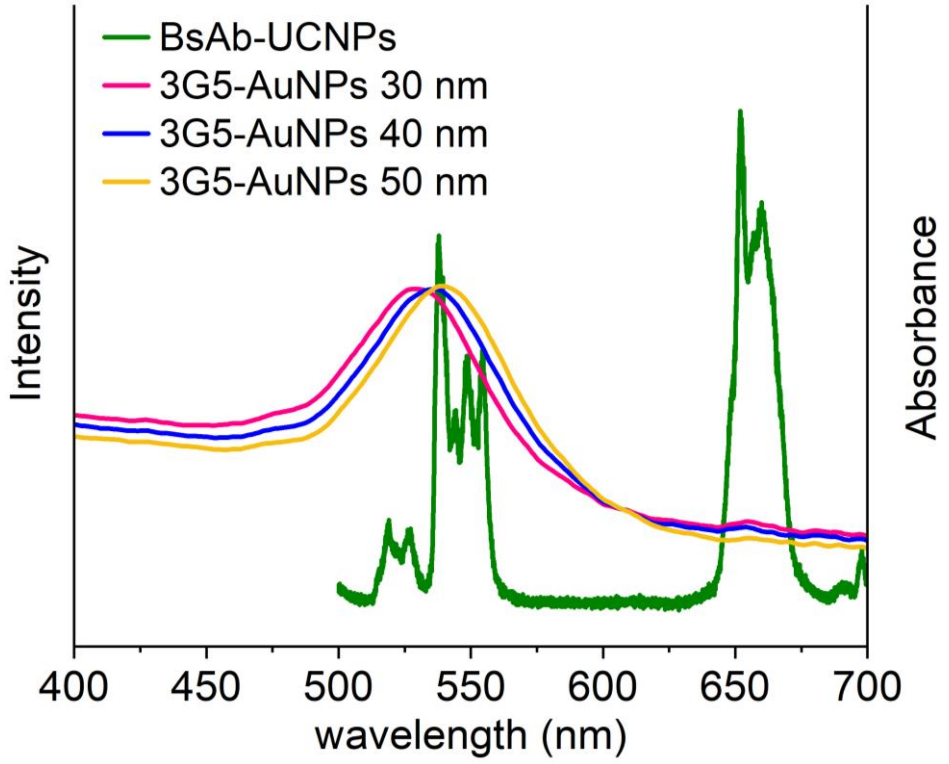

Figure 4.7 Absorbance spectrum of the 3G5-AuNPs at three sizes (30, 40 and 50 nm) and the upconversion luminescence spectrum of BsAb-UCNPs.

4.3.5 Microparticles-based Sandwich Immunoassay for GPC-1 with BsAb-UCNPs

In order to evaluate the immune-affinity of BsAbs after conjugated onto UCNPs to GPC-1 antigen, a 3G5-antibody modified microparticles-based sandwich immunoassay for GPC-1 detection with BsAb-UCNP as the signal probe has been designed and conducted.

Conjugation of 3G5-antibodies onto microparticles. In order to test the conjugation efficiency of 3G5-antibodies onto microparticles using EDC chemistry, a tube-based ELISA was conducted. Both 3G5-microparticles and BSA-microparticles were incubated with anti-mouse-IgG-HRP secondary antibodies in Tris-buffer containing 0.5% BSA for 30 min. After washing four times, 100 ul of TMB substrate was added into each tube for observation of the colour change. Figure 4.8 shows the tube-based ELISA result, all three groups of 3G5-microparticles show positive blue colour, meaning the existence of 3G5-antibodies on the surface of microparticles. Anti-mouse-IgG-HRP secondary antibodies can target primary antibodies (3G5-antibodies), and HRP enzyme can catalyse the TMB substrate being oxidised under acidic condition. In contrast, all three groups of BSA-microparticles show negative result as there was no colour change. Because anti-mouse-IgG-HRP secondary antibodies cannot target BSA, after reaction and washing steps, there is no HRP enzyme presenting on the microparticles, therefore the TMB substrate cannot be oxidised for colour change.

Figure 4.8 Tube-based ELISA for confirming the attachment of 3G5-antibodies onto the surface of microparticles. Beads mean microparticles.

Microparticles-based sandwich immunoassay for GPC-1 with BsAb-UCNPs. When 3G5-conjugated microparticles incubated with GPC-1 and, consequently with BsAB-UCNPs, the microparticles show obvious upconversion luminescence when viewed under the microscope with external 980 nm laser excitation (Figure 4.9A). This means that it forms the sandwich structure among 3G5-microparticles and GPC-1 and BsAb-UCNPs. BsAb-UCNPs demonstrate strong immuno-affinity to GPC-1 antigens, and the conjugation step does not influence the bioactivity of BsAbs. For the control group, BSA-microparticles show only background levels of upconversion luminescence when viewed under the microscope with an external 980 nm laser excitation (Figure 4.9B), meaning it cannot form the sandwich structure among BSA-microparticles and GPC-1 and BsAb-UCNPs. The low upconversion luminescence is due to some non-specific adsorption of BsAb-UCNPs on surface of microparticles.

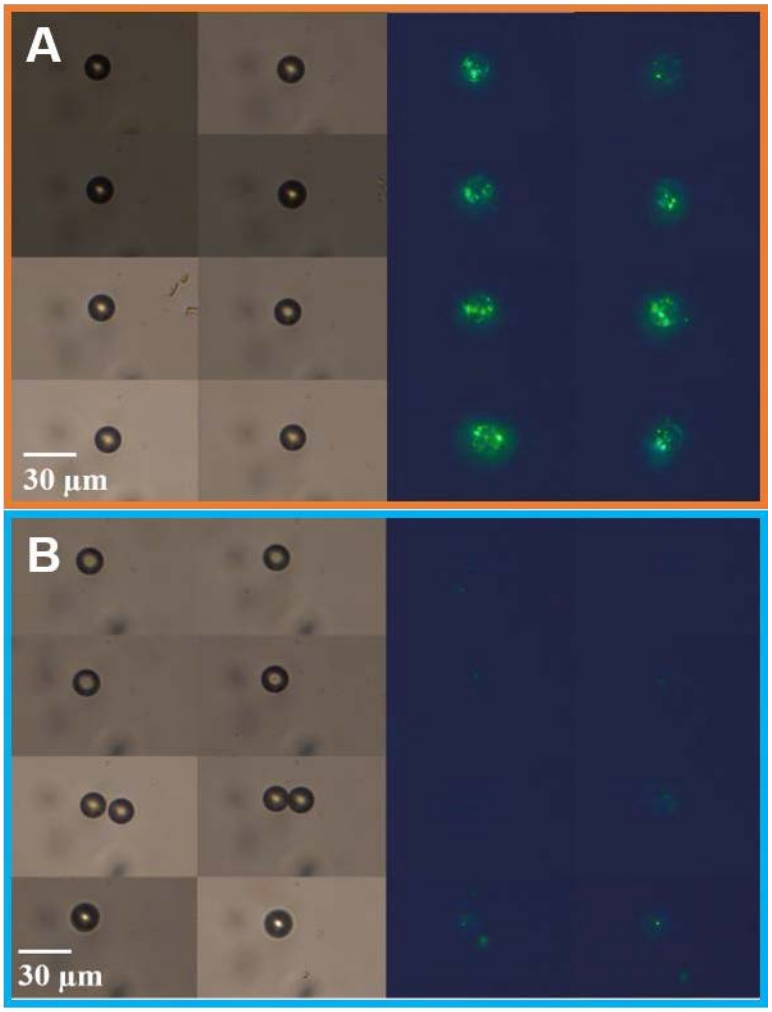

Figure 4.9 Upconverting microscopy measurement of sandwich beads-assay for GPC-1 detection. Microscopy measurement of 3G5-microparticles (A) and BSA-microparticles (B) with BsAb-UCNPs in the presence of GPC-1 antigen. These are four replicates experiments with completely same condition. Each arrow stands for one sample with two different areas. The left two columns are images under bright field, and the right two columns are images under 980 nm excitation corresponded with the left ones.

4.3.6 Plate-based Direct ELISA Assay with 3G5-AuNPs

The plate-based direct ELISA assay was used to check the specific immune-affinity of 3G5-AuNPs to GPC-1 antigens. For assay group, pre-coating GPC-1 antigens onto the

bottom of the wells showed the colour change to blue (Figure 4.10, three wells in red box). For control group, the wells pre-coated with BSA has shown negative results as there is no colour changing of TMB substrate (Figure 4.10, three wells in green box). This outcome demonstrates that 3G5-antibodies are attached to the AuNPs, and their specific binding-affinity against GPC-1 antigens are preserved, therefore, 3G5-AuNPs can be applied as probes in subsequent assays.

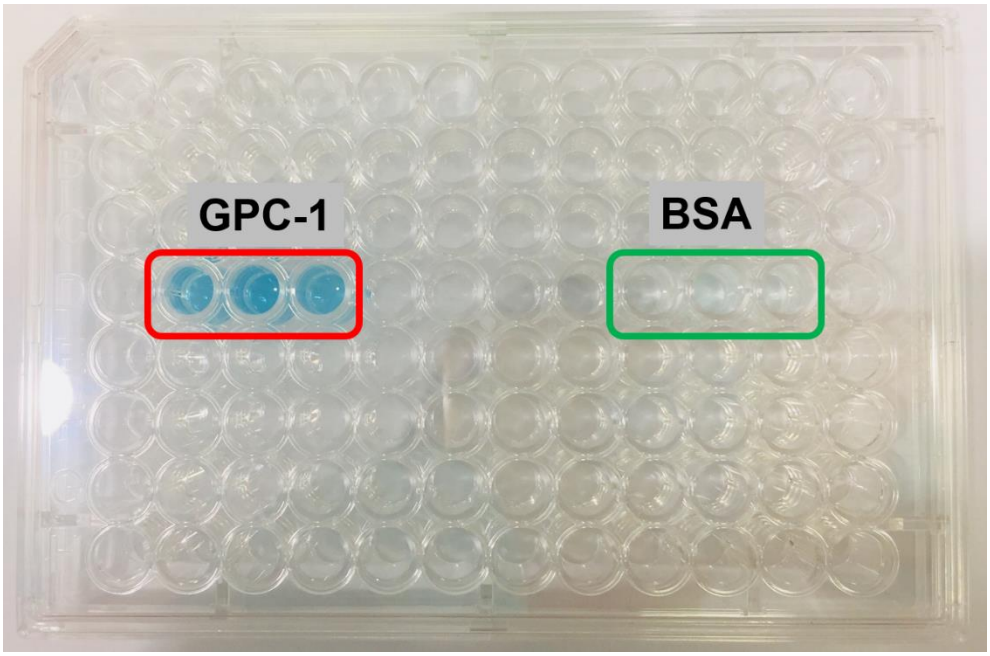

Figure 4.10 Plate-based direct ELISA assay with 3G5-AuNPs. Three wells in red box were pre-coated with GPC-1 antigens, and the other three wells in green box were pre-coated with BSA proteins as control.

Successful conjugation of BsAbs onto UCNPs and the remained bioactivity of the BsAbs, are the key elements to ensure the developed homogenous FRET assay performing well. In addition, the immune-affinity based conjugation also makes itself promising in biological imaging for prostate cancer diagnosis, as the antigen target for MIL-38 was detected in two forms: a membrane bound cell surface one and soluble secreted one.

4.3.7 Optimisation

Molar ratio between BsAb-UCNPs and 3G5-AuNPs. For this part of experiment, it is aiming to observe the influence on the two luminescent peaks by adding different amount of AuNPs, and also to investigate the quenching efficiency at various molar ratios between BsAb-UCNPs and 3G5-AuNPs. The results in Figure 4.11 show the upconversion luminescence spectrum of the mixture of BsAb-UCNPs/3G5-AuNPs at different molar ratio, for the three sizes of AuNPs. The quenching level of green emission at around 539 nm increases as the molar ratio of AuNPs to UCNPs increases. It is obvious that the quenching of green emission is much stronger than that of red emission, which is in accordance with the fact that the maximum spectrum cross-section between UCNPs and AuNPs is around green emission. Thus, to calculate the quenching efficiency of upconversion luminescence by AuNPs, two formulas are applied: (1), directly comparing the intensity of green emission between the BsAb-UCNPs solutions with/without the addition of 3G5-AuNPs. The formula is $(I_0\text{-}I)/I_0$, and I_0 stands for the upconversion green intensity without addition of 3G5-AuNPs and I stands for the addition of 3G5-AuNPs; (2), using the ratio of green/red emission as the comparative parameter, and the formula is $(R_0\text{-}R)/R_0$. R_0 stands for the ratio of upconversion green to red emission without addition of AuNPs, and R stands for that ratio with the addition of AuNPs. From the result, under both formulations, they all show almost linear correlation. In comparison, the quenching efficiency calculated under formula 1 is higher than that under formula 2. This phenomenon is reasonable as the red emission is also influenced to a small degree by the addition of AuNPs in the solution from the spectrum observation. However, formula 2, using ratio of green/red emission, is still considered the better choice for further assay. In the presence of GPC-1 antigen, the mixture of BsAb-UCNPs and 3G5-AuNPs creates the

"sandwich" formation among the three parts, resulting in large particle aggregates. In that case, calculation of quenching efficiency by the difference of green emission is inaccurate, as the particle-aggregations will likely show higher luminescent intensity than monodispersed UCNPs suspension. By using the ratio (formula 2) to calculate the quenching efficiency, the problem mentioned above can be avoided.

It is noticed that for different sizes of AuNPs at the same molar ratio to UCNPs, the quenching efficiency is different. Take the comparison between 40 nm and 50 nm as the example. The quenching efficiency of 3G5-AuNPs for 40 nm at the ratio of 1:1, is only about half of that for 50 nm. This phenomenon is rather expected as the commercially available AuNPs at different sizes all have 1 OD absorbance intensity for total 20 mL volume. However, the molar concentration of each size in 20 ml solution is different (demonstrated in experimental section), which results in the absorbance of individual AuNP at different sizes calculated according to the following formula: $Absorbance_{individual} = Absorbance_{total}/Molar\ concentration$. As for single AuNPs at 40 nm, the absorbance around green emission is fifty percent of that for single AuNP at 50 nm, and that is why the quenching efficiency of 3G5-AuNPs for 40 nm at the ratio of 1:1 is only about half of that for 50 nm

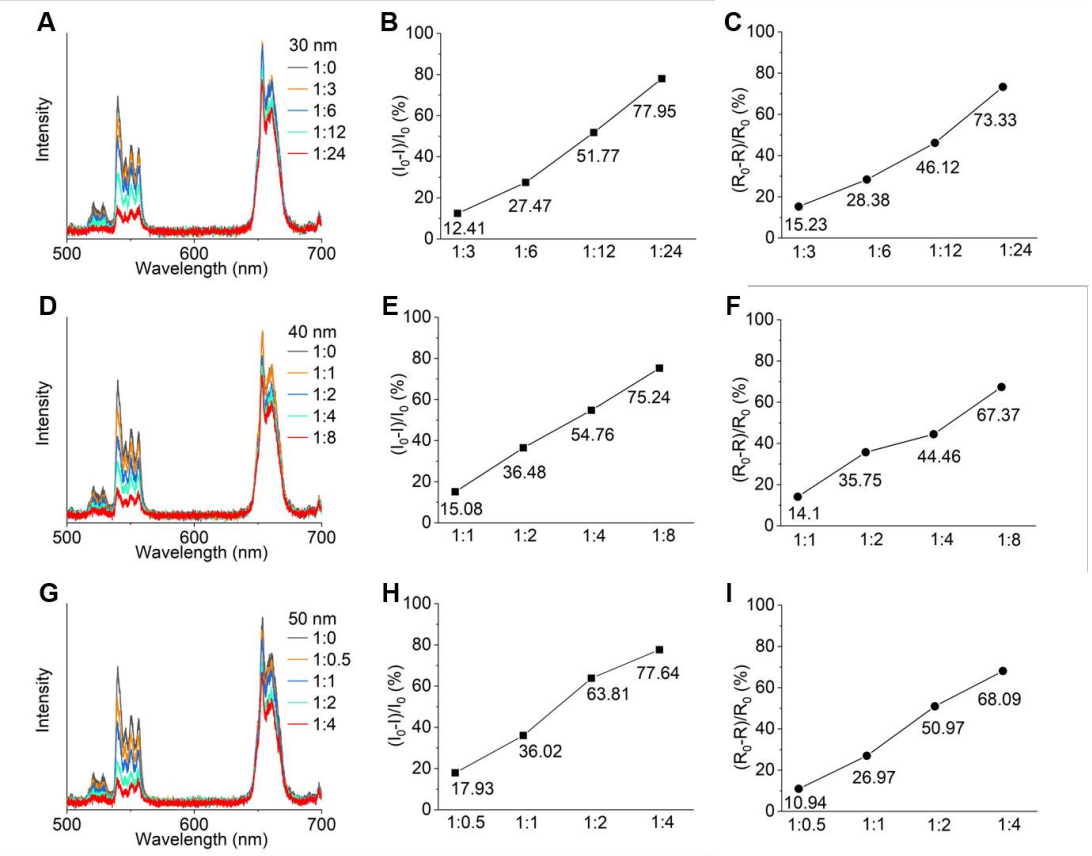

Figure 4.11 Investigation of the relationship between upconversion quenching with input amount of AuNPs. Upconversion spectrum at different molar ratios between upconversion nanoparticles with gold nanoparticles (A-30 nm, D-40 nm,G-50 nm). Quenching efficiency of upconversion luminescence by AuNPs at different molar ratios to UCNPs via directly comparing the intensity of green emission as formula $(I_0\text{-}I)/I_0$ (B-30 nm, E-40 nm, H-50 nm), and via comparing the ratio of green/red emission as formula $(R_0\text{-}R)/R_0$ (C-30 nm, F-40 nm, I-50 nm).

Distance-dependant energy transfer between BsAb-UCNPs and 3G5-AuNPs. In order to confirm that the energy transfer is distance-dependant between UCNPs and AuNPs, luminescence measurements were tested for the mixture of BsAb-UCNPs and 3G5-AuNPs at fixed molar ratio but different solution volumes. 2 ul of BsAb-UCNPs

were mixed with 3G5-AuNPs in the molar ratio of 1:4 for 50 nm, 1:8 for 40 nm and 1:24 for 30 nm, in the various volumes of Tris-buffer (100, 200, 300, 400, 500, 600 and 700 ul). Increasing overall volume of the mixture results in increasing the distance between BsAb-UCNPs and 3G5-AuNPs. The spectrum was measured under 980 nm excitation (Figure 4.12). As for the same amount of BsAb-UCNPs in various volumes show different luminescence intensity under spectrum measurement, formula 2 has been applied here for the calculation. The results clearly demonstrated that the quenching efficiency has been reduced gradually with the larger mixture volumes. This result indicates that the energy transfer between UCNPs and AuNPs is distance-dependent, by which it is confirmed that the sandwich formation inducing the distance shorten between two kinds of nanoparticles can trigger the LRET.

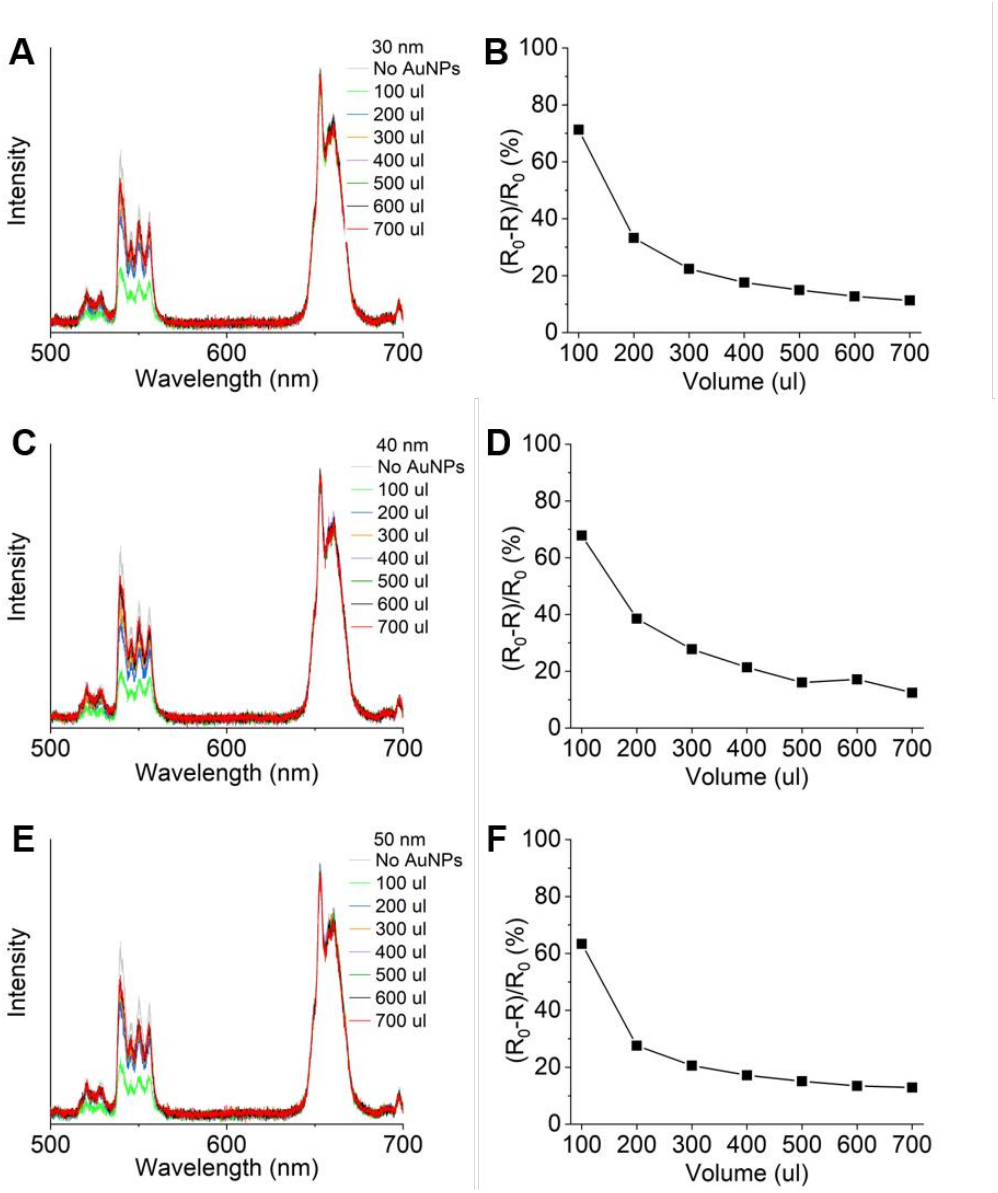

Figure 4.12 Spectrum of upconversion luminescence for the same ratio between BsAb-UCNPs with 3G5-AuNPs in different volumes of Tris-buffer (A, C, E). Quenching efficiency of upconversion luminescence at fixed molar ratio of UCNPs/AuNPs in various volumes via comparing the ratio of green/red emission as formula $(R_0-R)/R_0$ (B-30 nm, D-40 nm, F-50 nm).

4.3.8 GPC-1 Detection Based on Upconversion LRET Assay

As mentioned in the experimental section, 3G5-AuNPs at 40 and 50 nm tend to easily stick onto the inner wall of the eppendorf tube (1.5 ml) once dissolved in Tris-buffer (pH 7.6) even with a very gentle shaking. As a result of nanoparticles stuck to the walls of the tube, the molar concentration of 3G5-AuNPs in the tube is decreased, affecting the "sandwich" formation and, consequently, the energy transfer. However, for 3G5-AuNPs with the size of 30 nm, there is no sticking onto the wall of the tube. Therefore, for all further assays, all AuNPs used are 30 nm.

Figure 4.13 demonstrates the quenching efficiency of BsAb-UCNPs by 3G5-AuNPs as a function of changing concentration of GPC-1 from 25 to 200 ng/ml (n = 3). The quenching percentage of BsAb-UCNPs by 3G5-AuNPs is in correlation to the concentration of GPC-1 in the mixture, indicating that this newly designed upconversion LRET assay is applicable for GPC-1 detection in combination with sandwich immunoassay. However, in order to achieve good calibration curve for quantification of GPC-1, further optimization of the detecting condition is needed, as the standard deviation (SD) value of each point among three groups was high. The limit of detection for GPC-1 in this assay is 10 ng/ml, not as low as that reported recently[26]. The reaction volume is 100 ul, and as homogenous sample, the analyte can only be partly detected by the spectrometer through the cuvette. This disadvantage is considered as the probable factors to induce very big SD value of each point including the control sample without GPC-1, and influence the lower LOD achieved. Thus, to measure the quenching efficiency of single upconversion nanoparticle for detection and quantification of GPC-1 will be a good option, in order to improve the detection sensitivity. In that case, the total reaction volume as well as the concentration of two particles need to be significantly

reduced, so that it is applicable to analyse all luminescent quenching based on each upconversion nanoparticles measurement.

Even though, high detection sensitivity cannot be achieved via this assay at present, this assay demonstrates the potential to be applied in clinical detection in the future, as it is simpler and faster than other assays. In terms of clinic usage, the composition of human samples (e.g. whole blood, serum and plasma) is much more complicated than biological buffers, thus the stability of both UCNPs and GNPs will be a great challenge. Take traditional ELISA as an example, there is only one step where the human sample is incubated with the capture antibody. The following washing steps are designed to help remove almost all non-binding small and large molecules in the sample. However, for the homogenous assay in this chapter, antibody-modified UCNPs and GNPs are existing with human samples through the whole reaction, molecules from samples may induce the particles unstable. Particles' aggregation or antibodies' releasing will reduce the quenching efficiency, resulting in poor detection sensitivity.

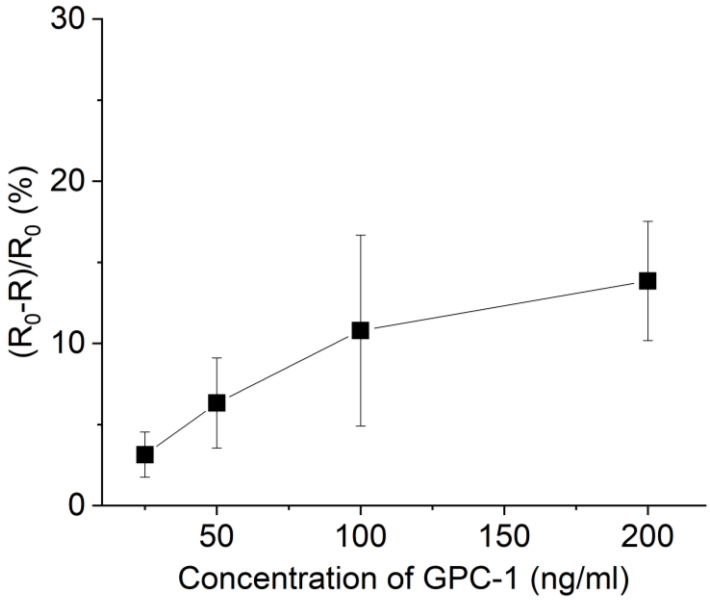

Figure 4.13 Quenching efficiency of upconversion luminescence in the existing of different concentration of GPC-1 antigen (25, 50, 100, 200 ng/ml) via comparing the ratio of green/red emission as formula $(R_0-R)/R_0$. (n = 3)

4.3.8 Specificity of Upconversion LRET Assay for GPC-1

The specificity of this designed assay for GPC-1 detection was compared with PSA, a widely used biomarker for prostate cancer in the commercially available test. The upconversion luminescence quenching is negligible in the presence of PSA (Figure 4.14), while there is distinguished ratio for GPC-1 antigen. This means that the developed upconversion LRET assay based on "sandwich" immunoassay in this chapter is highly specific to GPC-1 detection ($p < 0.05$).

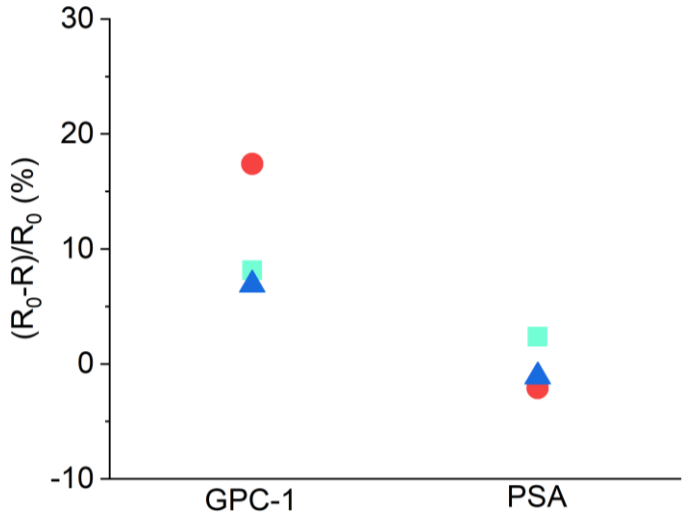

Figure 4.14 Quenching efficiency of upconversion luminescence in the existing of GPC-1 and PSA, respectively, at concentration of 100 ng/ml. Each colour stands for one single testing group (n = 3).

4.4 Conclusion

In summary, we have developed a simple assay that can rapidly and specifically detect for protein antigens, *via* a newly developed washing-free upconversion LRET technique in combination with traditional "sandwich" immunoassay. In this project, the rational core-shell structure of UCNPs was designed and applied in a very advanced strategy. Besides, the unique BsAb with specific binding-affinity to mPEG-UCNP were also introduced into this project, achieving labour-saving bioconjugation method and avoiding bioactivity influence of traditional chemical reaction.

The next step is to optimise the reaction conditions in order to achieve more accurate quantification of GPC-1, based on the upconversion LRET immunoassay developed in this project. In addition, more efforts will be given to investigate and solve sticking nature of the other two sizes of 3G5-AuNPs and to use them in the detection, as well as in quantification processes.

4.5 References

[1] Australian Government-Cancer Australia-Prostate cancer statistics. *https://prostate-cancer.canceraustralia.gov.au/statistics*. **(2018)**.

[2] Heidenreich, A., Bastian, P. J., Bellmunt, J., Bolla, M., Joniau, S., van der Kwast, T., Mason, M., Matveev, V., Wiegel, T. & Zattoni, F. Eau Guidelines on Prostate Cancer. Part 1: Screening, Diagnosis, and Local Treatment with Curative Intent–Update 2013. *European Urology* 65, 124-137 **(2014)**.

[3] Kobori, Y., Kitagawa, Y., Mizokami, A., Komatsu, K. & Namiki, M. Free-to-Total Prostate-Specific Antigen (PSA) Ratio Contributes to an Increased Rate of Prostate Cancer Detection in a Japanese Population Screened Using a PSA Level of 2.1–10.0 ng/ml as a Criterion. *International Journal of Clinical Oncology* 13, 229-232 **(2008)**.

[4] Catalona, W. J., Partin, A. W., Slawin, K. M., Brawer, M. K., Flanigan, R. C., Patel, A., Richie, J. P., Walsh, P. C., Scardino, P. T. & Lange, P. H. Use of the Percentage of Free Prostate-Specific Antigen to Enhance Differentiation of Prostate Cancer from Benign Prostatic Disease: A Prospective Multicenter Clinical Trial. *Jama* 279, 1542-1547 **(1998)**.

[5] Quach Truong, I. O. J., Nocon, A. L., Soon, J. T., Wissmueller, S., Campbell, D. H. & Walsh, B. J. Glypican-1 as a Biomarker for Prostate Cancer: Isolation and Characterization. *Journal of Cancer* 7, 1002 **(2016)**.

[6] Shore, N., Concepcion, R., Saltzstein, D., Paivanas, T., Beebe-Dimmer, J., Ruterbusch, J., Justiniano, I., Mazure, H., Nocon, A. & Soon, J. PII-LBA3 Glypican-1 as a Biomarker for Prostate Cancer. *The Journal of Urology* 193, e496 **(2015)**.

[7] Zhao, J., Jin, D., Schartner, E. P., Lu, Y., Liu, Y., Zvyagin, A. V., Zhang, L., Dawes, J. M., Xi, P. & Piper, J. A. Single-Nanocrystal Sensitivity Achieved by Enhanced Upconversion Luminescence. *Nature Nanotechnology* 8, 729 **(2013)**.

[8] Li, S., Xu, L., Ma, W., Wu, X., Sun, M., Kuang, H., Wang, L., Kotov, N. A. & Xu, C. Dual-Mode Ultrasensitive Quantification of Microrna in Living Cells by Chiroplasmonic Nanopyramids Self-Assembled from Gold and Upconversion Nanoparticles. *Journal of the American Chemical Society* 138, 306-312 **(2015)**.

[9] Deng, R., Xie, X., Vendrell, M., Chang, Y. T. & Liu, X. Intracellular Glutathione Detection Using MnO_2-Nanosheet-Modified Upconversion Nanoparticles. *Journal of the American Chemical Society* 133, 20168-20171 **(2011)**.

[10] Chen, Y., Duong, H., Wen, S., Mi, C., Zhou, Y., Shimoni, O., Valenzuela, S. M. & Jin, D. Exonuclease III-Assisted Upconversion Resonance Energy Transfer in a Wash-Free Suspension DNA Assay. *Analytical Chemistry* **(2017)**.

[11] Gu, B., Zhou, Y., Zhang, X., Liu, X., Zhang, Y., Marks, R., Zhang, H., Liu, X. & Zhang, Q. Thiazole Derivative-Modified Upconversion Nanoparticles for Hg^{2+} Detection in Living Cells. *Nanoscale* 8, 276-282 **(2016)**.

[12] Peng, J., Xu, W., Teoh, C. L., Han, S., Kim, B., Samanta, A., Er, J. C., Wang, L., Yuan, L. & Liu, X. High-Efficiency in Vitro and in Vivo Detection of Zn^{2+} by Dye-Assembled Upconversion Nanoparticles. *Journal of the American Chemical Society* 137, 2336-2342 **(2015)**.

[13] Liang, T., Li, Z., Song, D., Shen, L., Zhuang, Q. & Liu, Z. Modulating the Luminescence of Upconversion Nanoparticles with Heavy Metal Ions: A New Strategy for Probe Design. *Analytical Chemistry* 88, 9989-9995 **(2016)**.

[14] Saleh, S. M., Ali, R. & Wolfbeis, O. S. Quenching of the Luminescence of Upconverting Luminescent Nanoparticles by Heavy Metal Ions. *Chemistry-A European Journal* 17, 14611-14617 **(2011)**.

[15] Yuan, J., Cen, Y., Kong, X.-J., Wu, S., Liu, C. L., Yu, R. Q. & Chu, X. MnO2-Nanosheet-Modified Upconversion Nanosystem for Sensitive Turn-on Fluorescence Detection of H_2O_2 and Glucose in Blood. *ACS Applied Materials & Interfaces* 7, 10548-10555 **(2015)**.

[16] Wu, Y. M., Cen, Y., Huang, L. J., Yu, R. Q. & Chu, X. Upconversion Fluorescence Resonance Energy Transfer Biosensor for Sensitive Detection of Human Immunodeficiency Virus Antibodies in Human Serum. *Chemical Communications* 50, 4759-4762 **(2014)**.

[17] Alonso-Cristobal, P., Vilela, P., El-Sagheer, A., Lopez-Cabarcos, E., Brown, T., Muskens, O., Rubio-Retama, J. & Kanaras, A. Highly Sensitive DNA Sensor Based on Upconversion Nanoparticles and Graphene Oxide. *ACS Applied Materials & Interfaces* 7, 12422-12429 **(2015)**.

[18] Li, C., Zuo, J., Li, Q., Chang, Y., Zhang, Y., Tu, L., Liu, X., Xue, B., Zhao, H. & Zhang, H. One-Step in Situ Solid-Substrate-Based Whole Blood Immunoassay Based on Fret between Upconversion and Gold Nanoparticles. *Biosensors and Bioelectronics* 92, 335-341 **(2017)**.

[19] Wu, M., Wang, X., Wang, K. & Guo, Z. Sequence-Specific Detection of Cytosine Methylation in DNA Via the FRET Mechanism between Upconversion Nanoparticles and Gold Nanorods. *Chemical Communications* 52, 8377-8380 **(2016)**.

[20] Wu, S., Duan, N., Ma, X., Xia, Y., Wang, H., Wang, Z. & Zhang, Q. Multiplexed Fluorescence Resonance Energy Transfer Aptasensor between Upconversion Nanoparticles and Graphene Oxide for the Simultaneous Determination of Mycotoxins. *Analytical Chemistry* 84, 6263-6270 **(2012)**.

[21] He, M., Li, Z., Ge, Y. & Liu, Z. Portable Upconversion Nanoparticles-Based Paper Device for Field Testing of Drug Abuse. *Analytical Chemistry* 88, 1530-1534 **(2016)**.

[22] You, H., Hua, X., Feng, L., Sun, N., Rui, Q., Wang, L. & Wang, M. Competitive Immunoassay for Imidaclothiz Using Upconversion Nanoparticles and Gold Nanoparticles as Labels. *Microchimica Acta* 184, 1085-1092 **(2017)**.

[23] Fan, G., Wang, Z., Hao, M. & Li, J. Bispecific Antibodies and Their Applications. *Journal of Hematology & Oncology* 8, 130 **(2015)**.

[24] Howard, C. B., Fletcher, N., Houston, Z. H., Fuchs, A. V., Boase, N. R., Simpson, J. D., Raftery, L. J., Ruder, T., Jones, M. L. & de Bakker, C. J. Overcoming Instability of Antibody-Nanomaterial Conjugates: Next Generation Targeted Nanomedicines Using Bispecific Antibodies. *Advanced Healthcare Materials* 5, 2055-2068 **(2016)**.

[25] He, H., Howard, C. B., Chen, Y., Wen, S., Lin, G., Zhou, J., Thurecht, K. J. & Jin, D. Bispecific Antibody-Functionalized Upconversion Nanoprobe. *Analytical Chemistry* 90, 3024-3029 **(2018)**.

[26] Levin, R. A., Lund, M. E., Truong, Q., Wu, A., Shore, N. D., Saltzstein, D. R., Concepcion, R. S., Paivanas, T. A., van Breda, A. & Beebe-Dimmer, J. Development of a Reliable Assay to Measure Glypican-1 in Plasma and Serum Reveals Circulating Glypican-1 as a Novel Prostate Cancer Biomarker. *Oncotarget* 9, 22359 **(2018)**.

CHAPTER 5

Conclusions and Perspectives

5.1 Conclusions

This PhD thesis mainly focuses on developing optical biosensors for molecular biomarker detection and quantification with upconversion nanoparticles (UCNPs). The exploration of the suitable surface modification ligand of UCNPs, ultimately results in the development of a set of optical biosensors for both nucleic acid and protein antigen detection and quantification.

The main research achievements through my PhD program are in final summary below:

1) The literature review in Chapter 1, has provided a comprehensive understanding of upconversion luminescence resonance energy transfer technique (LRET) in molecular biomarker detection and quantification during the latest five years, for researchers in biology, diagnosis, analytical chemistry and nanotechnology.

2) The newly designed polymer ligand used to form highly water stable and bio-compatible UCNPs in Chapter 2, has solved the bottle-neck of nanoparticles' surface modification. The polymer-coated nanoparticles demonstrate potential application in both molecular monitoring and cellular imaging, even the excellent monodispersion in cytoplasm makes the polymer-coated nanoparticles used for subcellular study.

3) The robust developed Exo III-assisted upconversion resonance energy transfer in a wash-free suspension DNA assay (Chapter 3), has achieved an ultra-high detection

sensitivity with a detection limit of 15 pM. For upconversion optical probes, the cooperation with enzyme-catalyzed target-triggered signal amplification in isothermal condition, has enhanced one order of magnitude detection sensitivity compared to conventional LRET DNA assay. It is a good example of combining upconversion probes with various kinds of advanced techniques to realize trace amounts of DNA biomarker monitoring in simplified process, and it paves the way of the real clinic application of upconversion DNA probes in the further.

4) It is a big challenge that merging upconversion LRET technique into the sandwich immunoassay for protein antigen monitoring. The smart core-shell structure of UCNPs has been used to increase the on/off ratio of quenching efficiency aiming to achieve sensitive detection. And the special bispecific antibody has been used to improved immune-affinity and simplicity. This project broadens the application of upconversion probes in protein assay, and shows the capacity of nano-biotechnology to compete and substitute the traditional immunoassay.

5.2 Perspectives

5.2.1 Clinical testing

The purpose of the work done in the thesis is to develop a proof-of-concept for various diagnostic applications. The developed proof-of-concepts are currently adopted by other researchers to detect various diseases. For example, the Exo-III assisted upconverting LRET assay is being developed with the aim of detecting miRNA in tuberculosis serum patient samples. The assay involves using carbodiimide chemistry. Since serum contains a lot of proteins and other small molecules with amino groups, there will be competition between amine-probe-DNA and other non-specific biomolecules to conjugate with EDC-

activated carboxyl-UCNPs. This disadvantage may be the big challenge during applying the developed assay into clinical serum/plasma samples. To overcome this challenge, different conjugation methods of conjugation chemistry, such as click-chemistry, may need to be applied.

For the upconverting LRET assay with gold nanoparticles developed in chapter 4 for GPC-1 detection, the technique is still currently being developed to improve the sensitivity and reproducibility for clinic application with human samples. Assay measurements using a spectrometer and a cuvette is currently the bottle-neck of the assay and most likely is the underlying factor leading to the poor reproducibility and influencing the detection sensitivity. The alternative would include measurement of the quenching efficiency based on single upconversion nanoparticles. To address this, the total reaction volume as well as the concentration of nanoparticles needs to be significantly reduced to analyse all luminescent quenching based on each upconversion nanoparticle measurements. It is worth mentioning that the stability of BsAb-UCNPs conjugate should also be assessed in serum or plasma, as the complicated environment of human samples may damage the immunoaffinity between BsAb with PEG linker.

5.2.2 Multiplexing

In this thesis, application of upconversion LRET in combination with signal amplification technique has achieved an ultrahigh detection sensitivity for a particular DNA target. This work can be expanded to realize multiplex DNA assay. High throughput multiplexing detection and quantification of various biomolecules has been become popular over last decade[1,2]. Multiplex sample analysis can provide more information about different biomolecules in a shorter time, with a smaller amount of sample to deliver a more

comprehensive diagnosis.

To achieve multiplexing using UCNPs, most of the current research uses colour emission derived by doping with various lanthanide ions[3,4,5]. There are two models to expand multiplexing properties of UCNPs: UCNP-doped bead-based barcode and UCNP-based fluorescent reporter. Referring to UCNP-doped bead-based barcode, UCNPs are encapsulated within microparticles, and then the microparticles show different luminescent colour as various doped lanthanide ions[6]. Besides the colour emission, luminescence lifetime is also potential for multiplexing by adjusting the concentration of doped lanthanide ions [7].

To develop multiplexing DNA assay with developed Exo III-assisted upconverting LRET approach in Chapter 3, the biggest challenge might be the sophisticated design of complementary probe-DNA for each target DNA sequence, in order to get rid of the cross-section. Searching well-matched chromophores is another key element. For protein antigen detection with upconversion LRET immunoassay, simultaneously monitoring various protein targets is also our next challenge. Distinguished from multiplexing DNA assay, the key element to apply this approach in protein multiplexing with gold nanoparticles is the synthesis of multi-colour UCNPs, being as barcode and signal at the same time.

5.2.3 Point-of-Care

Transferring lab-based molecular assay into small-scale integrated devices is a trend to broaden the application of experimental techniques into the real world[8,9]. How to shrink the experimental scale to be performed in a tiny platform, in integration of input, mixture,

separation and measurement, needs great efforts. In particular, the enzyme-assisted upconverting LRET assay for nucleic acids detection, factors including reacting temperature and volume should are two key elements. Currently, the assay is semi-isothermal, and the signal amplification step in requisition of high temperature is a trouble. The involvement of smartphone for optical signal measurement and analysis can further extend the product market because that extremely overcome the access limitation of expensive and sophisticated machines. In fact, the whole reaction can be conducted at room temperature, realizing fully-isothermal. The activity of Exo III is temperature-dependent, room temperature with a little bit longer reaction time is also suitable for the enzyme-assisted signal amplification. The following stopping-step with 70°C, can be substituted by addition of EDTA. In this case, the whole assay is isothermal at RT, ideal for the development of point-of-care.

Another factor is reaction volume. In chapter 3, the reaction volume used is 100 ul, and the sample was filled into a cuvette for spectral measurement. This volume is too high, resulting in loss of sample information. Thus, reduction of the overall measurement volume to less than 10 ul for optical fiber measurement provides a good option for translating this assay into a point-of-care test. In chapter 4, the upconverting LRET assay with gold nanoparticles for protein biomarker detection, is one-step homogenous assay at RT. Reduction of the reaction volume and use of optical fibre is necessary for point-of-care development. To develop the optical biosensor into point-of-care, there are integrated opportunities, including paper-testing[10,11], array assay[12,13] and microfluidics[14,15], which have already been reported in the literature. Specifically for the Exo III assisted upconverting LRET assay in chapter 3, use of microfluidics is a good choice to satisfy multiple reaction steps[15]; for the one-step homogeneous upconverting LRET assay with

gold nanoparticles, suspension array assay is suitable, especially for further multiplexing development[12].

In conclusion, the further goal of my research contains both broadening the designs and techniques for multiplexing in parallel, and exploring the user-friendly point-of-care devices for marketing in progression. All efforts for these two advanced scopes will pave the way for transferring laboratory outcomes into real world application, in more reasonable, productive as well as long-term healthy.

5.3 References

[1] Schouten, J. P., McElgunn, C. J., Waaijer, R., Zwijnenburg, D., Diepvens, F. & Pals, G. Relative Quantification of 40 Nucleic Acid Sequences by Multiplex Ligation-Dependent Probe Amplification. *Nucleic Acids Research* 30(12), 57-57 **(2002)**.

[2] Elshal, M. F. & McCoy, J. P. Multiplex Bead Array Assays: Performance Evaluation and Comparison of Sensitivity to Elisa. *Methods* 38, 317-323 **(2006)**.

[3] Ehlert, O., Thomann, R., Darbandi, M. & Nann, T. A Four-color Colloidal Multiplexing Nanoparticle System. *ACS Nano* 2(1), pp.120-124 **(2008)**.

[4] Wu, S., Duan, N., Zhu, C., Ma, X., Wang, M. & Wang, Z. Magnetic Nanobead-based Immunoassay for the Simultaneous Detection of Aflatoxin B1 and Ochratoxin A Using Upconversion Nanoparticles as Multicolor Labels. *Biosensors and Bioelectronics* 30(1), pp.35-42 **(2011)**.

[5] Zhou, L., Wang, R., Yao, C., Li, X., Wang, C., Zhang, X., Xu, C., Zeng, A., Zhao, D. & Zhang, F. Single-band Upconversion Nanoprobes for Multiplexed Simultaneous in situ Molecular Mapping of Cancer Biomarkers. *Nature Communications* 6, p.6938 **(2015)**.

[6] Shikha, S., Zheng, X. & Zhang, Y. Upconversion Nanoparticles-Encoded Hydrogel Microbeads-Based Multiplexed Protein Detection. *Nano-Micro Letters* 10(2), p.31 **(2018)**.

[7] Lu, Y., Zhao, J., Zhang, R., Liu, Y., Liu, D., Goldys, E.M., Yang, X., Xi, P., Sunna, A., Lu, J. & Shi, Y. Tunable Lifetime Multiplexing Using Luminescent

Nanocrystals. *Nature Photonics* 8(1), p.32 **(2014)**.

[8] Wang, J. Electrochemical Biosensors: Towards Point-of-Care Cancer Diagnostics. *Biosensors and Bioelectronics* 21, 1887-1892 **(2006)**.

[9] Chin, C. D., Linder, V. & Sia, S. K. Commercialization of Microfluidic Point-of-Care Diagnostic Devices. *Lab on a Chip* 12, 2118-2134 **(2012)**.

[10] He, H., Liu, B., Wen, S., Liao, J., Lin, G., Zhou, J. & Jin, D. Quantitative Lateral Flow Strip Sensor Using Highly Doped Upconversion Nanoparticles. Analytical Chemistry 90(21), pp.12356-12360 **(2018)**.

[11] He, M., Li, Z., Ge, Y. & Liu, Z. Portable Upconversion Nanoparticles-based Paper Device for Field Testing of Drug Abuse. Analytical Chemistry 88(3), pp.1530-1534 **(2018)**.

[12] Kale, V., Päkkilä, H., Vainio, J., Ahomaa, A., Sirkka, N., Lyytikaï en, A., Talha, S.M., Kutsaya, A., Waris, M., Julkunen, I. & Soukka, T. Spectrally and Spatially Multiplexed Serological Array-in-well Assay Utilizing Two-color Upconversion Luminescence Imaging. *Analytical Chemistry* 88(8), pp.4470-4477 **(2018)**.

[13] Ylihaï silä, M., Alaranta, S., Lahdenperä, S., Lahtinen, S., Arku, B., Hedman, K., Soukka, T. & Waris, M. Array-in-well Serodiagnostic Assay Utilizing Upconverting Phosphor Label Technology. *Journal of Virological Methods* 222, 224-230 **(2015)**.

[14] Fang, S., Tian, H., Li, X., Jin, D., Li, X., Kong, J., Yang, C., Yang, X., Lu, Y., Luo, Y. & Lin, B. Clinical Application of a Microfluidic Chip for Immunocapture and Quantification of Circulating Exosomes to Assist Breast Cancer Diagnosis and Molecular Classification. *PLoS One* 12(4), p.e0175050 **(2017)**.

[15] Xu, H., Liao, C., Zuo, P., Liu, Z. & Ye, B.C. Magnetic-Based Microfluidic Device for On-Chip Isolation and Detection of Tumor-Derived Exosomes. *Analytical Chemistry* 90(22), 13451-13458 **(2018)**.